

AV 8201 683
Crop micrometeorology:
a simulation study

J. Goudriaan

NN08201.683

Crop micrometeorology: a simulation study

Stellingen

I

De meeste belangrijke micrometeorologische grootheden in veldgewassen kunnen thans voldoende nauwkeurig voor toepassing in modellen voor groei en ontwikkeling van gewassen en van hun ziekten en plagen worden gesimuleerd. Als belangrijke uitzondering moet de bladnatperiode in verband met simulatie van schimmelziekten genoemd worden.

II

De helderheidsverdeling van de standaard-bewolkte hemel en de randverzwakking van de helderheid van de zonneschijf kunnen uit dezelfde modelberekeningen theoretisch worden verklaard.

Dit proefschrift

J. Grace, 1971. *J. appl. Ecol.*, 8: 155–165

C. W. Allen, 1973. *Astrophysical Quantities*, Londen.

III

De aërodynamische gewaseigenschappen ruwheidslengte en nulvlaksverplaatsing kunnen eenvoudiger en nauwkeuriger uit gewasgeometrie en de aërodynamische planteigenschappen worden berekend dan d.m.v. windprofielen worden gemeten. Meting van windprofielen leent zich er evenmin toe om de turbulente uitwisselingscoëfficiënt in het gewas of aërodynamische planteigenschappen te bepalen.

IV

De bladhoekverdeling van veldgewassen kan voldoende nauwkeurig met één getal worden gekarakteriseerd.

J. Ross, 1975. (Editor: J. L. Monteith), Londen.

V

De hoekafhankelijkheid van de reflectie van straling door elk willekeurig oppervlak voldoet aan een reciprociteitsrelatie, die zegt dat de helderheid van het oppervlak dezelfde blijft als de hoeken van inval en van uittreding worden verwisseld onder gelijkblijvende inkomende flux.

Dit proefschrift.

VI

Bij enkele belangrijke landbouwgewassen wordt de huidmondjesweerstand zo geregeld dat het CO₂-gehalte in de substomataire holte constant blijft. Verhoging van het CO₂-gehalte in de lucht leidt daarom lang niet altijd tot verhoging van de fotosynthese.

J. Goudriaan en H. H. van Laar, in druk. *Photosynthetica*.

VIII

Tot nog toe is veel te weinig aandacht besteed aan de ontwikkeling en verbreiding van goed bruikbare computerprogramma's voor:

- a. het uitwerken van wiskundige vergelijkingen langs analytische weg,
- b. continue simulatie van systemen waarbinnen sterk verschillende tijdsconstanten voorkomen,
- c. het controleren van simulatieprogramma's op consequent gebruik van dimensies.

VIII

Voor het bereiken van een evenwichtiger verdeling van arbeid en inkomen, is het gewenst dat geleidelijk een arbeidsloos inkomen voor elke Nederlander wordt ingevoerd, dat bekostigd dient te worden uit indirecte belastingen.

IX

In discussies over gebruik van kernenergie worden de gevaren van fossiele energie vaak veronachtzaamd.

X

Groenzones hebben als buffer tegen lawaai geen betekenis.

XI

Met de in de Machtigingswet Inschrijving Studenten aangewezen methode om vast te stellen wie in het geval van een numerus clausus kan gaan studeren, zou ook de kabinetsformatie aanzienlijk vereenvoudigd kunnen worden.

Art. 4, lid 2 van de Wet van 6 juli 1972, Stb. 355.

Proefschrift van J. Goudriaan

Crop micrometeorology: a simulation study.

Dit proefschrift met stellingen van Jan Goudriaan, natuurkundig ingenieur, geboren te Capelle a/d IJssel op 7 mei 1946, is goedgekeurd door de promotoren, dr. ir. C. T. de Wit, buitengewoon hoogleraar in de theoretische teeltkunde, en dr. ir. J. Schenk, hoogleraar in de natuurkunde en weerkunde.

Wageningen, 17 februari 1977

De rector magnificus
van de Landbouwhogeschool,
J. P. H. van der Want

Crop micrometeorology: a simulation study

J. Goudriaan

Proefschrift

ter verkrijging van de graad van

doctor in de landbouwwetenschappen,

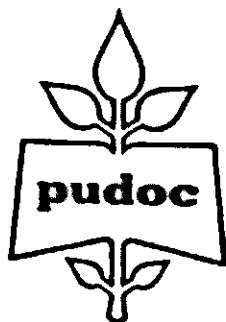
op gezag van de rector magnificus,

dr. ir. J. P. H. van der Want, hoogleraar in de virologie,

in het openbaar te verdedigen

op 22 april 1977 des namiddags te vier uur

in de aula van de Landbouwhogeschool te Wageningen



Wageningen

Centre for Agricultural Publishing and Documentation

1977

The author works at the Department of Theoretical Production Ecology of the Agricultural University, Wageningen, the Netherlands

Keywords

energy balance, hierarchical approach, photosynthesis, radiation, sensitivity analysis, stiff systems, transpiration

ISBN 90-220-0614-X

This thesis will also be published in the series Simulation Monographs

© Centre for Agricultural Publishing and Documentation, Wageningen, the Netherlands, 1977

No part of this book may be reproduced or published in any form, by print, photoprint, microfilm or any other means without written permission from the publisher

Cover design: Pudoc, Wageningen

Printed in the Netherlands

Voorwoord

Toen ik in 1970 solliciteerde naar aanleiding van een advertentie waarin een medewerker werd gevraagd voor de afdeling Theoretische Teeltkunde van de Landbouwhogeschool, had ik er nog geen vermoeden van in welke omgeving ik terecht zou komen. Die bleek gekenmerkt door een goede wetenschappelijke sfeer, maar ook door bijzonder plezierige menselijke verhoudingen. Deze werksfeer is een belangrijke factor geweest voor het tot stand komen van dit proefschrift, en ik wil allen danken die er een bijdrage aan hebben geleverd. Dit geldt wel in de eerste plaats voor prof. dr. ir. C. T. de Wit. Hij heeft ook de aanzet gegeven tot dit onderzoek, en als leermeester en inspirator voortdurend een actieve rol gespeeld bij de uitvoering en verslaglegging ervan.

Enige ervaring in het vak heb ik opgedaan tijdens een studieverblijf in 1971 in Engeland bij prof. J. L. Monteith. Hem en zijn medewerkers wil ik van harte danken voor hun bereidwilligheid mij te ontvangen en te begeleiden. Verder maak ik graag van de mogelijkheid gebruik dr. P. E. Waggoner en dr. T. R. Sinclair te bedanken die beiden enige tijd in Wageningen hebben verbleven en met wie ik heb mogen samenwerken. Hun bezoek was voor mij zeer leerzaam en stimulerend.

Zolang ik bij de Landbouwhogeschool werk heb ik gastvrijheid genoten bij het CABO (IBS vroeger). Dit heb ik altijd bijzonder gewaardeerd.

Hoewel dit proefschrift grotendeels van theoretische aard is, waren experimentele gegevens voor modevaluatie onmisbaar. Deze gegevens zijn verzameld en ter beschikking gesteld door de vakgroep Natuur- en Weerkunde van de Landbouwhogeschool, die ik hiervoor zeer erkentelijk ben. In het bijzonder hebben zich hierbij ingespannen dr. C. J. Stigter en dr. F. A. Bottemanne. Ook de voorzitter van de vakgroep, prof. dr. ir. J. Schenk, wil ik hiervoor danken. Later heeft hij ook een grote bijdrage geleverd aan het tot stand komen van het proefschrift en is bereid geweest als tweede promotor op te treden.

Ondanks zijn eigen drukke werkzaamheden wist dr. ir. R. Rabbinge altijd wel tijd te vinden om te helpen bij het oplossen van wat voor

problemen dan ook. Mevrouw H. H. van Laar heeft veel tijd besteed aan het werken van gegevens en is ook op tal van andere wijzen steeds behulpzaam geweest. Ir. C. de Jonge heeft op conscientieuze wijze mijn computerprogramma's voor publikatiedoeleinden aangepast. De heer M. van den Born heeft met groot enthousiasme en vindingrijkheid stralingsmeters vervaardigd, die later o.a. op de proefbedrijven Flevoland en De Eest opgesteld zijn geweest. De heer G. C. Beekhof heeft de tekeningen bij dit proefschrift vervaardigd. Mevrouw E. Brouns heeft veel tijd besteed aan correctie van de Engelse tekst en aan de bespreking van de verbeteringen. Vele anderen met wie ik in de loop der jaren wetenschappelijke en technische problemen heb besproken hebben direct of indirect het hunne bijgedragen.

Ik ben Pudoc erkentelijk voor het scheppen van de mogelijkheid mijn proefschrift in deze vorm te laten verschijnen. Tenslotte wil ik de Landbouwhogeschool, en hierbij denk ik in het bijzonder aan de administratieve en bestuurlijke sektor daarvan, bedanken voor de mogelijkheid dat dit onderzoek verricht kon worden.

Curriculum vitae

Jan Goudriaan werd geboren op 7 mei 1946 te Capelle aan de IJssel. Hij volgde de middelbare school in Rotterdam en behaalde het diploma Gymnasium-B in 1964. Daarna begon hij met de studie in de Technische Natuurkunde aan de Technische Hogeschool te Delft en behaalde in 1970 het ingenieursdiploma met lof op een onderwerp uit de akoestiek. Gedurende het laatste jaar van de studie werd dit onderzoek tevens als part-time werk verricht voor de Technisch Fysische Dienst TNO-TH. In maart 1970 kwam hij als wetenschappelijk medewerker in dienst bij de vakgroep Theoretische Teeltkunde van de Landbouwhogeschool te Wageningen. Daar kreeg hij de gelegenheid om zijn werk, onderzoek en onderwijs in de simulatie van gewasgroei en microklimaat en in de simulatietechniek, te laten resulteren in dit proefschrift.

Samenvatting

Dit proefschrift geeft de resultaten van een gedetailleerde studie in de micrometeorologie. Dit wetenschapsgebied is van groot belang voor de studie van de groei en ontwikkeling van gewassen en van de ziekten en plagen die daarin voor kunnen komen.

Het doel van dit onderzoek is het microweer te kunnen verklaren als functie van plant- en bodemeigenschappen, en van de weersgesteldheid op enige hoogte boven het gewas. Er zijn zoveel factoren betrokken bij de micrometeorologie dat het nodig is een simulatie techniek te gebruiken om het resultaat van hun gezamenlijke effect te kunnen berekenen.

In de hoofdstukken 2, 3 en 4 worden de submodellen, die de basiselementen vormen van het micrometeorologische systeem, beschreven en besproken. In hoofdstuk 5 worden de programmeringsaspecten in beschouwing genomen en in hoofdstuk 6 worden de resultaten van het samengestelde model en een evaluatie ervan gegeven. De waarden van de parameters die nodig zijn in de submodellen zijn bijna uitsluitend afkomstig van literatuurgegevens. Daarentegen is de structuur van de submodellen speciaal voor dit onderzoek ontwikkeld met het oog op hun onderlinge afstemming en een evenwichtige verhouding tussen nauwkeurigheid en eenvoud.

In hoofdstuk 2 worden modellen gegeven voor de straling in gewassen onder verschillende omstandigheden en aannames.

Voor horizontale bladeren is de uitdoving van straling van één golflengte zuiver exponentieel, zowel voor zwarte als voor verstrooiende bladeren. Het numerieke model toont aan dat voor niet-horizontale bladeren de uitdoving weliswaar niet exponentieel verloopt, maar er gewoonlijk toch slechts weinig van afwijkt. Alleen bij lage zonnestand wordt door de bovenste gewaslagen meer en door de onderste minder geabsorbeerd dan volgens een exponentiële uitdoving het geval zou zijn. De waarden van de extinctie- en reflectiecoëfficiënten kunnen met enkele eenvoudige formules, die een generalisering vormen van de

resultaten voor horizontale bladeren, benaderd worden. Ross (1975) had reeds aangetoond dat de bladhoekverdeling bij benadering door een enkel getal gekarakteriseerd kan worden. Onze evaluatie laat zien dat de extinctie- en reflectiecoëfficiënten met behulp van het numerieke stralingsmodel en de vereenvoudigde formules goed geschat kunnen worden. Dagelijkse gangen, en ook het verschil tussen de zichtbare en nabij infrarode stralingsgebieden, worden er goed door weergegeven. De numerieke resultaten van het model tonen een reciprociteitsrelatie met interessante theoretische aspecten en belangrijke conclusies voor bijv. de zgn. remote sensing techniek. De vergelijkingen voor de warmtestraling kunnen eenvoudig worden gehouden omdat de temperatuur van de bladeren en van het bodemoppervlak als toestandsvariabelen worden beschouwd.

Door toepassing in het model van een verstrooiingscoëfficiënt van één kan de helderheidsverdeling van de standaard bewolkte hemel (SOC) verklaard worden. Een andere modeluitbreiding betreft het geval dat de reflectie- en transmissiecoëfficiënten van individuele bladeren niet aan elkaar gelijk zijn. Vervolgens wordt aangetoond dat, verlopend vanaf een regelmatige tot aan een geclusterde bladplaatsing, de reflectie- en extinctiecoëfficiënten voor een gewas afnemen, evenals het verschil in uitdoving tussen zichtbare en nabij infrarode straling. Deze effecten zijn inderdaad in de literatuur vermeld. Uit een model voor lichtonderschepping door een gewas in rijen is gebleken dat verlies van diffuse straling tussen de rijen niet ernstig is. Ook voor deze situatie zijn vereenvoudigde formules afgeleid en geëvalueerd.

De modellen, die in dit hoofdstuk zijn gegeven, zijn voldoende algemeen enerzijds en hun resultaten zijn voldoende vereenvoudigd anderzijds om met succes toegepast te kunnen worden in simulatiemodellen voor fotosynthese en verdamping van gewassen.

In hoofdstuk 3 wordt de verdeling van de beschikbare energie over plant- of bodemverdamping, voelbare warmteverlies, opslag van warmte en fotosynthese afgeleid uit de eigenschappen van de planten en de bodem, en van de gesteldheid van de lucht. Het plantwatergehalte heeft invloed op de huidmondjesweerstand en wordt gevonden door integratie van de berekende plantverdamping en wateropname uit de grond. Wegens de ongelijke verdeling van straling over de bladeren en wegens het verticale verloop van de temperatuur en de vochtigheid van de lucht, is een indeling van de bladeren in hoogte en in

hoek van inval van de straling nodig. De warmte- en waterdampstromen vanaf de bladeren en het grondoppervlak komen vrij in de lucht. De profielen van luchttemperatuur en vochtigheid worden gevonden door integratie van de netto-stromen naar de tijd, voor de verschillende horizontale lagen in het gewas afzonderlijk. Een soortgelijke methode wordt gebruikt om de bodemtemperaturen uit te rekenen, zij het dat alleen de warmteflux aan het bodemoppervlak een drijvende kracht is. De warmtegeleidbaarheid en capaciteit in de grond zijn konstant verondersteld. Voor de turbulente uitwisseling tussen de lagen in het gewas wordt de theorie van het volgende hoofdstuk gebruikt.

In hoofdstuk 4 wordt enige theorie betreffende wind en turbulentie in en boven gewassen behandeld. Het vaak geobserveerde logaritmische windprofiel wordt gebruikt als basis voor de berekening van de uitwisselingscoëfficiënt boven het gewas. Als een verticaal temperatuurverloop in de lucht aanwezig is, wordt het logaritmische windprofiel verstoord en moeten de waarden van de uitwisselingscoëfficiënt gewijzigd worden. De hiervoor benodigde formules zijn uit de literatuur afkomstig en aangepast voor gebruik in het simulatiemodel.

De vorming van een inversielaag boven het gewas gedurende de nacht, als de netto straling negatief is, kan met deze formules worden beschreven. Wat betreft de turbulente uitwisseling binnen het gewas is gevonden, dat de profielen van zowel de windsnelheid als de uitwisselingscoëfficiënt redelijk goed benaderd kunnen worden door een exponentiële uitdoving met de diepte. De theoretische waarden van de uitdovingsfactor zijn in goede overeenstemming met experimentele gegevens. Als er binnen het gewas een temperatuurverloop aanwezig is, wordt de uitwisselingscoëfficiënt op dezelfde manier gecorrigeerd als boven het gewas. Er blijkt een ondergrens te bestaan voor de uitwisselingscoëfficiënt als de windsnelheid tot nul nadert. Daarom blijft ook onder een inversie de uitwisseling binnen het gewas gehandhaafd. De aerodynamische macrogrootheden zoals de nulvlaksverplaatsing d en de ruwheidslengte z_0 worden uitgedrukt in de aerodynamische microgrootheden en in de gewasgeometrie. De theoretische resultaten voor grasland, een maïsgewas en een naaldbos blijken goed overeen te komen met experimentele gegevens voor de aerodynamische macrogrootheden. Uit een modelonderzoek naar het effect van ruimtelijke variatie blijkt dat ondanks niet-lineaire effecten een ééndimensionaal schema toereikend is, voorzover men alleen geïnteresseerd is in de

horizontale gemiddelden van de resultaten. Variaties in de tijd echter, zoals die optreden door fluctuaties in windsnelheid, hebben ook op gemiddelde waarden van temperatuur en vochtigheid vrij veel invloed.

In hoofdstuk 5 komen de programmeringsaspecten aan de orde. Eerst wordt het initialiseringsprobleem besproken. Dit kan worden opgelost d.m.v. de gedachte van een cyclisch evenwicht. Wat betreft de ruimtelijke grenzen van het systeem; de ene wordt zo diep in de grond gelegd dat de invloed van de dagelijkse warmtegolf verdwijnt, de andere wordt niet hoger dan 3 m boven het grondoppervlak gelegd om de invloed van horizontale advectie zoveel mogelijk te vermijden. De methode wordt gegeven om de weersgegevens die op dit niveau gemeten zijn in een voor het programma bruikbare vorm te brengen. Vervolgens wordt de hiërarchische benadering en ook de voorwaarden voor de toepassing ervan aan de hand van enkele voorbeelden besproken. Er wordt een overzicht gegeven van enkele oplossingstechnieken voor verschillende probleemgebieden (Fig. 27). In een volgende sectie wordt een techniek gegeven waarmee het aantal berekeningen in een simulatieprogramma voor een stijf systeem drastisch verminderd kan worden. Deze methode wordt toegepast in het micrometeorologische simulatiemodel. De teksten van de gebruikte programma's staan in sectie 5.6.

In hoofdstuk 6 worden de resultaten van het micrometeorologisch simulatiemodel gegeven. Voor een kenmerkend voorbeeld worden de dagelijkse gangen van enkele karakteristieke uitvoervariabelen gesimuleerd en aan de hand van de submodellen verklaard. Als het grondoppervlak nat is blijkt de bodemverdamping wel één derde van de totale evapotranspiratie te bedragen. Dauw op de bladeren bestaat grotendeels uit water, overgedestilleerd van het grondoppervlak. Gedurende de nacht ontwikkelt zich een inversie boven het gewas. Water-spanning gedurende de namiddag heeft een sterke verlaging van de CO₂ opname tot gevolg.

De gevoeligheidsanalyse laat zien dat sensoren voor invoer weersgegevens traag mogen zijn, aangezien uurgemiddelden toereikend zijn. Een uitzondering moet echter gemaakt worden voor windsnelheid: vlagerigheid heeft een aanzienlijk effect op de simulatiere-sultaten. De inkomende straling moet bij voorkeur in diffuse en directe straling apart worden geregistreerd. De hoeveelheid dauw en de

bladnat periode kunnen niet met een vuistregel worden geschat. De indeling van de bodem in tien lagen is zeker voldoende nauwkeurig, en voor de gewasruimte blijkt een aantal van slechts drie lagen toereikend te zijn. Belangrijke planteigenschappen zijn de verstrooiingscoëfficiënt van de bladeren, de cuticulaire weerstand en het huidmondjesgedrag. In overeenstemming met vroegere bevindingen van De Wit (1965) blijkt de bladhoekverdeling van ondergeschikt belang, zodat de vereenvoudigingsmethode van Ross (sektie 2.3.3) zeker voldoende nauwkeurig is. Voor een gesloten gewas heeft de bladoppervlakteindex weinig invloed op de CO₂ opname en op de transpiratie, bovendien zijn de aerodynamische gewasgrootheden van gematigde betekenis. De thermische bodemeigenschappen hebben een grote invloed op de bodemtemperaturen en de warmteflux de grond in, maar niet op het tijdstip van hun maximum. Gedurende de nacht is het effect van de thermische bodemeigenschappen op de profielen in de lucht vrij groot, gedurende de dag is deze echter te verwaarlozen.

De variatie van de uitwisselingscoëfficiënt met de hoogte is één van de overheersende factoren voor de vorm van de temperatuur- en vochtprofielen in de lucht binnen het gewas, evenals de variatie in de tijd. De resultaten van het model worden vergeleken met meetresultaten in een maïsgewas voor drie verschillende dagen. De profielen van nettostraling, windsnelheid en bladgeleidbaarheden stemmen voldoende overeen. De gesimuleerde bodemwarmteflux en grondoppervlaktetemperatuur wijken aanzienlijk van de gemeten waarden af. Dit komt waarschijnlijk door het weglaten in de simulatie van opdrogen van het grondoppervlak en ook door meettechnische moeilijkheden. Zoals reeds hiervoor opgemerkt kunnen deze afwijkingen echter niet de eveneens aanwezige afwijkingen in de profielen in de lucht verklaren. Deze afwijkingen zijn grotendeels te wijten aan overschatting van de relatieve turbulentie intensiteit, en aan het weglaten van het effect van vlagerigheid van wind. Door deze factoren beter in rekening te brengen blijken de afwijkingen aanzienlijk gereduceerd te worden. Daarom is het goed meer aandacht aan deze factoren te geven in toekomstig micrometeorologisch onderzoek.

Het gepresenteerde model is een verantwoorde en betrouwbare basis voor de berekening van de verschillende componenten van het microweer in een gewas. De resultaten van dit model kunnen goed gebruikt worden voor de simulatie van de groei van gewassen, en van enkele ziekten en plagen die hierin voorkomen.

In de toekomst zal het model voor toepassing in andere situaties, zoals een grasland, geschikt gemaakt moeten worden. De resultaten ervan moeten in eenvoudige formules samengevat worden zoals dat ook voor de stralingsmodellen gedaan is. Een volgende stap zal zijn om de kloof te overbruggen tussen het veld waar het gewas groeit, en het veld waar de meteorologische waarnemingen worden gedaan. Tenslotte is het goed zich te realiseren dat onze plantenfysiologische kennis, in nog sterkere mate dan onze meteorologische kennis, een beperkende factor vormt voor de mogelijkheid gewasgroei en opbrengst door middel van simulatie te voorspellen.

Contents

1	Introduction	1
1.1	Definition of the problem	1
1.2	Outline of the book	2
1.3	Symbols and units	3
2	Radiation in plant canopies	5
2.1	Introduction	5
2.2	Basic elements	6
2.2.1	Geometry	6
2.2.2	Incoming radiation	8
2.2.3	Optical properties	12
2.3	Elementary models	13
2.3.1	Horizontal leaves	13
2.3.2	Canopies with a non-horizontal leaf angle distribution	15
2.3.3	Simplifying formulations	25
2.3.4	Evaluation	32
2.3.5	An important reciprocity relation	36
2.3.6	Thermal radiation	39
2.4	Model extensions	41
2.4.1	The origin of the radiance distribution of the standard overcast sky	41
2.4.2	Leaves with unequal reflection and transmission	46
2.4.3	The influence of spatial correlation of leaf positions	51
2.4.4	Plants in rows	54
2.5	List of symbols used in Chapter 2	67
3	Energy and mass balances	73
3.1	Introduction	73
3.2	Single leaves	73
3.3	The soil surface	79
3.4	The canopy	81
3.4.1	Introduction	81
3.4.2	Leaf area index less than 0.2	82

3.4.3	Leaf area index more than 0.2	83
3.4.4	Water status	86
3.5	The air inside the canopy	88
3.6	List of symbols used in Chapter 3	89
4	Turbulence and wind	94
4.1	Introduction	94
4.2	Exchange above the canopy	95
4.2.1	Neutral conditions	95
4.2.2	Non-neutral conditions	98
4.3	Exchange inside the canopy	108
4.3.1	Neutral conditions	108
4.3.2	Non-neutral conditions	111
4.4	A fundamental approach to the derivation of z_0 and d	115
4.5	Variability in time and space	118
4.6	List of symbols used in Chapter 4	122
5	Programming aspects	124
5.1	Introduction	124
5.2	Boundaries in time and space	124
5.2.1	Initialization	124
5.2.2	Spatial boundaries	126
5.2.3	Conversion of measured weather data	127
5.3	Hierarchical approach	129
5.4	Solution techniques	130
5.5	Stiff systems	133
5.6	Programs and lists of abbreviations	141
6	Results	175
6.1	Introduction	175
6.2	A case study	175
6.2.1	Description	175
6.2.2	Daily courses of energy fluxes	177
6.2.3	Daily courses of temperatures and humidities	180
6.2.4	Net CO ₂ -assimilation	182
6.2.5	Dew	184
6.3	Sensitivity analysis	185
6.3.1	Introduction	185
6.3.2	Input weather data	186

6.3.3	Compartmentalization in canopy and soil	192
6.3.4	Height of reference	194
6.3.5	Plant properties	196
6.3.6	Soil properties	201
6.3.7	Turbulent exchange	204
6.4	Experimental evaluation	207
6.4.1	Introduction	207
6.4.2	Experimental conditions	209
6.4.3	Comparison of measured and simulated output values	211
6.4.4	Discussion	224
	Summary	231
	Acknowledgments	236
	References	237
	Appendix A	242
	Appendix B	245
	Index	247

1 Introduction

1.1 Definition of the problem

Production ecology is the study of how internal and external factors influence the growth and development of crops, pastures and their pests and diseases. Some examples are the primary production of grasslands in semi-arid conditions (van Keulen, 1975) or the population growth of the fruit-tree red spider mite (Rabbinge, 1976). The choice and definition of these problem areas depend on socio-economic factors, whose relevance is taken for granted here. In almost every applied study of this kind different scientific disciplines are involved such as soil science, physics, meteorology, plant physiology, phytopathology and entomology. How important these specialisms are and to what extent they should be considered, must be answered by a detailed study. This monograph presents the results of such a study in the field of micrometeorology. Since in micrometeorology many factors are involved that partly interact, a quantitative evaluation of their combined effect can only be successful with the aid of a simulation technique.

In micrometeorology, more than in meteorology, the feedback of plants or soil on their environment has to be taken into account. The plants modify their environment for instance by shading, by the release of water vapour and by reduction of the wind velocity. The plant's own properties play a role in this modification. These are considered as given parameters, though in fact they may have been partly influenced by past meteorological conditions.

However, this study is limited to a time scale of a few days, so that morphogenetic effects of the microweather on plants are not considered. Short-term effects, such as plant water stress caused by transpiration, are taken into account. Not only micrometeorological factors that are directly important for crop growth and development are treated, but also those that play a role in the development of pests and diseases, such as leaf wetness duration. The limitation to a short period is the reason why here the term microweather is preferred to

6.3.3	Compartmentalization in canopy and soil	192
6.3.4	Height of reference	194
6.3.5	Plant properties	196
6.3.6	Soil properties	201
6.3.7	Turbulent exchange	204
6.4	Experimental evaluation	207
6.4.1	Introduction	207
6.4.2	Experimental conditions	209
6.4.3	Comparison of measured and simulated output values	211
6.4.4	Discussion	224
	Summary	231
	Acknowledgments	236
	References	237
	Appendix A	242
	Appendix B	245
	Index	247

1 Introduction

1.1 Definition of the problem

Production ecology is the study of how internal and external factors influence the growth and development of crops, pastures and their pests and diseases. Some examples are the primary production of grasslands in semi-arid conditions (van Keulen, 1975) or the population growth of the fruit-tree red spider mite (Rabbinge, 1976). The choice and definition of these problem areas depend on socio-economic factors, whose relevance is taken for granted here. In almost every applied study of this kind different scientific disciplines are involved such as soil science, physics, meteorology, plant physiology, phytopathology and entomology. How important these specialisms are and to what extent they should be considered, must be answered by a detailed study. This monograph presents the results of such a study in the field of micrometeorology. Since in micrometeorology many factors are involved that partly interact, a quantitative evaluation of their combined effect can only be successful with the aid of a simulation technique.

In micrometeorology, more than in meteorology, the feedback of plants or soil on their environment has to be taken into account. The plants modify their environment for instance by shading, by the release of water vapour and by reduction of the wind velocity. The plant's own properties play a role in this modification. These are considered as given parameters, though in fact they may have been partly influenced by past meteorological conditions.

However, this study is limited to a time scale of a few days, so that morphogenetic effects of the microweather on plants are not considered. Short-term effects, such as plant water stress caused by transpiration, are taken into account. Not only micrometeorological factors that are directly important for crop growth and development are treated, but also those that play a role in the development of pests and diseases, such as leaf wetness duration. The limitation to a short period is the reason why here the term microweather is preferred to

microclimate. Typical microclimatic effects such as exposure on a hill side, are not considered in this study.

The purpose of this monograph is to explain the microweather as a function of the properties of plant and soil, and of the weather conditions at some height above the canopy. This choice of the location of these input data seriously limits the scope of the work since an important gap remains to be bridged: the relation between the weather conditions at some height above the crop surface studied and the weather conditions as recorded on standard meteorological observation sites. Nevertheless, the results of this work mean a considerable simplification of the input data that are needed for a study of growth and development of crops, pastures and their pests and diseases.

1.2 Outline of the book

The complexity of the subject of this study is illustrated by the number of publications on micrometeorology. Most of these studies are experimental and together they signify an impressive collection of information. There is also a considerable mass of literature on the basic elements of micrometeorological systems, such as heat and mass transfer, radiation, plant ecophysiology. A simulation technique that permits evaluation of their combined effects, is the proper instrument for a quantitative synthesis of present knowledge. Moreover, in a simulation program one must state explicitly how one conceives reality in each of the submodels in relation to the purpose of the simulation and so provide a basis for discussion and further improvement, as will be shown in this study.

The submodels used are given and discussed in Chapters 2, 3 and 4. Chapter 2 describes the modelling of radiation in crops. This model gives results both on a macroscale (crop reflectance and transmittance) and on a microscale (distribution of absorbed radiation intensity over the leaves). Two quotations from Lemeur & Blad (1974) point out exactly what was aimed at: "a synthesis of fundamental models into workable expressions is badly needed" and "the calculation of empirical constants from the theoretical models and the experimental verification of the corresponding formulae are high priority needs". In Chapter 3 the energy and mass balances of leaves and soil surface are modelled and discussed. By the combination of Chapters 2 and 3

another requirement of Lemeur & Blad (1974) is fulfilled: "It is necessary to relate radiation models to the phenomena of transpiration and photosynthesis". In Chapter 4 wind and turbulence are treated as related phenomena above as well as inside the canopy.

The parameter values that were needed in the submodels were almost exclusively taken from existing literature sources. But the structure of the submodels was especially developed for this study in view of their compatibility and of an optimal balance between accuracy and simplicity.

The synthesis of the submodels in a simulation program for the micro-weather results in some programming difficulties which are discussed in Chapter 5. Also some general considerations on the modelling of systems are given in this chapter.

In Chapter 6 the result of two applications of the model are presented. First the behaviour of the model as a whole and a sensitivity analysis are discussed for a typical case, and thereafter the model behaviour is evaluated with experimental data in another situation.

Each chapter begins with an introduction, which outlines its scope. The results of these chapters are summarized in Chapter 7, which also forms the summary of the whole book. By reading these introductions and summaries a general impression of the book can be easily obtained.

1.3 Symbols and units

The symbols and their units are listed at the end of Chapters 2, 3 and 4. Apart from a few exceptions they are in accordance with the international system (SI). Relicts of previous systems are the unit of water vapour pressure (mbar), the unit of plant water stress (bar) and the unit of CO₂-concentration (volume parts per million, abbreviated as vpm).

The rate of energy production (J s^{-1}) is indicated by the name 'flow' and the rate of passage of energy through a surface ($\text{J m}^{-2} \text{s}^{-1}$) by the name 'flux', instead of the normalized but somewhat impractical terms 'flux' and 'flux density', respectively. The symbols correspond closely to those chosen by Monteith (1973). An exception is the symbol 's', which I use for the slope of the saturated vapour pressure curve, instead of the symbol ' Δ '. The combination *LAI* denotes one variable, leaf area index. The great number of variables made it

necessary to list the symbols for Chapters 2, 3 and 4 separately. These lists also give the computer symbols if they are used in the programs. Moreover, the number of the equation is given in which the variable occurs for the first time in the text. Variables that occur only once or twice are omitted.

2 Radiation in plant canopies

2.1 Introduction

In simulation models of plant growth, the absorption of radiation by the leaves of a canopy is a major factor governing photosynthesis and transpiration. During the last few years there have been several publications on this subject. Lemeur & Blad (1974) gave an excellent review of these light models, so that it suffices here to give a short survey of the work done.

In 1953 Monsi & Saeki introduced the idea of the exponential extinction of radiation in a canopy. In 1959, de Wit first used an analytical method to calculate the light distribution, but applied later in 1965 an entirely numerical method. Some extensions to this work were presented by Anderson (1966), Cowan (1968), Lemeur (1971) and Ross & Nilson (1966). They used primarily analytical methods, but sometimes computer programs as well. Cowan's analytical method is only applicable to a canopy with horizontal leaves. Ross & Nilson used a more general, but also a more complicated and laborious method.

An attempt was made to design models, sufficiently general to be realistic, and to formulate their results in terms sufficiently simple to be applicable without excessive effort.

First the basic elements of the model are presented (Section 2.2). Subsequently an analytical study is made for canopies with horizontal leaves (Section 2.3.1). In Section 2.3.2 the more general case of non-horizontal leaf angle distributions is studied by an extension of de Wit's numerical method to multiple scattering. The results of this numerical model are summarized in Section 2.3.3, mainly by generalizing the earlier results for horizontal leaves. In Section 2.3.4, the results obtained so far are evaluated by checking with experimental data, largely from literature. The model presented is also used for the treatment of thermal radiation. In Section 2.4 some model extensions are given. The first one concerns the case of individual elements with a very high scattering coefficient. In the next extension the constraint is

removed that the leaf reflection should equal the leaf transmission coefficient. Subsequently leaf positionings other than random are considered. The radiation field in plant stands, cultivated in rows, deserves special attention and is treated in Section 2.4.4.

2.2 Basic elements

2.2.1 Geometry

The canopy is supposed to be homogeneous in a horizontal plane so that there is no horizontal clustering of leaves. The leaf area density is height dependent with the dimension m^2 leaf per m^3 air. The number of leaves expected in a layer is equal to the leaf area density multiplied by the air volume of this layer and divided by the area per leaf. In maize the actual number of leaves in a volume element can be described by a Poisson distribution (Sinclair & Lemon, 1974), but in this model only the expectation values of leaf area and radiant fluxes are considered. This is allowed if the horizontal extension of the layers is sufficiently large. Thus there is no correlation between the positions of leaves in subsequent layers and the horizontal layers are considered continuous. Each layer has a leaf area L_s per unit of ground area. L_s is made so small that mutual shading within such a layer can be neglected. For this purpose a value for L_s of 0.1 is sufficiently small. The total number of layers equals leaf area index LAI divided by L_s .

The leaves may have different inclinations, given by the leaf angle distribution, which may be a function of height and consists of nine classes of ten degrees each. Absence of azimuthal preference is assumed. The average projection of leaves with inclination λ in a direction with inclination β can then be calculated.

The sine of the angle of incidence θ on a leaf was given by de Wit (1965).

$$\sin\theta = \sin\beta \cos\lambda + \cos\beta \sin\lambda \sin\alpha \quad (2.1)$$

where α is the difference in azimuth between the leaf's normal and the incident ray.

The mean projection of the leaves can be found by averaging over α :

$$O(\beta, \lambda) = \frac{\int_0^{\pi/2} \sin\theta \, d\alpha}{\int_0^{\pi/2} d\alpha} \quad (2.2)$$

As the interception of the rays by the under and the upper side of a leaf has the same effect, the absolute value of $\sin\theta$ must be taken in the integration. Thus

$$O(\beta, \lambda) = \sin\beta \cos\lambda \quad \lambda \leq \beta \quad (2.3a)$$

$$O(\beta, \lambda) = \frac{2}{\pi} \left\{ \sin\beta \cos\lambda \arcsin\left(\frac{\text{tg}\beta}{\text{tg}\lambda}\right) + (\sin^2\lambda - \sin^2\beta)^{0.5} \right\} \quad \lambda > \beta \quad (2.3b)$$

The average projection of all the leaves together is given by

$$\bar{O}(\beta) = \sum_{\lambda=1}^9 F(\lambda) O(\beta, \lambda) \quad (2.4)$$

where $F(\lambda)$ describes the leaf inclination distribution, so that

$$\sum_{\lambda=1}^9 F(\lambda) = 1.$$

Some special leaf angle distributions are

– horizontal

$$\text{Here } O(\beta, \lambda) \text{ is given by } O(\beta, \lambda) = \sin\beta \quad (2.5)$$

– vertical

$$\text{Here } O(\beta, \lambda) \text{ is given by } O(\beta, \lambda) = 2/\pi \cos\beta \quad (2.6)$$

– spherical or isotropic

The distribution function of the leaf inclinations is the same as for the surface elements of a sphere. Then $F(1 - 9)$ is given by

$F(1 - 9) = 0.015; 0.045; 0.074; 0.099; 0.124; 0.143; 0.158; 0.168; 0.174$
calculated from $\cos 0 - \cos 10, \cos 10 - \cos 20, \text{ etc.}$

The word isotropic is also used because the projection $\bar{O}(\beta)$ is the same in all directions and equal to 0.5. This value is the ratio between the area of the base of a hemisphere and that of the hemisphere itself.

Section 2.3.4 gives an important simplification for the calculation of $\bar{O}(\beta)$, which was developed by Ross (1975).

The radiation at each level in the canopy is divided in upward and downward radiant fluxes. Both are subdivided into 9 classes of 10 degrees each, thus covering the upper and the lower hemisphere. An azimuthal classification of the radiation is not needed because the leaves have no azimuthal preference. The direct solar flux is treated separately. Its extinction can be calculated with the same equations as used for extinction of radiation in a canopy with black leaves.

2.2.2 Incoming radiation

The incoming radiation may be divided into four spectral regions. For each of these regions the geometric composition should be known which has to be classified only in terms of an inclination distribution, as the leaves do not have an azimuthal preference. Still, with four main spectral regions and nine inclination classes, there are 36 classes of incoming radiation. Fortunately a great simplification is possible.

Spectral regions

The first division of the incoming radiation concerns the distinction between thermal radiation (wavelength larger than 3000 nm) and short-wave radiation (wavelength less than 3000 nm). Compared with the thermal radiation of the sky and that of other spectral regions in the solar radiation the direct solar contribution to the thermal radiation can be neglected. In principle the treatment of the thermal or long-wave radiation is more complex than that of the short-wave radiation, because the leaves themselves radiate in the thermal region. Therefore the modelling of thermal radiation is given after that of the short-wave radiation (Section 2.3.6). There is no practicable correlation between the net thermal radiant flux and the incoming solar radiation, so that they must be measured separately. The thermal radiant flux can best be characterized by an apparent sky temperature. The solar or global radiation can be roughly divided in to three regions: the ultraviolet, the visible and the near-infrared region. At sea level the ultraviolet region (wavelength less than 400 nm) contains only about 3 percent of the total solar radiant energy so that it is neglected further. Thus the spectral composition of the solar radiation is characterized by the ratio of the incoming visible and near-

infrared radiation. Under a clear sky each of them contains about half of the incoming flux, and under an overcast sky the ratio shifts to about 0.6 : 0.4 in favour of the visible region.

More detailed figures can be found in Smithsonian Meteorological Tables (List, 1949) and in Šul'gin (1973).

Geometric distribution

The measured incoming radiation must be distributed over direct and diffuse radiation. The direct radiation has a known inclination, that of the sun. For the distribution of the diffuse light over the nine inclination classes there are two alternative assumptions. According to the first assumption the sky has a uniform radiance, resulting in an isotropic downward radiation. When the radiance is N , the contribution to the irradiance of a horizontal surface from a infinitesimal solid angle $d\omega$, at inclination β and azimuth α amounts to

$$dS = N \sin\beta d\omega \quad (2.7)$$

The solid angle $d\omega$ is given by

$$d\omega = \cos\beta d\beta d\alpha \quad (2.8)$$

so that dS can also be written as

$$dS = N \sin\beta \cos\beta d\beta d\alpha \quad (2.9)$$

Integration of the azimuth α from 0 to 2π results in the contribution from an infinitesimal zone $d\beta$ at inclination β given by

$$dS = 2\pi N \sin\beta \cos\beta d\beta \quad (2.10)$$

Integration of β from zero to $\pi/2$ gives $S = \pi N$ for a constant N . When the diffuse downward flux is denoted by S_d , dS equals:

$$dS = 2S_d \sin\beta \cos\beta d\beta \quad (2.11)$$

Integration of dS/S between the zone boundaries at ten-degree intervals gives a distribution table, denoted by B_u :

$$B_u(1 - 9) = 0.030; 0.087; 0.133; 0.163; 0.174; 0.163; 0.133; 0.087; 0.030.$$

This is the uniform overcast sky distribution (UOC). It will be used for the diffuse radiation from an overcast sky, a clear sky and for radiation reflected by the soil surface.

Some investigations will be made with the other assumption, the standard overcast sky (SOC). According to an empirical relation, proposed by Moon & Spenser (1942) and later verified by Grace (1971), the radiance of the standard overcast sky is given by

$$N = N_z (1 + 2\sin\beta)/3 \quad (2.12)$$

In this formula the radiance rises gradually by a factor 3 from the radiance at the horizon to the radiance in the zenith N_z . In Section 2.4.1 this empirical relation will be given a theoretical foundation. Integration of Eqn (2.12) gives

$$S_d = 7\pi N_z/9 \quad (2.13)$$

so that

$$dS = \frac{6}{7} S_d (1 + 2\sin\beta) \sin\beta \cos\beta d\beta \quad (2.14)$$

Integration of dS/S between the zone boundaries at ten-degree intervals gives the distribution table for the SOC, denoted by B_s ,

$$B_s(1 - 9) = 0.015;0.057;0.106;0.150;0.180;0.184;0.160;0.110;0.038$$

The numerical investigations, presented in Section 2.3.2, Table 5 and 6, show that the light extinction and reflection hardly differ under a uniform and a standard overcast sky. Therefore the calculations are done with the simpler UOC distribution, unless stated otherwise.

Table 1. The proportion of diffuse radiation for a very clear sky and some solar heights, for the visible region.

Inclination of the sun	Diffuse/total
5	1.00
15	0.32
25	0.22
35	0.18
45	0.16
90	0.13

Fig. 1 Scheme of the classification of the incoming radiation in diffuse and direct radiation and in the four main spectral regions.

	short-wave radiation			long-wave or thermal radiation
	ultraviolet	visible	near-infrared	
total	negligible	clear: $580 \sin\beta$ overcast: $116 \sin\beta$	clear (S_c): same as visible overcast: 70% of the visible	see diffuse
diffuse	negligible	clear ($S_{d,c}$): proportion diffuse/total, see Table 1 overcast ($S_{d,o}$): $116 \sin\beta$	clear: same as visible overcast: 70% of the visible	both clear and overcast, from apparent radiant sky temperature (Section 2.3.6)
direct	negligible	clear (S_b): proportion direct/total is complement of Table 1 overcast: none	clear: same as visible overcast: none	clear: negligible overcast: none

The proportion of diffuse radiation for a very clear sky is given in Table 1, according to de Wit (1965), for some solar inclinations. For intermediate inclinations a linear interpolation is used. The total visible radiant flux under a very clear sky is given by $580 \sin\beta$ in $\text{J m}^{-2} \text{s}^{-1}$, and one fifth of this value ($116 \sin\beta$) under an overcast sky. In the near-infrared region, the radiant flux is taken equal to the visible flux for a clear sky and to 0.7 of the visible flux for an overcast sky. The classification given in this section is summarized in Fig. 1.

2.2.3 Optical properties

The distinction between visible and near-infrared radiation is justified by the shape of the spectral dependence of leaf reflectance and transmittance (Fig. 2). At about 700 nm there is a sharp increase of both. Moreover the reflection and transmission coefficients are almost equal to each other in both regions. In the visible region an average value of 0.1 can be used and of 0.4 in the near-infrared region. These figures hold for many plant species (Brandt & Tageeva, 1967; Gates et al., 1965; Woolley, 1971). Sometimes reflection contains a specular component, but this effect will be neglected in this study. It is assumed

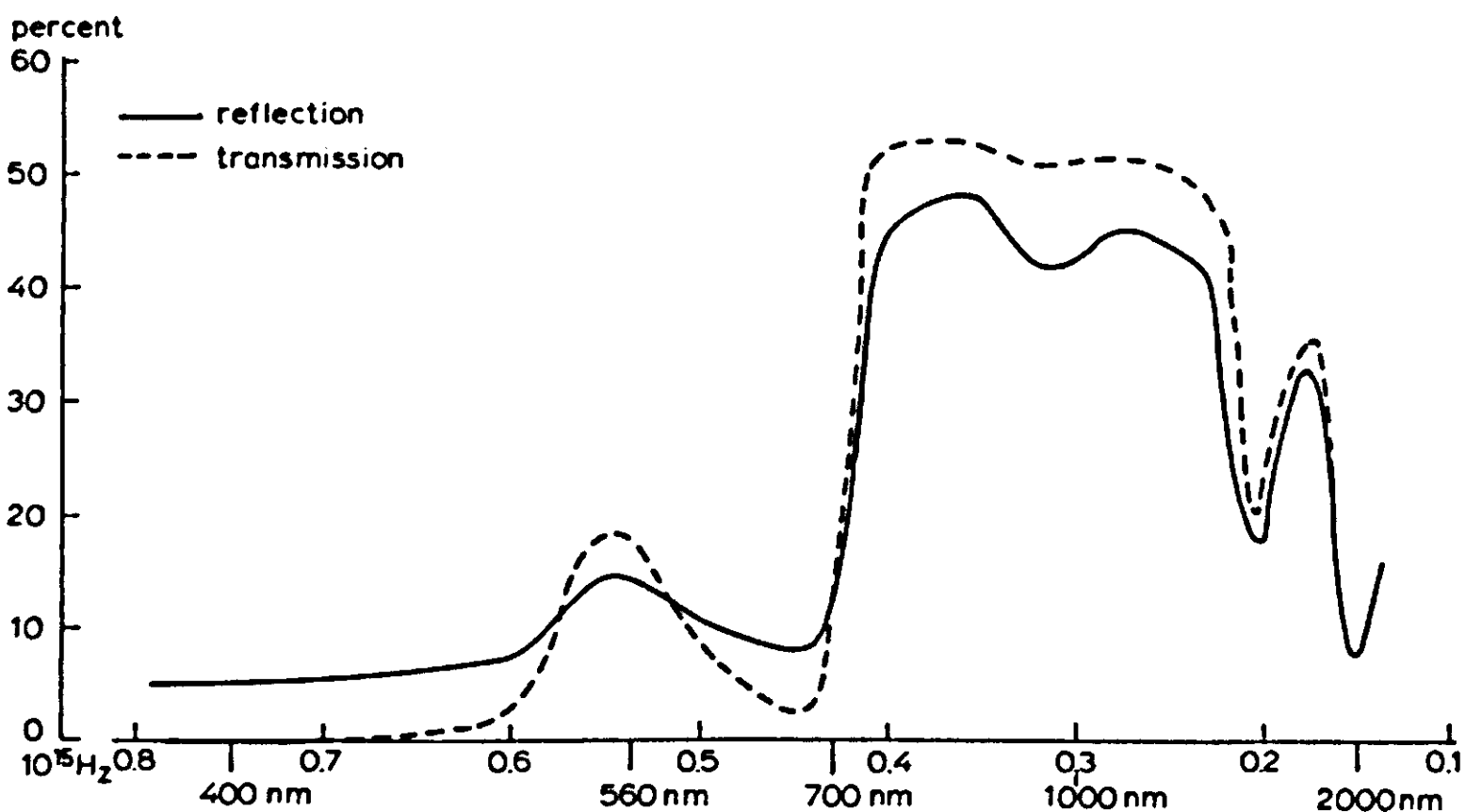


Fig. 2 | Spectral dependence of the leaf reflection and transmission coefficient of a healthy maize leaf.

that leaves reflect and transmit radiation isotropically. It will be shown that this assumption results in isotropically scattered radiation only for horizontal leaves.

Radiation reflected by the soil surface is assumed to be always isotropic. The reflection coefficient of soil does not exhibit a sharp increase at 700 nm, but rises gradually from about 0.1 at 400 nm via 0.2 at 700 nm to 0.35 at 1600 nm for a dry soil and from about 0.04 at 400 nm via 0.1 at 700 nm to 0.25 at 1600 nm for a moist soil (Verhoef & Bunnik, 1975). Thus an average value of 0.1 in the visible region and of 0.25 in the near-infrared region can be used as a first approximation for soil reflectance.

2.3 Elementary models

2.3.1 Horizontal leaves

For horizontal leaves the fraction of radiation intercepted per layer is always equal to the leaf area per layer L_s , independent of the light inclination. Let us denote the downward and upward radiant fluxes between layer j and $j-1$ by $\varphi_d(j)$ and $\varphi_u(j)$, the leaf reflection coefficient by ρ and the leaf transmission coefficient by τ . The equations for the downward and upward radiation leaving the j th layer then read

$$\varphi_d(j+1) = (1 - L_s)\varphi_d(j) + L_s\{\tau\varphi_d(j) + \rho\varphi_u(j+1)\} \quad (2.15a)$$

$$\varphi_u(j) = (1 - L_s)\varphi_u(j+1) + L_s\{\rho\varphi_d(j) + \tau\varphi_u(j+1)\} \quad (2.15b)$$

To find a solution for this set of equations, it is assumed that for each subsequent layer both downward and upward fluxes are reduced by the same constant reduction factor M . Such an assumption is justified if a solution exists. We therefore try

$$\varphi_d(j+1) = M\varphi_d(j) \quad (2.16a)$$

$$\varphi_u(j-1) = M\varphi_u(j) \quad (2.16b)$$

The whole procedure is considerably simplified by assuming that $\tau = \rho$. From a physical point of view this is a good approximation (Section 2.2.3). The sum of reflection and transmission coefficient is called the scattering coefficient and denoted by σ . After combination of Eqns (2.15) and (2.16) it is found that

$$\frac{\varphi_u(j)}{\varphi_d(j)} = \frac{(M - 1 + L_s)}{\{1 - M(1 - L_s)\}} \quad (2.17)$$

The assumption of a constant M is equivalent to the assumption of exponential extinction. The extinction coefficient K is related to M as

$$M = \exp(-KL_s) \quad (2.18)$$

For small values of L_s this expression approaches

$$M = 1 - KL_s \quad (2.19)$$

When this equation is combined with Eqns (2.17), (2.16) and (2.15), and the simplification is used that $\tau = \rho = 0.5\sigma$, we obtain

$$K_h = (1 - \sigma)^{0.5} \quad (2.20)$$

as was also found by Cowan (1968). The subscript h is used for reference to horizontal leaves. The expression for K can now be substituted into Eqn (2.19) for M , and M is used in Eqn (2.17) to find the ratio of the upward and downward flux. This ratio is independent of j , so that it also represents the reflection coefficient of the stand. We thus find:

$$\rho_h = \frac{\{1 - (1 - \sigma)^{0.5}\}}{\{1 + (1 - \sigma)^{0.5}\}} \quad (2.21)$$

A similar, but more complicated procedure is followed when τ does not equal ρ . For small values of L_s the extinction and reflection coefficient are then given by

$$K_h = \{(1 - \tau)^2 - \rho^2\}^{0.5} \quad (2.22)$$

$$\rho_h = (1 - \tau - K_h)/\rho \quad (2.23)$$

For low values of the leaf area index the reflection of the soil surface considerably disturbs the profiles found above, since in general the reflection coefficient of the soil surface ρ_s is not equal to the reflection of a closed leaf canopy ρ_h . Because of this boundary effect at the bottom, a second exponential profile in the opposite direction appears in the following equation:

$$\varphi_d(LAI) = \varphi_{1d}(0)\exp(K.LAI) + \varphi_{2d}(0)\exp(-K.LAI) \quad (2.24a)$$

$$\varphi_u(LAI) = \frac{\varphi_{1d}(0)\exp(K.LAI) + \varphi_{2d}(0)\rho_h \exp(-K.LAI)}{\rho_h} \quad (2.24b)$$

where ρ_h is given by Eqn (2.21) and $\varphi_{1d}(0)$ and $\varphi_{2d}(0)$ by

$$\varphi_{1d}(0) = \frac{(\rho_h - \rho_s)\exp(-K.LAI)\varphi_d(0)}{\left(\rho_s - \frac{1}{\rho_h}\right)\exp(K.LAI) + (\rho_h - \rho_s)\exp(-K.LAI)} \quad (2.25a)$$

$$\varphi_{2d}(0) = \frac{\left(\rho_s - \frac{1}{\rho_h}\right)\exp(K.LAI)\varphi_d(0)}{\left(\rho_s - \frac{1}{\rho_h}\right)\exp(K.LAI) + (\rho_h - \rho_s)\exp(-K.LAI)} \quad (2.25b)$$

Here ρ_s is the reflection coefficient of the soil surface and $\varphi_d(0)$ the downward flux at the top of the canopy.

Now the effective reflection coefficient of the canopy-soil system is given by

$$\rho_{\text{eff}} = \frac{(\rho_s \rho_h - 1)\exp(K.LAI) + (1 - \rho_s/\rho_h)\exp(-K.LAI)}{\left(\rho_s - \frac{1}{\rho_h}\right)\exp(K.LAI) + (\rho_h - \rho_s)\exp(-K.LAI)} \quad (2.26)$$

The transmitted fraction below the canopy is

$$\tau_{\text{eff}} = \frac{\rho_s - \frac{1}{\rho_h}}{\left(\rho_s - \frac{1}{\rho_h}\right)\exp(K.LAI) + (\rho_h - \rho_s)\exp(-K.LAI)} \quad (2.27)$$

The apparent reflection coefficient is given in Fig. 3 as a function of the leaf area index for visible and near-infrared radiation. For the visible radiation (solid lines) ρ_s was taken as 0 and 0.1 and for the near-infrared radiation (broken lines) ρ_s was taken as 0 and 0.25. The scattering coefficients of the leaves are 0.2 and 0.8, respectively. Above a LAI of 2 the influence of the soil surface can be practically neglected.

2.3.2 Canopies with a non – horizontal leaf angle distribution

The fraction intercepted by a layer with leaf area L_s is proportional to the average projection $\bar{O}(\beta)$ (Eqn (2.4)) and inversely proportional to the sine of the inclination of the incident light $\sin\beta$. Therefore the intercepted fraction is given by

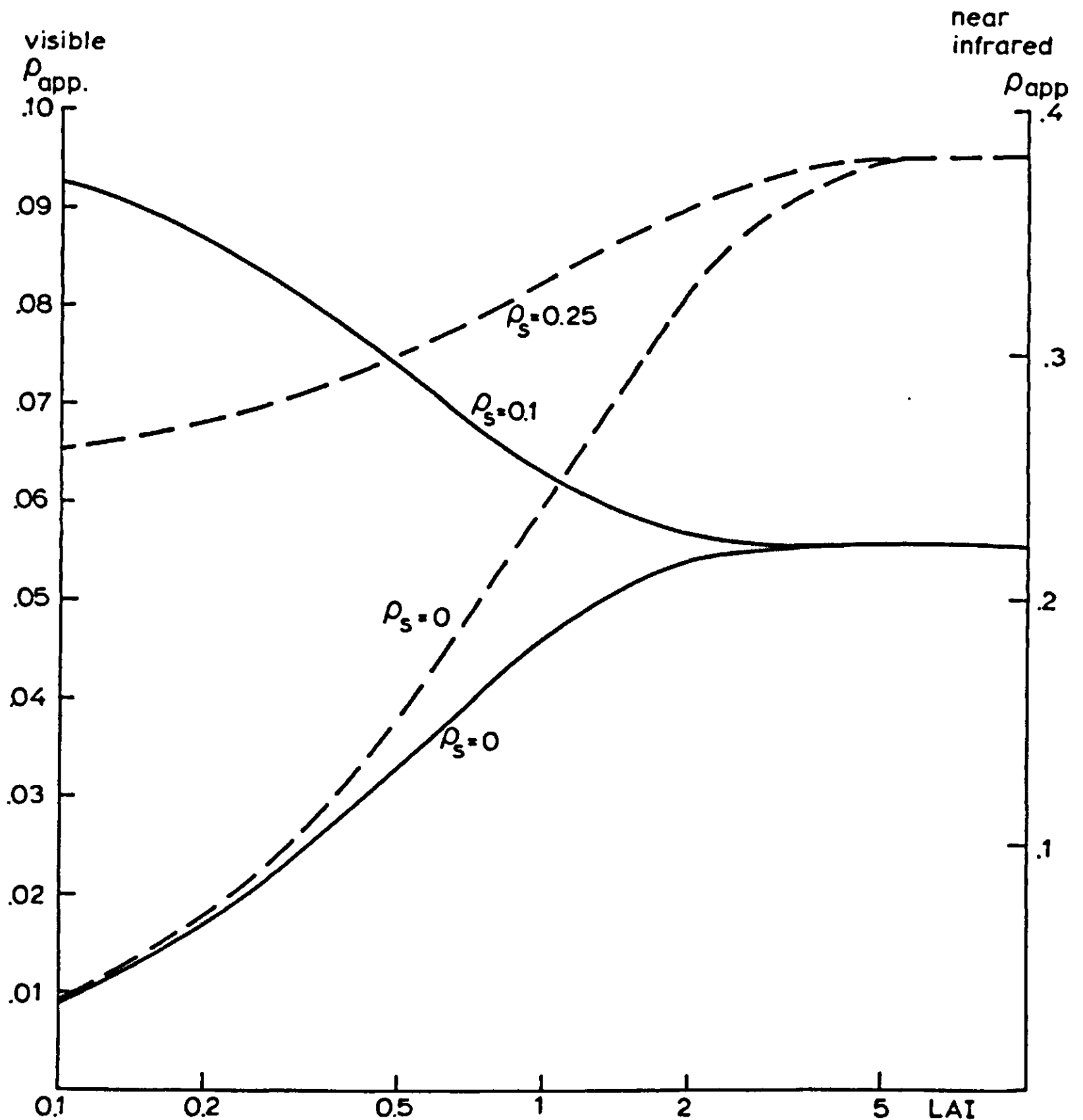


Fig. 3 | Apparent reflection coefficient of the canopy-soil system as function of the leaf area index for two values of the soil reflectance ρ_s . For the visible region (solid lines) the values are indicated on the left ordinate and for the near-infrared region (broken lines) on the right ordinate.

$$M_i(\beta) = L_s \bar{O}(\beta) / \sin \beta \quad (2.28)$$

The fraction of light transmitted through a layer is

$$M_t(\beta) = 1 - M_i(\beta) \quad (2.29)$$

In each subsequent layer the same fraction is transmitted and intercepted. This follows from the assumptions that the leaf angle distribution is not a function of height, that the positions of the leaves in

subsequent layers are not correlated and that they do not have preference for either sunny or shaded positions.

The directional composition of the light will change with depth because the intercepted fraction $M_i(\beta)$ varies with direction β . Since M_i is generally a decreasing function of β , the vertical light predominates in the deeper layers, causing a relatively slower extinction.

The radiant flux in a downward direction φ_d , and in an upward direction φ_u are related to the fluxes in adjacent layers as

$$\varphi_d(\beta, j + 1) = M_i(\beta)\varphi_d(\beta, j) \quad (2.30a)$$

$$\varphi_u(\beta, j) = M_i(\beta)\varphi_u(\beta, j + 1) \quad (2.30b)$$

where j is the index of the layer, running from 1 to m in downward direction. In this equation the leaves are assumed black.

The total number of layers is

$$m = LAI/L_s \quad (2.31)$$

The distribution of the incoming radiation was discussed in Section 2.2.2. Under the canopy the radiation is isotropically reflected:

$$\varphi_u(\beta', m + 1) = \rho_s B_u(\beta') \sum_{\beta=1}^9 \varphi_d(\beta, m + 1) \quad (2.32)$$

where ρ_s is the reflection coefficient of the soil surface.

The prime means that the angle refers to scattered radiation. The profile of the downward radiation can be calculated by repeated application of Eqn (2.30a), starting at the top with the given distribution of the incoming radiation. The reflected radiation at the soil surface (Eqn (2.32)) gives the boundary condition for the upward radiation. Then Eqn (2.30b) is applied repeatedly. In this way the profiles of both the downward and upward radiation fields are found when the leaves are black. Results of these calculations are given in Table 2 for a spherical leaf angle distribution. For direct radiation the profile is exponentially extinguished according to

$$\varphi_d = S_b \exp\{-K_b(\beta)LAI'\} \quad (2.33)$$

where the extinction coefficient K_b is given by

$$K_b(\beta) = \bar{O}(\beta)/\sin\beta \quad (2.34)$$

for small values of L_s .

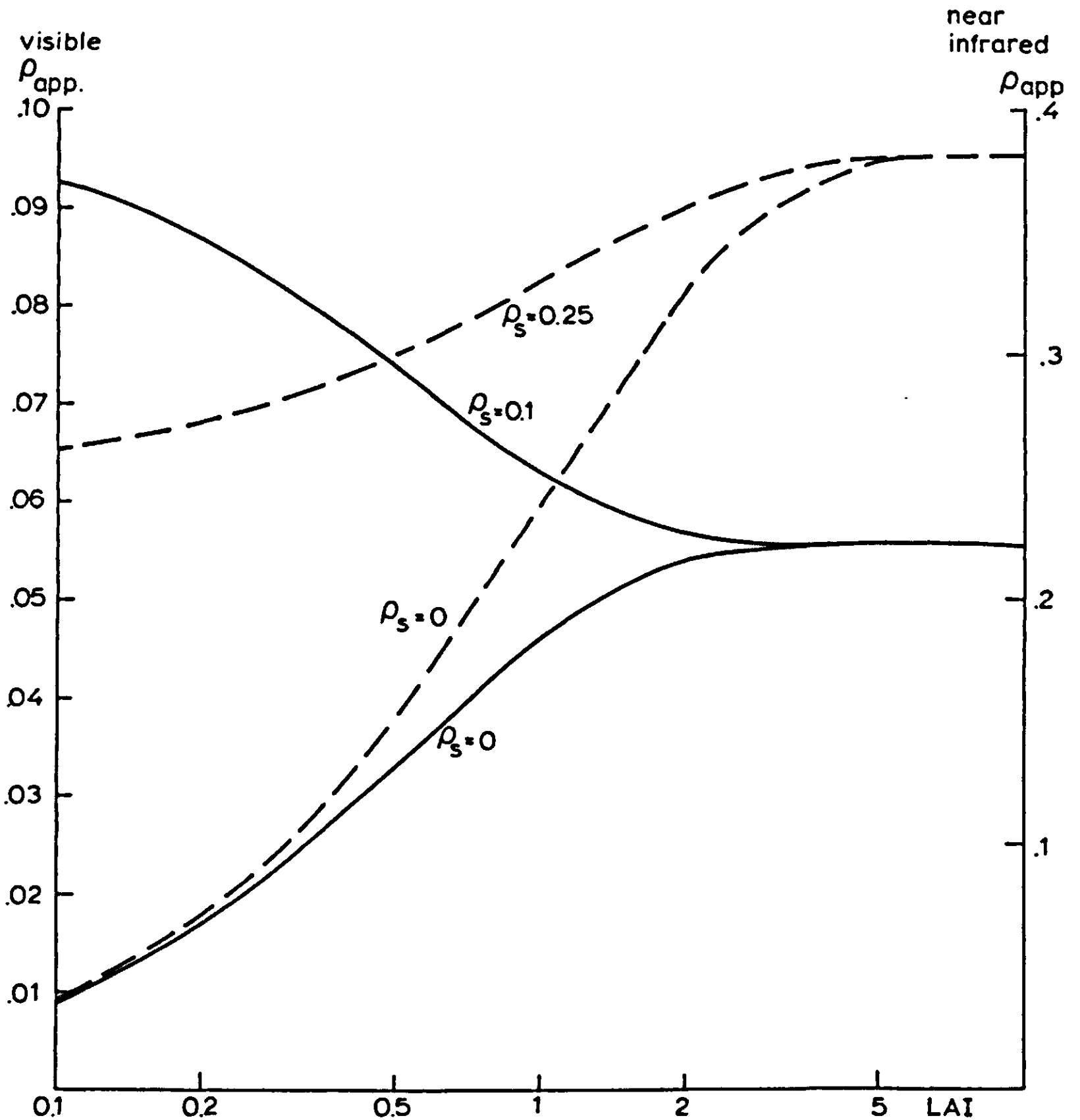


Fig. 3 | Apparent reflection coefficient of the canopy-soil system as function of the leaf area index for two values of the soil reflectance ρ_s . For the visible region (solid lines) the values are indicated on the left ordinate and for the near-infrared region (broken lines) on the right ordinate.

$$M_i(\beta) = L_s \bar{O}(\beta) / \sin \beta \quad (2.28)$$

The fraction of light transmitted through a layer is

$$M_t(\beta) = 1 - M_i(\beta) \quad (2.29)$$

In each subsequent layer the same fraction is transmitted and intercepted. This follows from the assumptions that the leaf angle distribution is not a function of height, that the positions of the leaves in

subsequent layers are not correlated and that they do not have preference for either sunny or shaded positions.

The directional composition of the light will change with depth because the intercepted fraction $M_i(\beta)$ varies with direction β . Since M_i is generally a decreasing function of β , the vertical light predominates in the deeper layers, causing a relatively slower extinction.

The radiant flux in a downward direction φ_d , and in an upward direction φ_u are related to the fluxes in adjacent layers as

$$\varphi_d(\beta, j + 1) = M_i(\beta)\varphi_d(\beta, j) \quad (2.30a)$$

$$\varphi_u(\beta, j) = M_i(\beta)\varphi_u(\beta, j + 1) \quad (2.30b)$$

where j is the index of the layer, running from 1 to m in downward direction. In this equation the leaves are assumed black.

The total number of layers is

$$m = LAI/L_s \quad (2.31)$$

The distribution of the incoming radiation was discussed in Section 2.2.2. Under the canopy the radiation is isotropically reflected:

$$\varphi_u(\beta', m + 1) = \rho_s B_u(\beta') \sum_{\beta=1}^9 \varphi_d(\beta, m + 1) \quad (2.32)$$

where ρ_s is the reflection coefficient of the soil surface.

The prime means that the angle refers to scattered radiation. The profile of the downward radiation can be calculated by repeated application of Eqn (2.30a), starting at the top with the given distribution of the incoming radiation. The reflected radiation at the soil surface (Eqn (2.32)) gives the boundary condition for the upward radiation. Then Eqn (2.30b) is applied repeatedly. In this way the profiles of both the downward and upward radiation fields are found when the leaves are black. Results of these calculations are given in Table 2 for a spherical leaf angle distribution. For direct radiation the profile is exponentially extinguished according to

$$\varphi_d = S_b \exp\{-K_b(\beta)LAI'\} \quad (2.33)$$

where the extinction coefficient K_b is given by

$$K_b(\beta) = \bar{O}(\beta)/\sin\beta \quad (2.34)$$

for small values of L_s .

Table 2 The downward fluxes for different depths (LAI') in the canopy. The leaves are black and the leaf angle distribution is spherical.

LAI'	$\beta = 5^\circ$ only direct	$\beta = 45^\circ$ only direct	$\beta = 85^\circ$ only direct	UOC only diffuse
0	1	1	1	1
0.1	0.426	0.929	0.950	0.900
0.2	0.181	0.863	0.902	0.819
0.5	0.014	0.693	0.773	0.634
1.0	0.000	0.480	0.595	0.428
2.0	0.000	0.231	0.357	0.208
5.0	0.000	0.025	0.076	0.029
10.0	0.000	0.001	0.006	0.001

When the leaves scatter intercepted radiation, the equations used must be extended. First it is assumed that the reflection and transmission coefficients of the leaves are equal. This assumption is reasonable for thin leaves, like those of maize, and simplifies considerably, since the scattered fluxes upwards and downwards are always the same then, irrespective of the leaf angle distribution. Section 2.4 deals with the situation when the reflection and transmission coefficients of the leaves are not the same.

Although the leaves in the model are Lambertian radiators, the light scattered by a layer is not isotropic, contrary to an assumption of de Wit (1965). For a certain leaf inclination the projection in direction β is given by Eqns (2.3). The intercepted fraction follows from Eqn (2.28) whereby $\bar{O}(\beta)$ equals $O(\beta, \lambda)$. Now the anisotropy of the scattered light is due to the variation of this intercepted fraction M_i with inclination β , because the scattered radiation is proportional to M_i . Only for horizontal leaves is $M_i(\beta)$ invariant with β . The scattered light is then isotropic so that the scattered radiant flux through a horizontal surface is distributed with β' as $B_u(\beta')$.

In general the flux is distributed as:

$$B_i(\beta') = \frac{B_u(\beta') M_i(\beta')}{\sum_{\beta=1}^9 B_u(\beta) M_i(\beta)} \quad (2.35)$$

Ideally, the summation in the denominator should equal L_s , as can be seen from the integration result of

$$J = \int_0^{\pi/2} B_u(\beta) M_i(\beta) d\beta \quad (2.36)$$

given in Appendix A(c). However, the discretization to nine classes causes a small deviation resulting in an effective scattering coefficient which is slightly different from the one intended. Therefore the sum-

mation is not replaced by L_s , so that $\sum_{\beta=1}^9 B_i(\beta)$ is not different from unity.

The total amount of radiation to be distributed as scattered light equals the scattering coefficient times the total intercepted amount which consists of radiation intercepted from the upward direction but also from downwards. The total intercepted amount per layer is thus given by

$$I_t(j) = \sum_{\beta=1}^9 M_i(\beta) \{ \varphi_d(\beta, j) + \varphi_u(\beta, j + 1) \} \quad (2.37)$$

The resulting extension of the equations (2.30) is now:

$$\varphi_d(\beta', j + 1) = M_i(\beta') \varphi_d(\beta', j) + 0.5\sigma B_i(\beta') I_t(j) \quad (2.38a)$$

$$\varphi_u(\beta', j) = M_i(\beta') \varphi_u(\beta', j + 1) + 0.5\sigma B_i(\beta') I_t(j) \quad (2.38b)$$

When the leaf inclination is not one-valued, but distributed, two approaches can be followed.

In the simpler approach Eqns (2.38a, b) are used, whereby M_i and M_t are calculated with $\bar{O}(\beta')$. Then it is assumed that all leaves in the layer have the same radiance, so that the distribution of the scattered light is only determined by the projection $\bar{O}(\beta')$ in the direction of emittance.

However, in fact the radiance of the leaves in a layer depends on the leaf inclination. When the sun is in the zenith, the more horizontally inclined leaves have a higher radiance than the vertically inclined leaves. Because the angular distribution function of the light scattered by horizontal leaves differs from that for vertical leaves, this effect should be accounted for.

Then the variables B_i and I_t must not only be classified with respect

to the layer number j , but also to inclination class λ by executing the calculations of Eqns (2.28), (2.35) and (2.37) for each λ separately. The thus calculated scattered fluxes are added, and weighted according to $F(\lambda)$:

$$\varphi_d(\beta'j + 1) = M_i(\beta')\varphi_d(\beta'j) + 0.5\sigma \sum_{\lambda=1}^9 F(\lambda)B_i(\beta',\lambda)I_i(\lambda,j) \quad (2.39a)$$

$$\varphi_u(\beta'j) = M_i(\beta')\varphi_u(\beta'j + 1) + 0.5\sigma \sum_{\lambda=1}^9 F(\lambda)B_i(\beta',\lambda)I_i(\lambda,j) \quad (2.39b)$$

Surprisingly, the numerical results of the more correct model (Eqns (2.39)) and the simpler model (Eqns (2.38)) are hardly different. As expected, the extinction coefficients are larger for the simpler method (Table 3), but it could not be predicted that the effect of the simplification would be so small. This fortunate result permits the use of the

Table 3 Comparison of the results of the correct method (upper value) and the simplified method (lower value) for the redistribution of scattered radiation. The leaf angle distribution is sperical.

		Reflection coefficients of the canopy		
		only direct		only diffuse
σ	$\beta = 5^\circ$	$\beta = 45^\circ$	$\beta = 85^\circ$	UOC
0.3	0.1478	0.0720	0.0591	0.0781
	0.1472	0.0726	0.0614	0.0787
0.8	0.5223	0.3343	0.2898	0.3497
	0.5224	0.3347	0.2924	0.3502
		Extinction coefficients for the same conditions		
0.3		0.636	0.461	0.684
		0.640	0.463	0.686
0.8		0.374	0.302	0.383
		0.375	0.299	0.383

simpler method (Eqns (2.38)).

The equations for the fluxes are all connected by the scattered light. A formal solution can be obtained by writing the equations in the form of a matrix, and solving it by calculation of the determinant and subdeterminants. However, this method is not feasible because of the extraordinary matrix size. When the LAI is 5 and L_s is 0.1, the number of unknowns is 900 ($2 \times 9 \times 5/0.1$). Therefore a relaxation

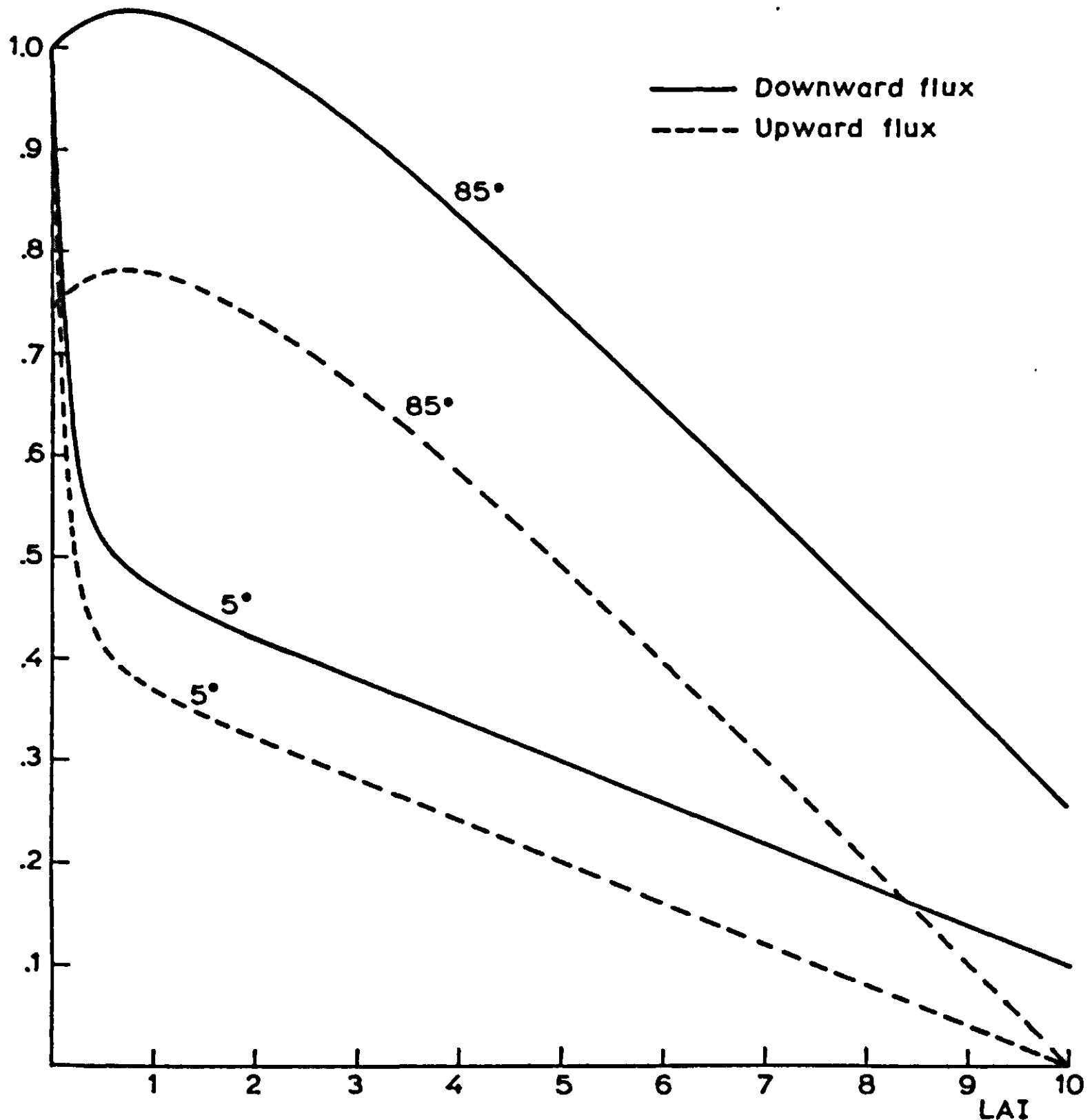


Fig. 4 | Downward and upward radiant fluxes, relative to the incoming value, as a function of depth in the canopy. The scattering coefficient of leaves is unity, and the leaf angle distribution is spherical. There is no diffuse component in the incoming flux. The inclination of the direct incoming flux is 5 degrees in one case and 85 degrees in the other.

to the layer number j , but also to inclination class λ by executing the calculations of Eqns (2.28), (2.35) and (2.37) for each λ separately. The thus calculated scattered fluxes are added, and weighted according to $F(\lambda)$:

$$\varphi_d(\beta'j + 1) = M_i(\beta')\varphi_d(\beta'j) + 0.5\sigma \sum_{\lambda=1}^9 F(\lambda)B_i(\beta',\lambda)I_i(\lambda,j) \quad (2.39a)$$

$$\varphi_u(\beta'j) = M_i(\beta')\varphi_u(\beta'j + 1) + 0.5\sigma \sum_{\lambda=1}^9 F(\lambda)B_i(\beta',\lambda)I_i(\lambda,j) \quad (2.39b)$$

Surprisingly, the numerical results of the more correct model (Eqns (2.39)) and the simpler model (Eqns (2.38)) are hardly different. As expected, the extinction coefficients are larger for the simpler method (Table 3), but it could not be predicted that the effect of the simplification would be so small. This fortunate result permits the use of the

Table 3 Comparison of the results of the correct method (upper value) and the simplified method (lower value) for the redistribution of scattered radiation. The leaf angle distribution is sperical.

		Reflection coefficients of the canopy		
		only direct		only diffuse
σ	$\beta = 5^\circ$	$\beta = 45^\circ$	$\beta = 85^\circ$	UOC
0.3	0.1478	0.0720	0.0591	0.0781
	0.1472	0.0726	0.0614	0.0787
0.8	0.5223	0.3343	0.2898	0.3497
	0.5224	0.3347	0.2924	0.3502
		Extinction coefficients for the same conditions		
0.3		0.636	0.461	0.684
		0.640	0.463	0.686
0.8		0.374	0.302	0.383
		0.375	0.299	0.383

simpler method (Eqns (2.38)).

The equations for the fluxes are all connected by the scattered light. A formal solution can be obtained by writing the equations in the form of a matrix, and solving it by calculation of the determinant and subdeterminants. However, this method is not feasible because of the extraordinary matrix size. When the LAI is 5 and L_s is 0.1, the number of unknowns is 900 ($2 \times 9 \times 5/0.1$). Therefore a relaxation

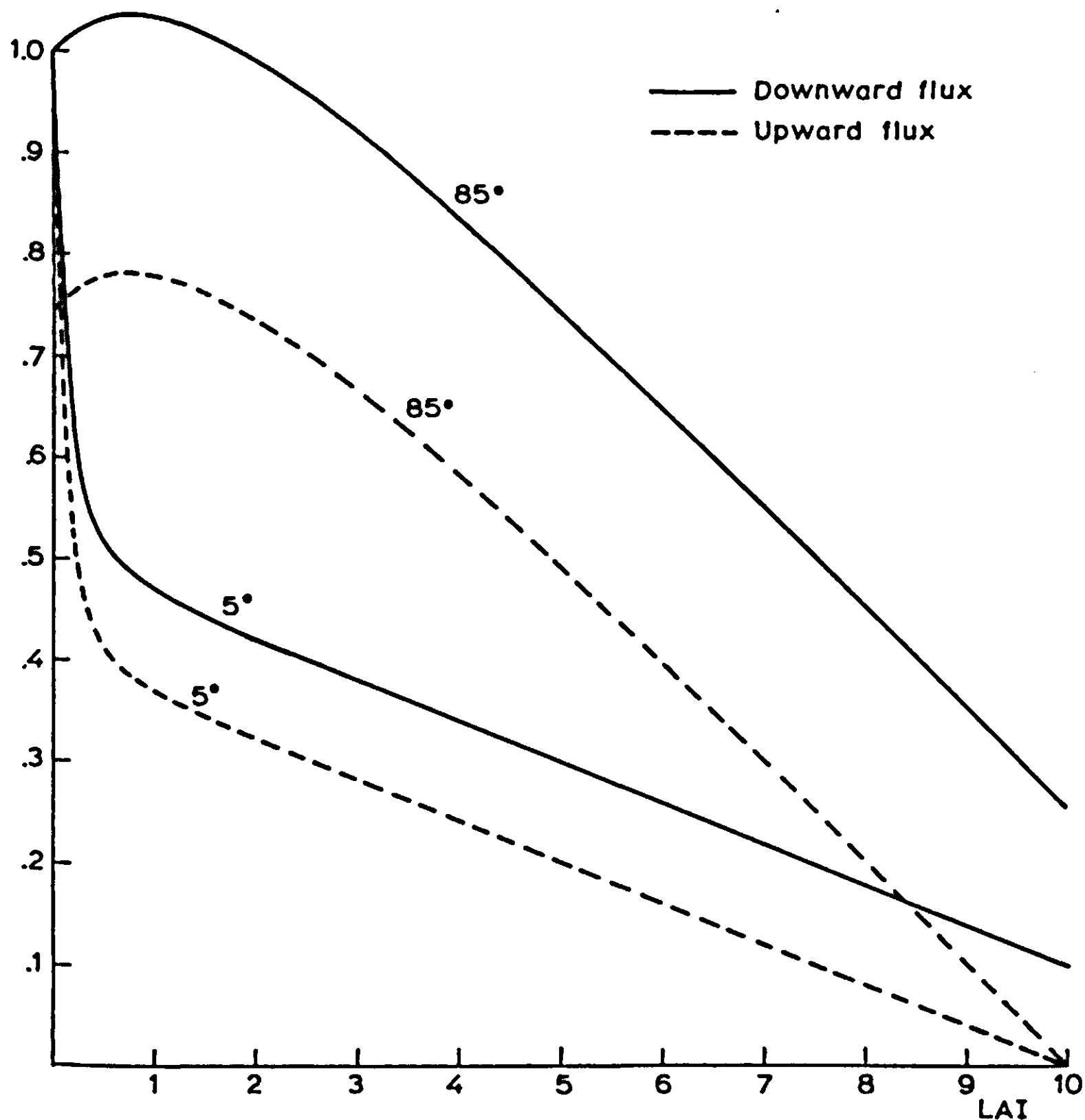


Fig. 4 | Downward and upward radiant fluxes, relative to the incoming value, as a function of depth in the canopy. The scattering coefficient of leaves is unity, and the leaf angle distribution is spherical. There is no diffuse component in the incoming flux. The inclination of the direct incoming flux is 5 degrees in one case and 85 degrees in the other.

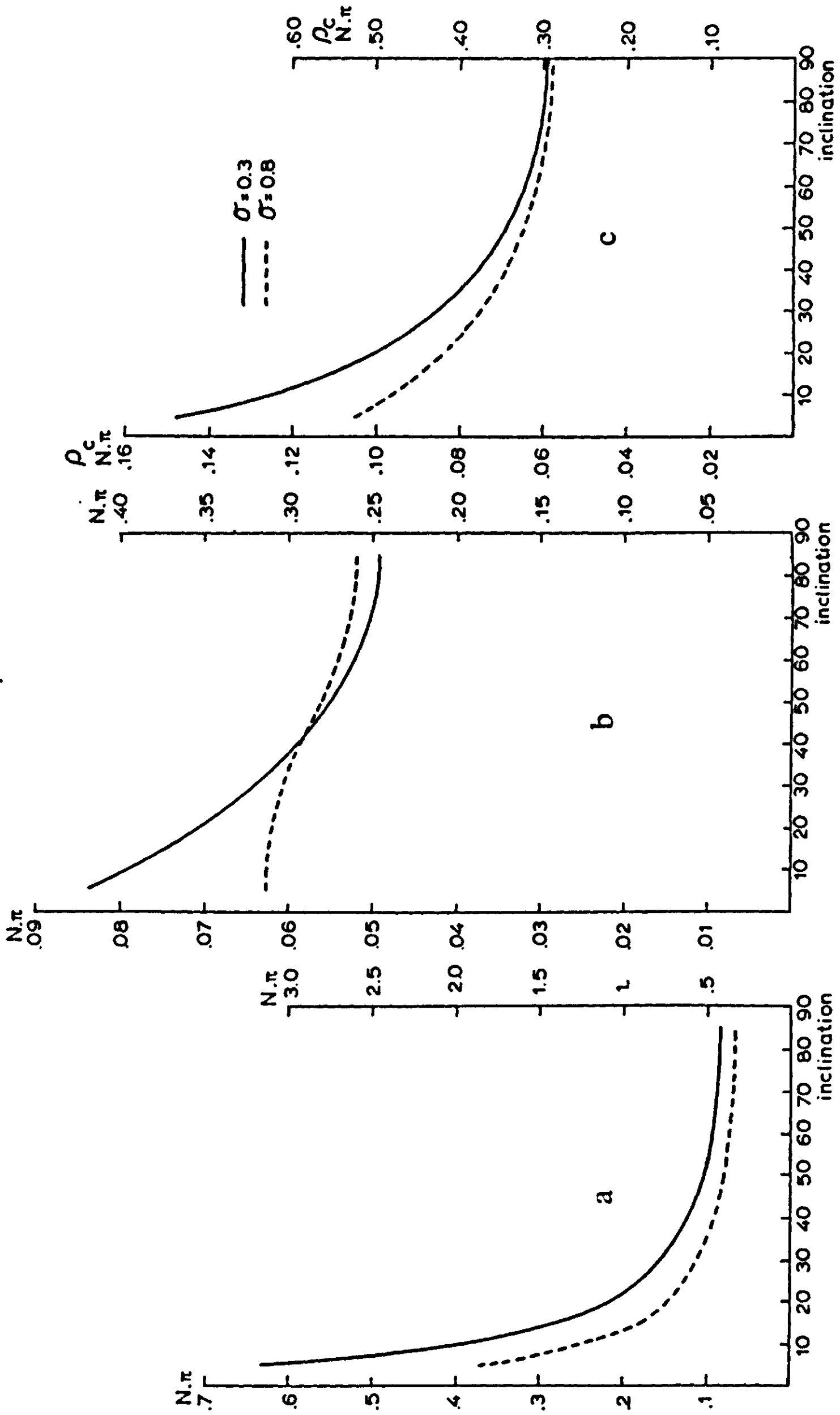


Fig. 5

method is applied by which scattered fluxes are added to the fluxes already there. The basic radiation field is provided by the calculation for the black leaves, which takes one computation in the downward direction and another one upwards. Then this procedure is repeated, adding the scattered fluxes, first downwards and then upwards. In this way the convergence is fast. When the scattering coefficient is 0.3 two full runs are needed and when it is 0.8 five. To test whether radiation is artificially generated or lost anywhere, the computations are also done with a scattering coefficient of unity. Then 20 full runs are needed to establish equilibrium. Over the whole depth of the system the net radiant flux is constant and equal to the amount lost at the bottom, so that the balances are all right.

In Fig. 4 two computed profiles are given. Because of the loss at the bottom the apparent reflection coefficient is not unity, but it does increase with the leaf area index. It is remarkable that under vertically incident radiation, the upward and downward fluxes in top of the canopy are even higher than that above it, because of trapping of radiation. In Table 4, the computed fluxes and some directional distributions of the incoming radiation are tabulated for the scattering coefficients of 0.3, 0.8 and 1. The soil is black and the LAI equals 10. Another output of the model is the dependence of the radiance of the reflecting canopy on the angle of view. This is given in Fig. 5 for some cases with a spherical leaf angle distribution.

A listing of the program is given in Section 5.6.

Fig. 5 | Dependence of the radiance of the reflecting canopy on the angle of view, in the visible ($\sigma = 0.3$, solid line, left ordinate) and in the near-infrared region ($\sigma = 0.8$, broken line, right ordinate). The leaf angle distribution is spherical.

- a. Incident radiation direct at an inclination of 5 degrees.
- b. Incident radiation direct at an inclination of 85 degrees.
- c. Incident radiation diffuse (UOC). The same curves also represent the hemispherical reflection coefficient ρ_c as a function of the angle of incidence of direct radiation (reciprocity, Section 2.3.5).

Table 4 Downward and upward fluxes, relative to the incoming value, as a function of the depth in the canopy (LAI') for three values of the scattering coefficient. The leaf angle distribution is spherical and for direct radiation three solar heights are considered.

LAI' UOC	$\sigma = 0.3$		$\sigma = 0.8$		$\sigma = 1.0$	
	φ_d	φ_u	φ_d	φ_u	φ_d	φ_u
0.	1.000	0.078	1.000	0.349	1.000	0.798
0.1	0.916	0.070	0.955	0.332	0.991	0.788
0.2	0.846	0.064	0.914	0.316	0.982	0.780
0.5	0.679	0.050	0.807	0.278	0.957	0.754
1.	0.482	0.035	0.662	0.229	0.916	0.713
2.	0.253	0.019	0.451	0.152	0.835	0.633
5.	0.043	0.003	0.149	0.048	0.598	0.397
10.	0.003	0.000	0.021	0.000	0.200	0.000
$\beta = 5^\circ$, no diffuse radiation						
0.	1.000	0.148	1.000	0.522	1.000	0.899
0.1	0.513	0.071	0.673	0.319	0.735	0.653
0.2	0.292	0.037	0.510	0.221	0.631	0.531
0.5	0.112	0.010	0.345	0.128	0.516	0.415
1.	0.065	0.005	0.263	0.093	0.472	0.371
2.	0.032	0.002	0.172	0.059	0.422	0.321
5.	0.004	0.000	0.054	0.019	0.298	0.198
10.	0.000	0.000	0.007	0.000	0.099	0.000
$\beta = 45^\circ$, no diffuse radiation						
0.	1.000	0.072	1.000	0.334	1.000	0.790
0.1	0.941	0.068	0.972	0.327	1.005	0.795
0.2	0.884	0.064	0.941	0.319	1.005	0.796
0.5	0.732	0.053	0.849	0.290	0.995	0.786
1.	0.531	0.039	0.706	0.242	0.963	0.753
2.	0.278	0.020	0.481	0.165	0.881	0.671
5.	0.040	0.003	0.150	0.050	0.623	0.415
10.	0.002	0.000	0.020	0.000	0.207	0.000

Table 4 (Continued)

LAI'	$\sigma = 0.3$		$\sigma = 0.8$		$\sigma = 1.0$	
	φ_d	φ_u	φ_d	φ_u	φ_d	φ_u
$\beta = 85^\circ$, no diffuse radiation						
0.	1.000	0.059	1.000	0.300	1.000	0.744
0.1	0.958	0.057	0.982	0.288	1.012	0.755
0.2	0.917	0.055	0.962	0.284	1.020	0.764
0.5	0.802	0.048	0.896	0.270	1.033	0.776
1.	0.638	0.039	0.786	0.241	1.032	0.776
2.	0.399	0.024	0.588	0.185	0.990	0.735
5.	0.094	0.006	0.222	0.070	0.747	0.492
10.	0.008	0.000	0.034	0.000	0.253	0.000

2.3.3 Simplifying formulations

The downward radiation of each inclination class separately is extinguished exponentially, but only if the leaves are black. The extinction profile of downward diffuse radiation thus consists of the sum of many exponential curves with different coefficients. When the leaves are not black, radiation of all inclinations is generated even under pure direct irradiation. Therefore extinction is only strictly exponential for black leaves under direct irradiation, or for horizontal leaves. In all other cases the profiles must be calculated as described in the previous section.

Investigation of the numerically calculated profiles shows, however, that most of them are very close to exponential extinction. An example is given in Fig. 6. Therefore the definition of the extinction coefficient can be broadened to the coefficient of the closest fitting exponential curve. The criterion for closest fitting is taken as the sum of the squares of the absolute deviations at equidistant depths. If the absolute deviation exceeds at some depth an error limit of 5 percent of the incoming radiation even for the closest fitting curve, exponential extinction is rejected. For these situations no other mathematical equations were introduced the profile being characterized by the

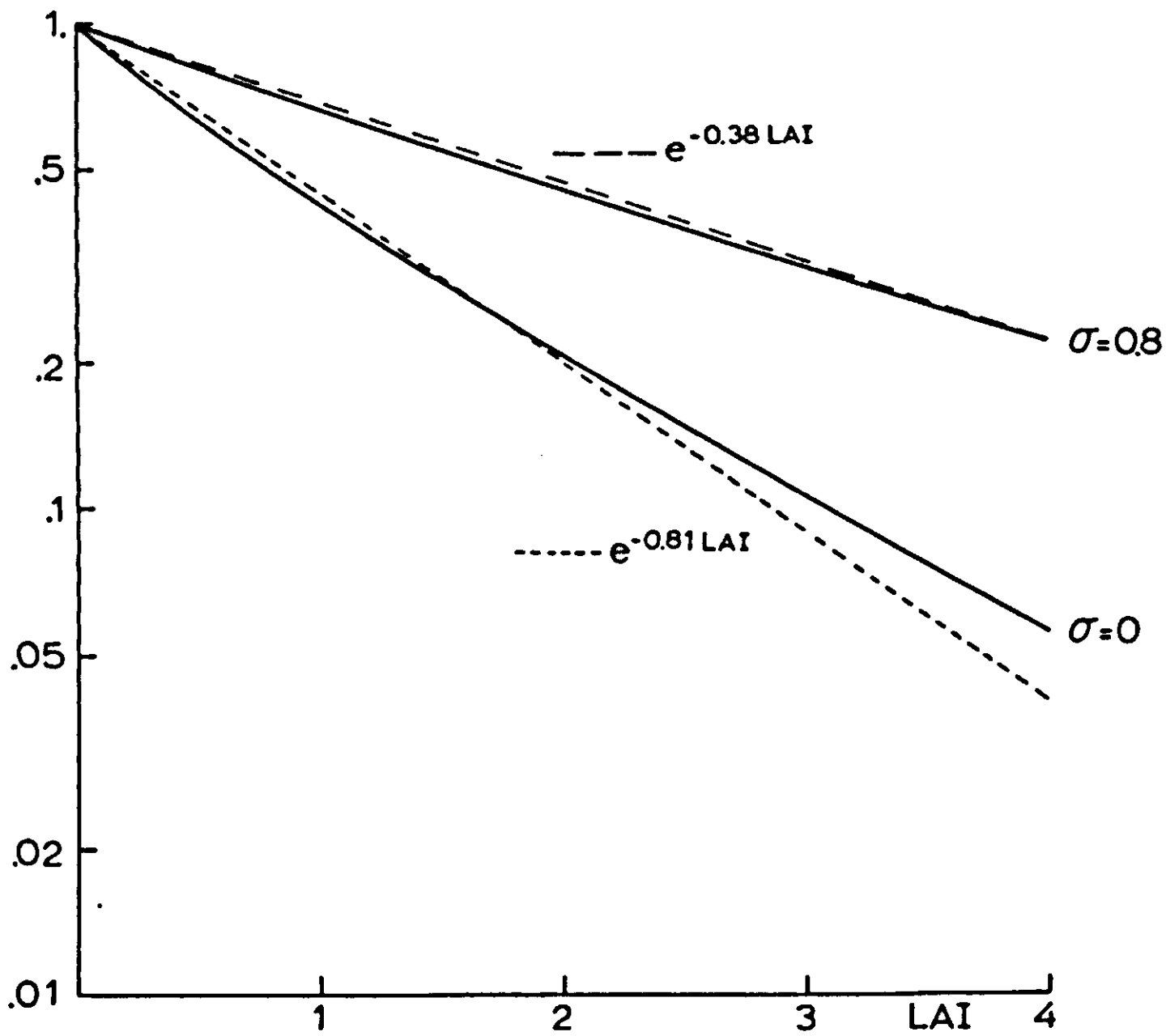


Fig. 6 | Downward radiant flux, relative to the incoming value, as a function of depth in the canopy, for two scattering coefficients of the leaves. The leaf angle distribution is spherical and the incoming radiation is diffuse (UOC). The numerically calculated profiles (solid lines) are compared to exponential curves (broken lines). The ordinate is logarithmic.

numerical values at different depths.

The extinction coefficients that do satisfy the above definition are listed in Table 5 for a few different conditions. They always refer to extinction of $\varphi_d - \varphi_u$, in other words of the net radiation within the considered wave band. These values of the extinction coefficients may be approximated by an equation, very similar to the one for horizontal leaves (Eqn (2.20))

$$K_f = K_b (1 - \sigma)^{0.5} \quad (2.40)$$

where K_b is the extinction coefficient for black leaves (Eqn (2.34)) that have the same leaf angle distribution as the ones considered. Consequently the coefficient for diffuse radiation is found by

$$\exp(-K_d LAI) = \sum_{\beta=1}^9 B_u(\beta) \exp\{-K_r(\beta) LAI\} \quad (2.41)$$

so that K_d depends on the total leaf area index.

Table 5 Extinction coefficients with the best fit for the net flux $\varphi_d - \varphi_u$. When the maximum deviation exceeds 5 percent of the incoming flux, K_m is omitted. Between 5 and 3 percent deviation K_m is marked with an asterisk.

σ	Only direct					Only diffuse	
	$\beta = 5^\circ$	$\beta = 25^\circ$	$\beta = 45^\circ$	$\beta = 65^\circ$	$\beta = 85^\circ$	UOC	SOC
Horizontal leaves							
0	1.050	1.050	1.050	1.050	1.050	1.050	1.050
0.3	0.872	0.872	0.872	0.872	0.872	0.872	0.872
0.5	0.730	0.730	0.730	0.730	0.730	0.730	0.730
0.8	0.440	0.440	0.440	0.440	0.440	0.440	0.440
Leaves under 45 degrees							
0	7.29	1.130	0.734	0.734	0.734	0.829	.
0.3		0.939	0.638	0.638	0.638	0.708	.
0.5		0.781	0.553	0.553	0.553	0.606	.
0.8		0.458*	0.351	0.351	0.351	0.376*	.
Vertical leaves							
0	12.9	1.46	0.658	0.306	0.088		.
0.3		1.20	0.586	0.282	0.083		.
0.5		0.986	0.517	0.257	0.076	0.399*	.
0.8			0.340	0.179	0.054	0.261	.
Spherical leaf angle distribution							
0	8.55	1.26	0.733	0.568	0.515	0.81*	0.745
0.3		1.03	0.636	0.504	0.461	0.684	0.643
0.8		0.48*	0.370	0.320	0.300	0.380	0.348

In Figure 7 the extinction coefficients, some of which were tabulated in Table 5, are plotted, against those given by Eqns (2.40) and (2.41). As the correlation is apparently very high the extinction coefficients can be calculated with Eqns (2.40) and (2.41), without the use of the numerical model. The regression equation is

$$\hat{K}_m = 0.0353 + 0.94623K_f \quad (2.42)$$

where K_f is the result of Eqn (2.40) or (2.41), and \hat{K}_m is an estimate for the result of the model K_m .

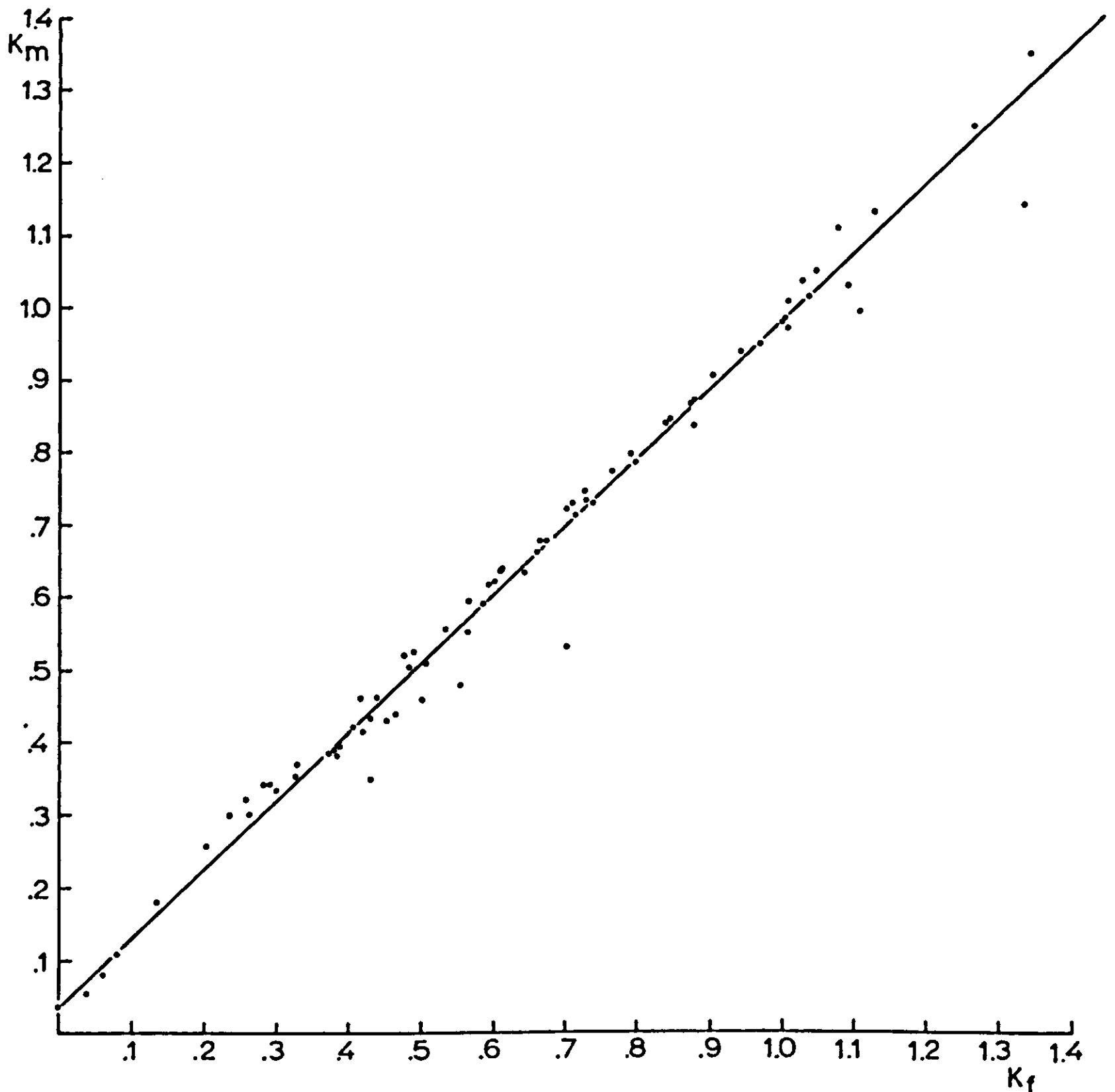


Fig. 7 | Extinction coefficients according to the model (K_m) against extinction coefficients according to a simple equation (K_f) for many situations differing in leaf angle distribution, scattering coefficient and geometry of the incoming radiation. The solid line represents the regression equation (Eqn (2.42)).

This equation is better written as

$$\hat{K}_m = 0.7541 + 0.94623(K_f - 0.7597) \quad (2.43)$$

where the origin is shifted to the centre of gravity of the 200 points considered. The standard deviation of the mean of \hat{K}_m is 0.0077 and that of the slope 0.0081. This means that there is 95 percent probability that the value of \hat{K}_m is correct within 0.015 in the region of 0.75. This range increases to 0.03 for \hat{K}_m as small as 0.1. These numbers are much more meaningful than the regression coefficient which is as high as 0.9928.

A similar procedure is followed for the reflection coefficient. Table 6 lists some values of reflection coefficients computed with the model. It must be kept in mind that these values apply to a canopy with a high

Table 6 Reflection coefficients according to the numerical model.

σ	Only direct					Only diffuse	
	$\beta = 5^\circ$	$\beta = 25^\circ$	$\beta = 45^\circ$	$\beta = 65^\circ$	$\beta = 85^\circ$	UOC	SOC
Horizontal leaves							
0.3	0.0928	0.0928	0.0928	0.0928	0.0928	0.0928	0.0928
0.5	0.178	0.178	0.178	0.178	0.178	0.178	0.178
0.8	0.387	0.387	0.387	0.387	0.387	0.387	0.387
Leaves under 45 degrees							
0.3	0.146	0.0905	0.0736	0.0736	0.0736	0.0794	.
0.5	0.266	0.175	0.145	0.145	0.145	0.155	.
0.8	0.517	0.386	0.332	0.332	0.332	0.350	.
Vertical leaves							
0.3	0.151	0.0897	0.0617	0.0381	0.0138	0.0590	.
0.5	0.274	0.174	0.124	0.0780	0.0287	0.117	.
0.8	0.526	0.388	0.297	0.199	0.0764	0.275	.
Spherical leaf angle distribution							
0.3	0.148	0.0922	0.0720	0.0626	0.0591	0.0781	0.0743
0.8	0.522	0.396	0.334	0.302	0.290	0.350	0.333

LAI only. Starting from the equation for horizontal leaves Eqn (2.21), the following formulas are used for approximation, which are semi-empirical. They introduce the dependence of the reflection coefficient on solar height through the dependence of $K_b(\beta)$ on solar height. The exponential relationship has no physical meaning but is only a means to remove most of the curvature in the relation between ρ_r and ρ_m . L_s accounts for the increase of the reflection coefficient with the leaf area index per sublayer, or with the regularity of leaf arrangement (see also Section 2.4.3).

$$\rho_r(\beta) = 1 - \exp[-2\rho_h\{1 + L_s K_d/(1 + K_d)\}K_b(\beta)/\{1 + K_b(\beta)\}] \quad (2.44)$$

where ρ_h follows from Eqn (2.21), K_d from Eqn (2.41) and L_s is the leaf area index per layer. For small values of L_s this equation simplifies to

$$\rho_r(\beta) = 1 - \exp[-2\rho_h K_b(\beta)/\{1 + K_b(\beta)\}] \quad (2.45)$$

Correlation of ρ_r with ρ_m gives

$$\hat{\rho}_m = 0.2057 + 1.1170 (\rho_r - 0.19414) \quad (2.46)$$

This equation does not work as well as the one for the extinction coefficient. It may be worthwhile to search for an equation with a better physical foundation. In Fig. 8 $\hat{\rho}_m$ is compared with ρ_m for $\sigma = 0.2$ and 0.8 , for a spherical leaf angle distribution. For high solar elevations $\hat{\rho}_m$ underestimates ρ_m in the near-infrared region by about 4 percent.

For diffuse light the reflection coefficient is found by weighted summation of $\hat{\rho}_m$ over the nine inclination classes.

These formulas for \hat{K}_m and $\hat{\rho}_m$ give a description of the radiation field that is in good agreement with the results of the model as long as the conditions are not too extreme. They are used as a substitute for the radiation model in larger computer models for microclimate, plant growth etc.

A simple calculation of $\bar{O}(\beta)$

Ross (1975) found that the following simplification can be applied for the naturally occurring leaf angle distributions. An index χ_L is introduced characterizing the deviation of the actual leaf angle

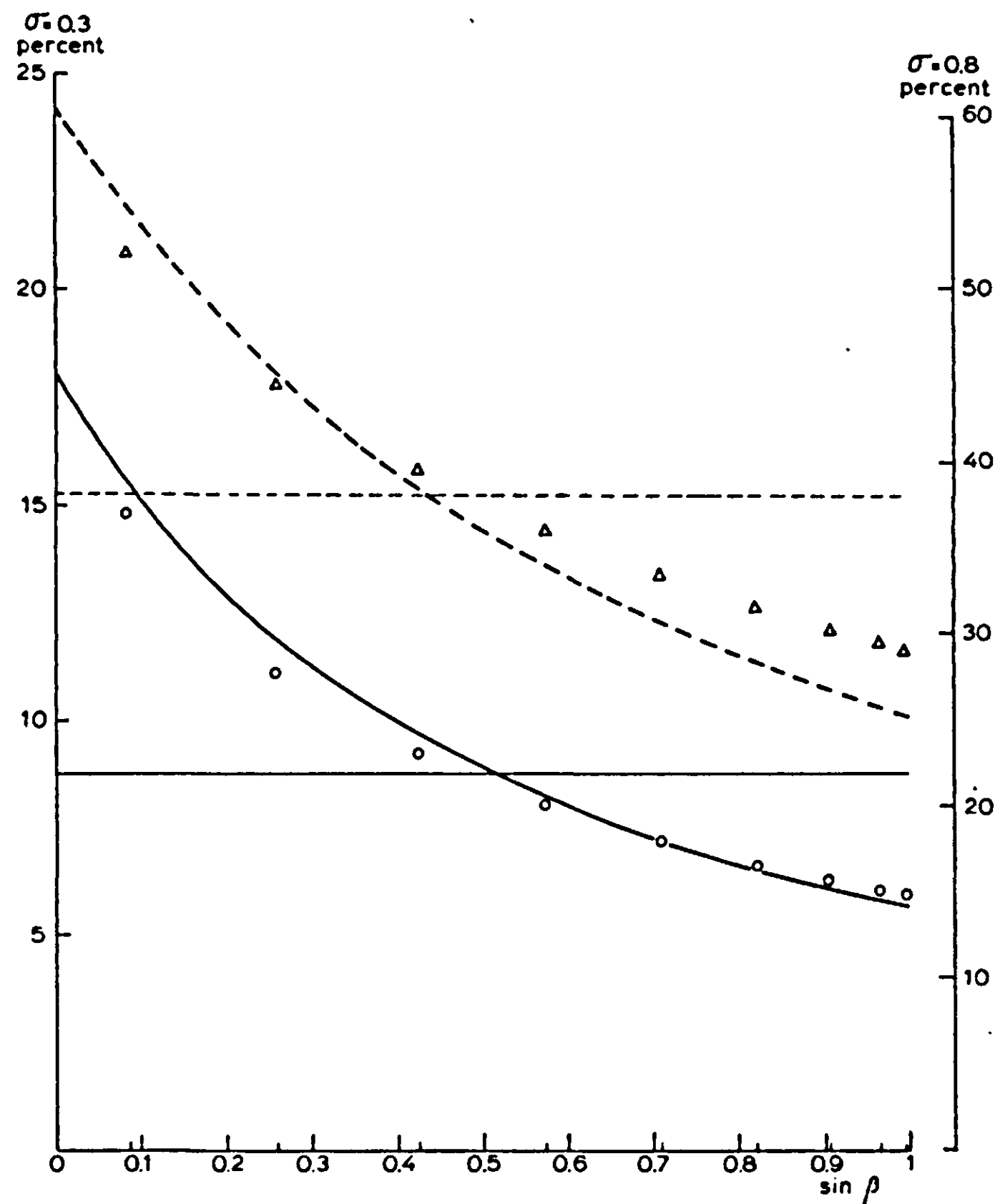


Fig. 8 | Comparison of the hemispherical reflection coefficient, calculated by the model (ρ_m) and calculated by a regression of the result of a simple equation ($\hat{\rho}_m$), both as function of the inclination of the direct incident radiation. The leaf angle distribution is spherical. The horizontal lines give the values for a horizontal leaf angle distribution.

	ρ_m	$\hat{\rho}_m$
visible ($\sigma = 0.3$)	—————	○
near-infrared ($\sigma = 0.8$)	- - - - -	△

distribution from the spherical one. χ_L is defined as:

$$\chi_L = \pm 1/2 \left\{ |0.134 - \sum_{\lambda=1}^3 F(\lambda)| + |0.366 - \sum_{\lambda=4}^6 F(\lambda)| + |0.5 - \sum_{\lambda=7}^9 F(\lambda)| \right\} \quad (2.47)$$

In this equation the nine leaf angle classes are reduced to three only. The numbers in the equation correspond to a spherical leaf angle distribution. The sign of χ_L is the same as the sign of the last term so that a tendency towards the horizontal leaf angle distribution is indicated by a positive sign, and towards a vertical leaf angle distribution by a negative sign. It is remarkable that for natural leaf inclination distributions, there is an almost unique relation between χ_L and the the average projection $\bar{O}(\beta)$. This semi-empirical relation is given by

$$O_1 = 0.5 - 0.633\chi_L - 0.33\chi_L^2 \quad -0.4 < \chi_L < 0.6 \quad (2.48)$$

$$\bar{O}(\beta) = O_1 + 0.877(1 - 2O_1) \sin\beta \quad (2.49)$$

This relation is not satisfactory for rare leaf angle distributions such as the extremophile and plagiophile (de Wit, 1965), but works very well in the whole range of naturally occurring leaf angle distributions for which χ_L appears to lie within the range of validity of Eqn (2.48). This method provides a valuable simplification for laborious determinations of leaf angle distributions, since it shows that only three classes of leaf angle give sufficient information.

2.3.4 Evaluation

The models discussed so far differ in complexity. It is not necessary in every situation to use the most complex model, on the contrary, the simplification should be carried out as far as possible. As pointed out before, for thin leaves the assumption that reflection equals transmission, is quite reasonable. The simplifying relations based on this assumption (Section 2.3.3) are a good approximation for a model with scattering leaves and a non-horizontal leaf angle distribution. The most natural non-horizontal leaf angle distribution is the spherical one, especially for maize and other grain crops (Ross, 1975). Therefore the evaluation is restricted to this case, formulated in terms of the simplifying relations.

Reflection

According to this model, under a clear sky the reflection coefficient will decrease with increasing solar height. This phenomenon has indeed been confirmed by many research workers. In Fig 9, the measured reflection coefficient of a maize crop for total short-wave radiation as a function of solar height is compared with the calculated values (solid line). The measurements were made by Burikov (1968) and by Kyle (1971). The calculations are done with Eqns (2.45), (2.44), (2.41) and (2.21), and with the values 0.2 and 0.8 for σ_v and σ_n , respectively. The theoretical and measured values depend similarly on the inclination but their absolute values differ slightly, probably because of a small difference in the scattering coefficient of the individual leaves.

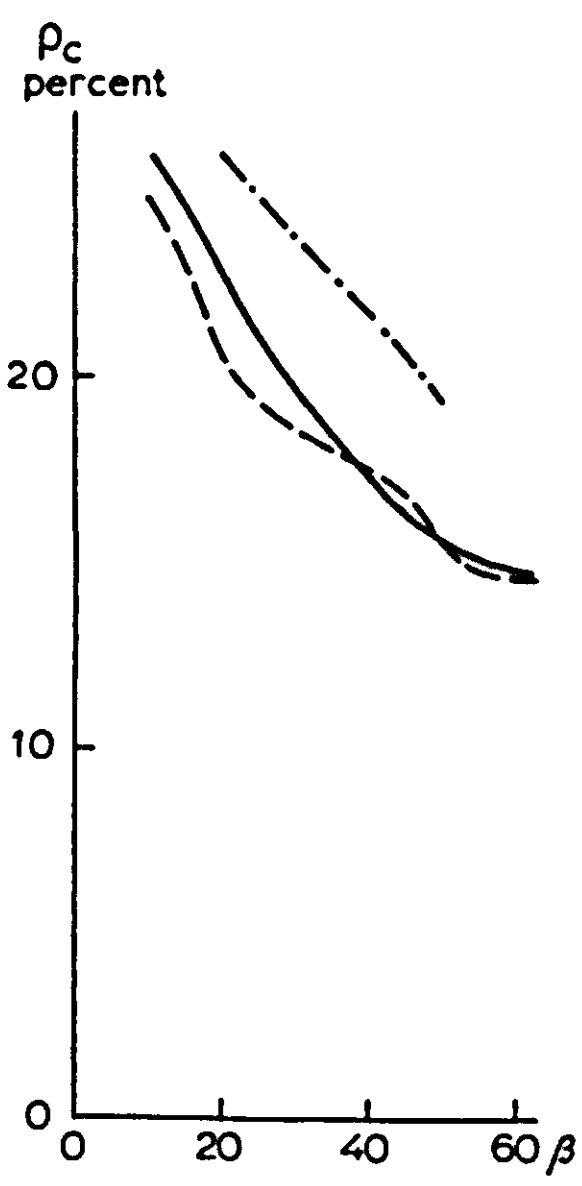


Fig. 9 | Comparison of measured and calculated reflection coefficients of a maize crop for total short-wave radiation as function of the inclination of the direct incoming radiation (see Section 2.3.4).

———— calculated; - - - - - measured by Burikov (1968); - · - · - measured by Kyle (1971).

In Fig. 10 my own measurements for wheat are compared with the theoretical lines, calculated in the same way as before. The lower solid line holds for 4 July and the upper one for 13 August. The small shift is due to the decrease in the declination of the sun in this period. The measurements were done with tube solarimeters of one metre long and of the type described by Szeicz et al. (1964). On 13 August the crop was already mature and the spectral composition of the reflected radiation had certainly changed, but the final effect on the total reflectance seems small.

Kanemasu (1974) reported that the reflection coefficient in the near-infrared region varies with solar height for wheat, sorghum and soya bean. For these crops ρ_c increased from 30% at 70 degrees to 43%

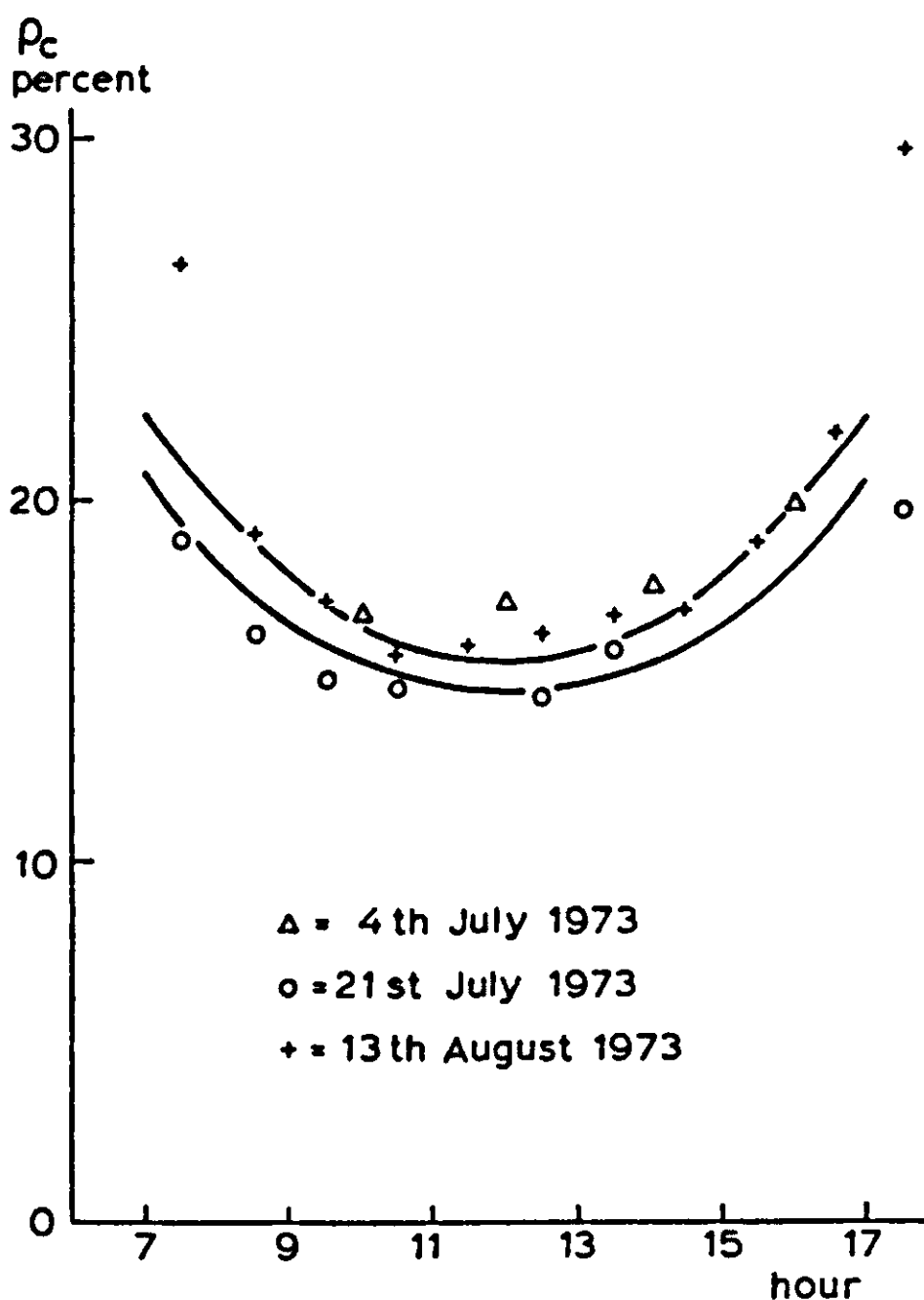


Fig. 10 | Comparison of measured and calculated reflection coefficients of a wheat crop for total short-wave radiation as function of the hour of the day. The sky is assumed to be clear.

The solid lines are the calculated daily courses on 4 July and 13 August.

Table 7 Reflection and extinction coefficients for solar radiation in rice as a function of solar height, according to measurements of Udagawa et al. (1974). The theoretical values are calculated for $\sigma_v = 0.3$ and $\sigma_n = 0.8$ and a spherical leaf angle distribution.

solar height in degrees	ρ_c		K	
	measured	theoretical	measured	theoretical
10	0.38	0.37	0.8	1.0 ¹
30	0.26	0.24	0.65	0.6
60	0.18	0.18	0.4	0.41

¹ The exponential profile with the best fit deviates between 3 and 5 percent from the profile according to the numerical model.

at 20 degrees. With the same assumptions as before $\hat{\rho}_m$ is calculated as 24.9% and 39.5% respectively for both solar heights.

Many authors reported a diurnal trend, such as given in Fig. 10, for reflection coefficients of canopies. Examples are given by Kalma & Badham (1972), Monteith (1976).

Measurements of Udagawa et al. (1974) for the reflection of solar radiation (ρ_c) by a rice canopy are given in Table 7. They are compared with the theoretical values for $\sigma_v = 0.3$ and $\sigma_n = 0.8$.

Extinction

In the same table Udagawa's data are given for the extinction coefficient (K), and compared with the calculated values. The agreement in this table is good.

Rodskjer (1972) measured downward radiant fluxes in the visible and near-infrared region in barley and oats. He calculated their values relative to the flux densities above the canopy and found a linear relation between the logarithms of the relative values for visible and near-infrared radiation. This result is consistent with an exponential extinction in both wave bands. The slope of the line represents the ratio of the extinction coefficients. According to Eqn (2.40) the ratio

is given by

$$n = \left(\frac{1 - \sigma_n}{1 - \sigma_v} \right)^{0.5} \quad (2.50)$$

so that n is not dependent on crop geometry neither on solar height. Rodskjer found values ranging between 0.46 and 0.53 for n in the green period of the crop. When σ_n and σ_v are taken as 0.8 and 0.2 as done before, the result of Eqn (2.50) is 0.5 so that the agreement with the experimental results is good. Rodskjer gave also values for wheat, both in the green and the ripe stage. In the green stage n was 0.51 and in the ripe stage 0.71. The value for the green stage was the same as for barley and oats. For the ripe stage he found a reflection coefficient of the canopy of 0.15 and 0.33 for visible and near-infrared radiation, respectively. These results give calculated values of $\sigma_v = 0.45$ and $\sigma_n = 0.75$ by Eqn (2.21), and then a value of 0.67 for n in the ripe stage. This is close to the measured value of 0.71.

The model extensions explain the radiance distribution of the standard overcast sky (Section 2.4.1) and the lower reflection of a forest compared with a grass field for equal optical properties of the leaves (Section 2.4.3).

These examples show that the radiation model is sufficiently reliable and can be used in a micrometeorological simulation model. Because of the reported dependences of the reflection and extinction coefficients on solar height, the model with horizontal leaves resulting in constant values, is too simple.

2.3.5 *An important reciprocity relation*

According to calculations with the model as described in Section 2.3.2, the radiance of a reflecting surface at inclination β_1 with direct light incident from β_2 , is equal to the radiance at inclination β_2 with direct light incident from β_1 , provided the fluxes through a horizontal plane are the same in both cases.

This is an attractive relation which seems like a physical law. It must be a logical consequence of the structure of the model, but I could not find which feature of the model is essential for this reciprocity relation. It could not be invalidated by changing leaf inclination distribution, scattering coefficient, the value of L_s , uniform all over the canopy or even as a function of height. However, a striking restric-

tion is that this relation only holds for radiances at the boundaries of the system, that means for crop reflection and also for crop transmission, if the reflection of the soil surface is zero. It does not hold for radiances at any level inside the canopy.

One of the consequences of this property is that the dependence of the hemispherical reflection coefficient of a surface on the inclination of the incoming direct radiation is the same as the dependence of the radiance, under a UOC sky on the inclination of the angle of view. Thus reflection coefficients for all inclinations of direct light can be found from a single run for a UOC sky. This property is used in Fig. 5c where the radiance πN and the hemispherical reflection coefficient ρ_c are put on the same ordinate.

This can be proven as follows.

When $S_b(\beta)$ is a direct downward flux with inclination β , the radiance of a reflecting surface, as seen from direction β' , can be written as

$$N(\beta') = N_{r,\rho}(\beta',\beta)S_b(\beta) \quad (2.51)$$

Reciprocity as described above can be mathematically expressed as

$$N_{r,\rho}(\beta',\beta) = N_{r,\rho}(\beta,\beta') \quad (2.52)$$

The reflection coefficient of the reflecting surface can be found by integration of $N(\beta') \sin\beta'$ over the upper hemisphere.

$$\rho_c(\beta) = \frac{1}{S_b(\beta)} \int N(\beta') \sin\beta' d\omega' \quad (2.53)$$

The solid angle $d\omega'$ can be written as

$$d\omega' = \cos\beta' d\beta' d\alpha' \quad (2.54)$$

when α' is the azimuth of the reflected ray.

After substitution of Eqns (2.51) and (2.54) in Eqn (2.53) the expression for $\rho_c(\beta)$ becomes

$$\rho_c(\beta) = \int_0^{2\pi} \int_0^{\pi/2} N_{r,\rho}(\beta',\beta) \sin\beta' \cos\beta' d\beta' d\alpha' \quad (2.55)$$

or

$$\rho_c(\beta) = 2\pi \int_0^{\pi/2} N_{r,\rho}(\beta',\beta) \sin\beta' \cos\beta' d\beta' \quad (2.56)$$

According to the reciprocity relation (2.52) $\rho_c(\beta)$ is also equal to

$$\rho_c(\beta) = 2\pi \int_0^{\pi/2} N_{r,\rho}(\beta,\beta') \sin\beta' \cos\beta' d\beta' \quad (2.57)$$

The radiance of the canopy in direction β' under a diffuse (UOC) sky equals, by combination of Eqns (2.11) and (2.51)

$$N_d(\beta') = \int_0^{\pi/2} N_{r,\rho}(\beta',\beta) 2S_d \sin\beta \cos\beta d\beta \quad (2.58)$$

This equation has the same structure as Eqn (2.57) when β and β' are interchanged so that

$$N_d(\beta) = \rho_c(\beta) S_d/\pi \quad (2.59)$$

Hence the dependences of $N_d(\beta)$ and $\rho_c(\beta)$ on β are the same.

The reciprocity relation only holds for the outer boundaries of the system, but not anywhere inside. Thus it also applies to transmitted radiation, provided that no reflected radiation, for example from the soil surface, returns.

The mathematical proof of the reciprocity relation in its general form is very difficult. For only one sublayer it proceeds as follows.

When a direct flux $S_b(\beta)$ is incident, the flux scattered into a zone with index β' is given by

$$\varphi_u(\beta') = 0.5\sigma S_b(\beta) \int_0^{\pi/2} F(\lambda) B_1(\beta',\lambda) M_i(\beta,\lambda) d\lambda \quad (2.60)$$

The radiance into direction β' is given by

$$N(\beta') = \frac{\varphi_u(\beta')}{\pi B_u(\beta')} \quad (2.61)$$

Substitution of Eqns (2.51) and (2.61) into Eqn (2.60) gives

$$N_{r,\rho}(\beta,\beta') = \frac{0.5\sigma \int_0^{\pi/2} F(\lambda) B_1(\beta',\lambda) M_i(\beta,\lambda) d\lambda}{\pi B_u(\beta')} \quad (2.62)$$

By substitution of Eqns (2.35) and (2.36), this expression is simplified to

$$N_{r,\rho}(\beta,\beta') = \frac{0.5\sigma}{\pi L_s} \int_0^{\pi/2} F(\lambda) M_i(\beta',\lambda) M_i(\beta,\lambda) d\lambda \quad (2.63)$$

In this equation β and β' occur symmetrically so that reciprocity holds. For more than one layer probably a similar, but more complicated procedure has to be executed to give the mathematical proof of reciprocity. The mathematical investigation of the conditions for this

reciprocity relation is a challenging problem. It may have important practical implications for remote sensing techniques.

2.3.6 Thermal radiation

According to the Law of Stefan-Boltzmann a black body emits thermal radiation related to its surface temperature as

$$B = \sigma T^4 \quad (2.64)$$

where T is here the absolute temperature expressed in degrees Kelvin. The Stefan-Boltzmann constant σ has the value $5.668 \cdot 10^{-8} \text{ W m}^{-2} \text{ K}^{-4}$. For two black parallel plates with temperatures T_1 and T_2 the net thermal radiant flux is thus given by

$$B_n = \sigma(T_1^4 - T_2^4) \quad (2.65)$$

When the temperature difference $\Delta T = T_1 - T_2$ is small compared with the absolute temperatures, B_n can be written as

$$B_n = 4\sigma T_m^3 \Delta T \quad (2.66)$$

where T_m is the arithmetic mean of the absolute temperatures T_1 and T_2 . At 25°C the differential thermal radiation according to Eqn (2.66) is $6 \text{ W m}^{-2} \text{ K}^{-1}$. For a heat capacity of the air of $1240 \text{ J m}^{-3} \text{ K}^{-1}$, this value corresponds to a resistance of about 200 s m^{-1} . Since this resistance can be considered to be connected in parallel to the boundary layer resistance, it need only be taken into account in still air or for large surfaces (see Eqn (3.5)). Therefore the thermal radiant exchange between leaves can usually be neglected in the daytime. This does not apply to thermal radiant exchange with the relatively cold sky, because it is the only means of exchange and the apparent temperature difference may be of the order of 20 K. According to Monteith (1973), the apparent temperature of a clear sky may be estimated as

$$T_{\text{sky}} = T_a - 21 + 0.2T_a \quad (2.67)$$

with all temperatures in $^\circ\text{C}$, and T_a is the air temperature at a height of 2 m (screen height). For cloudy skies the apparent sky temperature has an estimated value of 2 degrees less than air temperature at 2 m. Hence typical values for the net thermal radiation are -80 to -100 W m^{-2} for a clear sky and -10 W m^{-2} for an overcast sky.

The temperatures of the leaves and the soil surface are known during the simulation because they are considered as state variables. The fluxes of thermal radiation can then be computed in the same way as those of the short-wave radiation. Scattered radiation must be replaced by emitted radiation, which depends on the temperature of the leaves. In Section 2.3.3 it was shown that extinction of diffuse radiation can be approximated by an exponential profile. This approximation is now used for the extinction of the net thermal radiation per leaf area. The extinction coefficient for the diffuse 'black' radiation is $K_{b,r}$ and according to Table 5 equal to 0.81 for a spherical leaf angle distribution. A layer with index j not only exchanges thermal radiation with the sky, but also with layers of leaves above and below it and also with the soil surface. The total number of layers of leaves is denoted by m . The index of the layer considered is denoted by j , of the other layers by i . The index 0 refers to the sky and the index n refers to the soil surface. The equations for the net thermal radiation per leaf area are now:

$$R_l(j) = \frac{\{1 - \exp(-K_{b,d}L_s)\}}{L_s} [\sigma'_{0,j}\{T_{\text{sky}} - T_l(j)\} + \sigma'_{i,j}\{T_l(i) - T_l(j)\} + \sigma'_{n,j}\{T_{\text{soil}} - T_l(j)\}] \quad (2.68)$$

where the σ' are given by

$$\sigma'_{0,j} = 4\sigma T_m^3(0,j) \exp\{-K_{b,d}L_s(j-1)\} \quad (2.69a)$$

$$\sigma'_{i,j} = 4\sigma T_m^3(i,j) \exp\{-K_{b,d}L_s(|i-j|-1)\} \{1 - \exp(-K_{b,r}L_s)\} \quad (2.69b)$$

$$\sigma'_{n,j} = 4\sigma T_m^3(n,j) \exp\{-K_{b,d}L_s(m-j)\} \quad (2.69c)$$

For the mutual exchange between leaves and with the soil surface Eqn (2.66) is used in a linearized form:

$$B_n = \{4.61 + 0.0281(T_1 + T_2)\}(T_1 - T_2) \quad (2.70)$$

where T_1 and T_2 are expressed in °C. The term 4.61 stands for $4\sigma 273^3$ and 0.0281 for $4 \times 3 \times \sigma \times 273^2/2$.

Because the estimation of the apparent sky temperature is inaccurate one can neglect that the emission coefficient of leaves is about 0.96 rather than unity. However, as soon as the thermal radiation from the leaves is indeed used for a remote measurement of their temperature, this small difference may not be overlooked, since it results in an underestimation of the leaf temperature by about 3 K.

2.4 Model extensions

2.4.1 *The origin of the radiance distribution of the standard overcast sky*

Table 4 and Fig. 4 give the radiation profiles that are calculated for a scattering coefficient σ of unity and a spherical leaf angle distribution. This exercise was intended to test the balances in the model. These were found in order and now these results can also serve a more direct purpose.

Physical media with a very high reflection coefficient due to multiple scattering are for instance clouds, snow and some powders. It is well known that a powder becomes whiter when it is ground finer. There are two reasons for this.

When each particle is considered as a scattering element, the surface area index ('*LAI*') increases as the particles get finer so that the effect of absorption at the underlying surface is reduced (Fig. 3). Secondly the absorption in each element itself decreases, just because the light path in the elements is shortened. The reflection coefficient of the medium is approximately given by Eqn (2.21), and when in this equation $1 - \sigma$ is replaced by the absorption coefficient per particle α , it reads:

$$\rho_h = \frac{1 - \sqrt{\alpha}}{1 + \sqrt{\alpha}} \quad (2.71)$$

When the particle size tends to zero, the absorption coefficient α approaches zero, so that ρ_h approaches unity. Inversion of this relation gives

$$\alpha = \left(\frac{1 - \rho_h}{1 + \rho_h} \right)^2 \quad (2.72)$$

By this equation one can calculate the value of the absorption α of the individual particles, resulting in the reflection coefficient ρ_h . When the reflection coefficient is close to unity, α becomes extremely small. For instance, for ρ_h is 0.9 and 0.99, α is $2.77 \cdot 10^{-3}$ and $25.2 \cdot 10^{-6}$, respectively. In practice reflection coefficients of 0.98 can be realized (Budde, 1960), with a powder of barium sulphate. Such a highly reflecting surface is used in black and white radiometers.

For thin layers or a low ' LAI ', absorption of the underlying surface causes a depression in the reflection of the medium (Fig. 3). For a high scattering coefficient the extinction coefficient K will approach zero, so that $\exp(K \times LAI)$ can be written as $1 + K \times LAI$. The reflection coefficient ρ_h (Eqn (2.21)) can be expressed in K as

$$\rho_h = \frac{1 - K}{1 + K} \quad (2.73)$$

By substituting this expression into Eqn (2.26) ρ_{eff} can be calculated for K approaching zero. When ρ_s is zero the result is

$$\rho_{eff} = LAI/(2 + LAI) \quad (2.74)$$

These relations hold for a horizontal leaf angle distribution, whereas Table 8 gives the computed values for a spherical leaf angle distribution. Presumably this is approximately the situation in clouds, because droplets are spherical interceptors and scatter almost all radiation. They do, however, not act as Lambertian radiators and this peculiarity must be considered separately.

The directional distribution of the transmitted radiation under the

Table 8 Reflection and transmission coefficients of a medium with a scattering coefficient unity of the individual particles. Three optical thicknesses, denoted by LAI , are considered and five inclinations of the direct radiation. The 'leaf' angle distribution is spherical and the underlying surface is black.

$LAI = 2$	$\beta = 5^\circ$	$\beta = 25^\circ$	$\beta = 45^\circ$	$\beta = 65^\circ$	$\beta = 85^\circ$
ρ_c	0.727	0.548	0.430	0.371	0.349
τ_c	0.273	0.452	0.570	0.629	0.651
$LAI = 5$					
ρ_c	0.835	0.734	0.656	0.606	0.584
τ_c	0.165	0.266	0.344	0.394	0.416
$LAI = 10$					
ρ_c	0.899	0.838	0.790	0.759	0.744
τ_c	0.099	0.160	0.207	0.239	0.253

medium (the sky) is especially interesting. According to the model the distribution is independent of the angle of incidence of the direct radiation at the top of the medium, when the ' LAI ' (optical thickness) is large enough. The empirical equation for the standard overcast sky (SOC) is of the form (Eqn (2.12))

$$N(\beta') = a + b \sin\beta' \quad (2.75)$$

From a simple theoretical argument follows that this structure is not coincidental but has a theoretical basis. The radiance of the sky consists of the radiances of elements at different depths:

$$N(\beta') = \int_0^{LAI} K_b(\beta') N_1(\beta', LAI') \exp\{-K_b(\beta') LAI'\} dLAI' \quad (2.76)$$

where LAI' is reckoned from beneath and not from above. N_1 is the radiance of the elements.

To account for the interception in the direction of view, the extinction coefficient for black leaves K_b must be used. The radiance of the elements N_1 will be approximately proportional to the sum of the upward and downward flux at depth LAI' :

$$N_1(\beta', LAI') \sim \varphi_d + \varphi_u \quad (2.77)$$

Below the first few top layers the fluxes are a linear function of depth, so that φ_d and φ_u can be approximately written as

$$\varphi_d \approx \tau_{\text{eff}} + (1 - \tau_{\text{eff}}) \frac{LAI'}{LAI} \quad (2.78)$$

$$\varphi_u \approx (1 - \rho_{\text{eff}}) \frac{LAI'}{LAI} \quad (2.79)$$

Since $\tau_{\text{eff}} + \rho_{\text{eff}}$ equal unity when soil reflectance is zero and the scattering coefficient is unity, the sum of φ_d and φ_u can be written as

$$\varphi_d + \varphi_u \approx \tau_{\text{eff}} + \frac{LAI'}{LAI} \quad (2.80)$$

According to Eqn (2.74) τ_{eff} will be approximately equal to

$$\tau_{\text{eff}} \approx 2/(2 + LAI) \quad (2.81)$$

For large values of LAI $\varphi_d + \varphi_u$ will thus be given by

$$\varphi_d + \varphi_u \approx \frac{2}{LAI} (1 + 0.5LAI') \quad (2.82)$$

so that

$$N_1(\beta, LAI') \sim (1 + 0.5LAI') \quad (2.83)$$

For a sufficiently large value of LAI integration of Eqn (2.76) gives

$$N(\beta') \sim 1 + 0.5LAI'/K_b(\beta') \quad (2.84)$$

For spherical particles $K_b(\beta')$ equals $0.5/\sin\beta'$ so that

$$N(\beta') \sim 1 + \sin\beta' \quad (2.85)$$

The structure of this simple theoretical equation corresponds to the empirical one (Eqn (2.12)). It underestimates, however, the angle dependence probably because of approximation Eqn (2.77).

The results of the computer model in which these approximations need not be made, are compared to the SOC equation in Fig. 11.

The model prediction and the empirical relation practically coincide at least for a low reflection coefficient of the underlying surface. When ρ_s increases, the angle dependence of the radiance decreases simultaneously. It would be worthwhile to investigate how the radiance distribution of an overcast sky changes above a snow cover. According to the model prediction the uniform overcast sky (UOC) should be a better representation then.

One model simplification remains to be discussed. So far the individual elements scatter radiation isotropically. This is not so for real droplets of water. Although it will be difficult to incorporate the real angular scattering distribution of the individual particles one step in this direction can be made. With the use of the results of the following section, the model is run for leaves with zero transmission on one hand ($\tau = 0$ and $\rho = 1$) and zero reflection on the other ($\tau = 1$ and $\rho = 0$). With these values there is a drastic change in the angular distribution of scattered radiation. The results of these runs are also given in Fig. 11. In both cases the SOC distribution is again closely approached.

It may thus be concluded that the SOC distribution emerges rather independently of the angular scattering distribution of the individual particles. The radiance distribution of the sky is, however, strongly

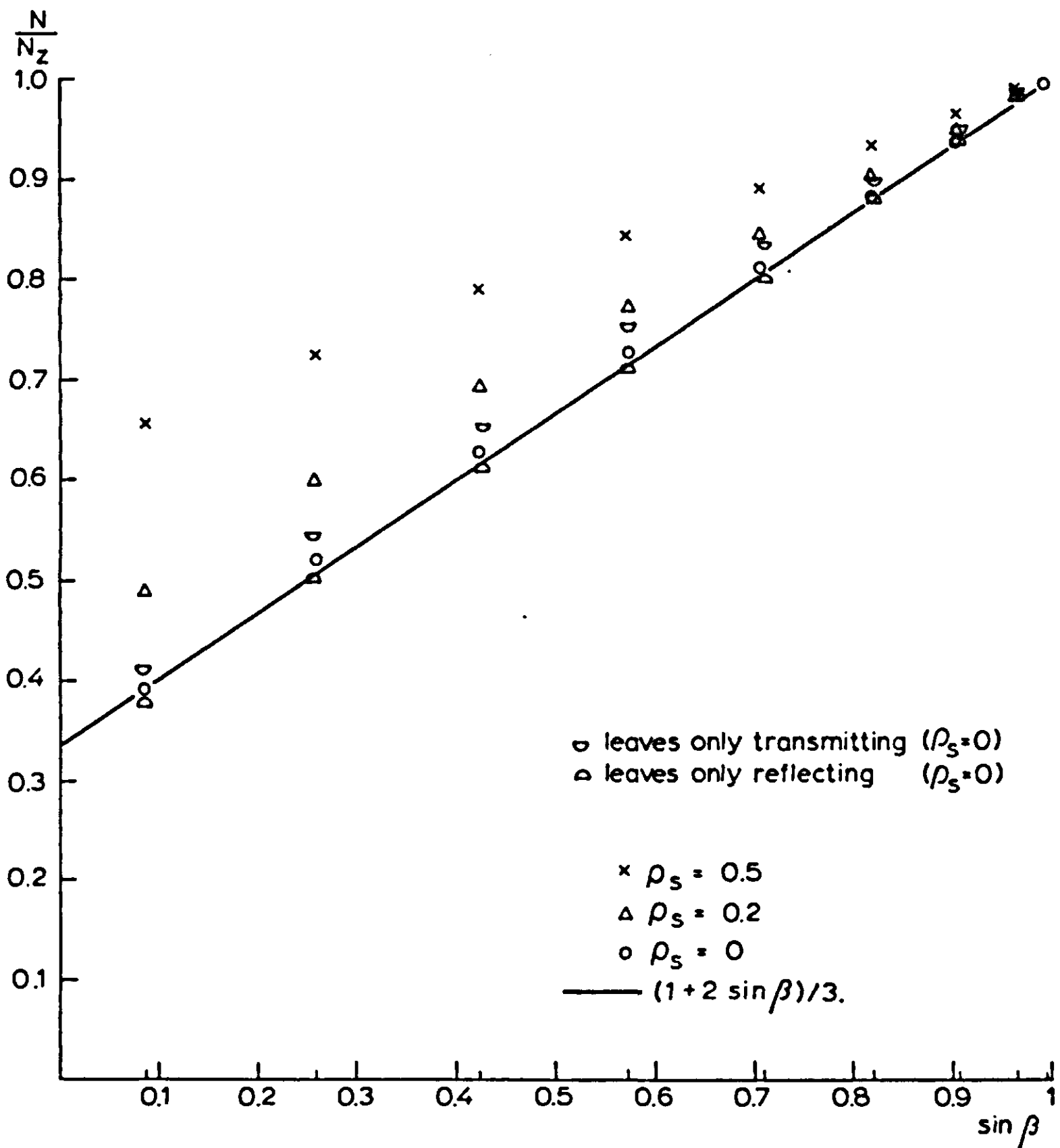


Fig. 11 | Comparison of the empirical relation of the standard overcast sky (SOC), (solid line), and some values of the radiance of the sky computed by the model. The scattering coefficient is unity, and the leaf angle distribution spherical. The hemicircles indicate the values computed for either only transmitting or only reflecting leaves; in the other cases leaf reflection and transmission were equal.

influenced by the reflection coefficient of the underlying surface. Above a snow cover it will probably tend to the UOC distribution.

2.4.2 Leaves with unequal reflection and transmission

Now the theory is extended to leaves with unequal reflection and transmission coefficients. Thick, succulent leaves usually reflect more than they transmit as do pine needles. Other scattering elements like the air-water transitions inside a leaf or the droplets in a foggy air transmit more than reflect.

For horizontal scattering elements Eqns (2.22) and (2.23) were derived in Section 2.3.1. However, for the general case a numerical model must be used. This is achieved by modification of the following equations

$$\varphi_d(\beta'j + 1) = M_i(\beta')\varphi_d(\beta'j) + 0.5\sigma B_i(\beta')I_i(j) \quad (2.38a)$$

$$\varphi_u(\beta'j) = M_i(\beta')\varphi_u(\beta'j + 1) + 0.5\sigma B_i(\beta')I_i(j) \quad (2.38b)$$

The term on the right which represents the addition of scattered radiation must be separated into one term with the reflection coefficient ρ and another with the transmission coefficient τ . The contribution to $\varphi_d(\beta'j)$ originating from $\varphi_d(\beta, j - 1)$ contains purely transmitted radiation only if both the inclination of the incident ray β and the inclination of the scattered ray β' are larger than the inclination of the leaves λ . The same argument, in complementary form, applies to reflected radiation. Thus in general both reflected and transmitted components are present.

For a single leaf inclination λ Eqns (2.38a) and (2.38b) can be changed into:

$$\begin{aligned} \varphi_d(\beta'j + 1) = & M_i(\beta')\varphi_d(\beta'j) + \\ & + B_i(\beta') \sum_{\beta=1}^9 M_i(\beta)[\varphi_d(\beta, j)\{\rho(1 - \xi) + \tau \xi\} + \\ & + \varphi_u(\beta, j - 1)\{\tau(1 - \xi) + \rho \xi\}] \end{aligned} \quad (2.86)$$

$$\begin{aligned} \varphi_u(\beta'j) = & M_i(\beta')\varphi_u(\beta'j + 1) + \\ & + B_i(\beta') \sum_{\beta=1}^9 M_i(\beta)[\varphi_d(\beta, j)\{\tau(1 - \xi) + \rho \xi\} + \\ & + \varphi_u(\beta, j - 1)\{\rho(1 - \xi) + \tau \xi\}] \end{aligned} \quad (2.87)$$

ξ is the reflection-transmission distribution function for a single leaf inclination λ , and depends further on the angle of incidence β and the angle of scattering β' . When both β and β' are larger than λ , ξ is one. The minimum value of ξ is 0.5, which is reached for β and β' both tending to zero and λ to 90 degrees.

The expression for ξ as dependent on β , β' and λ can be derived as follows.

The radiance N ($\text{J m}^{-2} \text{sr}^{-1} \text{s}^{-1}$) of an inclined surface element dA , with a Lambertian reflection coefficient ρ , and receiving a direct radiant flux S_p at an angle of incidence θ , is given by

$$N = \rho S_p \sin\theta/\pi \quad (2.88)$$

The energy flow ψ (J s^{-1}) of radiation reflected under an angle θ' into a solid angle $d\omega'$ equals

$$\psi = N \sin\theta' dA d\omega' \quad (2.89)$$

where $d\omega'$ is given by

$$d\omega' = \cos\beta' d\beta' d\alpha' \quad (2.90)$$

All angles without a prime refer to incident radiation and with a prime to reflected, transmitted or emitted radiation.

The angles of incidence and reflection are calculated according to Eqn (2.1)

$$\sin\theta = \sin\beta \cos\lambda + \cos\beta \sin\lambda \cos\alpha \quad (2.91a)$$

$$\sin\theta' = \sin\beta' \cos\lambda + \cos\beta' \sin\lambda \cos\alpha' \quad (2.91b)$$

where λ is the inclination of the surface element, and α and α' are the azimuths of the incident and reflected rays, respectively.

For reflected radiation $\sin\theta$ and $\sin\theta'$ should be either both positive or both negative. The critical values of the azimuths α and α' for which the sines are zero, are denoted by α_c and α'_c and given by

$$\alpha_c = \pi/2 + \arcsin\left(\frac{\text{tg}\beta}{\text{tg}\lambda}\right) \quad \beta < \lambda \quad (2.92a)$$

$$\alpha_c = \pi \quad \beta \geq \lambda \quad (2.92b)$$

and likewise for α'_c where β is replaced by β' .

The energy flow reflected into the zone $d\beta'$ can be found by integra-

tion of Eqn (2.89) over the azimuth ranging from 0 to 2π . Because of the azimuthal isotropy of the leaves the average flow $\bar{\psi}$ for α ranging from 0 to 2π is found by another integration over this interval and dividing by 2π . For both integrations the region from π to 2π is identical to the region from 0 to π , so that only integrations in the latter region are done and the result is multiplied by 4 instead.

As both sines should have the same sign, the integrated expression for reflected radiation becomes

$$\bar{\psi}_{\text{refl}} = \frac{4}{2\pi} \int_0^{\alpha_c'} \int_0^{\alpha_c} \psi \, d\alpha d\alpha' + \int_{\alpha_c'}^{\pi} \int_{\alpha_c}^{\pi} \psi \, d\alpha d\alpha' \quad (2.93)$$

To find the transmitted amount the integration intervals must be combined crosswise, and of course ρ must be replaced by τ in Eqn (2.88).

Integration gives for the average reflected and transmitted flows into the zone $d\beta'$:

$$\begin{aligned} \bar{\psi}_{\text{refl}} = S_p \rho \frac{4}{2\pi^2} \{ & a_1(\pi^2 + 2\alpha_c \alpha_c' - \pi\alpha_c - \pi\alpha_c') + \\ & + a_2 \sin\alpha_c' (2\alpha_c - \pi) + a_3 \sin\alpha_c (2\alpha_c' - \pi) + \\ & + 2a_4 \sin\alpha_c \sin\alpha_c' \} \cos\beta' \, d\beta' \, dA \end{aligned} \quad (2.94a)$$

$$\begin{aligned} \bar{\psi}_{\text{trans}} = S_p \tau \frac{4}{2\pi^2} \{ & a_1(2\alpha_c \alpha_c' - \pi\alpha_c - \pi\alpha_c') + a_2 \sin\alpha_c' (2\alpha_c - \pi) + \\ & + a_3 \sin\alpha_c (2\alpha_c' - \pi) + 2a_4 \sin\alpha_c \sin\alpha_c' \} \cos\beta' \, d\beta' \, dA \end{aligned} \quad (2.94b)$$

Apart from the multiplication by ρ or τ , these expressions are only different in the term π^2 , by which a_1 must be multiplied. The auxiliary variables a_1, a_2, a_3 and a_4 are given by

$$a_1 = \sin\beta \sin\beta' \cos^2\lambda \quad (2.95a)$$

$$a_2 = \sin\beta \cos\beta' \sin\lambda \cos\lambda \quad (2.95b)$$

$$a_3 = \cos\beta \sin\beta' \sin\lambda \cos\lambda \quad (2.95c)$$

$$a_4 = \cos\beta \cos\beta' \sin^2\lambda \quad (2.95d)$$

The fraction $\xi(\beta, \beta', \lambda)$ is now given by

$$\xi(\beta, \beta', \lambda) = \frac{\psi_{\text{refl}}}{2 S_p \rho O(\beta, \lambda) O(\beta', \lambda) \, d\beta' \, dA} \quad (2.96)$$

where $O(\beta, \lambda)$ is the average projection of the leaves with inclination λ in direction β (Eqn (2.3)). It should be noted that $\xi(\beta, \beta', \lambda) = \xi(\beta', \beta, \lambda)$.

The average value of ξ over the upper hemisphere can be found by integrating the numerator and the denominator of Eqn (2.96) for β from 0 to $\pi/2$. The integral of the denominator is $S_p \rho O(\beta, \lambda) dA$ for any leaf angle (Appendix A, Eqn (A12)). This is in fact the total amount of reflected radiation. The fraction reaching the upper hemisphere is found by integrating $\bar{\psi}_{\text{refl}}$ (Appendix A, (d)) from 0 to $\pi/2$. The ratio of the two integrals is thus given by

$$\frac{\int \bar{\psi}_{\text{refl, up}}}{\int \bar{\psi}_{\text{refl, tot}}} = \frac{1}{2} \left(1 + \frac{\sin \beta \cos^2 \lambda}{O(\beta, \lambda)} \right) \quad (2.97)$$

When $\beta > \lambda$ this expression simplifies to

$$\frac{\int \bar{\psi}_{\text{refl, up}}}{\int \bar{\psi}_{\text{refl, tot}}} = \frac{1}{2} (1 + \cos \lambda) \quad \beta > \lambda \quad (2.98)$$

Results

Some computer runs were made with the model described for a spherical leaf angle distribution. The resulting reflection coefficients are listed in Table 9. The same results are plotted in Fig. 12 together with the results for equal reflection and transmission of the leaves. In the same graph the values of the analytic solution for horizontal leaves (Eqn (2.23)) are drawn as a horizontal line.

The extinction coefficients of the closest fitting exponential curves are listed in Table 10. When the largest deviation of the real profile from

Table 9 Reflection coefficient of a canopy with a high LAI as a function of the angle of incidence of direct radiation. The leaves either transmit or reflect. The leaf angle distribution is spherical.

ρ	τ	$\beta = 5^\circ$	$\beta = 25^\circ$	$\beta = 45^\circ$	$\beta = 65^\circ$	$\beta = 85^\circ$
0.3	0.0	0.162	0.119	0.100	0.090	0.087
0.0	0.3	0.132	0.063	0.041	0.031	0.028
0.8	0.0	0.559	0.450	0.390	0.356	0.343
0.0	0.8	0.468	0.310	0.240	0.205	0.190

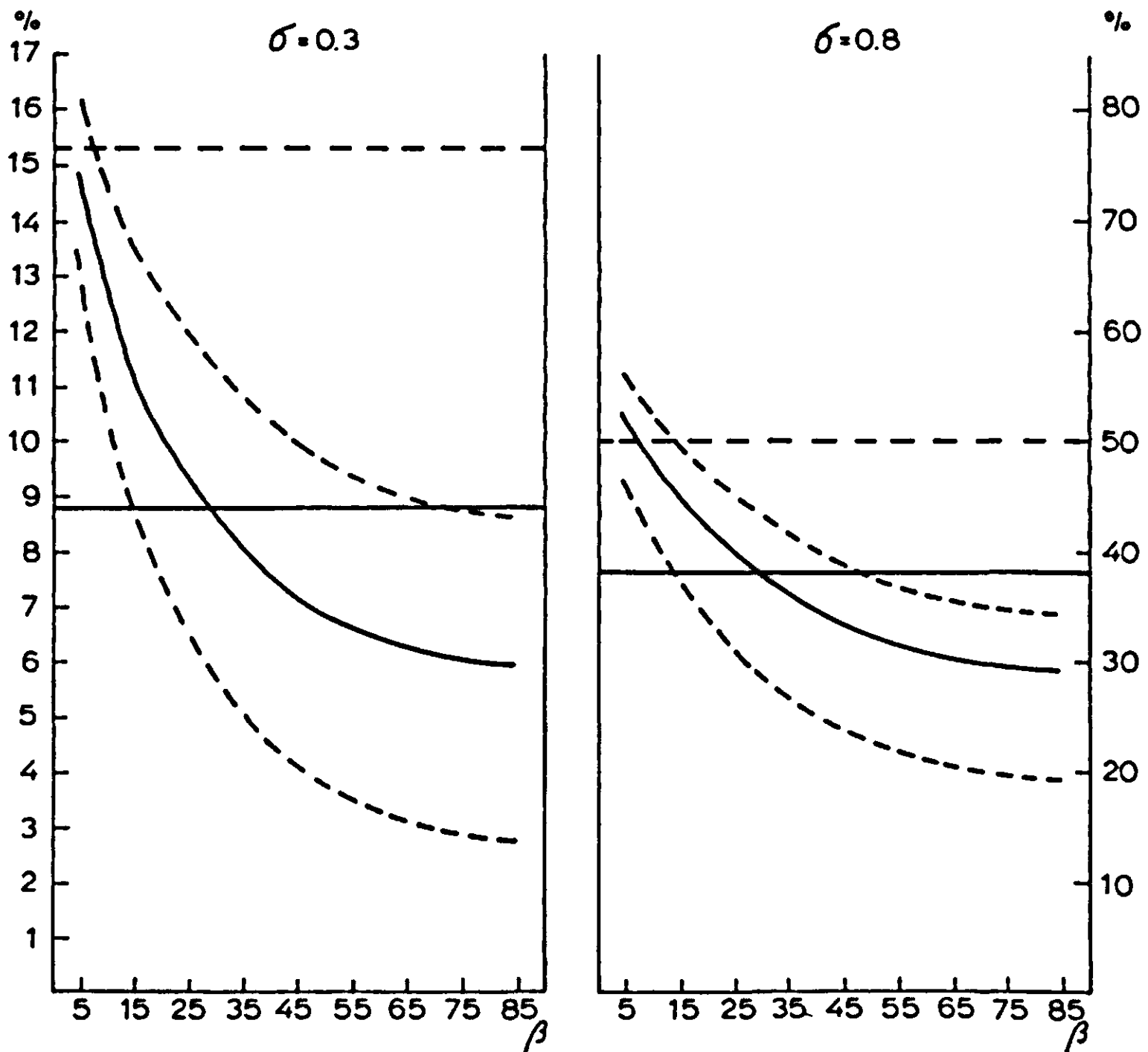


Fig. 12 | Computed reflection coefficients of a canopy as a function of the inclination of the direct incident radiation. For the solid lines the reflection and transmission coefficients of the leaves are equal, for the broken lines the leaves either only reflect (upper lines) or only transmit (lower lines). The curved lines give the results for a spherical leaf angle distribution and the horizontal lines for a horizontal leaf angle distribution. In the last case the reflection of the canopy is zero, when the leaves only transmit radiation.

an exponential curve exceeds 5%, the value is omitted. In general a shift from transmission to reflection of the individual leaves, the sum of them remaining equal, will increase both the reflection and extinction coefficients of the canopy. This effect is stronger, the smaller the inclination of the leaves. With vertical leaves it makes no difference whether the leaves reflect or transmit. For a spherical leaf angle distribution the effect of the shift of scattering to one side of a leaf is rather small. The shift to only reflecting

Table 10 Extinction coefficient of the exponential curve with the best fit. The conditions are the same as for Table 9.

ρ	τ	$\beta = 5^\circ$	$\beta = 25^\circ$	$\beta = 45^\circ$	$\beta = 65^\circ$	$\beta = 85^\circ$
0.3	0.0		1.097	0.675	0.532	0.485
0.0	0.3		0.966	0.602	0.487	0.436
0.8	0.0		0.575 ¹	0.409	0.336	0.311
0.0	0.8			0.292	0.244	0.226

¹ The maximum deviation between the exponential curve and the curve found by the numerical model has a value between 3 and 5 percent.

leaves results in a maximum increase in K of 0.04 and in ρ_c of 0.05 in the near-infrared region and 0.03 in the visible region. When the leaves only transmit the shift is larger. K decreases maximally by 0.08 and ρ_c maximally by 0.10 in the near-infrared region and by 0.04 in the visible region. Most leaves are intermediate between the case of $\tau = \rho$ and the case of only reflecting thick leaves. When ρ is only 20% larger than τ the idealization to $\tau = \rho$ has a negligible effect. When the difference is larger, the model described in this section should be used. The program is listed in Section 5.6.

2.4.3 *The influence of spatial correlation of leaf positions*

The distribution of leaves in space may range from very regular through random to a strongly clustered one. The equation derived so far hold for a random spatial distribution only. A deviation in either sense will influence both the reflection and extinction coefficients. This influence can be investigated for horizontal leaves.

Regular positions (or negatively clustered)

This term means that there are layers of leaves in which the internal shading is less than that for the random leaf arrangement. Since the leaves seem to avoid each other's presence, they are negatively clustered. De Wit (1965) mimicked this situation by increasing the leaf area index per sublayer L_s . In the extreme case L_s equals one, so that the sublayers form horizontal sheets without holes. It can be

derived that below every sheet radiation levels are reduced by a factor M , given by

$$M = \frac{1 - (1 - \sigma^2)^{0.5}}{\sigma} \quad (2.99)$$

The apparent extinction coefficient is thus given by

$$K_{app} = \ln \left\{ \frac{\sigma}{1 - (1 - \sigma^2)^{0.5}} \right\} \quad (2.100)$$

The equation for the reflection coefficient is

$$\rho_c = \frac{\sigma}{1 + (1 - \sigma^2)^{0.5}} \quad (2.101)$$

In comparison with the random arrangement of leaves (Table 11), both the extinction and reflection coefficients are increased.

Table 11 The calculated extinction and reflection coefficient for a regular, a random and a clustered leaf arrangement. In the last situation the reflection and transmission coefficients of the clusters are given as well.

Regular	$\sigma = 0.2$	$\sigma = 0.8$
K_{app}	2.29	0.693
ρ_c	0.101	0.500
Random		
K	0.894	0.447
ρ_c	0.056	0.382
Clustered		
ρ_{cl}	0.046	0.240
τ_{cl}	0.408	0.581
K_{app}	0.590	0.344
ρ_c	0.040	0.315

Clustered positions

In this case the internal shading in a layer is larger than that for the random leaf arrangement. It can be studied by considering groups of leaves as new elements of the canopy, for example needled twigs in a spruce canopy. The reflection and transmission of such a cluster (Eqns (2.26) and (2.27)) are given by

$$\rho_{cl} = \frac{\rho_h \{1 - \exp(-2 K L_c)\}}{1 - \rho_h^2 \exp(-2 K L_c)} \quad (2.102)$$

$$\tau_{cl} = \frac{(1 - \rho_h^2) \exp(-K L_c)}{1 - \rho_h^2 \exp(-2 K L_c)} \quad (2.103)$$

where L_c is the leaf area index of the cluster, and ρ_h and K are given by the Eqns (2.21) and (2.20). These clusters may now be considered as leaves with an unequal reflection and transmission coefficient, so that for the transmission of the whole canopy the Eqns (2.22) and (2.23) may be used. For simplicity L_c is taken as unity. The resulting extinction and reflection coefficients when σ is 0.2 and 0.8 are given in Table 11. It is evident that both coefficients are decreased in comparison with those for the random arrangement.

It is thus concluded that over the whole range from negative to positive clustering the reflection and extinction coefficients will decrease, the optical properties of the leaves remaining equal. This effect is probably one of the main reasons why heather, gorse and different types of woodland reflect less (about 0.16) than pastures and farm crops such as grains (about 0.23). It must be noted that broad-leaved species with a more regular leaf arrangement like sugar-beet, cucumber and bracken score even higher (0.26) (Monteith, 1973).

Clustering will also decrease the difference in transmission between visible and near-infrared radiation. For a random arrangement the ratio between the extinction coefficients is equal to 2, when the scattering coefficient is 0.2 for visible radiation and 0.8 for near-infrared. This ratio was found experimentally for barley by Rodskjer (1972). For sunflower Norman & Jarvis (1974) found a ratio of 2.5 between the amounts transmitted below a LAI of 2 in the near-infrared and visible regions. The difference between the extinction coefficients in

these regions is thus equal to $\frac{\ln(2.5)}{2} = 0.46$. For a random leaf ar-

rangement the theoretically calculated difference is 0.447 (Table 11) which is very close to the measured value.

For sitka pruce, however, Norman & Jarvis (1974) measured a ratio of only 1.3 under a LAI of 2. This means that the difference between the K values for near-infrared and visible radiation is reduced to only 0.13. This can be largely ascribed to the clustered leaf arrangement in sitka, as follows from Table 11. The calculated difference is 0.246 for the clustered leaf arrangement. Interception by woody material is responsible for the remaining difference between the reported 0.13 and the calculated 0.246, but is not the main factor.

2.4.4 *Plants in rows*

In the previous section it was seen that clustering of leaves decreases the extinction coefficient, so that more radiation falls on the ground. The same happens when plants are in rows, thus grouped in a regular pattern of clustering. In terms of light utilization this is a loss, but not one that should be taken too seriously as we will see later.

The geometric assumptions in this section are the following. The rows have a square cross-section, and within them the leaves are homogeneously distributed. The leaf angle distribution is taken as spherical. The azimuth of the sun and the row are both measured with respect to the south, with a positive sign to the west.

The azimuth of the sun is now given by

$$\alpha_s = \arcsin(\sin\gamma \cos\delta / \cos\beta) \quad (2.104)$$

where β is the height of the sun, δ the declination of the sun, and γ the hour angle given by

$$\gamma = 2\pi(t_h + 12)/24 \quad (2.105)$$

t_h should be expressed in true solar time in hours.

For completeness the equations for the inclination and the declination are given as well. They read:

$$\delta = \frac{-23.4 \pi}{180} \cos\{2\pi(t_d + 10)/365\} \quad (2.106)$$

where t_d is the number of the day in the year

$$\sin\beta = \sin\lambda \sin\delta + \cos\lambda \cos\delta \cos\{2\pi(t_h + 12)/24\} \quad (2.107)$$

where λ is the latitude of the site.

The azimuth of the row is denoted by α_r . The width of the shade, cast by a single row, can be calculated from

$$w_s = h_r \sin\{\text{abs}(\alpha_s - \alpha_r)\} / \text{tg}\beta \quad (2.108)$$

where h_r is the height of the row.

For convenience of notation, hereafter the symbol α (azimuth) will replace the difference in azimuths $\alpha_s - \alpha_r$. For the treatment of the interception of diffuse radiation by rows it is convenient to characterize the angular position of a point on the upper hemisphere by polar co-ordinates with the central axis parallel to the row (Fig. 13). In the co-ordinate system used so far, the central axis pointed through the zenith. The relations between the new azimuth $\bar{\alpha}$ and new inclination $\bar{\beta}$, and the old values are:

$$\sin\beta = \cos\bar{\alpha} \cos\bar{\beta} \quad (2.109)$$

$$\sin\bar{\beta} = \cos\alpha \cos\beta \quad (2.110)$$

There are two types of question about radiation and rows of plants. The first type concerns totals: how much radiation is absorbed by the rows and how large is the sunlit leaf area? The other type of question is about the distribution of direct and diffuse radiation over different

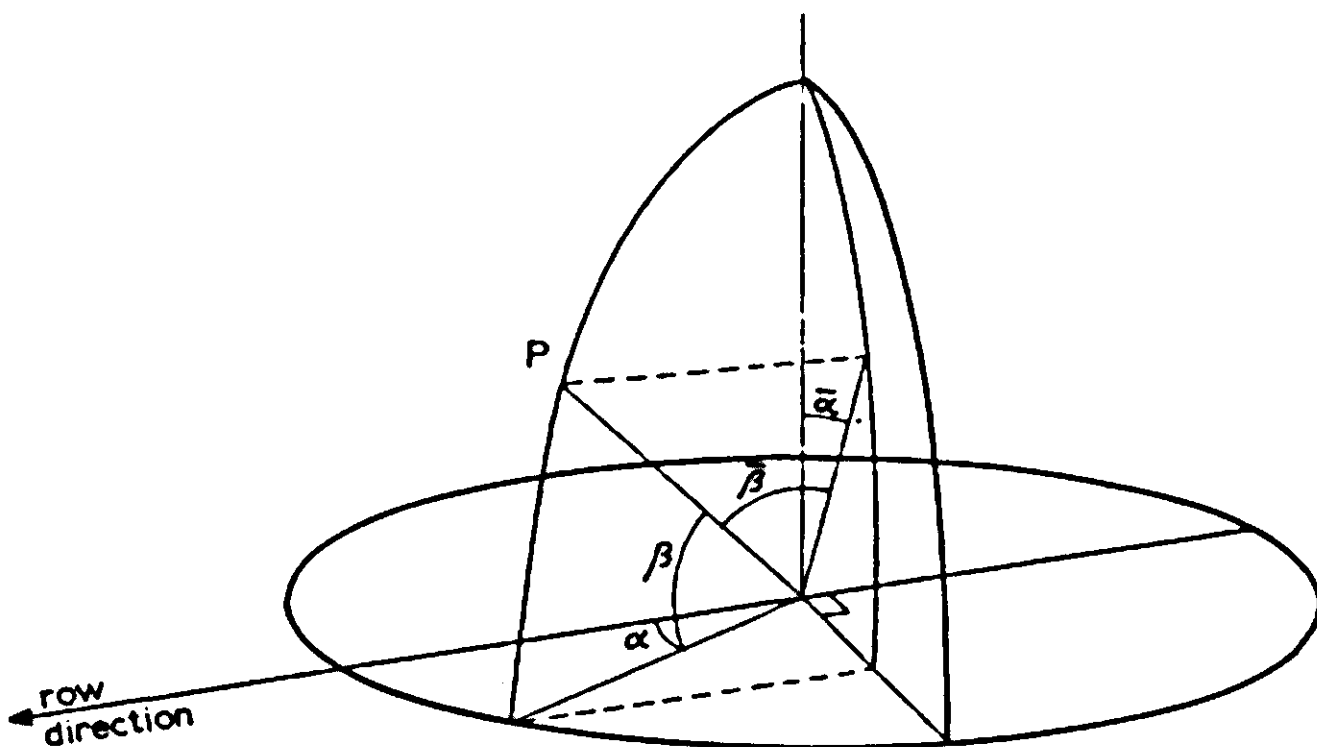


Fig. 13 | Two co-ordinate systems to characterize the position of a point P on the upper hemisphere. α and β are the azimuth and inclination in the normal polar co-ordinate system. The converted co-ordinates are provided with a bar.

parts of the rows. In principle the answer to the first type can be found by an integration of the solution of the second type, but this is far too complex. Approximate solutions are given for both questions but they are not entirely compatible.

Totals

The sunlit leaf area index in a single row can be calculated by integrating over the whole cross-section of the row of the expression:

$$LAI_s = \frac{1}{w_r} \int_0^{w_r} \int_0^{h_r} L_d \exp\{-\bar{O}(\beta) L_d l\} dx dy \quad (2.111)$$

where L_d is the leaf area density, l the path length of a solar ray from the point of entrance in the row to the point with the co-ordinates x and y . w_r is the width of the row.

For the characterization of the radiation geometry in the row the azimuth and inclination of the sun are converted according to Eqns (2.109) and (2.110) and Fig. 13. It follows from Eqns (2.109) and (2.110) that the tangent of the converted azimuth (Fig. 14) is given by

$$\operatorname{tg}\bar{\alpha} = \sin\alpha / \operatorname{tg}\beta \quad (2.112)$$

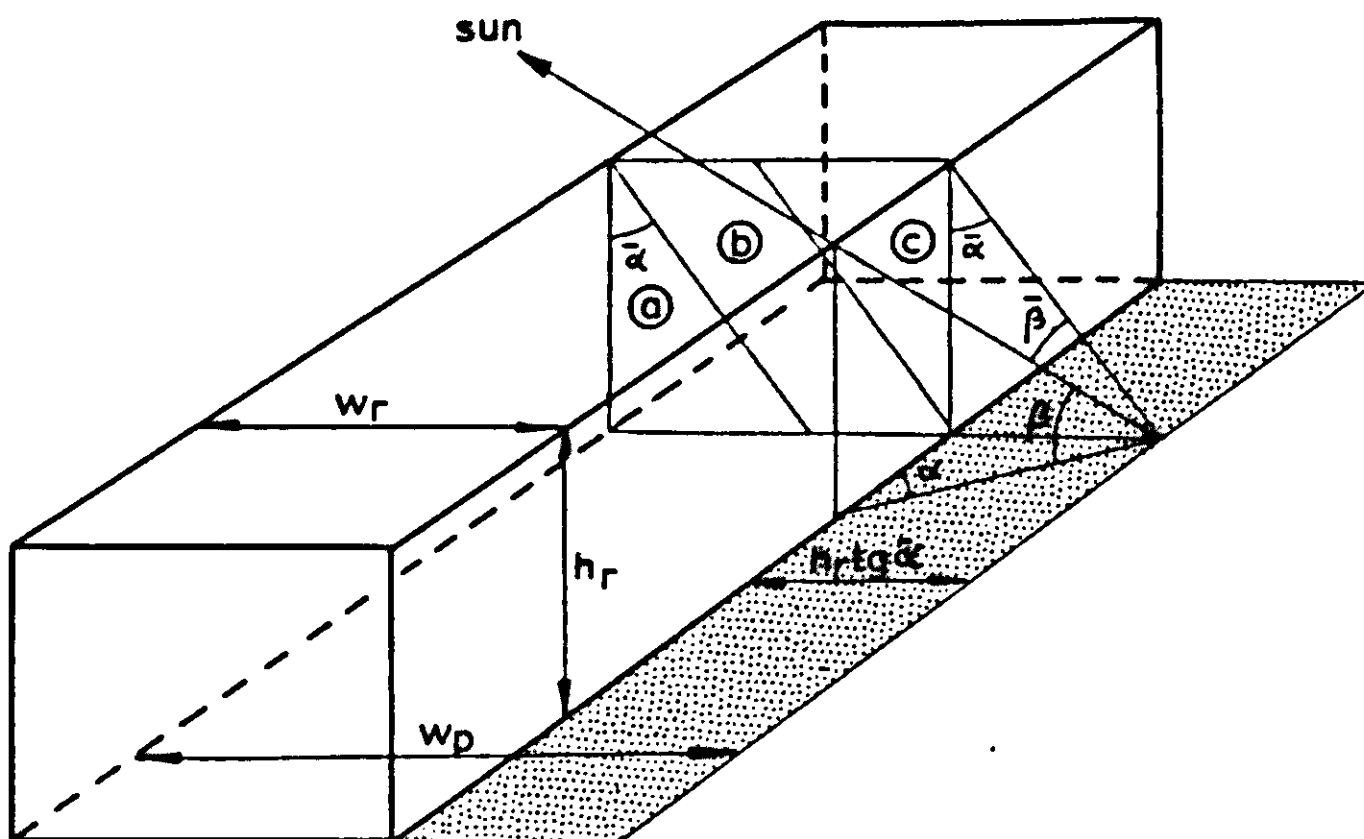


Fig. 14 | Radiation geometry of a row. The shaded width beside the row equals $h_r \operatorname{tg}\bar{\alpha}$. The polar co-ordinates of the sun are given in the normal and in the converted system.

Dependent on whether $h_r \text{tg} \bar{\alpha}$ is smaller than w_r or larger a different solution is obtained. In the first case, the shade of the sunlit side of the row falls entirely within the base of the row itself. The expression for LAI_s consists of the contributions of two triangles, (a and c in Fig. 14) which are essentially equal, and of a parallelogram, which can be treated as part of a homogeneous canopy (b in Fig. 14). The contribution of the two triangles is together:

$$\frac{2 \sin \beta h_r \text{tg} \bar{\alpha}}{\bar{O}(\beta) w_r} \left[1 - \frac{\sin \beta}{\bar{O}(\beta) LAI} \left\{ 1 - \exp \left(- \frac{\bar{O}(\beta) LAI}{\sin \beta} \right) \right\} \right] \quad (2.113)$$

and that of the parallelogram

$$\frac{\sin \beta}{\bar{O}(\beta)} \left(1 - \frac{h_r \text{tg} \bar{\alpha}}{w_r} \right) \left\{ 1 - \exp \left(- \frac{\bar{O}(\beta) LAI}{\sin \beta} \right) \right\} \quad (2.114)$$

When $h_r \text{tg} \bar{\alpha}$ is larger than w_r , the corresponding expression is

$$LAI_s = \frac{2 \sin \beta}{\bar{O}(\beta)} \left[1 - \frac{\sin \beta h_r \text{tg} \bar{\alpha}}{\bar{O}(\beta) LAI w_r} \left\{ 1 - \exp \left(- \frac{\bar{O}(\beta) LAI w_r}{\sin \beta h_r \text{tg} \bar{\alpha}} \right) \right\} \right] + \\ + \frac{\sin \beta h_r \text{tg} \bar{\alpha}}{\bar{O}(\beta) w_r} \left(1 - \frac{w_r}{h_r \text{tg} \bar{\alpha}} \right) \left\{ 1 - \exp \left(- \frac{\bar{O}(\beta) LAI w_r}{\sin \beta h_r \text{tg} \bar{\alpha}} \right) \right\} \quad (2.115)$$

The leaf area indices LAI and LAI_s refer both to row area only (paths excluded).

Now it is worthwhile to investigate whether these complicated expressions can be replaced by a simpler one, without too much loss of accuracy. As can be seen in Fig. 14, the total projected width of the row w_p is

$$w_p = w_r + h_r \text{tg} \bar{\alpha} \quad (2.116)$$

It seems a reasonable approximation to calculate LAI_s as the sunlit leaf area of a homogeneous canopy extending over the projected width w_p and with a corrected LAI of $LAI w_r/w_p$, so that the total leaf area remains the same.

In this approximation the width of the intercepted solar beam remains the same. In the extreme situation of a very low and wide row ($h_r \ll w_r$), it is obvious that such an approximation tends to the exact solution. In the extreme situation of a very high and narrow row ($h_r \gg w_r$), such as a single row of poplars, it may be surprising that the approximation tends to the exact solution as well. The exact solution is also obtained for the leaf area index tending either to zero or to infinity, irrespective

of h_r/w_r . For a homogeneous canopy the sunlit leaf area index is

$$LAI_s = \frac{\sin\beta}{\bar{O}(\beta)} \left\{ 1 - \exp\left(-\frac{\bar{O}(\beta)LAI}{\sin\beta}\right) \right\} \quad (2.117)$$

The approximation for a single row is now found by multiplying LAI by the ratio w_r/w_p , and by dividing the whole expression by the same ratio, because LAI_s should refer to the width of the row itself.

This leads to a simplified expression for LAI_s

$$LAI_s = \frac{w_p \sin\beta}{w_r \bar{O}(\beta)} \left\{ 1 - \exp\left(-\frac{\bar{O}(\beta)w_r LAI}{\sin\beta w_p}\right) \right\} \quad (2.118)$$

In Table 12 the results of this expression are compared with the exact one, for the sun perpendicular to the rows.

Table 12 The sunlit leaf area index, calculated with a numerical model (exact) and with a simple equation (Eqn (2.118)) for some different situations.

$\text{tg } \alpha$	h_r/w_r	LAI	Exact	Simple
Horizontal leaves				
1	1	0.5	0.401	0.422
1	1	1	0.657	0.716
1	1	2	0.942	1.070
Spherical leaf angle distribution				
1	1	0.5	0.446	0.458
1	1	1	0.801	0.842
1	1	2	1.315	1.434
1	0.5	0.5	0.434	0.445
1	0.5	1	0.759	0.797
1	0.5	2	1.193	1.295
2	1	0.5	0.446	0.456
2	1	1	0.802	0.835
2	1	2	1.314	1.410
2	0.5	0.5	0.419	0.436
2	0.5	1	0.712	0.766
2	0.5	2	1.074	1.204

The simple expression slightly overestimates the sunlit leaf area, but its results are still quite acceptable. Moreover, the examples listed represent the worst situations.

So far, the expressions referred to a single row. For normal conditions, when rows alternate with paths, the projected width w_p cannot exceed the distance between the centres of the rows so that w_p must then be expressed as

$$w_p = w_r + \min(p, h_r \tan \bar{\alpha}) \quad (2.119)$$

where p is the width of the path.

Thus in general, Eqn (2.118) must be used in combination with Eqn (2.119).

Total absorbed diffuse light

This amount can formally be found by integrating the above expression for LAI , over the whole upper hemisphere and weighting the radiance distribution of the sky. This laborious method can, however, be replaced by a simpler one. Each side of a vertical surface element will receive half the irradiance of the upper side of a horizontal element, at least under a UOC. Thus a fully black row with an infinitely high LAI absorbs the same amount of radiation as a black horizontal strip with a width of $w_r + h_r$, the width of the row plus its height. This now leads to the following approximation for a single row

$$H_d = S_d \frac{(w_r + h_r)}{w_r} \left[1 - \exp \left\{ -0.81 LAI \frac{w_r}{(w_r + h_r)} \right\} \right] \quad (2.120)$$

where H_d is the absorbed diffuse radiation per unit row area. The value 0.81 for the extinction coefficient was found in Section 2.3.3 (Table 5) for diffuse radiation, black leaves and a spherical leaf angle distribution. In Table 13 the results of this approximation are compared with the more exact numerical integration results (upper values). The approximate Eqn (2.120) appears to be good enough.

Two extensions must still be considered.

In the first place rows do not usually occur alone, but next to each other. For black, non-transmitting rows the irradiance on a point in the path is given by an integral of $N \sin \beta \cos \bar{\beta} d\bar{\alpha} d\bar{\beta}$ (cf. Eqns (2.7), (2.8), Fig. 13) between the appropriate boundaries. The converted inclination $\bar{\beta}$ runs from $-\pi/2$ to $\pi/2$ in all cases. The boundaries of the converted azimuth $\bar{\alpha}$ depend on the width of the path p and on the

Table 13 The absorbed radiation per row width, calculated with a numerical model (higher numbers of each pair) and with Eqn (2.120). The leaf angle distribution is spherical and the leaves are black. The incoming radiation is diffuse, and there is only one row.

LAI_z	LAI_l (lateral)				
	0.2	0.5	1	2	5
vertical					
0.2	0.196	0.184	0.178	0.174	0.169
	0.157	0.153	0.152	0.151	0.150
0.5	0.482	0.418	0.400	0.385	0.366
	0.382	0.367	0.355	0.346	0.339
1.0	0.824	0.780	0.727	0.665	0.606
	0.758	0.710	0.666	0.626	0.589
2.0	1.562	1.482	1.312	1.135	0.950
	1.506	1.384	1.252	1.110	0.960
5.0	4.004	3.600	2.946	2.349	1.627
	3.750	3.388	2.945	2.400	1.736

distance x of the point considered from the edge of the path. The boundaries are given by (Fig. 15)

$$\bar{\alpha}_1 = \text{arctg}\left(\frac{x-p}{h_r}\right) \quad (2.121)$$

$$\bar{\alpha}_2 = \text{arctg}\left(\frac{x}{h_r}\right) \quad (2.122)$$

The integral of the irradiance can be written as (Eqn 2.109).

$$S = \int_{-\pi/2}^{\pi/2} \int_{\bar{\alpha}_1}^{\bar{\alpha}_2} N \cos\bar{\alpha} \cos\bar{\beta} \cos\bar{\beta} \, d\bar{\alpha} \, d\bar{\beta} \quad (2.123)$$

or

$$S = \frac{\pi}{2} \int_{\bar{\alpha}_1}^{\bar{\alpha}_2} N \cos \bar{\alpha} \, d\bar{\alpha} \quad (2.124)$$

or

$$S = \frac{\pi}{2} N (\sin \bar{\alpha}_2 - \sin \bar{\alpha}_1) \quad (2.125)$$

Since the irradiance on a horizontal surface above the canopy equals πN , the relative irradiance I is given by

$$I = \frac{1}{2} (\sin \bar{\alpha}_2 - \sin \bar{\alpha}_1) \quad (2.126)$$

Substitution of $\bar{\alpha}_1$ and $\bar{\alpha}_2$ from Eqns (2.121) and (2.122) and integration of I with respect to x between the boundaries zero and p gives the average relative irradiance of the path, after division by p :

$$I_p = \frac{(h_r^2 + p^2)^{0.5} - h_r}{p} \quad (2.127)$$

The radiation falling on the path is lost for photosynthesis. The relative loss of radiation, weighted for the total width of row and path together is $pI_p/(w_r + p)$. In Table 14 some values of the relative loss are given, assuming that $w_r = p$.

These numbers apply to non-transmitting rows, that means with a very high LAI and black leaves. More generally spoken the absorbed radiation is given by

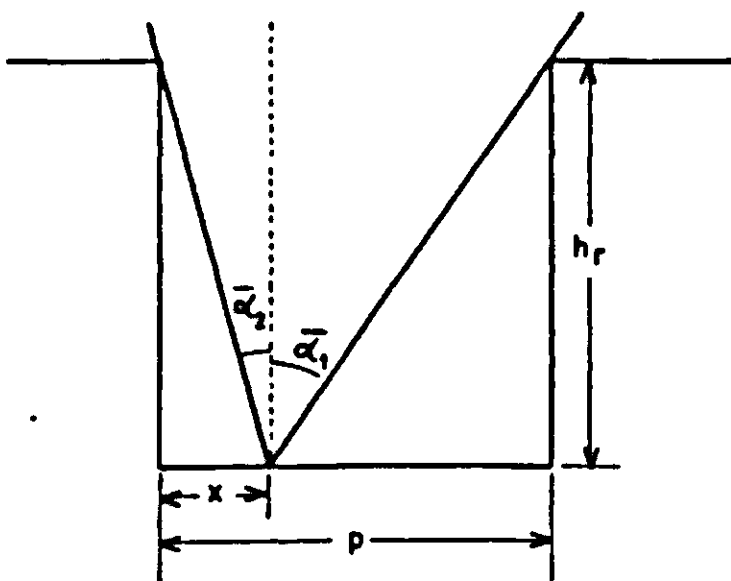


Fig. 15 | Boundaries of the part of the sky seen from a point at the bottom of the path between two rows.

$$H_d = S_d \frac{(w_r + \Delta w_r)}{w_r} \left\{ 1 - \exp\left(-0.81LAI \frac{w_r}{w_r + \Delta w_r}\right) \right\} \quad (2.128)$$

where Δw_r accounts for a row intercepting more radiation per row area than a homogeneous canopy per ground area. In Eqn (2.120) (a single row) the apparent increase Δw_r was equal to the height of the row h_r . This is the maximum possible value. When the rows are next to each other, the apparent increase of each is reduced and approaches p for a very narrow spacing. H_d can also be expressed in the radiation lost to the bottom of the path as

$$H_d = S_d \left\{ \frac{w_r + p(1 - I_p)}{w_r} \right\} \quad (2.129)$$

Thus for non-transmitting rows (Eqn 2.127) Δw_r is given by

$$\Delta w_r = p + h_r - (p^2 + h_r^2)^{0.5} \quad (2.130)$$

Table 14 The fraction of the diffuse incoming radiation, lost to the ground and absorbed by the rows, for black leaves, a very high leaf area density and row and path width the same.

h_r/p	fraction lost	fraction absorbed
0.1	0.45	0.55
0.2	0.41	0.59
0.5	0.31	0.69
1.0	0.21	0.79
2.0	0.12	0.88

For transmitting rows the loss of radiation to the paths can be assessed by comparing the absorbed radiation per total ground area for a homogeneous canopy with that for a crop in rows with the same leaf area index. This comparison is done in Table 15 for $h_r = p$ and $K = 0.81$ (spherical leaf angle distribution, black leaves).

Hence, the efficiency of light interception is not reduced much by cultivation in rows.

The other extension concerns non-black leaves and consequently

Table 15 The fraction of the diffuse incoming radiation, absorbed by a crop in rows and by a homogeneous canopy with the same leaf area index per total ground area, and with black leaves. For the crop in rows the height h_r is taken equal to the width of the path p .

LAI	in rows	homogeneous
0.5 (sparse)	0.317	0.333
1.	0.507	0.555
2.	0.690	0.802
5. (dense)	0.788	0.983
∞	0.79 ¹	1.000

¹ Compare with Table 14, $h_r/p = 1$

lower values for the extinction coefficients. For this situation no computations were made. Therefore it is assumed that as a first order approximation the equations derived so far may be applied, with the substitution of the extinction and reflection coefficients found for homogeneous canopies with scattering leaves. Further development on this point is still necessary.

Distribution of diffuse radiation

For diffuse light there is not such an easy and convenient concept as the sunlit leaf area. The average irradiance of the leaves at any point must be found by integrating the contributions from the upper hemisphere. For a spherical leaf angle distribution and a UOC, the average irradiance on a leaf is given by

$$I = S_d \frac{1}{\pi} \int_{-\pi/2}^{\pi/2} \int_{-\pi/2}^{\pi/2} \exp(-0.5l) \cos \bar{\beta} \, d\bar{\beta} d\bar{\alpha} \quad (2.131)$$

where l is the path length, that the light must travel inside the row to a point at a depth z from the top of the row and at a horizontal distance w from the side of the row. l is calculated as:

$$l = z/(\cos \bar{\beta} \cos \bar{\alpha}) \quad (2.132)$$

when a light ray enters the upper horizontal boundary, and as

$$l = w/(\cos \bar{\beta} \sin \bar{\alpha}) \quad (2.133)$$

when it enters the side.

First the distribution of the light near the edge of a field is studied, so that light entering from the other side can be neglected. In other words, only one side of an infinitely wide row is considered. Numerical integration of Eqn (2.131) gives the results presented in Table 16 as the upper value of each pair. The lower value of each pair is found by an approximation, which consists of the following elements. First the relative downward flux under an UOC in a homogeneous canopy with black leaves and a spherical leaf angle distribution is approximated by

$$\varphi_d = \exp(-0.81LAI'_z) \quad (2.134)$$

where LAI'_z is the LAI per row area reckoned from above.

Table 16 Average irradiance of the leaves as a function of the vertical and lateral distance from the edge. The leaves are black, the leaf angle distribution is spherical and the incoming radiation is diffuse. LAI'_z stands for vertical distance and LAI'_x for lateral distance. The upper value of each pair is found by a numerical model, and the lower value by Eqn (2.136).

LAI'_z	LAI'_x							
	0	0.1	0.2	0.5	1.	2.	5.	∞
0.1	0.914	0.873	0.860	0.845	0.836	0.830	0.828	0.828
	0.849	0.841	0.834	0.815	0.793	0.767	0.749	0.747
0.2	0.861	0.808	0.785	0.756	0.739	0.728	0.723	0.723
	0.815	0.805	0.796	0.773	0.745	0.714	0.691	0.689
0.5	0.760	0.690	0.653	0.596	0.557	0.531	0.519	0.518
	0.726	0.712	0.699	0.664	0.623	0.577	0.543	0.540
1.	0.663	0.585	0.541	0.461	0.398	0.353	0.329	0.327
	0.619	0.599	0.581	0.533	0.476	0.412	0.365	0.360
2.	0.574	0.491	0.441	0.347	0.263	0.194	0.153	0.149
	0.500	0.474	0.450	0.387	0.312	0.228	0.166	0.160
5.	0.510	0.424	0.372	0.270	0.176	0.089	0.028	0.020
	0.426	0.382	0.354	0.280	0.192	0.093	0.021	0.014
∞	0.500	0.414	0.361	0.259	0.163			
	0.405	0.373	0.344	0.270	0.180			

The light intensity absorbed per leaf area I_z is found as the derivative of φ_d with respect to LAI'_z . Near the edge some light must be added, coming from the side. Since each side of a vertical plane under a UOC receives half the irradiance of a horizontal plane, the contribution from the side can be estimated as

$$I_x = \frac{d}{d LAI'_x} \{0.5 \exp(-0.81 LAI'_x)\} \quad (2.135)$$

where LAI'_z is the leaf area index in the horizontal direction, reckoned from the side of the field. Both contributions are now added in the following way:

$$I = I_z + I_x - I_z I_x \quad (2.136)$$

This ensures linear addition for low values of I_z and I_x , but a saturation level at unity. This approximation is compared with the results of the numerical integration in Table 16 and given as the lower value of each pair. The approximation tends to overestimate the irradiation of the leaves in the bulk of the canopy, and to underestimate near the edges, but for most purposes it will be good enough. It can also be seen in Table 16 (broken line) how far the boundary effect of radiation penetrates from the side into a canopy. When the rather arbitrary criterion is used that a boundary effect exists as long as the additional light from aside exceeds 5 percent of the value from above, the boundary effect penetrates roughly spoken as far as the vertical depth considered. For an average LAI'_z of 2 the average depth of lateral penetration of the boundary effect will also be about 2. For a maize crop this is about two metres, and for a wheat crop about one metre. The results of the approximating method near the edge are sufficiently reassuring to use it in rows. In a row three terms must be added as:

$$I = I_z + I_{x1} + I_{x2} - I_z I_{x1} - I_z I_{x2} - I_{x1} I_{x2} + I_z I_{x1} I_{x2} \quad (2.137)$$

I_z is given by $0.81 \exp(-0.81 LAI'_z)$. For a single row I_{x1} and I_{x2} equal $0.5 \times 0.81 \exp(-0.81 LAI'_x)$ and $0.5 \times 0.81 \exp\{-0.81 (LAI \frac{w_r}{h_r} -$

$LAI'_x)\}$ where $LAI \frac{w_r}{h_r}$ is the total lateral leaf area index of the row.

In Table 17 the result of Eqn (2.137) (lower value) is compared with numerical integration results (upper values). Deeper than $LAI'_z = 1$

Table 17 Average irradiance of the leaves as a function of their position in a single row with a LAI_1 of 2. For the rest the conditions are the same as for Table 16.

LAI'_z	LAI'_x				
	0	0.1	0.2	0.5	1.
0.1	0.917	0.890	0.863	0.849	0.844
	0.862	0.857	0.850	0.838	0.830
0.2	0.867	0.814	0.792	0.765	0.755
	0.830	0.822	0.815	0.800	0.791
0.5	0.772	0.704	0.670	0.618	0.596
	0.748	0.737	0.727	0.705	0.691
1.	0.689	0.614	0.572	0.503	0.470
	0.650	0.634	0.620	0.589	0.570
2.	0.619	0.540	0.495	0.417	0.378
	0.540	0.520	0.501	0.461	0.436

the contribution from the other side gives an appreciable increase, compared with an edge (Table 16). The approximating equation gives again reasonable results.

For an ensemble of rows the maximum of the lateral contribution is not 0.5 but less. The relative irradiance on a vertical surface element of the side of a row is approximately given by

$$I_s = [1 - \sin\{\arctg(h_r - z)/p\}]/2 \quad (2.138)$$

where z is the height of the element.

In this expression it is assumed that the adjacent row transmits no radiation at all. For instance, when h_r equals p , the relative irradiance decreases from 0.5 at the top to 0.15 at the bottom. For an ensemble of rows, Eqn (2.138) must be used to replace 0.5 in the expression for I_{x1} and I_{x2} .

For some applications these rather sophisticated calculations can be replaced by much simpler ones. For instance, it can be assumed that the leaves are either illuminated like those at the top or are entirely in the dark. The leaf area of the illuminated leaves must be chosen such that the total absorbed radiation is still correct. For many purposes this approximation is good enough (Rabbinge, 1976).

2.5 List of symbols used in Chapter 2

symbol	description	first used in eqn	unit	name in program
A	area	2.89	m^2	
B	Total radiant flux emitted per unit area of a full radiator	2.64	$\text{J m}^{-2} \text{s}^{-1}$	
B_n	Net thermal radiation (B)	2.65	$\text{J m}^{-2} \text{s}^{-1}$	LWR, NLWRS
B_l	Zonal distribution of radiation scattered by a sublayer of leaves	2.35	–	BL
B_u	Zonal distribution of sky radiation (UOC), isotropic distribution	2.32, page	–	BU
B_s	Zonal distribution of sky radiation for a standard overcast sky (SOC)	page	–	BS
F	Leaf inclination distribution	2.4	–	F
h_r	Height of the row	2.108	m	
H_d	Absorbed diffuse radiation per unit row area	2.120	$\text{J m}^{-2} \text{s}^{-1}$	
I_t	Total intercepted fraction of radiation per layer of leaves	2.37	–	INTER
I	Relative irradiance as fraction of the global irradiance	2.126	–	
I_p	Relative irradiance on a path	2.127	–	
I_s	Relative irradiance on the side of a row	2.138	–	
I_z	Average relative irradiance of the leaves from the vertical direction	2.136	–	
I_x	Average relative irradiance of the leaves from a lateral direc- tion	2.135	–	
j	Running index for a leaf layer	2.15	–	J, I
K	Extinction coefficient for radiation	2.18	m^2 ground m^{-2} leaf	K

symbol	description	first used in eqn	unit	name in program
K_b	Extinction coefficient for direct radiation and black leaves	2.33	m^2 ground m^{-2} leaf	KB, KDR
$K_{b,d}$	Extinction coefficient for diffuse radiation and black leaves	2.68	m^2 ground m^{-2} leaf	KBDF
K_d	Extinction coefficient for diffuse radiation	2.41	m^2 ground m^{-2} leaf	KDFV, KDFN
K_r	Extinction coefficient derived from a simple formula	2.40	m^2 ground m^{-2} leaf	
K_h	Extinction coefficient when the leaves are horizontal	2.20	m^2 ground m^{-2} leaf	
K_m	Extinction coefficient as found by the numerical model	Table 5	m^2 ground m^{-2} leaf	KM
\hat{K}_m	Result of a regression between K_m and K_r (an estimation for K_m)	2.42	m^2 ground m^{-2} leaf	KDN, KDV, KDRN, KDRV
l	Path length of a ray inside a row	2.111	m	
L_d	Leaf area density	2.111	m^2 leaf m^{-3} air	LAID
L_s	Leaf area index of a sublayer	2.15	m^2 leaf m^{-2} ground	LAI, LS
LAI	Leaf area index (total)	2.24	m^2 leaf m^{-2} ground	LAI
LAI'	Current LAI	2.33	m^2 leaf m^{-2} ground	LAI
LAI_1	total LAI of a row in lateral direction	Table 13	m^2 leaf m^{-2} side area	
LAI_s	Sunlit leaf area index	2.111	m^2 leaf m^{-2} ground	
m	Total number of leaf layers	2.31	–	NUMLL, MAX
M	Reduction factor per sublayer	2.16	–	
M_i	Fraction intercepted by a sub-layer	2.28	–	MI

symbol	description	first used in eqn	unit	name in program
M_t	Fraction transmitted by a sub-layer	2.29	—	MT
N	Radiance	2.7	$\text{J m}^{-2} \text{sr}^{-1} \text{s}^{-1}$	
N_d	Radiance of a reflecting surface under diffuse irradiation	2.58	$\text{J m}^{-2} \text{sr}^{-1} \text{s}^{-1}$	
$N_{r,\rho}$	Relative radiance for reflected radiation	2.51	sr^{-1}	
N_z	Radiance in the zenith of the sky	2.12	$\text{J m}^{-2} \text{sr}^{-1} \text{s}^{-1}$	
$O(\beta,\lambda)$	Projection of leaves with inclination λ into inclination β	2.2	—	
$\bar{O}(\beta)$	Projection of leaves into inclination β averaged over the leaf inclination distribution	2.4	—	OAV
R_t	Net thermal radiation per leaf area	2.68	$\text{J m}^{-2} \text{s}^{-1}$	LWR
p	Width of the path between rows	2.119	m	
S	Downward radiant flux	2.7	$\text{J m}^{-2} \text{s}^{-1}$	
S_b	Direct radiant flux (visible or near-infrared) on a horizontal surface under a clear sky	2.33, fig. 1	$\text{J m}^{-2} \text{s}^{-1}$	SUNDCL
S_d	Downward diffuse visible radiant flux	2.11	$\text{J m}^{-2} \text{s}^{-1}$	
$S_{d,c}$	Downward diffuse visible radiant flux under a clear sky	fig. 1	$\text{J m}^{-2} \text{s}^{-1}$	DIFCL
$S_{d,o}$	Downward diffuse visible radiant flux under an overcast sky	fig. 1	$\text{J m}^{-2} \text{s}^{-1}$	DIFOV
S_p	Direct radiant visible flux, perpendicular to the solar beam	2.88	$\text{J m}^{-2} \text{s}^{-1}$	SUNPER
t_h	Time in hours	2.105	h	
T_a	Air temperature	2.67	$^{\circ}\text{C}$	TA
T_l	Leaf temperature	2.68	$^{\circ}\text{C}$	TL
T_m	Mean temperature of two radiating surfaces	2.69	$^{\circ}\text{C}$	

symbol	description	first used in eqn	unit	name in program
T_{sky}	Apparent sky temperature	2.67	°C	SKTCL, SKTOV
T_{soil}	Soil surface temperature	2.68	°C	TS
w_p	Projected width of a row	2.116 fig. 14	m	
w_r	Width of row	2.111	m	
w_s	Width of shade, cast by a row	2.108	m	
α	Absorption coefficient per particle	2.71	–	
α	Azimuth of an incident ray	2.1	rad	
$\bar{\alpha}$	Azimuth of an incident ray in a converted coordinate system	2.109, fig. 13	rad	
α'	Azimuth of an emitted or scattered ray	2.54	rad	
α_c	Azimuth of a ray for which the sine of incidence is zero	2.92	rad	ACKK
α'_c	Azimuth of a ray for which the sine of emission or scattering is zero	2.94	rad	ACK
α_s	Azimuth of the sun	2.104	rad	
α_r	Azimuth of a row	2.108	rad	
β	Inclination of an incident ray or its index	2.1	rad	K, KK
β'	Inclination of a scattered ray or its index	2.32	rad	K
$\bar{\beta}$	Inclination of an incident ray in a converted coordinate system	2.109, fig. 13	rad	
γ	Hour angle	2.104	rad	
δ	Declination of the sun	2.104	rad	
θ	Angle of incidence on a surface element	2.1	rad	
ξ	Distribution function for reflection and transmission	2.86	–	KSI
λ	Leaf inclination or its index	2.1	rad	IL

symbol	description	first used in eqn	unit	name in program
λ	Latitude of the site	2.107	rad	LAT
ψ	Radiant energy flow	2.89	J s^{-1}	
φ_d	Radiant downward flux	2.15	$\text{J m}^{-2} \text{s}^{-1}$	PHID
φ_u	Radiant upward flux	2.15	$\text{J m}^{-2} \text{s}^{-1}$	PHIU
ρ	Reflection coefficient of leaves	2.15	$\text{J m}^{-2} \text{s}^{-1}$	RHO
ρ_c	Reflection coefficient of a canopy	section 2.3.4	$\text{J m}^{-2} \text{s}^{-1}$	
ρ_h	Reflection coefficient of a canopy with horizontal leaves	2.21	–	REFV, REFN
ρ_f	Reflection coefficient of the canopy according to a simple formula	2.44	–	
ρ_m	Reflection coefficient of the canopy according to the numerical model	Table 6	–	
$\hat{\rho}_m$	Reflection coefficient of the canopy, estimated by a regression between ρ_m and ρ_f	2.46	–	
ρ_s	Reflection coefficient of the soil surface	2.25	–	RHOS
ρ_{cl}	Reflection coefficient of a cluster of leaves	2.102	–	
τ	Transmission coefficient of the leaves	2.15	–	TAU
τ_{cl}	Transmission coefficient of a cluster of leaves	2.103	–	
σ	Scattering coefficient of the leaves	2.20	–	SC
σ_n	Scattering coefficient in the near-infrared region	Section 2.3.4	–	SCN
σ_v	Scattering coefficient in the visible region	Section 2.3.4	–	SCV
σ	Stefan-Boltzmann constant	2.64	$\text{J m}^{-2} \text{s}^{-1} \text{K}^{-4}$	SIGMA
σ'	Effective Stefan-Boltzmann constant	2.69	$\text{J m}^{-2} \text{s}^{-1} \text{K}^{-4}$	

symbol	description	first used in eqn	unit	name in program
χ_L	Index, characterizing the leaf inclination distribution	2.47		
ω	Solid angle	2.7	sr	

3 Energy and mass balances

3.1 Introduction

A main problem in micrometeorology is the distribution of the available radiant energy, first between the soil and the plant organs, and second between transpiration, sensible heat loss, heat storage and photosynthesis.

Section 3.2 gives some relations to calculate the energy balance for single leaves, and the relation between photosynthesis and transpiration. In the next section the energy balance equations for the soil surface are presented. Section 3.4 shows how the theory about the radiation from the previous chapter is used to calculate the distribution of the available radiant energy over the leaves in the different canopy layers. Finally (Section 3.5) the equations are discussed for the transport in the air inside the vegetation of the heat and moisture produced by the leaves and by the soil. Simplifications for sparse canopies are indicated.

3.2 Single leaves

The radiant energy which is absorbed by the leaves is generally partitioned between heat storage, heat loss to the air, transpiration and photosynthesis. Since the time constant of heat storage in a leaf is small, of the order of a hundred seconds, equilibrium with the ambient air is soon reached and the storage term in the energy balance can be neglected.

The value of the boundary layer resistance between the leaf and the surrounding air is of primary importance for the other processes, which generally involve exchange of heat and mass. The boundary layer resistance for heat is related to the Nusselt number Nu , the diffusivity for heat in the air D_h and a characteristic leaf dimension w (taken as the width of the leaves) as

$$r_{b,h} = \frac{0.5w}{D_h Nu} \quad (3.1)$$

The factor 0.5 accounts for the resistance of the two sides of a leaf being connected in parallel. According to Monteith (1973), Nusselt number is almost the same for isothermal surfaces, such as metal plates, and surfaces with a uniform flux over the whole area as is probably the case with leaves. The mean Nusselt number for the whole surface is given by

$$Nu = aRe^{1/2}Pr^{1/3} \quad (3.2)$$

where a is an empirical constant, Re is Reynolds number and Pr Prandtl number, which are defined as

$$Re = uw/v \quad (3.3)$$

and

$$Pr = \nu/D_h \quad (3.4)$$

According to Pearman et al. (1972) the constant a has an average value of 1.1 under field conditions. This is about 1.5 times as large as the value of 0.66, which is normally found in wind tunnel experiments. This enlargement is due to the turbulence of the wind under field conditions. Using the values of the air properties at 20°C and the value of 1.1 for a , we can write Eqn (3.1) as:

$$r_{b,h} = 0.5 \times 1.8 \times 10^2 \times \left(\frac{w}{u}\right)^{0.5} \quad (3.5)$$

where u is the local wind speed in m s^{-1} .

From Eqn (3.2) we notice that the boundary layer resistance is proportional to $D^{-2/3}$. Hence the resistances for water vapour and carbon dioxide can be calculated from the one for heat by multiplication by $(D_v/D_h)^{-2/3}$ and $(D_c/D_h)^{-2/3}$, respectively:

$$r_{b,v} = 0.93r_{b,h} \quad (3.6)$$

$$r_{b,c} = 1.32r_{b,h} \quad (3.7)$$

For the leaf resistance it is assumed that the main transport occurs via the stomata, so that the ratio between the leaf resistances for water vapour and for carbon dioxide is equal to the ratio between the diffusivities. According to Goudriaan & van Laar (in press) there exists a linear relation between net CO_2 -assimilation and the inverse leaf resistance in maize leaves. This relation can be used for the

simulation of the leaf resistance, since the net CO₂-assimilation can be reasonably well deduced from the absorbed visible radiation per leaf area. Above a visible irradiation of about 200 J m⁻²s⁻¹ the net CO₂-assimilation is saturated so that the leaf resistance of sunlit leaves approaches a minimum when the angle of incidence is more than 15 degrees. This was indeed found by Stigter (1974).

The mentioned proportionality between net CO₂-assimilation and inverse leaf resistance implies a constant CO₂-concentration in the substomatal cavities. For a C₄ plant like maize the internal CO₂-concentration is fixed at about 120 vpm and for a C₃ plant like beans at about 210 vpm. More details are given by Goudriaan & van Laar (in press).

To find the leaf resistance the rate of net CO₂-assimilation must be known. This rate is found by an empirical representation of measured curves (van Laar & Penning de Vries, 1972):

$$F_n = (F_m - F_d) \{1 - \exp(-R_v \varepsilon / F_m)\} + F_d \quad (3.8)$$

where F_m is the maximum rate of net CO₂-assimilation, F_d the net CO₂-assimilation in the dark (negative dark respiration), R_v the absorbed visible radiation per leaf area and ε the slope of the F_n , R_v curve at low light intensities, to be exact at the point where F_n is zero (the compensation point) ε can also be considered an efficiency and has an approximate value of 17.2 10⁻⁹ kg CO₂ per J of visible radiation in C₄ plants, and of 11.4 10⁻⁹ kg CO₂ per J of visible radiation in C₃ plants. Since 1 kg of assimilated CO₂ corresponds to an energy fixed in the form of carbohydrates of 10.8 10⁶ J, maximally 18.5 percent of the absorbed visible light energy in C₄ plants and 12 percent in C₃ plants is used for CO₂-assimilation. Hence by far the larger part is used for transpiration and sensible heat loss.

The maximum rate of CO₂-assimilation F_m is a function of leaf age, leaf temperature and ambient CO₂-concentration. In maize the net assimilation decreases little with age (van Laar et al., 1977). According to the model study the ambient CO₂-concentration does not drop by more than 50 vpm (from 330 to 280 vpm). Hence the influence of leaf age and ambient CO₂ concentration can be simplified by assuming that one average value may be used. The dependence on leaf temperature was simplified to a dependence on the ambient air temperature. On the average such an assumption is reasonable (Rabbinge, 1976), but for highly irradiated leaves it causes an underestimation of the

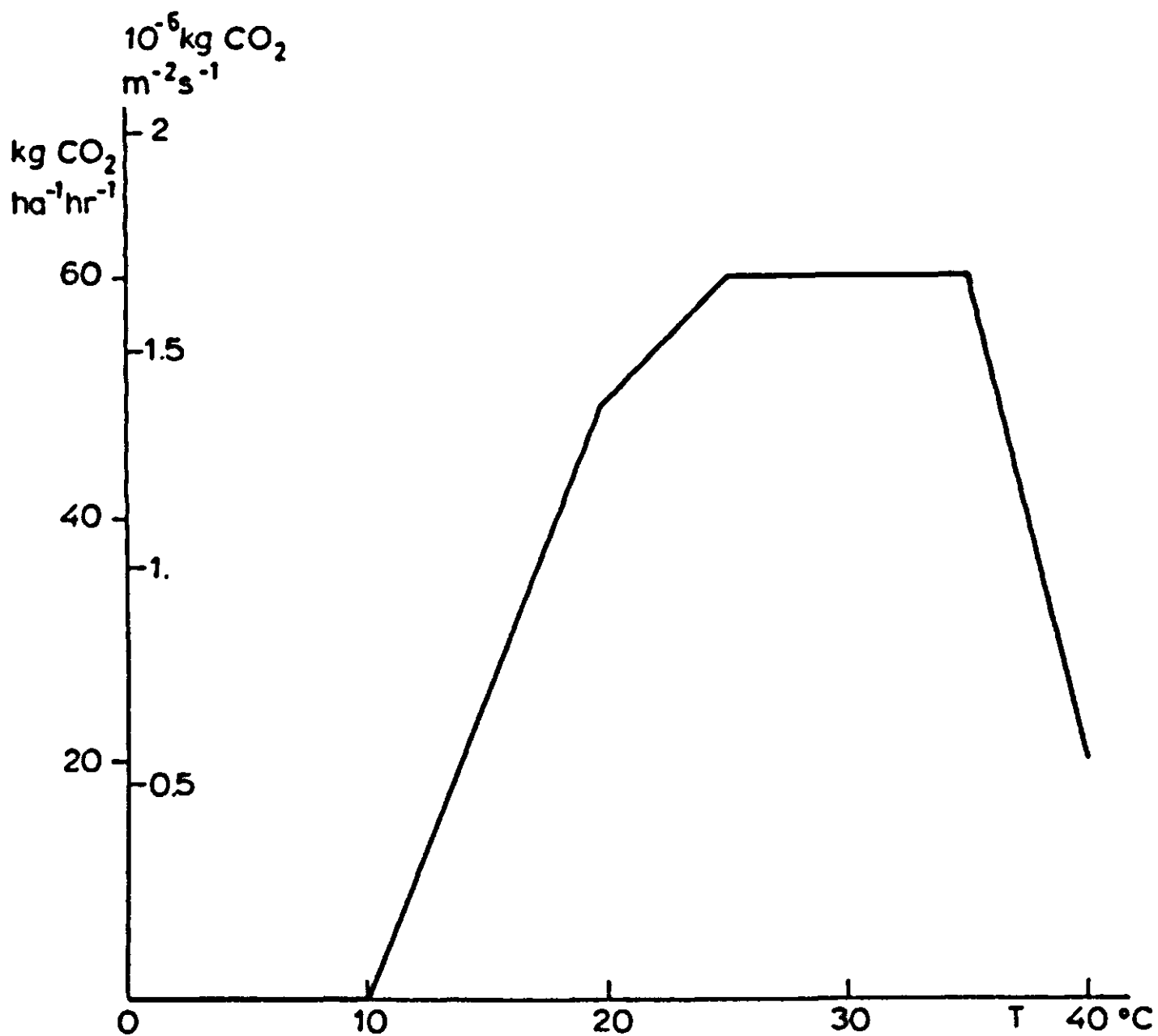


Fig. 16 | Maximum rate of net CO₂-assimilation (light saturated, external CO₂ concentration 300 vpm) of a healthy maize leaf as a function of the leaf temperature. On the ordinate two scales are given.

temperature. The relation between F_m and the temperature that is used in the model is given in Fig. 16. The assimilation in the dark F_d is also calculated from air temperature, with a reference value of $-0.17 \cdot 10^{-6} \text{ kg CO}_2 \text{ m}^{-2} \text{ s}^{-1}$ at 30°C and a Q_{10} of 2. Thus F_d is about -0.1 of F_m , in accordance with data of Tooming (1967).

From the net CO₂-assimilation so found the leaf resistance is calculated with

$$F_n = \frac{1.83 \cdot 10^{-6} (C_e - C_r)}{1.66r_{l,v} + 1.32r_{b,h}} \quad (3.9)$$

or

$$r_{l,v} = \frac{1.83 \cdot 10^{-6} (C_e - C_r)}{1.66F_n} - 0.783r_{b,h} \quad (3.10)$$

The conversion factor 1.66 is the ratio between D_v and D_c , and the conversion factor $1.83 \cdot 10^{-6}$ converts the CO_2 -concentration into $\text{kg CO}_2 \text{ m}^{-3}$ from vpm at 20°C . The CO_2 -concentrations (expressed in vpm) are the external value and the assumed regulatory concentration C_r . The value 1.32 originates from Eqn (3.7).

So far water stress did not come into the picture, but it may sometimes act as a limiting factor as when the minimum resistance, dictated by the water stress exceeds the leaf resistance calculated above. Then the larger resistance is used. At the same time the net CO_2 -assimilation is recalculated by Eqn (3.9) with the leaf resistance value based on the water stress. This procedure only slightly underestimates the assimilation under water stress conditions.

The energy flux used for assimilation, or released in respiration, is given by

$$M = 10.8 \cdot 10^{-6} F_n \quad (3.11)$$

where $10.8 \cdot 10^6 \text{ J}$ is the energy fixed in the form of carbohydrates, that correspond to an amount of 1 kg CO_2 .

The energy flux, used for transpiration, is given by (Monteith, 1973):

$$\lambda E = \frac{s(R - M) + \delta}{s + \gamma^*} \quad (3.12)$$

In this equation s is the slope of the saturated vapour pressure curve at air temperature in mbar K^{-1} , R is the absorbed radiation per leaf area, δ the drying power of the air (given below), and γ^* the apparent psychrometer constant. The drying power of the air is defined by

$$\delta = \frac{(e_s - e_a)\rho c_p}{r_{b,h}} \quad (3.13)$$

where e_s is the saturated vapour pressure at air temperature and e_a is the actual vapour pressure. ρc_p is the volumetric heat capacity of the air (about $1240 \text{ J m}^{-3} \text{ K}^{-1}$).

The apparent psychrometric constant is defined by

$$\gamma^* = \gamma \frac{(r_{b,v} + r_{l,v})}{r_{b,h}} \quad (3.14)$$

so that γ^* is 0.93γ for a wet surface (γ is 0.67 mbar K^{-1}).

By the energy balance equation the heat flux to the air can be found:

$$C = R - M - \lambda E \quad (3.15)$$

The equations presented above give a full description of the partitioning of the net absorbed radiant energy among photosynthesis, transpiration and heat loss to the air. Section 2.3.6 describes the feedback of leaf temperature on the net thermal radiation. Because of this the program contains a loop which is simply solved by substitution of the leaf temperature in the equation for net radiation during the next time-interval. This computational procedure may lead to instability, but when the feedback effect is small it converges fast. This condition is here fulfilled. After a few time intervals R_n and the leaf temperature T_1 are in equilibrium and the equation for T_1 is then simply

$$T_1 = T_a + C \frac{r_{b,h}}{\rho c_p} \quad (3.16)$$

where T_a is the air temperature.

The derivation of Eqn (3.12) is based on combination of the following four equations. Since this was first done by Penman (1948), Eqn (3.12) is often called the Penman equation.

$$R - M - C - \lambda E = 0 \quad (\text{energy balance}) \quad (3.17)$$

$$C = \frac{(T_1 - T_a)\rho c_p}{r_{b,h}} \quad (3.18)$$

$$\lambda E = \frac{\{e_s(T_1) - e_a\}\rho c_p}{\gamma(r_{1,v} + r_{b,v})} \quad (3.19)$$

$$e_s(T_1) = e_s(T_a) + s(T_1 - T_a) \quad (3.20)$$

The last equation is an approximation, but a good one if the leaf and air temperature are not too different. This can be checked in Table 18 where e_s and s are tabulated against temperature. In the simulation program e_s is approximated by

$$e_s = 6.11 \exp\{17.4T/(T + 239)\} \quad (3.21)$$

Table 18 The saturated water vapour pressure e_s , as a function of temperature. The results of an analytical expression to approximate e_s , are also given. The last column gives the derivative of e_s , with respect to temperature.

$T(^{\circ}\text{C})$	$e_s(\text{mbar})$	$6.11 \exp\{17.4 T/(T + 239)\}$	$s(\text{mbar K}^{-1})$
0	6.11	6.11	0.445
5	8.72	8.73	0.609
10	12.27	12.29	0.823
15	17.04	17.07	1.10
20	23.37	23.42	1.45
25	31.67	31.74	1.89
30	42.43	42.54	2.44
35	56.24	56.40	3.12
40	73.78	74.04	3.94

3.3 The soil surface

The equations for the energy balance of the soil surface are very similar to those for a leaf. However the photosynthesis term can be omitted. To find the temperature of the soil as a function of time and depth, a number of layers on top of each other are distinguished. The energy balance of the soil surface has to be extended with a storage term for the flux of heat into the top layer. This downward soil heat flux G is given by

$$G = \frac{(T_s - T_1)k'}{d_1} \quad (3.22)$$

where T_s is the temperature of the soil surface, T_1 the temperature of the centre of the first layer in the soil, d_1 the distance between the centre of this layer and the soil surface and k' the conductivity for heat in the soil. The energy balance on the other hand requires that

$$G = R - C - \lambda E \quad (3.23)$$

Since Eqn (3.22) is linear in T_s , a Penman type combination similar to that in the previous section is possible. The result is

$$\lambda E = \frac{sy \left\{ R + \frac{(T_1 - T_a)k'}{d_1} \right\} + \delta}{sy + \gamma^*} \quad (3.24)$$

This equation is very similar to Eqn (3.12). The only difference is the factor y , which occurs twice in Eqn (3.24). The dimensionless factor y accounts for the partitioning of the available energy between the soil heat flux and the fluxes to the air. It is defined by

$$y = \frac{\rho c_p d_1}{\rho c_p d_1 + k' r_{b,h}} \quad (3.25)$$

As expected y approaches unity for a low value of k' , because the storage term becomes negligible then. When the underlying substrate is highly conductive, y approaches zero.

The apparent psychrometer constant is here defined by

$$\gamma^* = \gamma \frac{(r_{b,v} + r_{s,v})}{r_{b,h}} \quad (3.26)$$

The resistance $r_{s,v}$ is the soil resistance for water vapour. For a wet soil it is zero, and for a dry soil very large.

In intermediate conditions more elaborate methods must be followed such as given by van Keulen (1975), van Keulen & Hillel (1974), Kaufmann (1976). The drying power of the air just above the soil surface, δ , is

$$\delta = \frac{(e_s - e_a) \rho c_p}{r_{b,h}} \quad (3.27)$$

This time $r_{b,h}$ is given by (see Eqns (3.1) and (3.5))

$$r_{b,h} = 1.8 \times 10^2 \times \left(\frac{w}{u} \right)^{0.5} \quad (3.28)$$

By this equation it is assumed that just above the soil surface there is a boundary layer as there was for a leaf. Beyond this boundary layer the air is fully turbulent. The thickness of this layer is determined by a wind speed u near the soil surface and the characteristic dimension w , which must be considered as the renewal length of the boundary layer. The average clod size is probably a reasonable guess for this characteristic dimension. Under a vegetative cover the result of Eqn (3.28) seems to be more realistic than the relation found by

Chamberlain (1968). His equation assumes a logarithmic profile over a certain height above the soil surface and an additional resistance to diffusion from between clods and ridges. A logarithmic profile equation may be well applicable for a bare soil with uniform surface roughness, but under a vegetative canopy such an air flow pattern will probably not develop.

Then it seems best to use the same approach as for leaves and to use Eqn (3.28). However, a direct empirical justification for this equation is still lacking.

When the latent heat of evaporation λE is found, the sensible heat loss to the air is given in the simplest way by an equation which emerges during the derivation of Eqn (3.24), and which is valid both for leaves and the soil surface:

$$C = (\gamma^* \lambda E - \delta) / s \quad (3.29)$$

The soil surface temperature is now found by applying Eqn (3.16) and consequently the soil heat flux G by Eqn (3.23).

After the soil heat flux G is found, the net fluxes of the soil layers can be integrated. G can be considered as the driving force for the temperature wave in the soil system. The procedure of solving the equations for the layers in the soil is well described by de Wit & van Keulen (1972) and needs no discussion here.

The dynamics of water movement in the soil is not considered in this study, because the duration of a simulation period was never longer than one day. However it can be easily incorporated, using the equations given by de Wit & van Keulen (1972) and by van Keulen (1975). It is assumed that the water content of the soil corresponds to field capacity, and that the soil properties are independent of depth. Hence also the thermal conductivity and the volumetric heat capacity are taken as constant.

3.4 The canopy

3.4.1 Introduction

In this section it will be described how the energy and mass balances of the individual leaves are summed to give the values for the whole canopy. For this purpose the distribution of the driving force, the radiant energy, over the different parts of the canopy is needed. The

basis for this calculation is given in Chapter 2.

When the leaf area index is low the problem of the radiation distribution can be treated in a simple way, because there is no mutual shading of leaves. Therefore this situation is first discussed separately.

3.4.2 Leaf area index less than 0.2

As long as the leaf area index is less than 0.2, mutual shading can be neglected, and all leaves are fully exposed to the incoming radiation. For diffuse radiation the assumption of the uniform overcast sky is adopted. Thus the radiation field is isotropic and the absorption per leaf area is independent of leaf inclination.

Hence the absorbed visible radiation under an overcast sky is given by

$$R_v = (1 - \sigma_v)S_{d,o} \quad (3.30)$$

and the absorbed near-infrared radiation

$$R_n = 0.7(1 - \sigma_n)S_{d,o} \quad (3.31)$$

Depending on the value of soil reflectance, the appropriate fraction must be added to these amounts.

The absorbed diffuse radiation under a clear sky is found in the same way, whereby $S_{d,c}$ is substituted for $S_{d,o}$ and the factor 0.7 for the near-infrared radiation is omitted. The direct light however is unevenly distributed over leaves in different positions. The fraction of leaves at which light is incident under a sine between $0.1 \times t$ and $0.1 \times (t - 1)$ is called $Z(\beta, t)$. β is the index connected with the inclination of the sun, and runs from 1 to 9. t runs from 1 to 10, since 10 incidence classes are distinguished. The Z function is derived from a cumulative Z_c function as

$$Z(\beta, t) = Z_c(\beta, t) - Z_c(\beta, t - 1) \quad (3.32)$$

Z_c is found as a weighted addition of the cumulative functions for each of the nine leaf inclinations.

$$Z_c(\beta, t) = \sum_{\lambda=1}^9 F(\lambda)S(\beta, \lambda, t) \quad (3.33)$$

$S(\beta, \lambda, t)$ is the cumulative distribution for the leaves in inclination class λ . Its calculation is given in Appendix B.

The absorbed direct visible radiation for leaves in incidence class t equals

$$R_{v,d} = (0.1t - 0.05) (1 - \sigma_v) S_p \quad (3.34)$$

where S_p is the incoming direct radiation on a surface perpendicular to the solar beam. A corresponding equation is applied for the near-infrared radiation. After the absorbed diffuse radiation has also been taken into account, the photosynthesis and transpiration of the leaves in this particular incidence class are calculated. The contributions of the incidence classes are added after multiplication by the weighting factor $Z(\beta, t)$, to find the total photosynthesis and transpiration.

3.4.3 Leaf area index more than 0.2

The radiation profile is characterized by the value of the extinction and reflection coefficients. The extinction coefficient for direct radiation is given by Eqn (2.34). When the scattered radiation is included, this value is multiplied by $(1 - \sigma)^{0.5}$ and regression equation (2.42) is used to approximate the value of the extinction coefficient given by the extensive radiation model. Subsequently Eqn (2.41) is used to find the extinction coefficient for the diffuse radiation. In a similar way the reflection coefficients are calculated, using equations (2.44), (2.45) and (2.46).

For an overcast sky the amount absorbed per leaf area in layer j is:

$$R_{v,o} = (1 - \rho_{dfv}) S_{d,o} [\exp\{-K_{dfv}(j-1)L_s\} - \exp\{-K_{dfv}jL_s\}]/L_s \quad (3.35)$$

where ρ_{dfv} and K_{dfv} are the reflection and extinction coefficients for diffuse visible radiation, which are found as described in Section 2.3.3. L_s is the leaf area index per layer. Since the integrated form with exponentials is used, L_s can be chosen quite large with an upper limit of about 3 but it will be limited by the variation of air conditions with height.

For the diffuse light under a clear sky the same equations are used, replacing $S_{d,o}$ by $S_{d,c}$ and $R_{v,o}$ by $R_{v,c}$. However, an additional source of diffuse illumination must now be accounted for, that is the radiation scattered by the sunlit leaves. The scattered light is already accounted for in the extinction coefficient as found by Eqn (2.42). As in Eqn (3.35) the visible absorbed radiation per leaf area, both

direct and diffuse, averaged over the whole layer is

$$R_{v,b} = S_b(1 - \hat{\rho}_m)[\exp\{-\hat{K}_m(j-1)L_s\} - \exp\{-\hat{K}_mjL_s\}]/L_s \quad (3.36)$$

where $\hat{\rho}_m$ and \hat{K}_m are estimated coefficients (Eqns (2.46) and (2.42)) under pure direct irradiation.

The average absorbed direct light per leaf area is

$$\bar{R}_{v,d} = S_b(1 - \sigma_v)[\exp\{-K_b(j-1)L_s\} - \exp\{-K_bjL_s\}]/L_s \quad (3.37)$$

K_b is the extinction coefficient for direct radiation according to Eqn (2.34). This expression can be simplified, with the fraction of sunlit leaves in a layer which is given by

$$s = [\exp\{-K_b(j-1)L_s\} - \exp\{-K_bjL_s\}]/(L_sK_b) \quad (3.38)$$

Combining the last two equations gives

$$\bar{R}_{v,d} = S_b(1 - \sigma_v)sk_b \quad (3.39)$$

The difference between $R_{v,b}$ and $\bar{R}_{v,d}$ is the absorbed diffuse radiation per leaf area, originating from scattering by sunlit leaves. It is assumed that this irradiation is the same for sunlit and shaded leaves. Hence, the absorbed diffuse visible radiation, common to all leaves at one level is

$$R_s = R_{v,c} + R_{v,b} - \bar{R}_{v,d} \quad (3.40)$$

This is the absorbed visible radiation for the shaded leaves, and for the sunlit leaves the additional absorbed direct radiation, given by Eqn (3.34), must be added to it. The rates of transpiration and CO₂-assimilation can now be calculated from of the equations in Section 3.2. Let F be the net CO₂-assimilation per leaf area, as function of the absorbed radiative energy R . For transpiration the total net radiation must be considered, but for CO₂-assimilation only the visible part. The contribution of the shaded leaves in a layer to the flux per ground area is

$$F_{sh} = L_s(1 - s)F(R_s) \quad (3.41)$$

and of the sunlit leaves

$$F_{su} = L_s s \sum_{t=1}^{10} Z(\beta, t) F(R_s + R_{v,d}) \quad (3.42)$$

The sum of F_{sh} and F_{su} gives the assimilation rate under a clear sky F_{c1} .

When the sky is overcast the contribution of a layer is

$$F_{ov} = L_s F(R_{v,o}) \quad (3.43)$$

Adding layer by layer gives the total rate of CO₂-assimilation per ground area. Similar procedures are followed for the transpiration rate and for the sensible heat loss. Since the classification into sunlit and shaded leaves is the same for transpiration and CO₂-assimilation, the respective calculations are executed simultaneously and not one after the other.

The calculations are executed separately for a supposed clear sky, and a fully overcast sky, for which the data from Table 1 are used.

For a partly overcast sky finally the rate is found by

$$\bar{F} = f F_{ov} + (1 - f) F_{cl} \quad (3.44)$$

This equation assumes a bimodal distribution of light intensity in time, either fully overcast or fully clear. This is a good approximation under cumulus clouds (Mullamaa & Pyldmaa, 1975) but for cirrus clouds it is better to use current values of both direct and diffuse radiation which must then be separately measured.

In well ventilated sparse canopies the air conditions do not vary too much with height, so that leaves need only be classified with respect to irradiation. The equations presented before can then be applied in a simplified way, to such an extent that only one layer is distinguished. However, to avoid a too high degree of dilution of the available light in the model, all absorbed light is restricted to the upper LAI of 3, when the leaf area is larger. With these assumptions the equations read as follows:

$$s = \{1 - \exp(-K_b LAI)\} / LAI_m \quad (3.45)$$

$$R_{v,o} = (1 - \rho_{dfv}) S_{d,o} \{1 - \exp(-K_{dfv} LAI)\} / LAI_m \quad (3.46)$$

where LAI_m equals LAI restricted to an upper value of 3. Similarly $R_{v,b}$ is given by

$$R_{v,b} = (1 - \hat{\rho}_m) S_b \{1 - \exp(-\hat{K}_m LAI)\} / LAI_m \quad (3.47)$$

$$R_s = R_{v,c} + R_{v,b} - R_{v,d} \quad (3.48)$$

$$F_{sh} = LAI_m (1 - s) F(R_s) \quad (3.49)$$

$$F_{su} = sLAI_m \sum_{i=1}^{10} Z(\beta, t) F(R_s + R_{v,d}) \quad (3.50)$$

However, for the respiration the lower part of the canopy cannot be neglected.

3.4.4 *Water status*

The water status of the canopy influences both transpiration and net photosynthesis by setting a lower limit to the stomatal resistance. The relation between this lower limit and the relative water content of the canopy is given in Fig. 17. The relative water content is calculated as the actual water content divided by the maximum water content ($2.5 \cdot 10^{-3} \text{ kg m}^{-2}$ times the leaf area index), which is based on a leaf thickness of about 3 mm. The actual water content is an integral of the water uptake of the canopy minus the transpiration rate. As initial condition a relative water content of 0.975 is chosen, which means that the plants are fully turgid. The calculation of the transpiration rate was discussed in Section 3.4.3¹, where it was found to be a function of stomatal resistance so that a feedback loop is formed. Actually, time lags in this loop may cause oscillations as recorded by Hopmans (1971). Another feedback loop functions through the water uptake, since a lower water content of the canopy forces more water to flow from the soil through the root to the plant. The soil water stress is supposedly at field capacity (-0.1 bar), the root resistance is a function of soil temperature (Fig. 18), and the plant water stress is a function of the relative water content (Fig. 17). Because the root resistance is non-zero, a considerable plant water stress may develop, even when the soil is moist, provided the transpiration stream is large enough.

Leaf flutter and rapid fluctuations in incoming radiation may affect the total average transpiration rate by preventing the stomata reaching equilibrium. Because detailed knowledge about the transient behaviour of stomatal conductance is lacking, leaf flutter is not taken into consideration.

¹ Only after finishing the simulation studies was the following error found in the program. The transpiration rate should be calculated as the total water loss of the soil-canopy system minus soil surface evaporation. The latter was not subtracted.

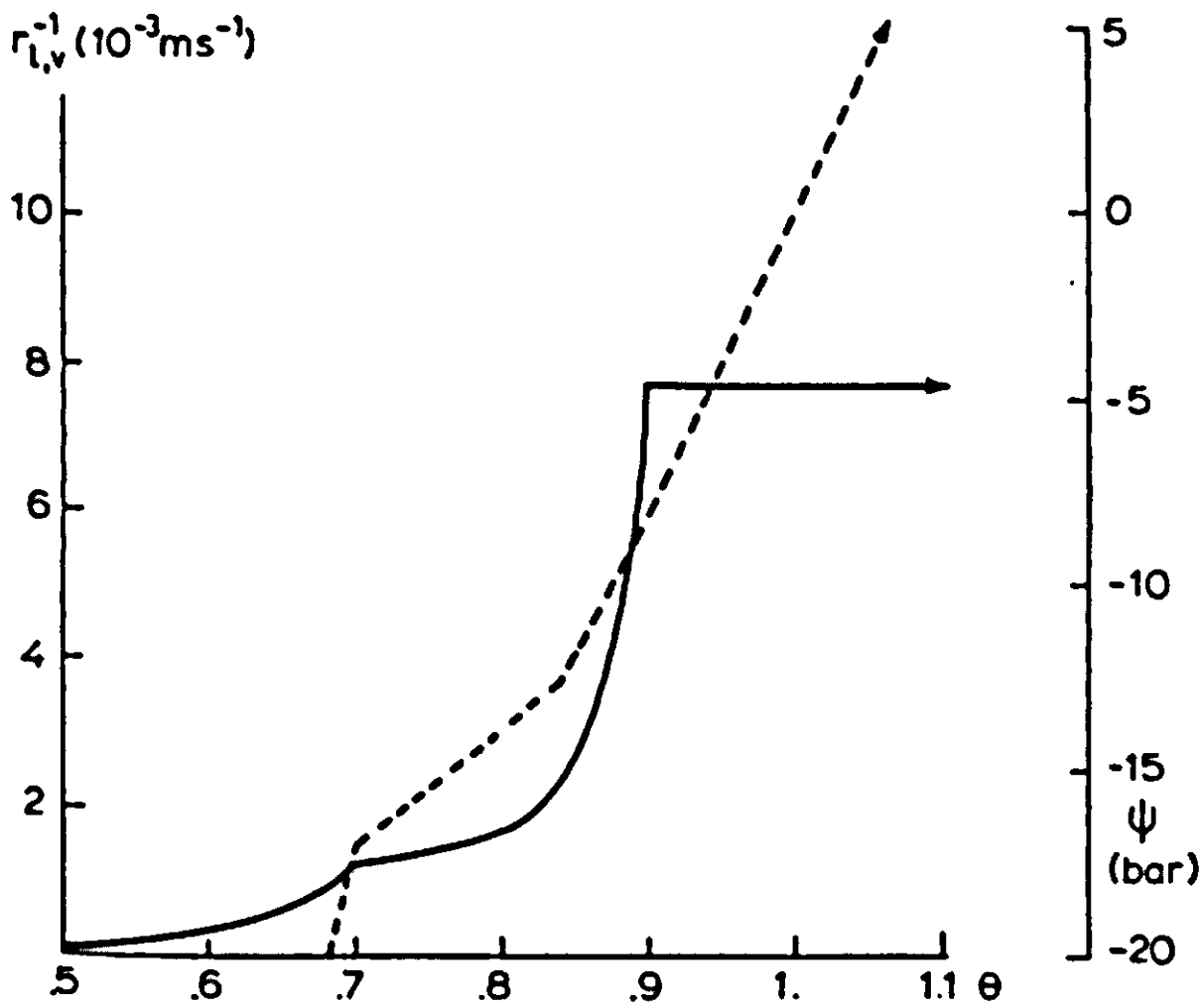


Fig. 17 | Inverse leaf resistance (solid line) and plant water stress (broken line) as a function of the relative water content of the canopy.

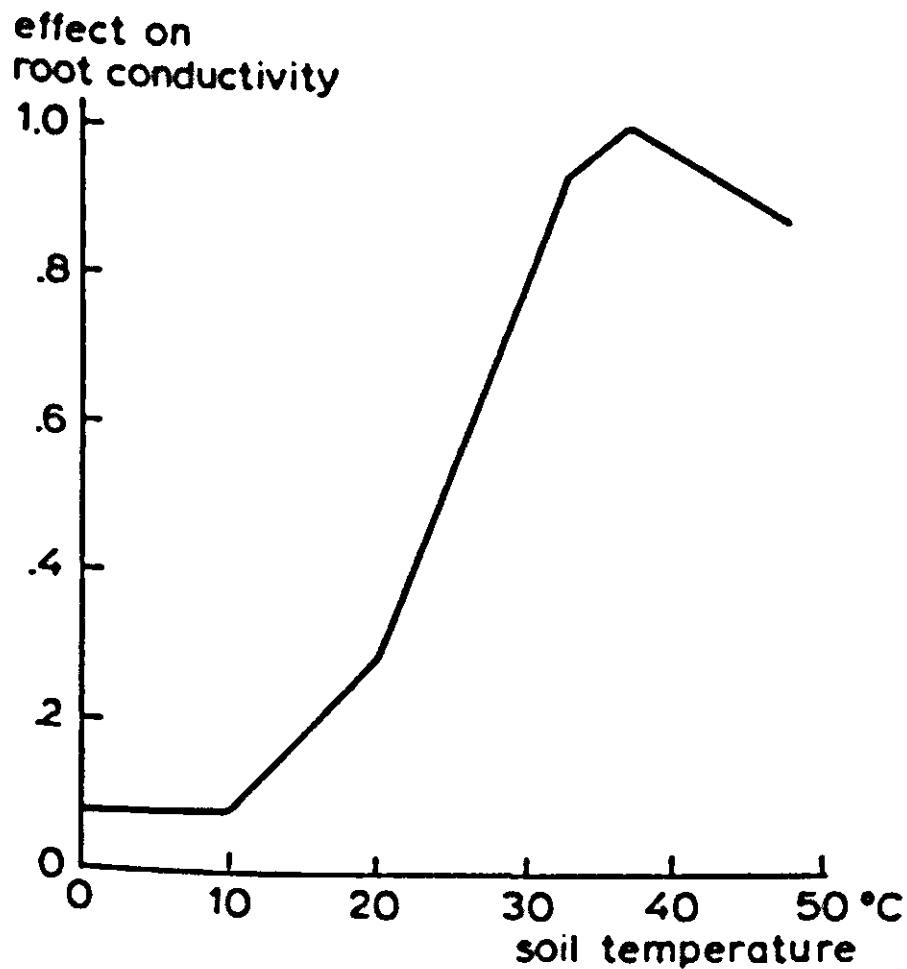


Fig. 18 | The effect of the soil temperature on the root conductivity, relative to the maximum value at 40°C.

3.5 The air inside the canopy

In Section 3.2 the fluxes of heat, water vapour and carbon dioxide per unit leaf area were calculated from the energy balance of the individual leaves. After summation of the contributions of the different leaf classes in a horizontal layer of leaves, it is checked whether the total released energy fluxes are equal to the total absorbed radiant energy per layer. This type of balance is used throughout the simulation program to check the consistency of programming. The total sensible heat flux released by a layer of leaves is related to the volume of air occupied by this particular layer. In this way a source strength is found with the dimension $\text{J m}^{-3} \text{s}^{-1}$ and which is called q .

The transport of heat, water vapour or carbon dioxide in the air is usually described by a second order partial differential equation. The one for temperature reads

$$\frac{\partial T_a}{\partial t} = \frac{\partial}{\partial z} \left(K \frac{\partial T_a}{\partial z} \right) + \frac{q}{\rho c_p} \quad (3.51)$$

where t is time, T_a the air temperature, K the exchange coefficient ($\text{m}^2 \text{s}^{-1}$) and ρc_p the volumetric heat capacity of the air ($1240 \text{ J m}^{-3} \text{K}^{-1}$). The term “exchange coefficient” is used with the same meaning as “diffusivity”, but is preferred here because turbulent exchange is included.

This equation cannot be solved analytically unless rather unrealistic assumptions are made about the dependence of K and q on height. To obtain a numerical solution the most obvious method is to divide the height into a number of layers, thus obtaining a number of simultaneous ordinary differential equations with respect to time. Here computational problems arise because of the small time constant of the amount of heat stored in the air. These problems are further discussed in Section 5.5.

Here it suffices to say that first the fluxes between the layers are calculated from the differences in temperature or concentration, the exchange coefficient and the distance between the centre of the layers. The fluxes at either side of a layer are subtracted, and the source flux released by the leaves is added, so that a net flux is obtained. Division by the capacitance of the air in the layer gives the net rate of change of temperature, humidity or CO_2 content in the layer considered. The values of the exchange coefficients will be discussed in Chapter 4.

3.6 List of symbols used in Chapter 3

symbol	description	first used in eqn	unit	symbol in computer program
a	Empirical constant	3.2	–	
C	Sensible heat flux per leaf area	3.15	$\text{J m}^{-2} \text{s}^{-1}$	SHL
C_e	External CO_2 -concentration	3.9	vpm*	ECO2C
C_r	Assumed regulatory CO_2 -concentration	3.9	vpm	RCO2I
d_1	Distance between soil surface and centre of the top soil layer	3.22	m	DIST1
D_h	Diffusivity of heat in air	3.1	$\text{m}^2 \text{s}^{-1}$	
D_c	Diffusivity of CO_2 in air		$\text{m}^2 \text{s}^{-1}$	
D_v	Diffusivity of water vapour in air		$\text{m}^2 \text{s}^{-1}$	
e_a	Actual water vapour pressure in the air	3.13	mbar	VPA
e_s	Saturated water vapour pressure	3.13	mbar	SVPA
E	Transpiration rate per leaf area	3.12	$\text{kg H}_2\text{O m}^{-2} \text{s}^{-1}$	
f	Fraction overcast of the sky	3.44	–	FOV
$F(\lambda)$	Leaf angle distribution function	3.33	–	F
F	Average flux of CO_2 -assimilation per ground area	3.44	$\text{kg CO}_2 \text{m}^{-2} \text{s}^{-1}$	TNCO2A
F_{cl}	Net assimilation flux under a clear sky	3.44	$\text{kg CO}_2 \text{m}^{-2} \text{s}^{-1}$	
F_d	Dark CO_2 -assimilation (negative respiration) flux	3.8	$\text{kg CO}_2 \text{m}^{-2} \text{s}^{-1}$	
F_m	Maximum net CO_2 -assimilation flux	3.8	$\text{kg CO}_2 \text{m}^{-2} \text{s}^{-1}$	AMAX
F_n	Net CO_2 -assimilation flux	3.8	$\text{kg CO}_2 \text{m}^{-2} \text{s}^{-1}$	NCO2A
F_{ov}	Net assimilation flux under an overcast sky	3.43	$\text{kg CO}_2 \text{m}^{-2} \text{s}^{-1}$	

* vpm is used for volume parts per million

symbol	description	first used in eqn	unit	symbol in computer program
F_{sh}	Net assimilation flux of a layer of shaded leaves per ground area	3.41	$\text{kg CO}_2 \text{ m}^{-2} \text{ s}^{-1}$	
F_{su}	Net assimilation flux of the sunlit leaves in a layer, per ground area	3.42	$\text{kg CO}_2 \text{ m}^{-2} \text{ s}^{-1}$	
G	Soil heat flux at the soil surface	3.22	$\text{J m}^{-2} \text{ s}^{-1}$	G
j	Running index of a layer of leaves	3.35	–	J
k'	Conductivity for heat in the soil	3.22	$\text{J m}^{-1} \text{ s}^{-1} \text{ K}^{-1}$	LAMBDA
K_{dfv}	Extinction coefficient for diffuse visible radiation	3.35	$\text{m}^2 \text{ ground m}^{-2} \text{ leaf}$	
\hat{K}_m	Extinction coefficient from the simple equation	3.36	$\text{m}^2 \text{ ground m}^{-2} \text{ leaf}$	
L_s	Leaf area index of a layer	3.35	$\text{m}^2 \text{ leaf m}^{-2} \text{ ground}$	DL
M	Energy flux released by respiration	3.11	$\text{J m}^{-2} \text{ s}^{-1}$	
Nu	Nusselt number	3.1	–	
Pr	Prandtl number	3.2	–	
q	Volumetric dissipation rate of heat	3.51	$\text{J m}^{-3} \text{ s}^{-1}$	
R	Absorbed radiant flux in the whole spectrum per leaf area	3.12	$\text{J m}^{-2} \text{ s}^{-1}$	ABSRAD
Re	Reynolds number	3.2	–	
R_n	Absorbed radiant flux in the near infrared region	3.31	$\text{J m}^{-2} \text{ s}^{-1}$	NIR
R_s	Absorbed visible radiation for the shaded leaves	3.40	$\text{J m}^{-2} \text{ s}^{-1}$	
R_v	Absorbed visible radiation	3.8	$\text{J m}^{-2} \text{ s}^{-1}$	VIS
$R_{v,b}$	R_v , averaged over a layer and including radiation diffused by other leaves	3.40	$\text{J m}^{-2} \text{ s}^{-1}$	
$R_{v,d}$	R_v , but only direct radiation	3.34	$\text{J m}^{-2} \text{ s}^{-1}$	

symbol	description	first used in eqn	unit	symbol in computer program
$\bar{R}_{v,d}$	R_v , but only direct radiation and averaged over a leaf layer	3.39	$J m^{-2} s^{-1}$	
$R_{v,c}$	Absorbed diffuse sky radiation under a clear sky	3.40	$J m^{-2} s^{-1}$	VISDF
$R_{v,o}$	R_v under an overcast sky	3.35	$J m^{-2} s^{-1}$	VISDFO
$r_{b,h}$	Boundary layer resistance for heat**	3.1	$s m^{-1}$	RA
$r_{b,c}$	Boundary layer resistance for CO ₂	3.7	$s m^{-1}$	
$r_{b,v}$	Boundary layer resistance for water vapour	3.6	$s m^{-1}$	
$r_{l,v}$	Leaf resistance for water vapour	3.9	$s m^{-1}$	SRES
$r_{s,v}$	Soil surface resistance for water vapour	3.26	$s m^{-1}$	RESS
s	Slope of the saturated water vapour pressure curve	3.12	$mbar K^{-1}$	SLOPE
s	Fraction of sunlit leaves in a layer	3.38	–	FSR
S	Cumulative distribution function of the leaves with respect to the sine of incidence	3.33	–	
S_b	Direct radiant flux on a horizontal surface under a clear sky (visible or near infrared)	3.36	$J m^{-2} s^{-1}$	SUNDCL
$S_{d,c}$	Diffuse radiant flux under a clear sky (visible only)	page	$J m^{-2} s^{-1}$	DIFCL
$S_{d,o}$	Diffuse radiant flux under an overcast sky (visible only)	3.30	$J m^{-2} s^{-1}$	DIFOV

** The resistances are in fact expressed per area. Therefore they are in literature sometimes called areal resistances. For reasons of convenience I will only use the name resistance.

symbol	description	first used in eqn	unit	symbol in computer program
S_p	Direct radiant flux, perpendicular to the solar beam (visible or near infrared)	3.34	$\text{J m}^{-2} \text{s}^{-1}$	SUNPER
i	Index for sine of incidence	3.34	–	SN
T_a	Air temperature	3.16	$^{\circ}\text{C}$	TA, TADT
T_l	Leaf temperature	3.16	$^{\circ}\text{C}$	TL
T_s	Soil surface temperature	3.22	$^{\circ}\text{C}$	TS
T_1	Temperature of the first soil layer	3.22	$^{\circ}\text{C}$	TEMP(1)
u	Wind speed	3.3	m s^{-1}	WIND
w	Average leaf width, characteristic soil surface dimension	3.1	m	WIDTH, CLOD
y	Dimensionless number for transport of heat in the soil	3.24	–	Y
Z_c	Same as S, but averaged over the leaf inclination distribution	3.32	–	
Z	Fraction of leaves in one class of the sine of incidence	3.32	–	Z, ZISSN
γ	Psychrometric constant	3.14	mbar K^{-1}	PSCH
γ^*	Apparent psychrometric constant	3.12	mbar K^{-1}	PSCHAP
δ	Drying power	3.12	$\text{J m}^{-2} \text{s}^{-1}$ mbar K^{-1}	DRYP
ϵ	Slope of photosynthesis-light response curve at compensation point	3.8	$\text{kg CO}_2 \text{J}^{-1}$ (visible)	
θ	Relative water content of the canopy	fig. 17	–	RWCP
λ	Latent heat of vaporization of water	3.12	$\text{J kg}^{-1} \text{H}_2\text{O}$	
λE	Latent heat flux	3.12	$\text{J m}^{-2} \text{s}^{-1}$	EHL
ν	Kinematic viscosity of air	3.3	$\text{m}^2 \text{s}^{-1}$	
ρ_{drv}	Reflection coefficient of the canopy for diffuse visible radiation	3.35	–	RFOVV

symbol	description	first used in eqn	unit	symbol in computer program
$\hat{\rho}_m$	Estimate for the reflection coefficient of the canopy according to the simple equations	3.36	–	
ρc_p	Volumetric heat capacity of the air	3.13	$\text{J m}^{-3} \text{K}^{-1}$	RHOCP
σ_v	Scattering coefficient of the leaves for visible radiation	3.30	–	SCV
σ_n	Scattering coefficient of the leaves for near-infrared radiation	3.31	–	SCN
ψ	Plant water stress	fig. 17	bar	WSTCP

4 Turbulence and wind

4.1 Introduction

The exchange in the air in the boundary layer close to the surface of leaves and soil clods is smaller by powers of ten than that in the air moving in the canopy space between the leaves and above the canopy. In the boundary layer the exchange proceeds virtually by molecular diffusion, so that the boundary layer resistance depends mainly on the depth of the boundary layer. In the formula for the boundary layer resistance (Eqn (3.5)), this depth is eliminated and a direct relation with the local wind speed is given instead. Outside the boundary layer the exchange is almost entirely maintained by turbulent transport due to moving parcels of air. The effectiveness of this exchange can be illustrated by the fact that a daily net CO_2 -assimilation of $300 \text{ kg CO}_2 \text{ ha}^{-1}$ corresponds to the CO_2 content of an air layer of 55 m thickness. The turbulence is primarily driven by gradients in wind speed, but also by the wind encountering obstacles such as leaves, stems and petioles. Differences in air density also contribute substantially. The turbulence is damped by viscous friction, which is a process on molecular level.

Upward moving air is cooled by expansion at a rate of 0.01 K m^{-1} . When the vertical temperature gradient has this value, decreasing upwards, the conditions are neutral because the temperature difference of an eddy and its surrounding is not affected by the direction of movement. When the temperature gradient is less negative, or even positive in the upward direction, an upward moving eddy will become colder compared with its surrounding and thus be decelerated. On the other hand a downward moving eddy will also be decelerated as it will gain heat in relation to its surrounding. Therefore this situation is called stable or an inversion (after the inverted temperature gradient). The vertical exchange processes are strongly reduced or even impaired then. In the opposite situation, under unstable or lapse conditions, the movement of eddies is enhanced by free convection effects. When the wind speed is too low, eddies may even spontaneously emerge, so

that free convection prevails.

Not only temperature, but also air humidity will influence the density. An increase in humidity of 1 mbar is equivalent to a temperature increase of about 0.1 K. Therefore the adiabatic vertical gradient of density is most conveniently related to the gradient of an equivalent temperature T' , defined by

$$T' = T_a + 0.1e_a + 0.01z \quad (4.1)$$

In some places the gradient of T' is used to calculate an equivalent sensible heat flux C' . It must be noted that this calculation is only done for notation purposes in the expression for the Monin-Obukhov length (Eqn (4.19)), and that there is no further physical meaning in C' . The turbulent exchange must be taken into account both inside and above the canopy. Above the vegetation the exchange processes are simpler because it may be at least assumed that the fluxes of momentum, mass and heat are almost constant with height. In this study the effects of fog formation and radiation absorption and emission by the air itself are not included. Inside the vegetation, however, sources and sinks are an essential part of the problem. These considerations justify a separate discussion of the exchange processes above and inside the vegetation. This is presented in Sections 4.2 and 4.3 respectively. Section 4.4 deals with some basic relations between the aerodynamic macro-characteristics of the canopy, e.g. the zero plane displacement d and the roughness length z_0 , and the aerodynamic micro-characteristics and geometry of the crop.

So far a one-dimensional model has been used, so that the phenomena observed at one height are supposed to be representative for what happens in the whole horizontal plane at that height. The influence of a variability in the horizontal direction as well as the influence of temporal variations in wind speed are discussed in Section 4.5.

4.2 Exchange above the canopy

4.2.1 Neutral conditions

Neutral conditions are characterized by a zero gradient of T' with respect to height. Experimental data, ubiquitous in literature, indicate that under neutral conditions the profile of wind velocity can be represented by a logarithmic relation

$$u = \frac{u^*}{k} \ln\left(\frac{z - d}{z_0}\right) \quad (4.2)$$

where d accounts for an upward shift in the whole profile above a tall vegetative cover. According to this equation the wind speed is zero at a height $d + z_0$, but normally the logarithmic profile cannot be extrapolated that far downwards. Near the vegetation the real profile shows a positive deviation from the logarithmic profile. d is usually called the zero plane displacement. Empirical data indicate that d is related to the height of the vegetation z_c . Monteith (1973) suggested a linear relation

$$d = 0.63z_c \quad (4.3)$$

The length z_0 is called the roughness length and is often supposed to be about one tenth of the height of the vegetation. In Section 4.4 the values of d and z_0 are considered theoretically.

When d and z_0 are known the whole profile above the canopy can be constructed from the value of u at a single height, by calculating u^*/k and applying Eqn (4.2) for the other levels.

The described logarithmic profile is consistent with the following assumptions about the turbulent exchange. In the same way as in the molecular gas theory, an exchange coefficient can be derived as the product of a velocity and a mixing length. For molecules the mixing length can be identified with the mean free pathway, but for eddies it is assumed that it is proportional to a corrected height $z - d$. The proportionality factor is given by k , the von Karman's constant, which has a value of about 0.4. The mixing length l_m is thus given by

$$l_m = k(z - d) \quad (4.4)$$

In the free air the turbulent movement of eddies is generated by the vertical velocity gradient. The difference in velocity over a height

interval l_m is of the order of $l_m \frac{du}{dz}$. Under the assumption that this

is also the velocity of the eddies, the turbulent exchange coefficient K is consequently given by

$$K = l_m l_m \frac{du}{dz} \quad (4.5)$$

or by

$$K = k^2(z - d)^2 \frac{du}{dz} \quad (4.6)$$

The momentum flux density or shear stress is independent of height and equals

$$\tau = \rho K \frac{du}{dz} \quad (4.7)$$

so that

$$\left(\frac{\tau}{\rho}\right) = k^2(z - d)^2 \left(\frac{du}{dz}\right)^2 \quad (4.8)$$

where ρ is the density of air.

The variable $\left(\frac{\tau}{\rho}\right)$ has the dimension of a velocity squared, that is independent of height. Hence one can define a characteristic velocity $(\tau/\rho)^{0.5}$ with the name *friction velocity*, and usually denoted by u^* . Now Eqn (4.8) can also be written as

$$u^* = k(z - d) \frac{du}{dz} \quad (4.9)$$

or

$$u^* = l_m \frac{du}{dz} \quad (4.10)$$

so that u^* can be identified with the velocity of the eddies, according to an earlier assumption. Thus this eddy velocity is not dependent on height. Equation (4.9) can be integrated to

$$u = \frac{u^*}{k} \ln(z - d) + u_i \quad (4.11)$$

where u_i is an integration constant. By comparison with the empirical equation (4.2) the integration constant must equal

$$u_i = - \frac{u^*}{k} \ln(z_0) \quad (4.12)$$

after which the derived equation (4.11) and the empirical equation

(4.2) are identical.

It is convenient to express the exchange coefficient K in the friction velocity by combination of (4.6) and (4.9):

$$K_m = k(z - d)u^* \quad (4.13)$$

The index m is added to indicate that this is the exchange coefficient for momentum and not necessarily for heat or mass. According to Businger et al. (1971), the exchange coefficient for heat is 1.35 times larger, at least under neutral conditions:

$$K_h = 1.35 k(z - d)u^* \quad (4.14)$$

The *resistance* between the top of the vegetation and the height of measurement (reference height), is to be found as the integral of the inverse of the exchange coefficient. For neutral conditions this can be solved analytically, and gives for heat

$$r_h = 0.74 \ln\left(\frac{z_r - d}{z_c - d}\right) / (ku^*) \quad (4.15)$$

In the simulation program this expression is used for the calculation of heat and mass transport under neutral conditions between the levels z_c and z_r .

4.2.2 Non-neutral conditions

The two best established parameters to characterize the degree of non-neutrality are Richardson's number Ri and the Monin-Obukhov length L . Essentially these two parameters are equivalent. Here a simple derivation is given, based on some fundamental physical concepts. A more precise derivation can be found in Monin & Obukhov (1954), Prandtl (1932) and Priestly (1959).

As pointed out before the exchange process can be considered as a result of movement of eddies, carrying heat, mass and momentum. It was assumed that the velocity u^* of the eddies was of the order of

$l_m \frac{du}{dz}$ where l_m is a characteristic length. From dimensional considerations we now conclude that the accelerations, caused by the friction forces, are of the order of $(u^*)^2/l_m$ or $l_m \left(\frac{du}{dz}\right)^2$. Under non-neutral con-

ditions eddies may also be accelerated by buoyancy, the forces caused by density differences between the air in the eddy and the surrounding air. This buoyancy acceleration is of the order of $\Delta T g/T_{\text{abs}}$, where g is the gravity acceleration and T_{abs} the absolute temperature (being equal to the thermal expansion coefficient for ideal gases). The difference ΔT is of the order $l_m \frac{dT}{dz}$. The ratio of the buoyancy and friction acceleration is given by

$$Ri_g = \frac{g \frac{dT}{dz}}{T_{\text{abs}} \left(\frac{du}{dz} \right)^2} \quad (4.16)$$

which is an expression often used for Richardson's number. The subscript g indicates that here Richardson's number is expressed in gradients. An equivalent expression in differences is also possible (Eqns (4.40) and (4.43)). It must be noted that the average mixing length l_m is cancelled out in this equation.

The Monin-Obukhov length can be simplest conceived as the height above the zero plane, where the buoyancy forces equal the friction forces. Close to the surface the friction forces are the prevailing factor, even under highly non-neutral conditions. With increasing height the mixing length l_m increases, and the gradients $\frac{du}{dz}$ and $\frac{dT}{dz}$ decrease.

According to Eqn (4.10) the product $l_m \frac{du}{dz}$ is constant with height, also under non-neutral conditions, because the momentum flux density and with this the friction velocity do not vary with height.

However the product $l_m \left(\frac{du}{dz} \right)^2$, the friction acceleration, decreases with height. If one assumes mathematical similarity of the wind speed and temperature profiles, because of the absence of sinks and sources in

both cases, the buoyancy acceleration $\frac{g}{T_{\text{abs}}} l_m \frac{dT}{dz}$ does not vary with

height. At a certain height L , the Monin-Obukhov length, above the zero plane both forces will be equal. At this height the following relation must be satisfied ($l_m = kL$)

$$kL \frac{dT}{dz} \frac{g}{T_{\text{abs}}} = \frac{(u^*)^2}{l_m} \quad (4.17)$$

The upward equivalent heat flux C' (see Eqn (4.1)) is of the order of

$$C' = - \rho c_p l_m u^* \frac{dT}{dz} \quad (4.18)$$

Substitution of this expression into Eqn (4.17) gives for L

$$L = - \frac{\rho c_p T_{\text{abs}} (u^*)^3}{kgC'} \quad (4.19)$$

This is the expression most frequently quoted for the Monin-Obukhov length. The ratio of the corrected height $z - d$ and the Monin-Obukhov length L is often used as a dimensionless height parameter and is denoted by ζ

$$\zeta = \frac{z - d}{L} \quad (4.20)$$

In this study the relations found by Businger et al., (1971) will be used to account for the effect of non-neutrality on the values of the exchange coefficients. To do this Eqns (4.13) and (4.14) are written as

$$K_m = ku^*(z - d)/\Phi_m \quad (4.21)$$

$$K_h = ku^*(z - d)/\Phi_h \quad (4.22)$$

The correction factors Φ_m and Φ_h are, according to Businger et al., (1971)

$$\Phi_m = (1 - 15\zeta)^{-0.25} \quad \text{unstable} \quad \zeta < 0 \quad (4.22a)$$

$$\Phi_m = 1 + 4.7\zeta \quad \text{stable} \quad \zeta > 0 \quad (4.22b)$$

$$\Phi_h = 0.74 (1 - 9\zeta)^{-0.5} \quad \text{unstable} \quad \zeta < 0 \quad (4.23a)$$

$$\Phi_h = 0.74 + 4.7\zeta \quad \text{stable} \quad \zeta > 0 \quad (4.23b)$$

Under neutral conditions the Monin-Obukhov length is infinite ($C' = 0$) and hence ζ is zero, so that $\Phi_m = 1$ and $\Phi_h = 0.74$ which values are consistent with Eqns (4.13) and (4.14).

In literature alternative solutions can be found for the formulation of the effect of non-neutrality on the profiles of the exchange coefficients. An extensive listing and discussion of these solutions is given by

Rijkoort (1968).

Now the relation between Ri_g and L can be derived. The expression for the fluxes of momentum and equivalent heat are

$$(u^*)^2 = K_m \frac{du}{dz} \quad (4.24)$$

$$C' = \rho c_p K_h \frac{dT}{dz} \quad (4.25)$$

so that after substitution of Eqns (4.21) and (4.22) the gradients can be expressed as

$$\frac{du}{dz} = \frac{u^* \Phi_m}{k(z-d)} \quad (4.26)$$

$$\frac{dT}{dz} = - \frac{C' \Phi_h}{\rho c_p k(z-d) u^*} \quad (4.27)$$

Substitution of these expressions into Eqn (4.16) for Ri_g , and combination with Eqns (4.19) and (4.20) gives

$$Ri_g = \frac{\Phi_h}{\Phi_m^2} \zeta \quad (4.28)$$

For unstable conditions $Ri_g = \zeta$ is a good approximation.

The equivalent heat flux C' can also be expressed in a difference ΔT and a resistance r_h , which is found by integration of K_h^{-1} . Note that k, u^* and Φ_h are assumed to be independent of temperature.

$$r_h = \int_{z_1}^{z_2} \frac{\Phi_h}{k u^* (z-d)} dz \quad (4.29)$$

$$C' = \frac{\rho c_p \Delta T}{r_h} \quad (4.30)$$

The difference ΔT is taken as $T(z_2) - T(z_1)$, which is positive under unstable conditions and negative under stable conditions.

The Monin-Obukhov length can now be expressed in the difference ΔT by substitution of Eqns (4.29) and (4.30) into (4.19):

$$L = - \frac{T_{\text{abs}}(u^*)^2 \int_{z_1}^{z_2} \frac{\Phi_h}{(z' - d)} dz'}{k^2 g \Delta T} \quad (4.31)$$

In the simulation program the level z_2 is chosen as z_r , the reference level, and z_1 as $d + z_0$. By this choice of z_1 the equations assume the simplest possible form. A problem is now, that the value of u^* , which is needed in Eqn (4.31), can not be found by the equation for the logarithmic wind profile (Eqn (4.2)). It must be derived from a general profile defined by Eqn (4.26). Integration of this equation gives

$$u_r = \frac{u^*}{k} \int_{d+z_0}^{z_r} \frac{\Phi_m}{(z' - d)} dz' \quad (4.32)$$

where u_r is the wind speed at the reference level. In the simulation program Eqns (4.20), (4.22), (4.23), (4.31) and (4.32) must be solved simultaneously.

Stable

In the stable case ($\zeta > 0$) the integrations in Eqns (4.32) and (4.31) can be done analytically. Then

$$u_r = \frac{u^*}{k} \left\{ \ln \left(\frac{z_r - d}{z_0} \right) + 4.7 \Delta \zeta \right\} \quad (4.33)$$

and

$$L = - \frac{T_{\text{abs}}(u^*)^2 \left\{ 0.74 \ln \left(\frac{z_r - d}{z} \right) + 4.7 \Delta \zeta \right\}}{k^2 g \Delta T} \quad (4.34)$$

where $\Delta \zeta$ is defined by

$$\Delta \zeta = \frac{z_r - d - z_0}{L} \quad (4.35)$$

Elimination of L and u^* from these equations results in a second order expression for $\Delta \zeta$. One of the two solutions can be excluded on physical grounds, because $\Delta \zeta$ should approach zero when ΔT approaches zero. Thus $\Delta \zeta$ is given by

$$\Delta\zeta = \frac{-b + (b^2 - 4ac)^{0.5}}{2a} \quad (4.36)$$

where

$$a = 4.7 (1 - 4.7 Ri_d) \quad (4.37)$$

$$b = (0.74 - 2 \times 4.7 Ri_d) \ln \left(\frac{z_r - d}{z_o} \right) \quad (4.38)$$

$$c = - Ri_d \ln \left(\frac{z_r - d}{z_o} \right) \quad (4.39)$$

Ri_d is a Richardson's number, expressed in differences (compare with Eqn (4.16))

$$Ri_d = - \frac{(z_r - d - z_o)g\Delta T}{u_r^2 T_{abs}} \quad (4.40)$$

At the level $d + z_o$ the wind speed is zero, so that u_r itself is the difference in wind speed over the range $z_r - d - z_o$. In the simulation program the equations for the neutral profile are used when Ri_d is between -0.001 and $+0.001$. When Ri_d is larger than $1/4.7$, the solution breaks down since a (Eqn (4.37)) becomes negative. Physically this breakdown means that a full inversion has emerged. The exchange processes are reduced to molecular diffusivity and to some turbulence generated by mechanical friction. In the simulation program this situation is treated as if there were no exchange at all, i.e. above canopy resistances for heat and mass exchange are made very large.

The behaviour of resistance and heat flux in the region $0 < Ri_d < 0.21$ is represented in Fig. 19. The relations are invariant with wind speed when $k^{-2} \bar{u}_r^{-1} \bar{r}_h^{-1}$ is used instead of resistance and $C \bar{u}_r^{-3}$ instead of heat flux as such. The occurrence of a third power illustrates the large influence of wind speed on the phenomenon of inversion formation. The geometry, that is the values of z_r, z_c, d and z_o , is not eliminated from the graph, but still the given curve is quite typical. Here the dimensions are $z_r = 3$ m, $z_c = 2.5$ m, $d = 2$ m and $z_o = 0.158$ m. The resistance r_h increases with increasing Ri_d to such an extent that beyond $Ri_d = 0.042$ $- C \bar{u}_r^{-3}$ starts to decrease. Once this point is passed, the gradients will collapse to a full inversion situation. The

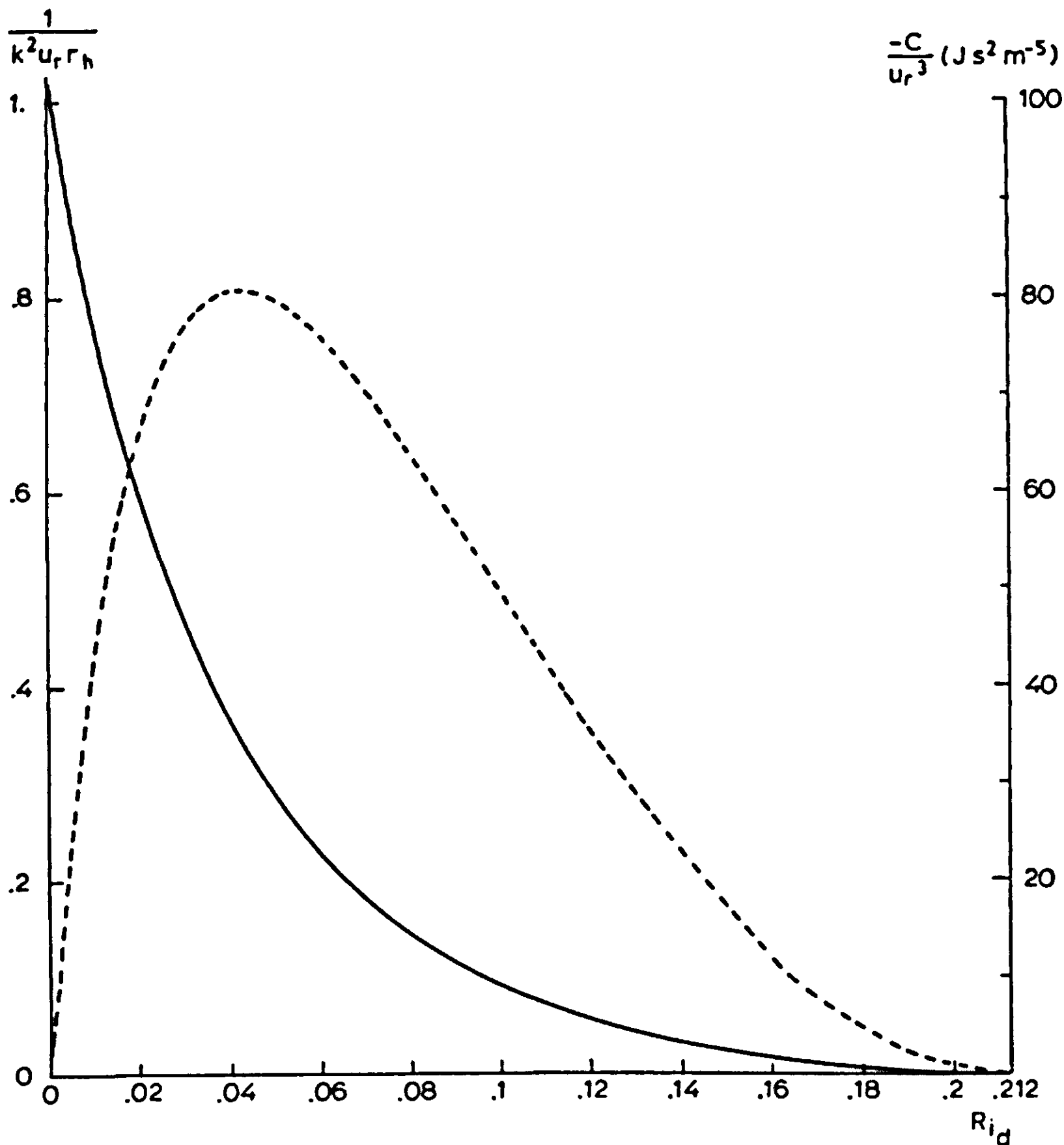


Fig. 19 | Simulated inverse resistance for heat exchange $k^{-2}\bar{u}_r^{-1}\bar{r}_h^{-1}$ (solid line) and the heat flux $-C\bar{u}_r^{-3}$ (broken line) as a function of Richardson number in the stable region, based on Businger's equations. The assumed geometrical data are $z_r = 3m, z_c = 2.5 m, d = 2m$ and $z_o = 0.158 m$. By the multiplication of the variables by \bar{u}_r^{-1} and \bar{u}_r^{-3} respectively the curve is made invariant with u_r .

duration of this process depends on the amount of heat that can be supplied by the soil. When the net radiation is negative, an inversion easily develops above a soil with a low conductivity and heat capacity, e.g. a dry soil, especially when it is covered with a dense vegetation. In practical terms this means an increased risk of night frost damage. In the inversion situation the sensible heat flux is zero, and the final temperature of the top of the vegetation is entirely determined by the balance in thermal radiative exchange with soil and air, and the aerial exchange inside the vegetation (see Section 4.3). In Fig. 20 a simulated relation is given between the temperature difference over 0.5 m height and the wind speed for a constant apparent sky temperature of 0°C and a constant air and soil temperature of 20°C . Effects of evaporation and condensation are excluded by assuming the soil and air to be very dry. With full inversion the air temperature in the canopy arrives at about 11.5°C ($20-8.5$), independently of the wind speed. However, when the wind speed exceeds a critical value, the full inversion breaks up and the temperature difference is decreased to about 1°C . In this region the actual value of the wind speed plays an important role. It must be noted that there is a hysteresis effect. The critical value of the wind speed is lower for a decreasing wind speed than it is for increasing wind speeds. In other words, the situation already established tends to be continued.

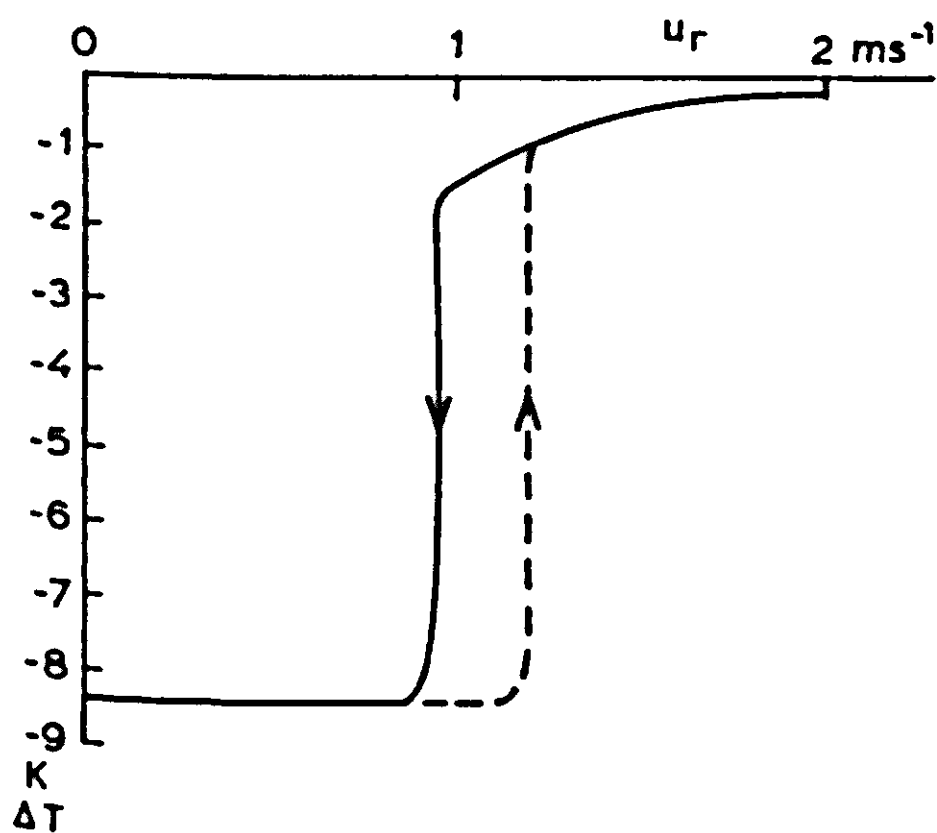


Fig. 20 | Simulated temperature difference as function of wind speed under a negative net radiation (see text). The system shows hysteresis for slowly changing wind speed. (arrows).

Unstable

A mathematical-analytical procedure such as that given for the stable case is not available for unstable conditions. The integrations over height in Eqns (4.31) and (4.32) must be executed numerically by expressing the correction factors Φ_m and Φ_h as the sum of a series of five terms

$$\Phi = A + B(z - d) + C(z - d)^2 + D(z - d)^3 + E(z - d)^4 \quad (4.41)$$

In principle the coefficients of these series may be found by differentiating Eqns (4.22a) and (4.23a) four times with respect to $(z - d)$ at the point $(z - d) = 0$ (Taylor series development). However, if this basic method is used the number of terms in the series must be very large for a reasonable accuracy. Therefore, the coefficients are calculated from the values of Φ at five equidistant heights between $d + z_0$ and z_r (see MACRO in computer program). Starting from Eqn (4.41) the integrals in Eqns (4.31) and (4.32) are then given by

$$I = A \ln \left(\frac{z_r - d}{z_0} \right) + B(z_r - d - z_0) + \frac{C}{2} \{(z_r - d)^2 - z_0^2\} + \\ + \frac{D}{3} \{(z_r - d)^3 - z_0^3\} + \frac{E}{4} \{(z_r - d)^4 - z_0^4\} \quad (4.42)$$

This gives a very accurate estimate for the value of the integrals over the range $d + z_0$ to z_r . The calculation, which is executed both for heat and momentum, is incorporated in an iteration (the IMPLICIT loop of CSMP). First a value is assumed for $\Delta\zeta$. The corresponding Monin-Obukhov length is then found by Eqn (4.35) and then the values of the dimensionless height at the five equidistant levels are calculated. The correction factors Φ_m and Φ_h follow, and both integrals are calculated by Eqn (4.42). The next estimate for $\Delta\zeta$ is found by the following relation, which is derived from Eqns (4.31), (4.32), (4.35) and (4.40):

$$Ri_d = \frac{\Delta\zeta I_h}{I_m^2} \quad (4.43)$$

The required value of Ri_d follows from Eqn (4.40). I_h and I_m stand for

$$\int_{d+z_0}^{z_r} \frac{\Phi_h}{z - d} dz \text{ and } \int_{d+z_0}^{z_r} \frac{\Phi_m}{z - d} dz, \text{ calculated with Eqn (4.42) for heat}$$

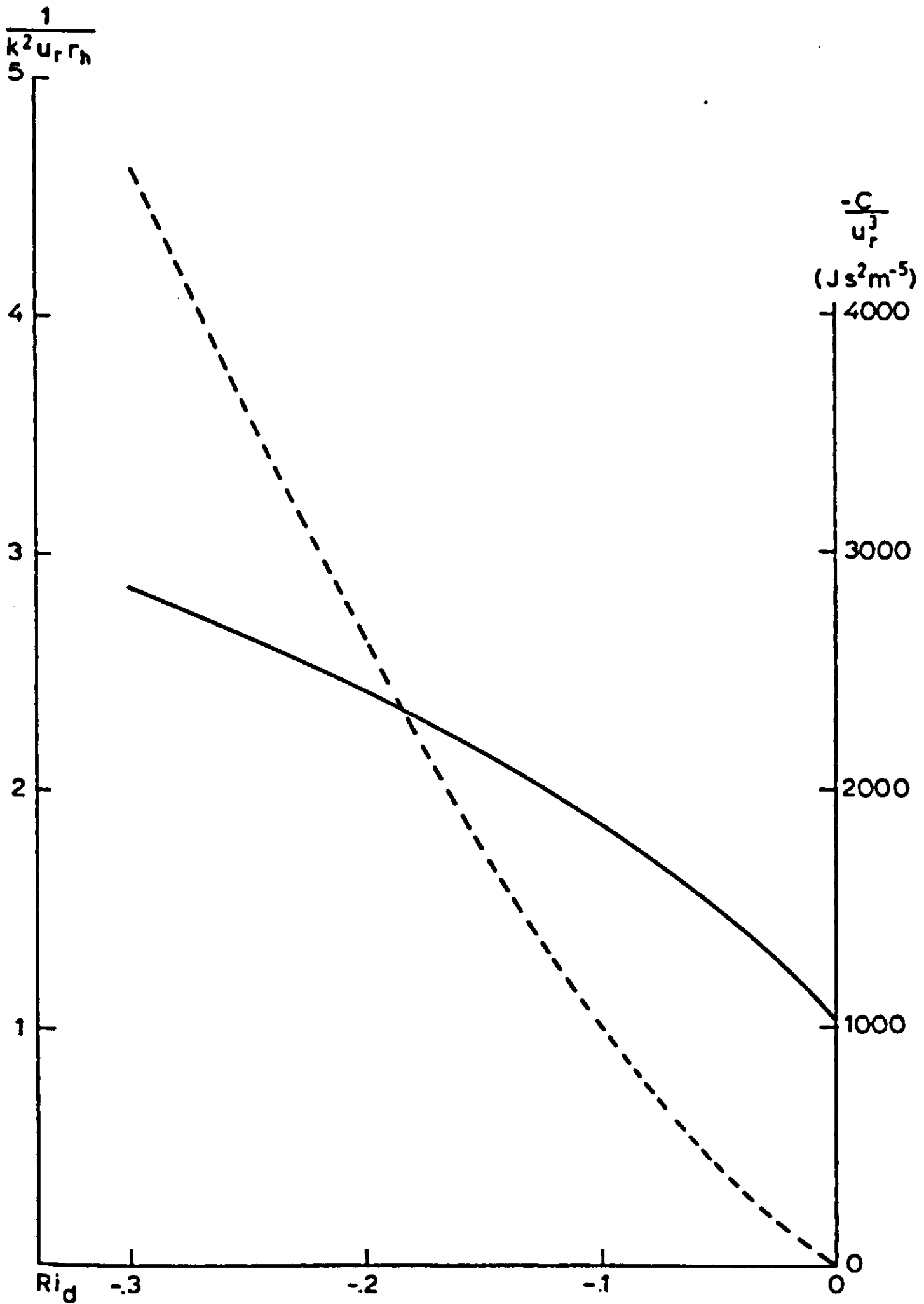


Fig. 21 | Same variables and geometry as for Fig. 19 but this graph represents the unstable case (negative Richardson number).

and momentum respectively. After convergence of the iteration, the value for u^* is found by Eqn (4.32). The resistance for heat r_h between the levels z_c and z_r is then calculated by Eqn (4.29). The integration needed is represented by Eqn (4.42) in which the lower boundary z_0 is replaced by $z_c - d$. A similar equation is used to find the wind speed at the level z_c , the top of the canopy. This wind speed is used as the upper boundary condition for the wind profile inside the vegetation. The performance of the equations used is further illustrated in Fig. 21 where the inverse resistance for heat $k^{-2} \bar{u}_r^{-1} r_h^{-1}$ and the heat flux $C \bar{u}_r^3$ are plotted against the negative Richardson's number Ri_d . The resistance decreases with the temperature difference, so that the heat flux shows an upward curvature. For large temperature differences free convection prevails ($Ri_d < -1$) and then the heat flux C should be independent of u_r . Thus $C \bar{u}_r^3$ should be proportional to $(-Ri_d)^{3/2}$. However, according to the equations used, $C \bar{u}_r^3$ becomes proportional to $(-Ri_d)^{7/4}$, so that these equations cannot be valid in the free convection region.

4.3 Exchange inside the canopy

4.3.1 Neutral conditions

As for the situation above the canopy, the working hypothesis is used that the exchange coefficient is given by the product of a mean mixing length and a mean eddy velocity. It must be admitted that this working hypothesis needs a firmer foundation by a more thorough experimental analysis of the relations between the mixing length of eddies of different sizes, their velocities, the spectra of turbulent energy and the correlations between vertical velocities and the transported quantities. As long as the above mentioned hypothesis is not invalidated by such an analysis, it is a good choice because of its conceptual attractiveness and its good performance.

For the mean mixing length in the canopy the free space between the leaves or stems is used. The number of leaves per volume is given by $L_d w^{-2}$ where w is the width of the square leaves and L_d the leaf area density. The mean distance between the leaves is

$$l_m = 2 \left(\frac{3w^2}{4\pi L_d} \right)^{1/3} \quad (4.44)$$

When the leaves are long and narrow, the mean mixing length is the diameter of a cylinder, containing on the average one leaf

$$l_m = \left(\frac{4w'}{\pi L_d} \right)^{0.5} \quad (4.45)$$

The length of the cylinder is the length of the leaf. For example, in maize with a LAI of 3, a crop height z_c of 2.5, so that L_d is 1.2, and a width of the leaves of 0.05 m, the mixing length is 0.23 m according to Eqn (4.45).

In reality leaves do not point in the same direction, so that there is a complicated effect on the mean value of the distance between leaves. However, in view of the crudeness of the working hypothesis used a more elaborate solution of this geometrical problem does not seem worthwhile.

The mean eddy velocity is assumed to be proportional to the local wind speed itself, with a proportionality factor i_w , which is called the relative turbulence intensity. According to measurements of Shaw et al. (1974) i_w ranges from 0.3 in the top of a maize crop to about 0.8 near the soil surface. Since i_w does not seem to vary with the wind speed, the exchange coefficient is proportional to the wind speed. The loss of momentum by dragging leaves may be assumed to be proportional to u^2 , and to a drag coefficient c_d that ranges from 0.05 to 0.5 depending on leaf inclination and shape (Monteith, 1973). The drag coefficient is here defined as the ratio between the force on the leaf and the volumetric kinetic energy of the air $0.5\rho u^2$ times the total leaf area (both sides). Since in the definition of the leaf area index and leaf area density the leaf area of one side is meant, the factor 0.5 disappears when the volumetric drag is related to the leaf area density (Eqn (4.47)). Den Hartog & Shaw (1975) found a value of 0.21 for the drag coefficient of maize leaves, when u is the wind speed registered by a cup anemometer at the same level as the leaf studied. The shear stress at any level is given by Eqn (4.7).

$$\tau = \rho K_m \frac{du}{dz} \quad (4.7)$$

Inside the canopy K_m is given by

$$K_m = l_m i_w u \quad (4.46)$$

The volumetric absorption of impulse by the leaves must be provided by a decrease in shear stress with depth in the canopy. Therefore the vertical gradient of the shear stress must equal the leaf area density L_d times the drag coefficient times ρu^2

$$\frac{d\tau}{dz} = L_d c_d \rho u^2 \quad (4.47)$$

If i_w , l_m , c_d , and L_d are independent of height, Eqns (4.7), (4.46) and (4.47) can be solved analytically and give

$$u = u_c \exp\left\{-a\left(1 - \frac{z}{z_c}\right)\right\} \quad (4.48)$$

where a is the extinction factor for wind speed. Mathematically the solution for u contains a second term, that increases exponentially with depth, but experimental evidence (Uchijima & Wright, 1963; Inoue, 1963), indicates that the second term can be neglected. The expression for a in Eqn (4.48) is

$$a = \left(\frac{c_d L A I z_c}{2 l_m i_w}\right)^{0.5} \quad (4.49)$$

In Table 20 some values for a are listed. These values agree well with those of 2–2.8 recorded by Cionco (1972) and of 2.21 by Shaw et al. (1974), both for maize.

The equations used cannot be solved analytically when i_w or L_d are height dependent, and do not yield an exponential extinction either. However, just as for radiation profiles (Section 2.3.3), it is remarkable how close the solutions found numerically are to an exponential curve. In Fig. 22 the solution for a uniform leaf area density (Curve a) with $L_d = 1$, $z_c = 3$, $c_d = 0.15$, $i_w = 0.6$ resulting in $a = 2.37$ is compared with the solution for a parabolic leaf area density distribution $L_d = 6 \left\{ \frac{z}{z_c} - \left(\frac{z}{z_c} \right)^2 \right\}$ chosen such that the total LAI is again 3,

and for the rest the same parameter values (Curve b). For Curve b the profile is still very close to exponential, except in the upper part, which makes a smooth transition to the logarithmic profile above the canopy. To determine the value of the extinction factor mean values of the parameters may be used. The exponential character of the wind profile inside the canopy appears to be insensitive to the validity of

Table 19 Values of $K_h(\text{min})$ for three types of crop and three values of the upward equivalent sensible heat flux. The geometrical characteristics of the crops are given in Table 20. The value of the resistance r_h from bottom to top ($z_c K_h^{-1}$) for $K_h(\text{min})$ and the corresponding difference in T are also given.

	$C' = 1$	$C' = 10$	$C' = 100$
Grass			
$K_h(\text{min})$	0.19×10^{-3}	0.41×10^{-3}	0.89×10^{-3}
r_h	1053.	488.	225.
ΔT	0.84	3.9	18.
dT/dz	4.2	19.5	90.
Maize			
$K_h(\text{min})$	6.7×10^{-3}	14.5×10^{-3}	31.2×10^{-3}
r_h	373.	172.	80.
ΔT	0.30	1.4	6.4
dT/dz	0.12	0.56	2.56
Coniferous forest			
$K_h(\text{min})$	55×10^{-3}	122×10^{-3}	260×10^{-3}
r_h	182.	82.	38.
ΔT	0.15	0.66	3.0
dT/dz	0.015	0.066	0.30

its underlying assumptions, and will thus remain valid in many different situations. Equations (4.48) and (4.46) are now used to describe the profiles of wind and exchange coefficient inside the canopy.

4.3.2 Non-neutral conditions

Since a well verified theory such as the similarity theory of Monin-Obukhov is not available for the exchange inside the canopy, the sweeping assumption is made that Richardson's number has the same effect on the values of the exchange coefficient inside the canopy as above it. Because inside the canopy the friction acceleration of eddies is determined by collisions with stationary objects like leaves and

Table 20 Some aerodynamic crop characteristics calculated from the upper 7 parameters which are assumed as typical values. In brackets the values according to Eqns (4.65) and (4.66).

	Grass	Maize	Coniferous forest
<i>input values</i>			
w	0.005	0.05	0.2
LAI	5.	3.	2.
z_c	0.2	2.5	10.
L_d	25.	1.2	0.2
i_w	0.5	0.5	0.5
c_d	0.2	0.2	0.2
k	0.4	0.4	0.4
<i>calculated values</i>			
z_c-d	0.053	0.84	4.33
d	0.147 (0.145)	1.66 (1.72)	5.67 (6.69)
l_m	0.016	0.23	1.13
a	3.54	2.55	1.88
z_o	0.018 (0.026)	0.26 (0.32)	1.27 (1.28)
$(z_c-d)/z_o$	2.90	3.21	3.41
d/z_c	0.735	0.664	0.567
z_o/z_c	0.0916	0.105	0.127
$s(w/l_m)$	0.31	0.22	0.18
η	0.376	0.343	0.326

stems, rather than by the wind gradient, Richardson's number is redefined as

$$Ri = \frac{g}{T_{abs}} \frac{dT}{dz} \left(\frac{l_m}{u} \right)^2 \quad (4.50)$$

However, the correction factors Φ are expressed as a function of a dimensionless height ζ and not of Ri . Therefore ζ must be derived from Ri . This derivation is done with Eqn (4.28). It can be checked from the parameter values in Eqns (4.22) and (4.23) that the ratio Φ_h/Φ_m^2 increases from 0.74 to nearly one for increasingly unstable conditions (ζ negative). The deviation from unity is so small that ζ is taken equal to Ri in the unstable region. For stable conditions ζ is

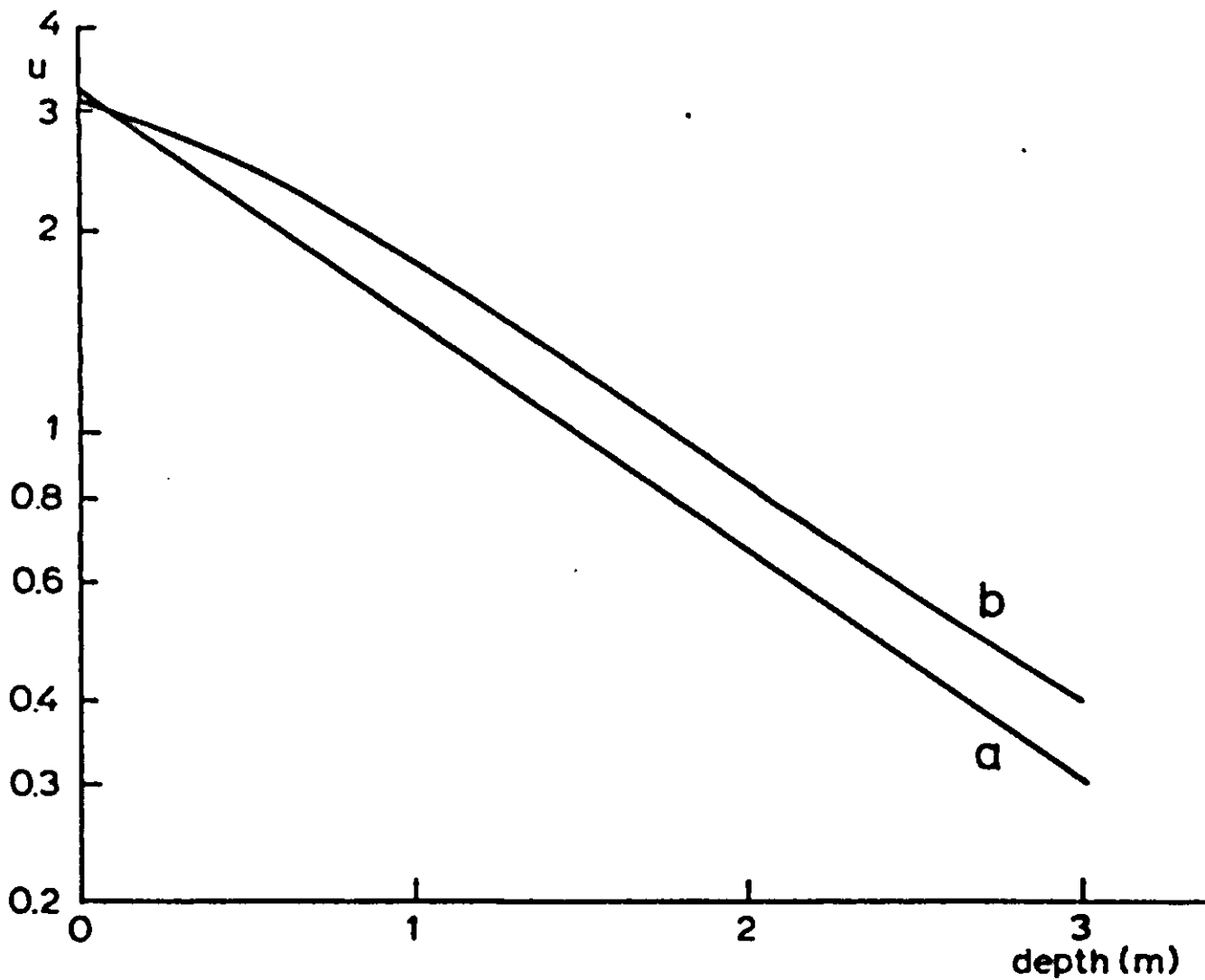


Fig. 22 | Numerically calculated wind profile inside the canopy for constant leaf area density (Curve a) and a parabolic leaf area density (Curve b). Other properties are invariant with height in both cases, and are given in the text.

substituted in the equations for Φ_h and Φ_m . Then Eqn (4.28) results in a second order equation for ζ . The solution of this equation is

$$\zeta = \frac{0.74 (1 + 8.926 Ri)^{0.5} + 2 \times 4.7 Ri - 0.74}{2 \times 4.7 (1 - 4.7 Ri)} \quad (4.51)$$

in which the factor 8.926 stands for $4 \times 4.7 \times (1 - 0.74) / (0.74)^2$. When the value of ζ is known, either by setting it equal to Ri (unstable) or from Eqn (4.51) (stable), it is substituted in the expression for Φ_h to calculate the correction for the exchange coefficient for heat. In principle the wind profile should also be affected by a correction through Φ_m . This is calculated as an average value of Φ_m over the whole height and used in the following equation

$$K_m = l_m i_w u / \Phi_m \quad (4.52)$$

as was done in Eqn (4.21). The new exponential extinction factor is then (cf Eqn (4.49)):

$$a' = a(\Phi_m)^{0.5} \quad (4.53)$$

Thus for stable conditions in the canopy the extinction of the wind speed is faster, and for unstable conditions slower¹.

At night, when a temperature minimum develops at the top of the canopy, the air is stable above the canopy but unstable inside because of the warm soil underneath. It is interesting that there is then a lower limit to the exchange coefficient for heat, when the wind speed drops to zero, as it usually does with an inversion above the canopy. Writing K_h as

$$K_h = l_m i_w u / \Phi_h \quad (4.54)$$

and using Eqns (4.23a), (4.50), we obtain for the lower limit:

$$K_h(\text{min}) = \frac{i_w l_m^2 3}{0.74} \left(\frac{g \frac{dT}{dz}}{T_{\text{abs}}} \right)^{0.5} \quad (4.55)$$

This equation can be combined with the expression for the equivalent heat flux C'

$$C' = \rho c_p K_h \frac{dT}{dz} \quad (4.56)$$

The gradient $\frac{dT}{dz}$ can be written explicitly and substituted in Eqn (4.55). Then the following expression for $K_h(\text{min})$ results

$$K_h(\text{min}) = \left(\frac{i_w l_m^2 3}{0.74} \right)^{2/3} \left(\frac{g C'}{T_{\text{abs}} \rho c_p} \right)^{1/3} \quad (4.57)$$

In Table 20 some values for the mixing length l_m are given for three types of crop. With these values $K_h(\text{min})$ is listed in Table 19 for C' is 1, 10 and 100 $\text{J m}^{-2} \text{s}^{-1}$. Under a nightly inversion C' is of the order of 10. The resistance r_h is calculated from bottom to top as $z_c / K_h(\text{min})$ together with the temperature difference over this distance. For the forest the temperature gradient is almost negligible, but for the grass it is large.

1. In the version of the model, used in Chapter 6, this feature was not yet included.

4.4 A fundamental approach to the derivation of z_0 and d^1

In principle the aerodynamic macrocharacteristics of a crop surface, i.e. z_0 and d , are a function of its aerodynamic microcharacteristics and its geometry. The theory of the previous section can be used to establish such a relationship. The fundamental requirement is that the boundary conditions should match at the interface between the flow regime above the canopy and that inside the canopy. The boundary conditions can be derived from the logarithmic wind profile above the canopy on the one hand and the exponential wind profile inside the canopy on the other. There is enough evidence for the correctness of both profiles in the main part of their region, but near the interface both profiles may slightly deviate. Then the outlined approach may break down, but according to the results this effect is not serious.

The three matching conditions concern wind speed, exchange coefficient and wind speed gradient. Combination of the last two implies continuity of shear stress. The three conditions are

$$u_c = \frac{u^*}{k} \ln \left(\frac{z_c - d}{z_0} \right) \quad (4.58)$$

$$k(z_c - d)u^* = l_{miw}u_c \quad (4.59)$$

$$\frac{u^*}{k(z_c - d)} = \frac{a}{z_c} u_c \quad (4.60)$$

which are found by combining the relevant equations above the canopy (4.2), (4.13) and (4.9) with those inside (4.46) and (4.48).

After elimination of u^* the following equations are obtained

$$z_c - d = k^{-1} \left(\frac{l_{miw}z_c}{a} \right)^{0.5} \quad (4.61)$$

$$z_0 = (z_c - d) \exp \left\{ - \frac{z_c}{a(z_c - d)} \right\} \quad (4.62)$$

1. This approach has not yet been incorporated in the simulation program that is presented in Section 5.6 and used in Chapter 6.

With the equations for l_m and a (4.45) and (4.49) given in the previous section, $z_c - d$ and z_o can be expressed in basic variables.

$$z_c - d = 2k^{-1}\pi^{-3/8}w^{3/8}i_w^{3/4}c_d^{-1/4}LAI^{-5/8}z_c^{5/8} \quad (4.63)$$

$$z_o = (z_c - d)\exp(-k\pi^{1/8}w^{-1/8}i_w^{-1/4}c_d^{-1/4}LAI^{-1/8}z_c^{1/8}) \quad (4.64)$$

In Table 20 the calculated aerodynamic crop characteristics are listed together with the assumed values for the crop geometry. For the forest, leafed branches are considered as effective leaves with a cross-section of 0.2 m. For the leaf (branch) area index a value of 2 is assumed. According to an empirical relation given by Tanner & Pelton (1960), z_o is

$$\log z_o = 0.997\log z_c - 0.883 \quad (4.65)$$

in which the lengths are expressed in cm. The results of this equation are given in brackets after the calculated number for z_o in Table 20. The same is done for d , according to a relation of Stanhill (1969):

$$\log d = 0.9793\log z_c - 0.1536 \quad (4.66)$$

The agreement of the calculated values with these empirical values (in brackets in Table 20) is quite satisfactory.

The ratio $\frac{u^*}{u_c}$, termed η by Jarvis et al. (1976), can be found from Eqn (4.58). The resulting values are also given in Table 20. According to Jarvis et al. (1976) η ranges between 0.25 and 0.35 for most types of coniferous forest. For a deciduous forest these values are about the same (Rauner, 1976).

The shear stress τ , divided by the air density ρ , is given by the product of K and $\frac{du}{dz}$. At the top of the canopy it can thus be found by multiplying Eqn (4.59) by Eqn (4.60)

$$\frac{\tau}{\rho} = \frac{l_m i_w a}{z_c} u_c^2 \quad (4.67)$$

The bulk drag coefficient C_d was defined by Den Hartog & Shaw (1975) with

$$\tau = \rho C_d u^2 \quad (4.68)$$

where u is a wind velocity anywhere above the canopy, so that C_d depends on height. According to the logarithmic wind profile C_d is

$$C_d = \frac{l_m i_w a}{z_c} \frac{\ln^2 \left(\frac{z_c - d}{z_0} \right)}{\ln^2 \left(\frac{z - d}{z_0} \right)} \quad (4.69)$$

Den Hartog & Shaw (1975) measured a value of 0.043 for C_d at a height of 3.55 m, for maize with a crop height of 2.5 m and a LAI of 3. Application of Eqns (4.68) and (4.69) gives a value of 0.041.

From Table 20 it is already evident that the ratio $\frac{z_c - d}{z_0}$ is fairly constant for quite different crops, because of the low values of the exponents in Eqn (4.64). It further appears that the geometrical characteristics in this equation can be combined in one factor s defined as the ratio of leaf width and mean leaf distance w/l_m . This is a leaf density number and closely connected to the leaf area index per sublayer, used in the radiation model. According to Table 20 s has a small range of values. By the use of the above definition for s (w/l_m) and the expression for l_m (Eqn (4.45), Eqn (4.64) can be written as

$$\frac{z_0}{z_c - d} = \exp(-k\pi^{1/4} i_w^{-1/4} c_d^{-1/4} s^{-1/4} 2^{-1/2}) \quad (4.70)$$

Similarly the value of $z_c - d$ is then given by

$$z_c - d = 2^{-1/4} k^{-1} \pi^{1/4} i_w^{3/4} c_d^{-1/4} w s^{-5/4} \quad (4.71)$$

Hence for a constant value of s , the distance $z_c - d$ is proportional to the leaf width w . From Table 20 the proportionality factor appears to range between 10 and 20.

The comparisons with empirical data give us enough confidence to use the above relations for calculations of z_0 and d when no direct measurements are available. It may even be that the accuracy of these calculations is better than the results of direct measurements that require the greatest care in calibrating and using anemometers and subsequent corrections for stability effects.

4.5 Variability in time and space

So far the variability has been limited to the vertical co-ordinate or to changes in time, much slower than the time constant (thermal) of the different layers of air in the canopy. It is likely that heterogeneities of plant density in horizontal directions cause corresponding variations in the exchange coefficient. Legg & Monteith (1975) gave some examples of this.

As a first approximation the effect of such heterogeneities on profiles of temperature or humidity can be studied by simple resistance schemes (Fig. 23). In such a scheme current (I) stands for flux of heat or mass, and voltage (V) for temperature or concentration. The release of heat and mass by the leaves is mimicked by applying currents at different nodes in the circuit. In the vertical direction four compartments are distinguished. In the horizontal direction there are two compartments which are repeated over and over again. In Fig. 23 only one such element is drawn. At the left side of an element the leaf area index is supposedly high. A high leaf area index means that more radiation is absorbed, so that the release of heat and mass is also higher. Therefore I made the source strength on the left two times larger than that on the right (Fig. 23). The other effect of a larger leaf area index is a decrease in mixing length for turbulent exchange. There-

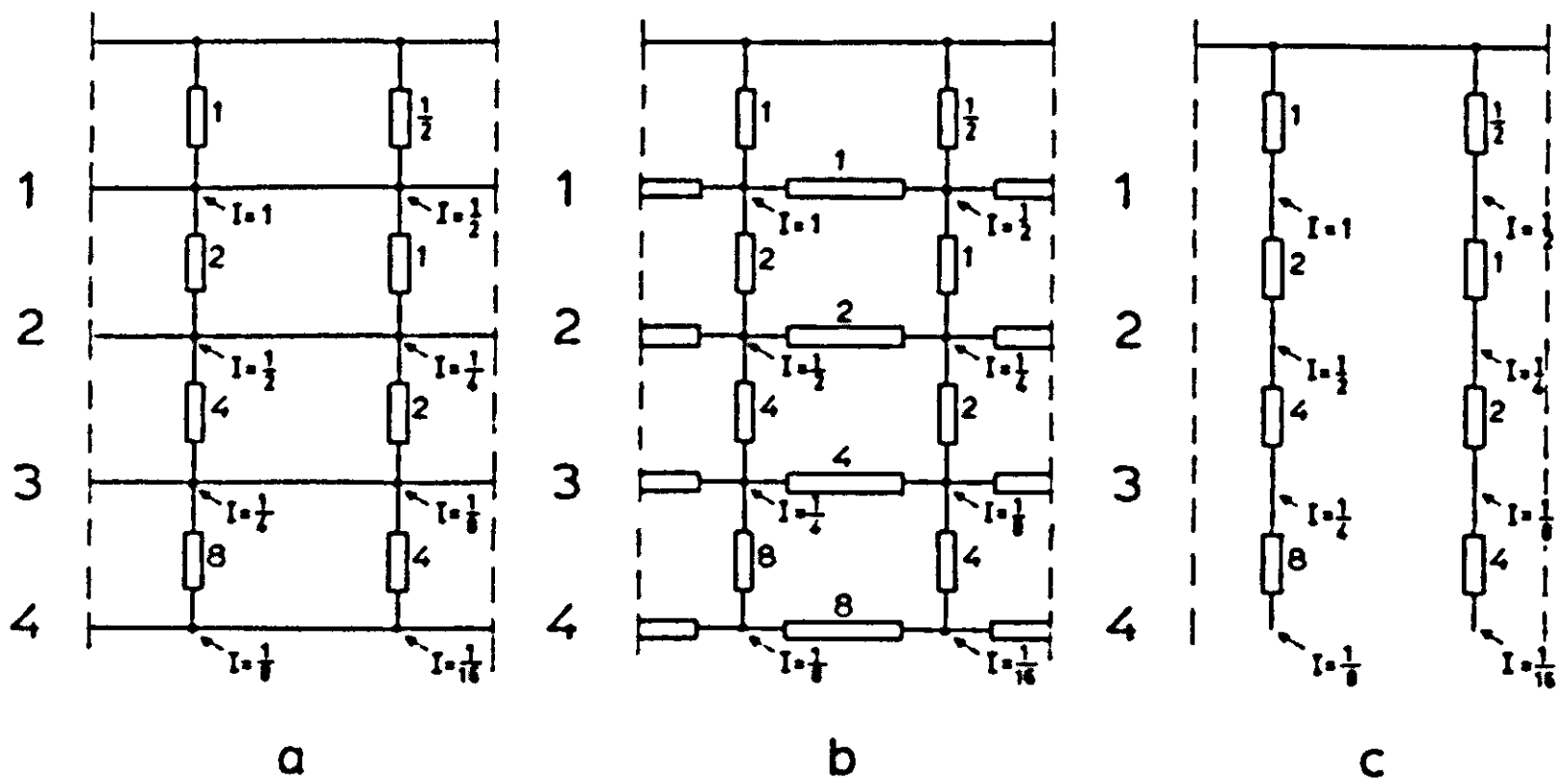


Fig. 23 | Three electric circuits as possible models for vertical and horizontal exchange between compartments inside the canopy, in the case of a repeating horizontal heterogeneity. For details see text.

fore the resistances on the left are two times larger than those on the right of the figure. This variation of a factor two in both characteristics is sufficiently large to obtain a basic insight in the effect of such a variability. In the downward direction the source strength is halved for each subsequent layer and the resistance is doubled, so that the exponential profiles of radiation and wind are mimicked. The alternating 'rows' of different leaf area index are connected by lateral resistances. The value of these resistances depends on the distance between these 'rows', or in other words on the characteristic size of the heterogeneity in the horizontal direction. When the distance is small enough, the horizontal resistances can be neglected (Case a, Fig. 23). This is equivalent to a one-dimensional scheme with a top resistance of $2/3$ and an applied current of $3/4$ that are doubled and halved, respectively in each lower layer. The resulting voltages at the four depths are given in Table 21. In the next scheme the horizontal resistances are of the same order as the vertical ones (Case b). This is probably typical for a crop in the last stage of vegetative development and in which the rows are closed. The characteristic size of the heterogeneity is of the order of the row distance. The solution for this scheme can be found by elementary algebra. The two voltages at the same level are averaged and listed in Table 21. From this table it appears that no substantial change in the average values occurs and that the one-dimensional scheme is still adequate. Finally the characteristic size of the horizontal heterogeneity may be so large that horizontal exchange may be neglected in comparison with the vertical exchange (Case c). The average figures for the voltages are a bit higher than in the one-dimensional case but no more than about 25 percent. However the variation in the horizontal direction is as

Table 21 The voltages calculated at the four depths for the three situations as presented in Fig. 23.

depth	a	b	c
1	0.938	0.970	1.172
2	1.813	1.852	2.266
3	2.563	2.604	3.203
4	3.063	3.104	3.828

large as a factor four. The results of these calculations are reassuring and suggest that a one-dimensional scheme is adequate as long as one is only interested in average figures.

However, because of the mean horizontal wind flow the heterogeneities, which have been transferred to the air conditions, do not stay where they are and are blown away. Thus a transient element is introduced in the system as air alternately passes the dense part of the foliage and the sparser part etc. The average temperature of a layer will always be somewhere between the extremes of Table 21. When the spatial variation only amounts to a factor two, as discussed above, this effect can be practically neglected.

However, temporal variations may be quite large due to gustiness of wind. Highly frequent changes in wind speed have an effect comparable to the discussed small distance variation in the spatial domain. Low frequencies are comparable with large-distance variation in the horizontal directions. In the high frequency or small-distance situation temperatures are almost constant because of the inertia of the system. In the low frequency or large-distance situation fluxes are constant and temperatures are proportional to resistances. For intermediate frequencies both vary. In Fig. 24 a simulation result is given where the sensible heat flux C above the canopy is plotted against the temperature difference over 0.5 m distance (from z_c to z_r). The radiant flux was constant, but the wind speed varied sinusoidally around an average of 2.4 m s^{-1} with an amplitude of 80 percent of the mean. Three frequencies are considered, a cycle period of 10, 100 and 1000 seconds respectively.

The square in the middle gives the equilibrium situation for a constant wind speed of 2.4 m s^{-1} . It is evident that for a low frequency the flux is almost constant whereas for a high frequency the temperature difference is almost constant. The low frequency oval is much sharper at its left end, because the time constant itself varies with the wind speed.

These results emphasize the need for studies on the frequency distribution of wind speed and exchange coefficients.

The non-linearity due to stability corrections may become quite important when an inversion develops. In Fig. 20 the relation was given between wind speed without gusts and the temperature difference. When the wind speed is subject to temporal variations, the transport above the canopy is maintained during certain fractions of

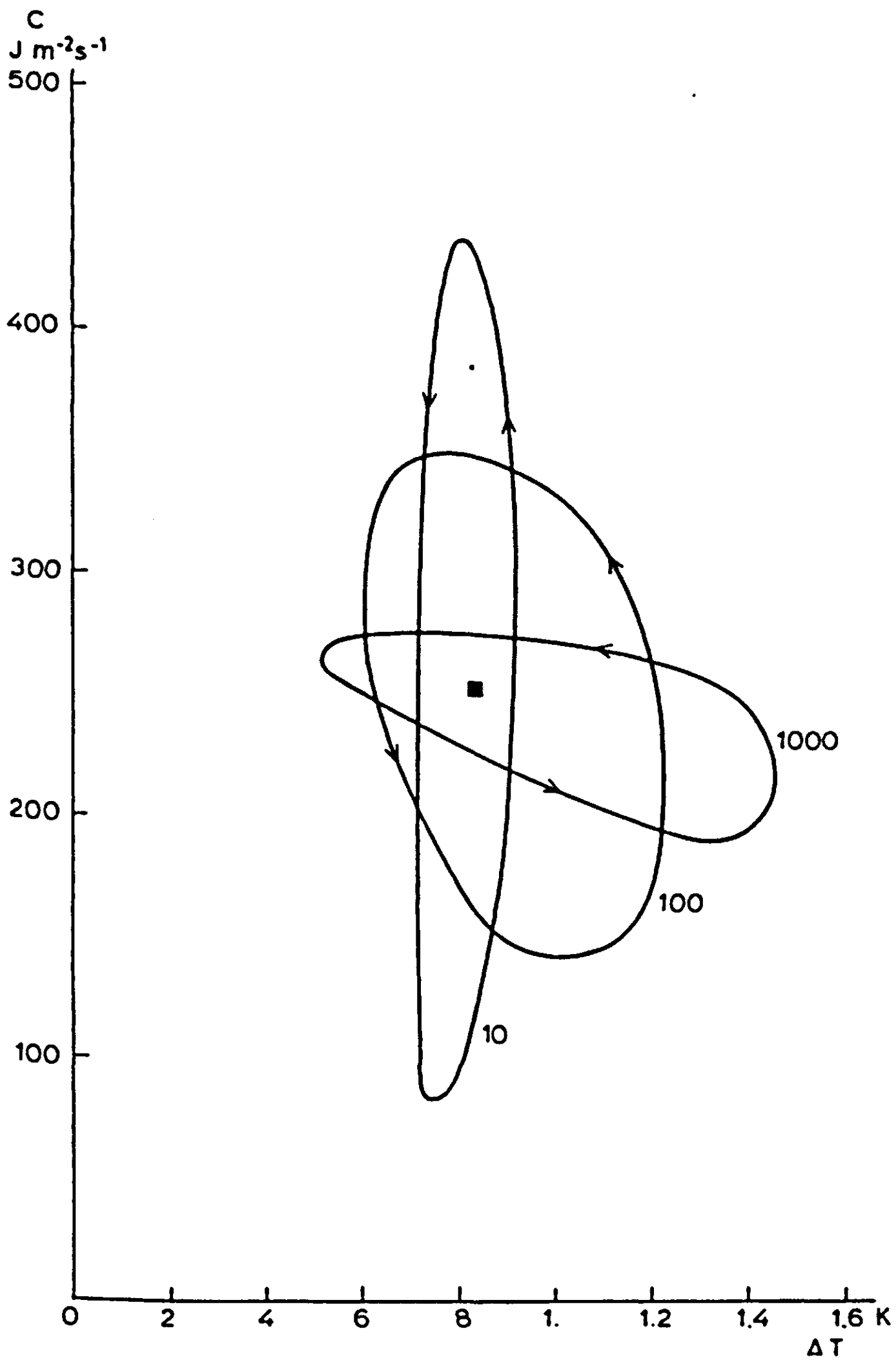


Fig. 24 | Simulated sensible heat flux against temperature difference, when the wind speed varies sinusoidally with a cycle period of 10,100 or 1000 seconds. The square in the middle of the curves gives the equilibrium situation when the wind speed has the mean value of the sinusoid. For further details see the text.

the time, even if the mean value is below the critical wind speed. Thus in general the simulated transition to inversion is too sudden if a steady average value is used for the wind speed (see also Section 6.3.7).

4.6 List of symbols used in Chapter 4

symbol	description	first used in equation	unit	name in simulation program
a	extinction factor for wind	4.48	–	ALPHAK
c_d	drag coefficient of the leaves	4.47	–	DRAGC
C_d	bulk drag coefficient	4.68	–	
C	sensible heat flux	Fig. 19	$\text{J m}^{-2} \text{s}^{-1}$	SHFL
C'	equivalent heat flux	4.18	$\text{J m}^{-2} \text{s}^{-1}$	
d	zero plane displacement	4.2	m	D
e_a	water vapour pressure in the air	4.1	mbar	VPA
g	gravity acceleration	4.16	m s^{-2}	GR
I	current	Fig. 23	A	
I	integral of $\Phi/(z-d)$	4.42	–	INTM, INTH
i_w	turbulence intensity	4.46	–	IW
k	Von Karman's constant	4.2	–	KARMAN
K	exchange coefficient	4.5	$\text{m}^2 \text{s}^{-1}$	
K_h	exchange coefficient for heat	4.14	$\text{m}^2 \text{s}^{-1}$	K
K_m	exchange coefficient for momentum	4.13	$\text{m}^2 \text{s}^{-1}$	
L	Monin-Obukhov length	4.19	m	MONOBL
l_m	mixing length	4.4	m	LMIX
L_d	leaf area density	4.44	$\text{m}^2 \text{ leaf m}^{-3} \text{ air}$	
r_h	resistance for transport of heat between z_c and z_r	4.15	s m^{-1}	ABTURR
Ri_d	Richardson's number in differences	4.37	–	RICHN
Ri_g	Richardson's number in gradients	4.16	–	

symbol	description	first used in equation	unit	name in simulation program
s	foliage density coefficient	4.70	m^2 leaf m^{-2} ground	
T_a	air temperature	4.1	$^{\circ}\text{C}$	TA
T	equivalent air temperature	4.1	$^{\circ}\text{C}$	
T_{abs}	absolute air temperature	4.16	K	TABS
u	wind velocity	4.2	m s^{-1}	WIND
u_c	wind velocity at the top of the canopy	4.48	m s^{-1}	WINDC
u_r	wind velocity at the reference level	4.32	m s^{-1}	WINDR
u^*	friction velocity	4.2	m s^{-1}	USTAR
w	average width of the leaves	4.44	m	WIDTH
z	height above the ground	4.1	m	
z_c	height of the canopy	4.3	m	CROPHT
z_r	reference height	4.15	m	REFHT
z_o	roughness length	4.2	m	ZNOT
$\Delta \dots$	difference of a variable between two levels	4.30	operator	
ζ	dimensionless height	4.20	–	ZETA
ρ	density of air	4.7	kg m^{-3}	
ρc_p	volumetric heat capacity of air	4.18	$\text{J m}^{-3} \text{K}^{-1}$	RHOCP
τ	shear stress	4.7	N m^{-2}	
Φ_m	correction factor for transport of momentum	4.21	–	PHIM
Φ_h	correction factor for transport of heat	4.22	–	PHIH

5 Programming aspects

5.1 Introduction

The theoretical considerations of the foregoing chapters can be quantitatively evaluated when they are formulated in terms of a computer program. Some difficulties that are encountered during this formulation are discussed in this chapter. The problem definition, as given in the introduction (Section (1.1)), largely defines the boundaries of the system, both in time and space, but for tactical reasons the boundaries must sometimes be shifted. This aspect, and also the formulation of the boundary and initial conditions, are discussed in Section 5.2. The model that results after connection of the different submodels, has such an exorbitant size that the employment of a hierarchical technique is necessary (Section 5.3).

In general different methods are available to solve a certain problem. A discussion of the choice of the computer language and the numerical technique is given in Section 5.4. Stiff systems are notorious for the computer time necessary to simulate their behaviour; a large system often turns out to be a stiff system. An approach to reduce the required computer time is given in Section 5.5.

The listings of the computer programs used are printed in Section 5.6.

5.2 Boundaries in time and space

5.2.1 Initialization

In Fig. 25 time is schematically presented along the horizontal axis and space along the vertical axis. The distance between the two boundaries in time stands for the simulation period. The natural cycle of micrometeorological processes is a day, so that one is usually interested in daily courses and daily totals of, for instance photosynthesis and transpiration. Hence the simulation period is chosen as 1 day or 86400 seconds. At the beginning of the simulation run, at midnight, the initial conditions of the integrals must be given. Initialization of

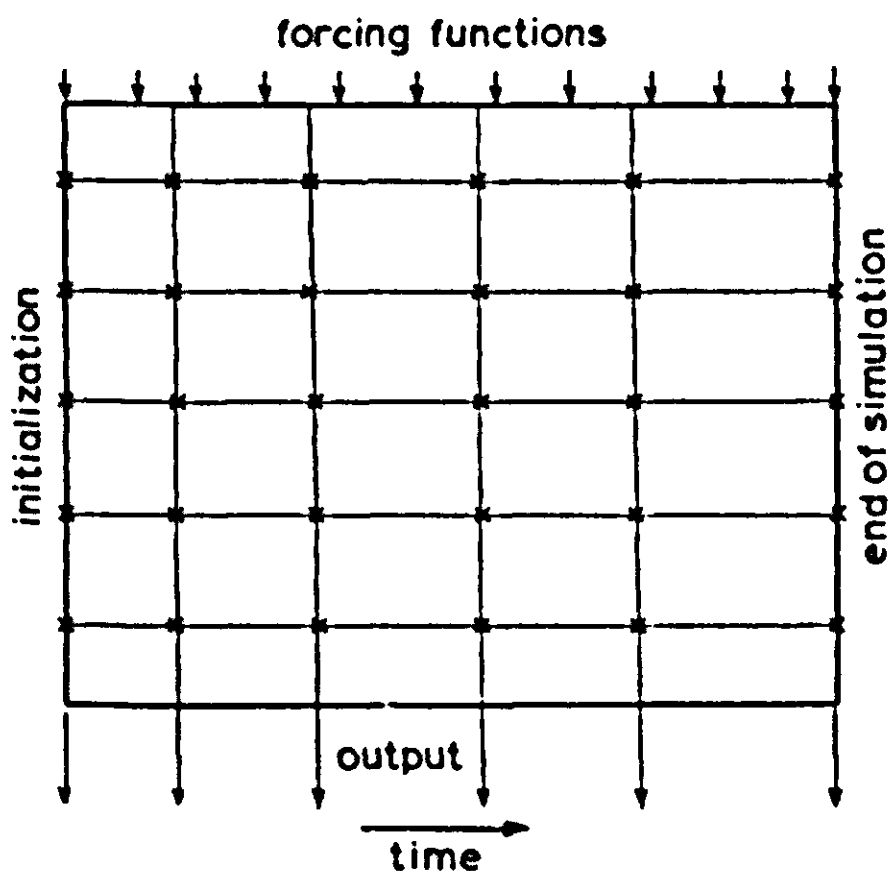


Fig. 25 | Scheme of the simulated space-time domain. Space is represented by the vertical axis and time by the horizontal axis. The forcing functions influence the system at its outer spatial boundaries. The initial values must be given for the whole system at time zero. At fixed moments of time the results of the model from different places in the system and for different variables are sent to the output devices.

air conditions is not a serious problem because of the small time constant. Therefore the aerial profiles of temperature and humidity start off as straight lines. After a few hundreds of seconds the equilibrium profile is reached. The time constants of plant water content and soil heat content are much larger, so that the effect of initialization is much longer noticeable. This effect can be eliminated by extending the simulation over some days, until a cyclic equilibrium has established. If a reasonable guess is made for the initial values, the second and the third day are already practically equal. Then the midnight values of the integrals after one single day of simulation are sufficiently accurate. The initial values for a standard run are also used in later runs of the sensitivity analysis. In theory this procedure introduces errors of initialization, but in practice the resulting change in initial conditions is so small that its effect is negligible.

5.2.2 *Spatial boundaries*

The spatial boundaries of the simulated system should be chosen such that the system does not influence its environment. Therefore the soil surface is not a good choice for the lower boundary. Instead the lower boundary should be taken so deep in the soil that the daily heat wave is damped out. The resulting increase in size of the system is not dramatic and is well compensated by the simplification of the boundary condition obtained.

For the upper boundary in the air such a solution is not possible. The large aerial exchange coefficient, which moreover increases with height, results in a damping 'depth' in the air of the order of a hundred metres. When the upper boundary is fixed so high above the ground, the assumption of horizontal homogeneity breaks down, because of the influence of adjacent fields that have different properties. By incorporating this influence into a model, one is trespassing on the field of macrometeorology.

Thus the height of the upper boundary should not exceed 2 or 3 m, at which normal meteorological observations are made. At this height the assumption of horizontal homogeneity is allowed, if the measurements are made not too close to the sides of the field. Limiting the height to 2 or 3 m has the great advantage that lateral boundaries need not be considered, but the disadvantage that system and environment are still mutually connected. Hence the condition of the air at the interface must be recorded and used as a forcing function, unlike the condition of the soil.

From a result of the simulation, which is given later in Section 6.3.2 we know that the input data need not be given with a high resolution in time. Hourly fluxes and hourly average profiles are not affected by noise with time constants less than a few minutes. An exception must be made for wind speed and radiation. However, most of the variation in radiation is attributable to transitions from the sun shining to being covered and vice versa. The resulting bimodal distribution is accounted for by separation into completely clear and completely overcast conditions (Section 3.4). In principle gustiness of wind can be represented by a probability distribution of wind speed and an auto-correlation function. These functions themselves change rather slowly. With these precautions the forcing functions can be given with a time resolution of about half an hour, so that the input tables

need not be very long.

5.2.3 Conversion of measured weather data

Temperature ($^{\circ}\text{C}$) and humidity (mbar) can be given directly as AFGEN functions of the hour of the day. Humidity may also be expressed as dew point, from which the water vapour pressure is calculated as

$$e_a = 6.11 \exp\{17.4T_d/(T_d + 239)\} \quad (\text{see Eqn (3.21)})$$

It may also be found from the measured relative humidity θ_a as

$$e_a = \theta_a e_s(T_a) \quad (5.1)$$

where $e_s(T_a)$ is the saturated vapour pressure at air temperature. The third possibility is that humidity is given as a wet bulb temperature T_w , from which e_a can be derived as

$$e_a = e_s(T_w) - \gamma^*(T_a - T_w) \quad (5.2)$$

where γ^* is the apparent psychrometric constant (0.623).

In this simulation program wind speed is characterized by the mean value in m s^{-1} only.

Radiation can be entered as incoming solar radiation or as net radiation, but preferably both figures should be available. Assuming a bimodal distribution, and using the figures given in Section 2.2.2, we can fully characterize the radiation regime with the fraction of overcast sky (FOV) and the apparent sky temperature (SKT).

The measured incoming flux supposedly consists of the contributions of the two possible sky conditions in appropriate fractions of time. A programming problem occurs when the measured flux exceeds the standard value under a clear sky. Then the fraction overcast (FOV) is fixed at zero, and the solar fluxes for the standard clear sky are enlarged so that the measured flux is used. As a guide line the weighted sum of the fluxes used in the program should always equal the measured fluxes. Alternatively, if the measured flux is less than the standard value under an overcast sky, the fraction overcast is fixed at unity, and the standard values are decreased by the appropriate fraction.

Type of radiation data available

There are three possible situations:

1 Both net and solar radiation data are available. Then the fraction overcast is based on the data for solar radiation and the apparent sky temperature is calculated from the difference between the measured net radiation and calculated net solar radiation. During the night the fraction overcast FOV is meaningless for this situation, and is set at unity for simplicity.

2 Only solar radiation data are available. Then FOV is first calculated, and the apparent sky temperature is found from a linear interpolation between the standard values for a clear sky and an over-

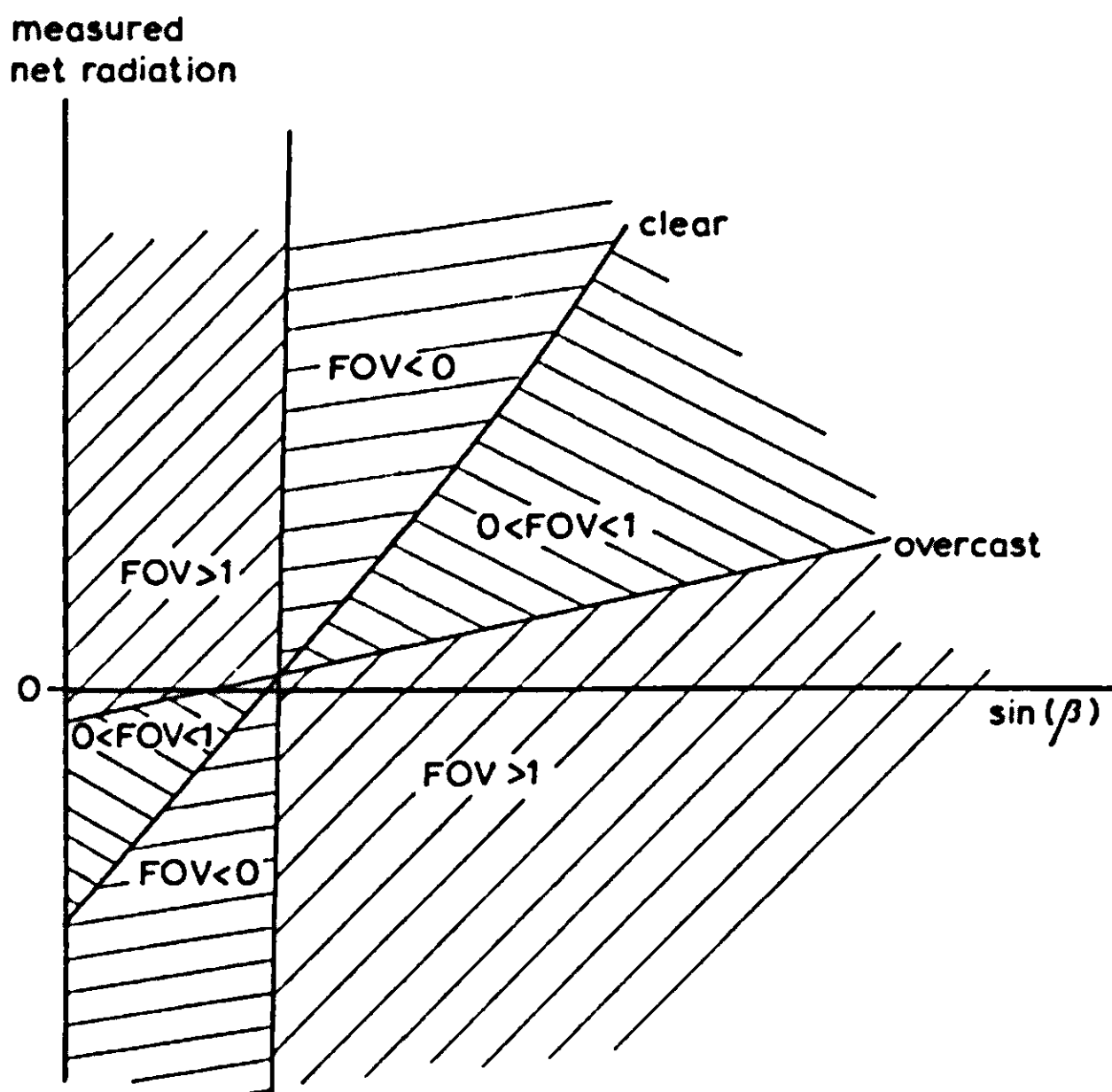


Fig. 26 | The graph of measured net radiation versus the sine of the solar height is divided into six regions according to the value of the fraction of overcast sky FOV. For the line "overcast" the value of FOV is unity, and for the line "clear" it is zero. The line "clear" shows an upward curvature because of the decrease in crop reflection with solar height. The value of FOV shows a singularity for the value of $\sin\beta$ at which the lines "clear" and "overcast" cross.

cast sky (Section 2.3.6). During the night the data required are missing here, and FOV is set to unity.

3 Only net radiation data are available. In this case FOV is calculated from the supposed net radiation under a clear sky and under an overcast sky, again with the use of the assumption for the apparent sky temperature of Section 2.3.6. Here the fraction overcast can also be calculated during the night. Computational difficulties may arise at low solar elevations when the net radiations computed for overcast and clear sky are almost equal (Fig. 26). Under a clear sky net radiation is zero at about 7 degrees solar height, and under an overcast sky at about $3\frac{1}{2}$ degrees height. Both computed fluxes are equal to about $12 \text{ J m}^{-2} \text{ s}^{-1}$ when the solar height is 8 degrees. Even when the measured fluxes deviate only slightly from this calculated value, the fractions of overcast sky that are calculated are exceptional. This is not a serious problem, since the truncation method described earlier for FOV is used. Still, one should be aware of errors in the radiation data causing exceptional values of FOV!

5.3 Hierarchical approach

The hierarchical approach is based on the idea that only two levels of causal depth should be distinguished in a model (van Keulen, 1975). The problem in applying this elegant principle is that in complicated systems the causal relations are so manifold that a relational diagram looks like a spider's web rather than a pyramid. Usually the causal connections are more numerous in some places than in others so that it is sometimes possible with some skill and effort in modelling to distinguish regions with relatively many relations inside and only a few outside. These regions are then called "submodels". After all one is often not interested in the internal behaviour of the variables inside a submodel. It is then quite useful to consider the submodel as a black box and to try to summarize the input-output relations of the submodel in some way or another, so that a simpler representation is obtained. The degree of simplification is very much a function of the accuracy one is willing to sacrifice.

For instance, the rate of growth respiration can be calculated from the rate and the type of the numerous biochemical conversions taking place in the growing tissue. Without a marked loss of accuracy, growth respiration can also be calculated as the growth rate times a weighted

sum of the chemical fractions of the growing plant material (Penning de Vries, 1973). The effect of the biochemical pathways can be neglected and temperature has only an indirect effect through the growth rate itself. When a larger loss of accuracy is acceptable, the growth respiration can be estimated as 25 percent of the gross photosynthesis. The simplified representation of a submodel can be called a *derived* model. An example is the calculation of reflection and extinction coefficients of radiation in a canopy (Section 2.3.3). Here the structure of the original and the simplified submodel are similar in the equations for horizontal leaves. However the structure of the derived model may also be entirely different from the original one. Van Keulen (1975) gave a soil evaporation submodel, that mimicks soil moisture extraction by an exponential extinction with depth. If a derived model is suggested by measurements, one often ends up with a regression equation that has lost all similarity in structure to the original submodel. The hierarchical approach is an essential tool in the reduction of the size of models. Submodels with few outside connections are replaced by simpler expressions for their input-output relations.

5.4 Solution techniques

A quantitative study of the dynamics of systems requires the solution of a set of differential equations. For simple linear systems well established mathematical techniques can provide solutions expressed in well known functions, such as sine waves, exponentials, Bessel, Legendre, gamma functions etc. Addition of non-linear terms to the differential equations often prevents the use of analytical techniques so that numerical methods are the only way out then.

Sometimes submodels with a fast time response are used. In these models one is not interested in the dynamic behaviour of the state variables but only in their equilibrium situation. Simulation is then not always necessary (Fig. 27). When there are only a few linear simultaneous differential equations, the equilibrium solution can be directly found by elimination (leaf temperature and transpiration, Section 3.2). When there are many simultaneous linear differential equations a matrix technique must be applied to find the equilibrium solution. Waggoner et al. (1969) and Goudriaan & Waggoner (1972) used this technique to find the equilibrium profiles of temperature and humidity of the air in a canopy. It is a very efficient technique in

Fig. 27 | Scheme of solution techniques to be applied, according to the type of problem.

	linear	nonlinear
fast	matrix algebra if few equations are parallel, then eliminate by hand (leaf energy balance) if too many equations are parallel, then use relaxation method (radiation model) if clarity is required, then integrate (aerial profiles)	iteration (wind and turbulence) if more than two equations are parallel, then integrate
slow	conventional methods of solving differential equations if too many equations are parallel, then integrate numerically	analytic solution rarely possible, usually numerical integration necessary

terms of computing time, but not very lucid. Because of its restriction to an equilibrium situation such effects as wind gustiness cannot be studied (Sections 4.5, 6). For reasons of clarity and sound physical representation, integration of the heat and humidity contents of the layers of air was preferred in this study.

Matrix inversion is the classical method for solving a set of linear equations. For large matrices inversion becomes unwieldy, but then the mathematical structure often permits other solution techniques like a relaxation method. Such a method is applied in the radiation model (Section 5.6). The principle of the relaxation method is to calculate consecutively each of the equations of the matrix, whereby the last calculated values of the unknowns are repeatedly substituted

until convergence, with or without a weighting factor. A substantial speeding up of convergence can be obtained by a careful choice of the sequence of calculation of the equations that form the matrix. In the radiation model an alternating downward and upward calculation is much faster than a repetitive downward calculation only. This mathematically efficient procedure is in fact suggested by the physical course of the rays from top to bottom and then from bottom to top. Also the formulation of the equations corresponds to the basic concept (Eqn (2.38)).

When the fast differential equations are non-linear, the equilibrium situation may be found by iteration. For a single non-linear differential equation this may be most conveniently done by using the IMPLICIT loop, available in CSMP (Section 4.2.2). For a pair of differential equations two unknowns must be found so that a nested iteration must be executed, or a two-dimensional method must be applied. The latter was described by de Wit & van Keulen (1972) for a situation where the equilibrium must be found between one-valued potassium and two-valued calcium ions, both in solution in the soil moisture and adsorbed onto the clay particles. When more state variables are introduced, iteration becomes unwieldy so that integration is the right method.

Integration over time or space

In a continuous simulation language like CSMP only one dimension at the same time can be considered as continuous. When a partial differential equation like Eqn (3.51) has to be solved, one is in principle free to choose whether the time or the space dimension is to be the continuous variable. Usually time will be chosen, but there are situations where another variable is preferable. When a step function is applied at one boundary of the system and the transient response of the diffusion process has to be studied, it is advantageous to choose the variable z/\sqrt{t} as the independent continuous variable. De Wit & van Keulen (1972) applied this method to simulate the wetting front in soil water infiltration. The height dimension z itself can be chosen as the continuous variable to check the effect of stratification in the conventional simulation. For a model of the type described here, Goudriaan & Waggoner (1972) found in this way that there are no objections to stratification. For equations with a diffusion term,

integration over space has the disadvantage that it usually concerns a two-boundary problem, whereas initialization can only occur at one boundary. Thus an iteration for an initial condition at one boundary has to be done until the boundary condition at the other end is met. In this special case the temperature and water vapour pressure profiles are coupled so that iteration should be done for two variables at the same time, which is even more impracticable. Finally compatibility with other simulation programs requires time as the continuous variable. For these reasons the integration was done over time, and the height dimension was discretized to a number of layers.

A simulation language like CSMP is adequate for the formulation of the model described. Most processes are continuous in time and deterministic. An exception may be the fluctuation of radiation and wind speed, but these can be dealt with by methods such as those given in Section 5.2.2. They do not justify the use of a discrete simulation language like SIMULA. CSMP has the advantage of compatibility with FORTRAN so that numerical techniques, such as those discussed earlier in this section, can be easily incorporated. There are convenient input and output facilities in CSMP, and the sorting routine allows grouping of statements corresponding to the submodels discussed in the previous chapters, instead of ordering them in computational sequence. A final and important argument in favour of CSMP is that different programs about related subjects should be as compatible as possible. For these reasons CSMP was chosen as the language in which the simulation model was to be formulated.

5.5 Stiff systems

Often the time constants of different processes, treated in one simulation model, differ by powers of ten. This is also the case for this micrometeorological model in which the time constant of the air conditions is of the order of seconds, but that of the heat content of the soil of the order of a thousand seconds. The integration of the fast processes requires small time intervals so that the computational costs are highly related to the degree of stiffness. The word stiffness originates from mechanical engineering. A complicated mass-spring system, with some stiff springs, shows both high and low frequencies when disturbed. The main problem for the simulation of a stiff system is how to reduce the number of computations. One method, the matrix

solution, has been indicated in the previous section. However this is only applicable if one is uninterested in the transient response and if the system is linear. Its main disadvantage, decisive in the micro-meteorological model, is its lack of clarity.

Conditional bypassing of the slow processes

Minimization of the number of computations can be achieved in the first place by bypassing the computations for the slow processes during most time intervals. This can only be properly organized if it is clear which parts of the model can be considered as fast and which as slow. In Fig. 28 the model comprizes an input segment, a central part and an output segment. The central part is divided into fast and slow processes, which are mutually connected. The coupling cannot be strong, otherwise the slow processes would become fast and the system would lose its stiffness. The coupling cannot be absent either, since then the system would fall apart in two isolated systems to be separately simulated. Therefore in a stiff system the coupling between fast and slow processes is weak by definition. The input segment is

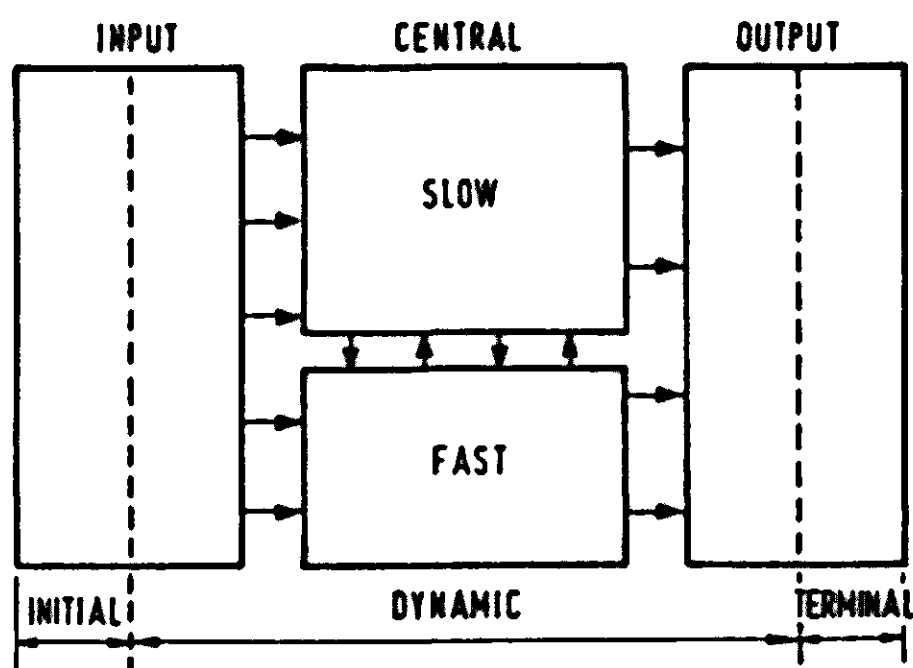


Fig. 28 | The main parts of a dynamic simulation model. The words "INITIAL" "DYNAMIC" and "TERMINAL" refer to the CSMP terms that are used to indicate the segments of a simulation model. The input part contains those calculations connected with initial values and forcing functions, in as far as they are not subject to a feedback from state variables of the model. The output part contains those calculations connected with output variables, from the point where they no longer influence state variables.

characterized by a one-way flow of information to the central segment, and by absence of state variables or integrals in the calculations. The same applies to the output segment, which only receives information from the central part but does not return it. Because of these definitions the INITIAL segment of CSMP is always a part of the input segment, and likewise the TERMINAL segment is a part of the output segment. The calculations given in the INITIAL segment are only executed at time zero, and the calculations in the TERMINAL segment only after termination of the simulation run. The DYNAMIC segment, which is executed every time-interval, may contain input, central and output type calculations. Because the slow processes are conditionally bypassed, only part of the DYNAMIC segment is executed every time-interval (Fig. 28). Hence the number of calculations can be considerably reduced.

Conditional bypassing of the fast processes

Not only the number of calculations of the slow processes, but also that of the fast processes can be reduced. Here the fast processes are so much damped by diffusion that they soon reach equilibrium after a disturbance. Once an initial disturbance is damped out, the fast processes remain in a state of pseudo-equilibrium, determined by input forces and the state of the slow processes. In this stage there is no longer the necessity for recomputation of the rates, and the states can be fixed, until some condition affecting the pseudo-equilibrium has changed. Then the computations are resumed, and the fast variables can adapt to the new situation. A new equilibrium is soon established, after which the computations are bypassed again.

The methods of bypassing fast or slow processes are supplementary. Before their application in the micrometeorological simulation program is discussed, a simple fictive technical example is given.

The temperature of a water bath is to be regulated at 50°C. The heat exchange of the bath with the surrounding air and the heating power of the element in the bath have such values that at most a temperature difference of 100 K with the surrounding can be maintained. The heat storage capacity of the water bath is such that the time constant for the exchange with the surroundings is 1 h. The heating element is controlled by a thermometer immersed in the bath with an on-off mechanism that switches at 50°C. The time constant of

the thermometer with respect to the water is denoted by $TAU2$ and has a value of 10^{-6} h. The time constant of the water bath is denoted by $TAU1$. The air temperature is assumed to be 20°C . The equations for this system, written in CSMP are

$$TM = \text{INTGRL}(0., DTM)$$

$$TW = \text{INTGRL}(0., DTW)$$

$$DTM = (TW - TM)/TAU2$$

$$DTW = (20. - TW)/TAU1 + \text{INSW}(50.- TM, 0., 100.)$$

$$\text{PARAM } TAU1 = 1., TAU2 = 1.E-6$$

$$\text{TIMER } \text{FINTIM} = 1., \text{PRDEL} = 0.1$$

PRINT TW, TM

TM is the temperature of the thermometer and TW the temperature of the water bath. The process of heating is simulated for 1 hour, starting at a temperature of 0°C . It is clear that the easiest way to solve this problem is not the simulation method, but the mathematical-analytical method, perhaps with equalization of TM to TW . The solution is then:

$$TW = \min(120. \times (1 - \exp(-t/TAU1)), 50.)$$

so that the level of 50°C is reached after 0.539 h.

However the simulation program is used for the purpose of illustrating the bypassing method. First the Runge-Kutta-Simpson method is employed for the integration and no special measures are taken. This method adapts its time interval to the rate of change of the fastest process. The program is then computed 2437600 times to cover the full hour of simulation. Hence this is of the order of the total simulation period divided by the smallest time constant.

Now the performance of the bypassing method is illustrated. The method of integration must be rectangular, and the time interval is chosen as 10^{-6} h. The slow process here only consists of the calculation of the rate of change in water temperature DTW . This equation is bypassed if TW differs by less than DEV from the value of TW during during the last calculation of DTW . For illustration purposes four values of DEV are used subsequently, 0.001, 0.01, 0.1 and 1. The fast process only consists of the calculation of DTM . This equation is bypassed and set to zero, if TW and TM differ by less than the same criterion DEV . In Table 22 the number of computations executed and the maximum deviation of TW and TM from the analytical solution are listed for four different values of the error criterion DEV . More-

Table 22 The number of computations for the straightforward RKS integration method and for the rectangular integration method in combination with the bypassing method with different values for the error criterion DEV. This table applies to the program listed in Table 23.

Integration method	TAU2	DEV	number of computations	maximum deviation of TW or TM
RKS	10^{-6}	–	2437600	0.0001
RECT	10^{-6}	0.001	66515	0.01
RECT	10^{-6}	0.01	6914	0.02
RECT	10^{-6}	0.1	695	0.2
RECT	10^{-6}	1.0	71	2.0
RKS	10^{-3}	–	52983	0.001
RECT	10^{-3}	0.001	1000	0.02
RECT	10^{-3}	0.01	1000	0.2
RECT	10^{-3}	0.1	511	0.2
RECT	10^{-3}	1.0	69	2.0

over the whole procedure was repeated for a time constant $TAU2$ of 10^{-3} h.

The time constant has little influence on the number of computations if the error criterion is chosen wide enough. The number of computations is about inversely proportional to the width of the error criterion. The listing of the program used for this purpose is given in Table 23.

The bypassing method, both for the slow and the fast processes, is also applied in the micrometeorological program. A scheme of the method is given in Fig. 29. Because of the additional input and output segments in the DYNAMIC, the scheme is more complicated than for the simple example of the water bath, but the basic idea of the method is the same.

The calculations of the weather conditions above the canopy, as described in Section 5.2.3, are input calculations and are executed with a fixed frequency of once every 180 seconds. Moreover within this time they are also done when the weather conditions have changed by more than a certain criterion. Transpiration and CO_2 -assimilation are already mainly determined by the outside weather conditions and

Table 23 Listing of the CSMP program to demonstrate the use of the bypassing method.

TITLE STIFF EQUATION

INITIAL

TELW = 0.

TELM = 0.

TEL = 0.

DYNAMIC

TM = INTGRL (0., DTM)

TW = INTGRL (0., DTW)

PARAM TR = 50., TA = 20., TAU2 = 1. E-6, TAU1 = 1.

METHOD RECT

TIMER FINTIM = 1., PRDEL = 0.1, DELT = 1. E-6, OUTDEL = 0.1

PROCED DTM, TELM = RATEM (TW)

IF (ABS (TW-TM). LT. DEV. AND. TIME. NE. 0.) GO TO 10

DTM = (TW-TM)/TAU2

TELM = TELM + 1.

GO TO 11

10 DTM = 0.

11 CONTINUE

ENDPRO

PROCED DTW, TELW = RATEW (TA)

PARAM DEV = (1., 0.1, 0.01, 0.001)

IF (ABS (TWL-TW). LT. DEV. AND. TIME. NE. 0.) GO TO 20

DTW = (TA-TW)/TAU1 + INSW (TR-TM, 0., 100.)

TELW = TELW + 1.

TWL = TW

20 CONTINUE

ENDPRO

PRINT TM, TW, TELW, TELM, TEL, DTM, DTW

PRTPLT TM, TW

NOSORT

TEL = TEL + 1.

END

STOP

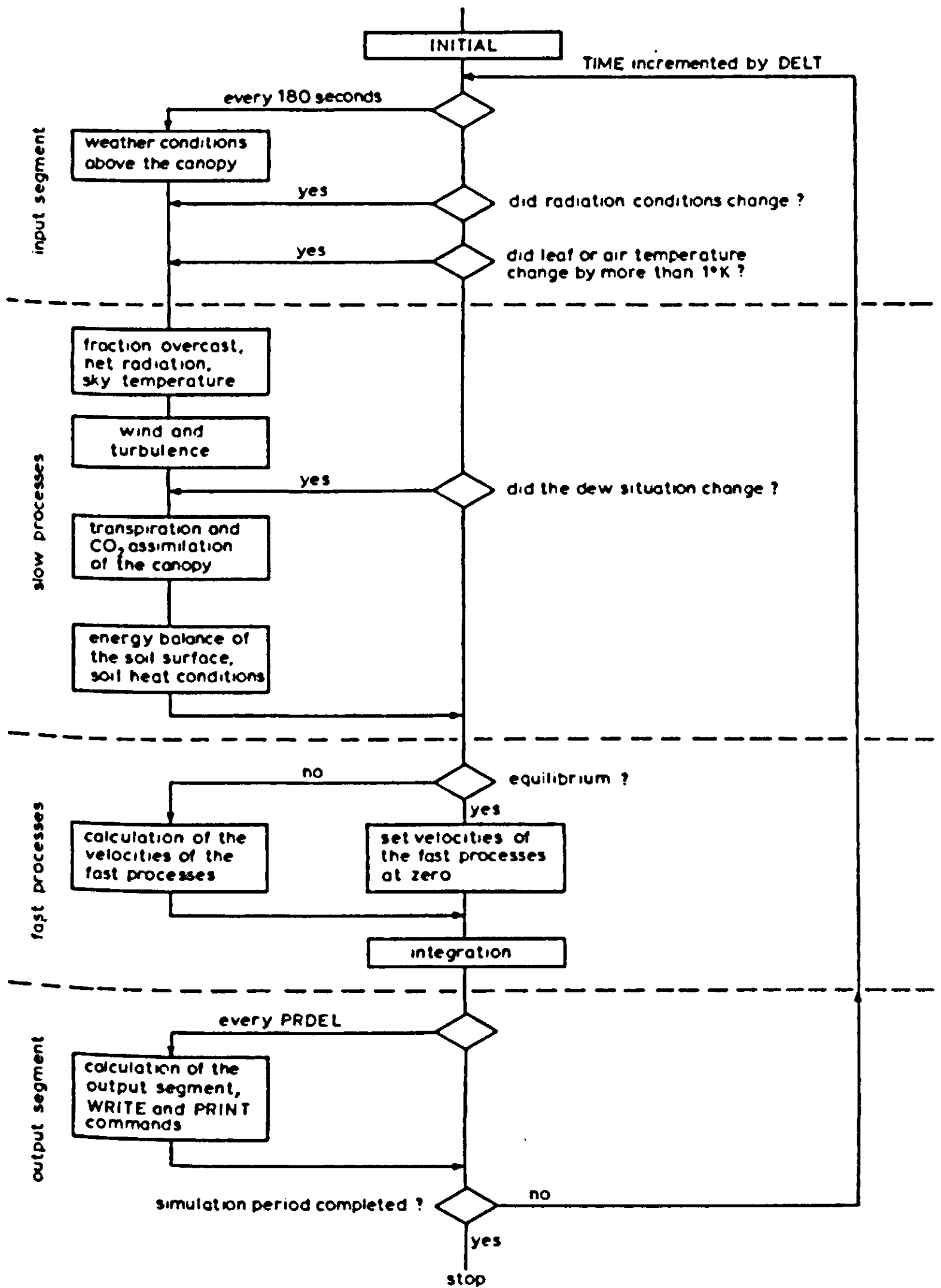


Fig. 29 | Scheme of the application of the bypassing methods in the micro-meteorological simulation model. The main segmentation is the same as in Fig. 28.

only slightly modified by the aerial profiles inside the canopy. Therefore these calculations are subject to the same frequency, except when the dew situation in any of the layers has changed. The influence of dew on the transpiration or condensation rate is so large that re-computation is necessary then.

The remaining slow processes in the central part concern the transport of heat in the soil and the energy balance at the soil surface. The calculation of these is also subject to the frequency of once every 180 seconds, safely below the smallest time constant of the thinnest top layer.

The output segment within the DYNAMIC has to be executed only when information is required by the user. Thus these calculations are subject to a fixed frequency of once every time interval of output, PRDEL. The value of PRDEL was usually 3600 seconds. The output calculations include the CO₂-profile inside the canopy. It was assumed that the feedback of CO₂-concentration to the CO₂-assimilation and the transpiration is negligible, which was later justified by the small simulated depletion of CO₂.

The computer time saved by the bypassing methods amounts to a factor one hundred in this case, when compared with a simple use of the RKS method. Because this amount of time can be saved, such a large model may be used. A disadvantage of these methods is that they require a rather sophisticated sorting of the statements. In the micro-meteorological program this has been accomplished by grouping of statements in PROCEDURES. The right sorting of the procedures is determined by the list of input and output variables mentioned in their headings. The IF statements of the conditional jumps are positioned in additional control PROCEDURES. In this way the whole program can still be divided in sections in accordance with the description in Chapters 2, 3 and 4.

The question may arise whether this method is more generally applicable. It probably is if diffusion is a prevailing factor in the system. Diffusion tends to level off peaks and dips. Irregularities never grow on account of diffusion alone as can be seen in the equations for the transport processes. With respect to time they are of the first order with a minus sign. In population dynamics the type of equations is quite different. An essential property of life is multiplication of itself, showing up in a first order derivative with respect to time, but with a positive sign. At regular or irregular periods of time

this may be offset by compensating forces like death and migration (diffusion). The combined result is that in population dynamics one often deals with oscillatory phenomena (May, 1973). Then the method of conditional bypassing cannot be applied as described here, but must be modified. The concept "equilibrium" must be replaced by a concept "cyclic equilibrium" which must be described by characteristics like mean, amplitude and frequency. When these characteristic quantities have reached equilibrium, they can take over the role of describing the state variables, so that the computations of the rates can be bypassed.

The given programming methods are used because the normally available software is both too accurate and too expensive in terms of computer time. In many agricultural and ecological problems the uncertainty in structure of the system and in the value of the input data is often so great that one would rather use less accurate and cheaper integration methods. Preferably there should be an inverse relation between the error criterion, specified by the user, and the computer time spent. This is indeed so in the conditional bypassing method discussed. The best solution would be a software package, organizing the user's source program. The commonly used integration methods like Runge-Kutta have sufficient power in normal problems, but since the computer time spent is almost independent of the specified error criterion they are not suitable for stiff systems. In stiff systems one is not really interested in the transient behaviour of the fastest processes, an accurate determination of their equilibrium values being usually sufficient.

5.6 Programs and lists of abbreviations

The first program EXTRAD.EQ is for the calculation of extinction and reflection of radiation in a plant canopy with leaves that have an equal reflection and transmission coefficient. The second program EXTRAD.NE is an extension of the first one for leaves with an unequal reflection and transmission coefficient. These programs were used in Chapter 2. They are followed by a list of abbreviations of the computer names used.

The next program is the micrometeorological simulation model MICROWEATHER. The results of this program are presented in Chapter 6. After completion of the sensitivity analysis the following

error was found and corrected. In Section 9 of the program I replaced the erroneous value 1 by the value 0.74 for the calculation of the heat exchange resistance in the MACRO-invocation NUMINT. The program thus corrected was used for the evaluation presented in Section 6.4. After this another error was found: for the calculation of WLOSS in Section 8 of the program LHFLB was not subtracted from LHFL1. This omission increases the severity of an afternoon depression. The input weather data used for the evaluation are listed. Finally the list of abbreviations of MICROWEATHER is presented.

TITLE EXTINCTION OF RADIATION, LEAF TRANSMISSION AND REFLECTION EQUAL

```

FIXED IS,J,K,MAX,MAXI,ITER,INVJ,ITERM,IL
/   DIMENSION MT(9),RN(101),PRN(101),NRRD(9),NRRU(9)
/   DIMENSION TPHID(101),TPHIU(101),PHID(9,101),PHIU(9,101),MI(9)
STORAGE SM(9),BU(9),F(9),OAV(9),RL(9)
TABLE BU(1-9)=.03,.087,.133,.163,.174,.163,.133,.087,.03
TABLE SM(1-9)=0.087,0.259,0.423,0.574,0.707,0.819,0.906,0.966,0.996
TABLE F(1-9)=.015,.045,.074,.099,.124,.143,.158,.168,.174
TABLE OAV(1-9)=9*0.5
*   OAV FOR A SPHERICAL LEAF ANGLE DISTRIBUTION
PARAM PI=3.141592
PARAM LS=0.1
PARAM LAI=10.,RHOS=0.,SD=1.,IS=9
PARAM SC=(0.,0.3,0.8,1.)

```

INITIAL
NOSORT

```

SBL=1.-SD
MAX=LAI/LS
MAXI=MAX+1
RAD=PI/180.
SBL=0.
DO 10 K=1,9
  FK=(10*K-5)*RAD
  SI=SIN(FK)
  CN=COS(FK)
  DD=0.
  DO 20 IL=1,9
    FLIL=(10*IL-5)*RAD
    AA=SI*COS(FLIL)
    BB=CN*SIN(FLIL)
    CC=AA
    IF(K.GE,IL) GO TO 20
    SQ=SQRT(BB*BB-AA*AA)
    CC=2.*(AA*ATAN(AA/SQ)+SQ)/PI
  20  DD=DD+CC*F(IL)
  OAV(K)=DD
  MI(K)=LS*OAV(K)/SM(K)
  MT(K)=1.-MI(K)
  10  SBL=SBL+BU(K)*MI(K)
  DO 30 K=1,9
    BL(K)=BU(K)*MI(K)/SBL
  30  PHID(K,1)=BU(K)*SD
  PHID(IS,1)=PHID(IS,1)+SB
  DO 40 K=1,9
    DO 40 J=1,MAXI
  40  PHIU(K,J)=0.
  ITERM=1
  IF (SC.GT.0.1) ITERM=2
  IF (SC.GT.0.5) ITERM=5
  IF (SC.GT.0.9) ITERM=10
  IF (SC.EQ.1.0) ITERM=20
  DO 240 ITER=1,ITERM
    DO 220 J=2,MAXI
    INTER=0.
    DO 215 K=1,9
  215  INTER=INTER+MI(K)*(PHID(K,J-1)+PHIU(K,J) )
    DO 220 K=1,9
    PHID(K,J)=PHID(K,J-1)+MT(K)
  220  PHID(K,J)=PHID(K,J)+.5*SC*INTER*BL(K)
  INTER=0.
  DO 225 K=1,9
  225  INTER=INTER+PHID(K,MAXI)
  DO 230 K=1,9
  230  PHIU(K,MAXI)=RHOS*INTER*BU(K)
  DO 240 INVJ=1,MAX
  J=MAXI-INVJ
  INTER=0.
  DO 235 K=1,9

```

```

235 INTER =INTER+MI(K)*(PHID(K,J)+PHIU(K,J+1) )
      DO 240 K=1,9
          PHIU(K,J)=PHIU(K,J+1)*MT(K)
240 PHIU(K,J)=PHIU(K,J)+.5*SC*INTER*BL(K)
      WRITE (6,245)
245 FORMAT ('1FLUXES')
      WRITE (6,250) ( (PHID(K,J),K=1,9),(PHIU(K,J),K=1,9),J=1,MAX1,5)
250 FORMAT (9E14.5/9E14.5//)

      WRITE (6,340)
340 FORMAT ('ORADIANCES')
      DO 360 J=1,MAX1
          TPHIU(J)=0.
          TPHID(J)=0.
          DO 345 K=1,9
              NRRU(K)=PHIU(K,J)/BU(K)
              NRRD(K)=PHID(K,J)/BU(K)
              TPHIU(J) =TPHIU(J)+PHIU(K,J)
              TPHID(J) =TPHID(J)+PHID(K,J)
345 IF (J.EQ.5*(J/5)+1) WRITE (6,350) NRRD, NRRU
350 FORMAT (9E14.5/9E14.5//)
          RN(J) =TPHID(J)-TPHIU(J)
360 RRN(J)=RN(J)/PN(1)
      WRITE (6,370)
370 FORMAT (' NET RADIATION, DOWNWARD FLUX, UPWARD FLUX, ',
      ' NET RADIATION RELATIVE')
      WRITE (6,380) (RN(J),TPHID(J),TPHIU(J),RRN(J),J=1,MAX1)
380 FORMAT (1H,4F15.5)
      RHOM =TPHIU(1)/TPHID(1)
      TRANSM =TPHID(MAX1)/TPHID(1)
      WRITE (6,390) RHOM,TRANSM
390 FORMAT ('OREFLECTIVITY AND TRANSMISSION'/2F10.5)

```

```

• BECAUSE THE LEAST SQUARES CRITERION DOES NOT RESULT IN AN
• EQUATION EASILY SOLVED FOR KM, AN ELEMENTARY APPROACH IS MADE
  KM =0.
  DELTA =0.1
  SUMDEV=100.
  DO 607 K=1,3
602 SUMDEI=SUMDEV
      SUMDEV=0.
      MAXDEV=0.
      DO 611 J=1,MAX1
          DEV =EXP(-KM*(J-1)*0.1)-RRN(J)
          MAXDEV=AMAX1(ABS(DEV),MAXDEV)
611 SUMDEV=SUMDEV+DEV*DEV
      IF (SUMDEV.GT.SUMDEI) GO TO 607
      KM =KM+DELTA
      GO TO 602
607 DELTA =-0.1*DELTA
      WRITE (6,601) KM,SUMDEV,MAXDEV
601 FORMAT ('OK, SUMDEV AND MAXDEV ARE'/3F15.5,' FOR NET RADIATION')

```

```

  KM =0.
  DELTA =0.1
  SUMDEV=100.
  DO 507 K=1,3
502 SUMDEI=SUMDEV
      SUMDEV=0.
      MAXDEV=0.
      DO 511 J=1,MAX1
          DEV =EXP(-KM*(J-1)*0.1)- TPHID(J)
          MAXDEV=AMAX1(ABS(DEV),MAXDEV)
511 SUMDEV=SUMDEV+DEV*DEV
      IF (SUMDEV.GT.SUMDEI) GO TO 507
      KM =KM+DELTA
      GO TO 502
507 DELTA =-0.1*DELTA
      WRITE (6,501) KM,SUMDEV,MAXDEV
501 FORMAT ('OK, SUMDEV AND MAXDEV ARE'/3F15.5,' FOR PAD, GOING DOWN')

```

```

DYNAMIC
TIMER DELT=1., FINTIM=1.
METHOD RECT
END

```


END
TABLE F(1-9)=0*0.,1.
END
STOP
ENDJOB

EXTRAD.NE

TITLE EXTINCTION OF RADIATION, LEAF TRANSMISSION AND REFLECTION ARE NOT EQUAL

```

FIXED IS,J,K,KK,MAX,MAX1,ITER,INVJ,ITEPM,IL
/   DIMENSION O(9,9),KSIAY(9,9)
/   DIMENSION MT(9),RN(101),RPN(101),NRRD(9),NRRU(9)
/   DIMENSION TPHID(101),TPHIU(101),PHID(9,101),PHIU(9,101),MI(9)
STORAGE SM(9),BU(9),F(9),OAV(9),BL(9)
TABLE BU(1-9)=.03,.087,.133,.163,.174,.163,.133,.087,.03
TABLE SM(1-9)=0.087,0.259,0.423,0.574,0.707,0.819,0.906,0.966,0.996
TABLE F(1-9)=.015,.045,.074,.099,.124,.143,.158,.168,.174
TABLE OAV(1-9)=9*0.5
*   OAV FOR A SPHERICAL LEAF ANGLE DISTRIBUTION
PARAM PI=3.141592
PARAM LS=0.1
PARAM LAI=10.,RHOS=0.,SD=1.,IS=9
PARAM RHO=1.,TAU=0.

```

INITIAL
NOSORT

```

SB=1.-SD
MAX =LAI/LS
MAX1=MAX+1
RAD=PI/180.
SBL =0.
DO 10 K=1,9
FK=(10*K-5)*RAD
SI=SIN(FK)
CO=COS(FK)
DD=0.
DO 20 IL=1,9
FLIL=(10*IL-5)*RAD
AA=SI*CO*(FLIL)
BB=CO*SIN(FLIL)
O(K,IL)=AA
IF(K.GE,IL) GO TO 20
SQ=SQRT(BB*BB-AA*AA)
O(K,IL)=2.*(AA*ATAN(AA/SQ)+SQ)/PI
20 DD=DD+O(K,IL)*F(IL)
OAV(K)=DD
MI(K) =LS*OAV(K)/SM(K)
MT(K)=1.-MI(K)
10 SBL =SBL+BU(K)*MI(K)
DO 24 K=1,9
FK=(10*K-5)*RAD
SIK=SIN(FK)
COK=COS(FK)
DO 24 KK=1,9
FKK=(10*KK-5)*RAD
SIKK=SIN(FKK)
COKK=COS(FKK)
SPSIR=0.
SDEN=0.
DO 25 IL=1,9
FLIL=(10*IL-5)*RAD
SIL=SIN(FLIL)
COL=COS(FLIL)
A1=SIK*SIKK*COL*COL
A2=SIK*COKK*SIL*COL
A3=COK*SIKK*SIL*COL
A4=COK*COKK*SIL*SIL
ACK=PI
ACKK=PI
IF(K.GE,IL) GO TO 26
AA=SIK*COL
BB=COK*SIL
SQ=SQRT(BB*BB-AA*AA)
ACK=PI*0.5+ATAN(AA/SQ)
26 IF(KK.GE,IL) GO TO 27
AA=SIKK*COL
BB=COKK*SIL

```

```

27  ACKK=PI*0.5+ATAN(AA/SQ)
    SIACK=SIN(ACK)
    SIACKK=SIN(ACKK)
    PSIR=4./(2.*PI*PI)*(A1*(PI*PI+2.*ACK*ACKK-PI*ACK-PI*ACKK)...
    +A2*SIACKK*(2.*ACK-PI)+A3*SIACK*(2.*ACKK-PI)+2.*A4*SIACK ...
    *SIACKK)
    DEN=2.*O(K,IL)*O(KK,IL)
    KSI=PSIR/DEN
    SPSIR=SPSIR+PSIR*F(IL)
    SDEN=SDEN+DEN*F(IL)
25  CONTINUE
24  KSI*V(K, KK)=SPSIR/SDEN
    DO 30 K=1,9
    BL(K) =BU(K)*MI(K)/SBL
30  PHID(K,1)=BU(K)*SD
    PHID(IS,1) =PHID(IS,1)+SB
    DO 40 K=1,9
    DO 40 J=1,MAX1
40  PHIU(K,J)=0.
    SC=TAU+RHO
    ITERM=1
    IF (SC.GT.0.1) ITERM=2
    IF (SC.GT.0.5) ITERM=5
    IF (SC.GT.0.9) ITERM=10
    IF (SC.EQ.1.0) ITERM=20
    DO 240 ITER=1,ITERM
    DO 220 J=2,MAX1
    DO 220 K=1,9
    SCAT=0.
    DO 215 KK=1,9
    SCAT=SCAT+MI(KK)*(PHID(KK,J-1)*(KSI*V(K, KK)*(TAU-RHO)+...
    RHO)+PHIU(KK,J)*(KSI*V(K, KK)*(RHO-TAU)+TAU))
215 CONTINUE
220 PHID(K,J)=PHID(K,J-1)*MT(K)+BL(K)*SCAT
    INTER=0.
    DO 225 K=1,9
225 INTER=INTER+PHID(K,MAX1)
    DO 230 K=1,9
230 PHIU(K,MAX1)=RHOS*INTER*BU(K)
    DO 240 INVJ=1,MAX
    J=MAX1-INVJ
    DO 240 K=1,9
    SCAT=0.
    DO 235 KK=1,9
    SCAT=SCAT+MI(KK)*(PHID(KK,J)*(KSI*V(K, KK)*(RHO-TAU) ...
    +TAU)+PHIU(KK,J+1)*(KSI*V(K, KK)*(TAU-RHO)+RHO))
235 CONTINUE
240 PHIU(K,J)=PHIU(K,J+1)*MT(K)+BL(K)*SCAT
    WRITE (6,245)
245 FORMAT ('1FLUXES')
    WRITE (6,250) ( (PHID(K,J),K=1,9),(PHIU(K,J),K=1,9),J=1,MAX1,5)
250 FORMAT (9E14.5/9E14.5//)

    WRITE (6,340)
340 FORMAT ('ORADIANCES')
    DO 360 J=1,MAX1
    TPHIU(J)=0.
    TPHID(J)=0.
    DO 345 K=1,9
    NRRU(K)=PHIU(K,J)/BU(K)
    NRRD(K)=PHID(K,J)/BU(K)
    TPHIU(J) =TPHIU(J)+PHIU(K,J)
345 TPHID(J) =TPHID(J)+PHID(K,J)
    IF (J.EQ.5*(J/5)+1) WRITE (6,350) NRRD, NRRU
350 FORMAT (9E14.5/9E14.5//)
    RN(J) =TPHID(J)-TPHIU(J)
360 RRN(J)=RN(J)/RN(1)
    WRITE (6,370)
370 FORMAT (' NET RADIATION, DOWNWARD FLUX, UPWARD FLUX, ',
    ' NET RADIATION RELATIVE')
    WRITE (6,380) (RN(J),TPHID(J),TPHIU(J),RRN(J),J=1,MAX1)
380 FORMAT (1H ,4F15.5)
    RHOM =TPHIU(1)/TPHID(1)
    TRANSM =TPHID(MAX1)/TPHID(1)
    WRITE (6,390) RHOM,TRANSM
390 FORMAT ('OREFLECTIVITY AND TRANSMISSION'/2F10.5)

```

```

• BECAUSE THE LEAST SQUARES CRITERION DOES NOT RESULT IN AN
• EQUATION EASILY SOLVED FOR KM, AN ELEMENTARY APPROACH IS MADE
  KM =0.
  DELTA =0.1
  SUMDEV=100.
    DO 607 K=1,3
602  SUMDEI=SUMDEV
    SUMDEV=0.
    MAXDEV=0.
      DO 611 J=1,MAXI
        DEV =EXP(-KM*(J-1)*0.1)-RRN(J)
        MAXDEV=AMAX1(ABS(DEV),MAXDEV)
611  SUMDEV=SUMDEV+DEV*DEV
      IF (SUMDEV.GT.SUMDEI) GO TO 607
      KM =KM+DELTA
      GO TO 602
607  DELTA =-0.1*DELTA
    WRITE (6,601) KM,SUMDEV,MAXDEV
601  FORMAT ('OK, SUMDEV AND MAXDEV ARE'/3F15.5,' FOR NET RADIATION')

  KM =0.
  DELTA =0.1
  SUMDEV=100.
    DO 507 K=1,3
502  SUMDEI=SUMDEV
    SUMDEV=0.
    MAXDEV=0.
      DO 511 J=1,MAXI
        DEV =EXP(-KM*(J-1)*0.1)-TPHID(J)
        MAXDEV=AMAX1(ABS(DEV),MAXDEV)
511  SUMDEV=SUMDEV+DEV*DEV
      IF (SUMDEV.GT.SUMDEI) GO TO 507
      KM =KM+DELTA
      GO TO 502
507  DELTA =-0.1*DELTA
    WRITE (6,501) KM,SUMDEV,MAXDEV
501  FORMAT ('OK, SUMDEV AND MAXDEV ARE'/3F15.5,' FOR RAD. GOING DOWN')

DYNAMIC
TIMER DELT=1., FINTIM=1.
METHOD RECT
END
PARAM RHO=0.,TAU=1.
END
STOP
ENDJOB

```

ACK	critical angle α'_c (Eqn(2.94))
ACKK	critical angle α_c (Eqn (2.92))
AA	auxiliary variable
BB	auxiliary variable
BL(K)	$B_l(\beta)$ see Eqn (2.35)
BU(K)	$B_u(\beta)$
CC	auxiliary variable
DD	auxiliary variable
DELTA	step size by which K_m is incremented in search for the best fitting value
DEN	denominator (see Eqn (2.96))
DEV	deviation between numerically calculated and exponential profile
F(IL)	leaf angle distribution ($F(\lambda)$)
FK	inclination of an incoming ray expressed in radians
FKK	inclination of a scattered ray expressed in radians
FLIL	leaf inclination, expressed in radians
INVJ	index of the layers, counted from beneath
INTER	intercepted amount (I_t)
ITER	number of executed full runs in iteration for multiple scattering
ITERM	maximum set to ITER
IS	index for the inclination of the sun
J	number of layer (j)
K	running index for inclination
KK	running index for inclination
KM	best fitting K according to the model (K_m)
KSI	ξ according to Eqn (2.96)
KSIKV(K,KK)	$\xi(\beta, \beta')$ weighted for the leaf angle distribution
LS	leaf area index per layer (L_s)
MAX	total number of layers
MAXDEV	maximum deviation between numerically calculated and exponential profile
MI(K)	$M_i(\beta)$
MT(K)	$M_t(\beta)$
NRRU(K)	relative radiance N_r in direction K (upward)
NRRD(K)	relative radiance N_r in direction K (downward)

O(K,IL)	$O(\beta, \lambda)$
OAV(K)	$\bar{O}(\beta)$
PHID(K,J)	$\varphi_d(\beta, j)$ Eqn (2.30) etc
PHIU(K,J)	$\varphi_u(\beta, j)$ Eqn (2.30) etc
PSIR	$\bar{\Psi}_{refl}$ see Eqn (2.94)
RAD	one degree in radians
RN(J)	net radiative flux at level j
RRN(J)	relative net radiative flux at level j
RHO	reflection coefficient of the leaves ρ
RHOS	reflection coefficient of the soil ρ_s
RHOM	reflection coefficient of the canopy-soil system ρ_m
TAU	transmission coefficient of the leaves τ
TRANSM	transmission coefficient of the canopy τ_m
TPHID(J)	$\sum_{\beta=1}^9 \varphi_d(\beta, j)$
TPHIU(J)	$\sum_{\beta=1}^9 \varphi_u(\beta, j)$
SB	direct component of incoming radiation S_b
SBL	$\sum_{\beta=1}^9 B_u(\beta) M_i(\beta)$ see Eqn (2.35)
SC	scattering coefficient of the leaves σ
SCAT	amount of scattered radiation, see Eqn (2.86)
SD	diffuse component of incoming radiation S_d
SDEN	DEN, weighted for the leaf angle distribution
SI	sine of inclination
SIK	sine of inclination
SIL	sine of leaf inclination
SIACK	$\sin(\alpha'_c)$ see Eqn (2.94)
SIACKK	$\sin(\alpha_c)$ see Eqn (2.94)
SUMDEV	sum of the squares of DEV
SQ	square root of some expression (auxiliary)

MICROWEATHER

TITLE MICROWEATHER SIMULATION

***** SECTION 1 *****

• FIXED AND ARRAY DECLARATIONS

FIXED N,I,NUMLL,NUML1,IS,IL,SN,L,ISUN,J,INVL

```
/ DIMENSION HC(10),HCI(10),NHFL(10),CO2(20),CO2FL(21),RINC(21)
/ DIMENSION DT(9),DV(9),DDTDT(9),DDVDT(9),DEW(9),DEWT(9),IDEW(9)
/      & DDEW(9),DDEWT(9),DEWL(9),IDEW(9),NCO2A(9),NLWR(21),NLWRM(9,9)
/ DIMENSION WIND(21),H(21),NSF(20),NLF(20),IDT(9),IDV(9)
/ DIMENSION S(9,10),Z(9,10),LHLL(9),SHLL(9),ZA(5),ZS(5)

/ EQUIVALENCE (DT(1),DT1),(DDTDT(1),DDTDT1),(DV(1),DV1),(DDVDT(1),
/      & DDVDT1),(DEW(1),DEW1),(DDEW(1),DDEW1),(IDEW(1),IDEW1),
/      & (IDEW(1),IDEW1),(DEWT(1),DEWT1),(DDEWT(1),DDEWT1),
/      & (HC(1),HC1),(HCI(1),HCI1),(NHFL(1),NHFL1),(IDT(1),IDT1),
/      & (IDV(1),IDV1)
```

```
STORAGE K(21),TI(9),TCOND(20),VCOND(20),ITCAP(20),IVCAP(20)
STORAGE LHFL(21),DIK(20),SHFL(21),RFN(11),KDY(11),KB(11),TCOM(10)
STORAGE HFL(11),TEMP(10),DIST(11),RICH1(9),TI(10)
STORAGE F(9),BU(9),OAV(9),RFV(11),KDV(11)
```

***** SECTION 2 *****

• MACRO FOR NUMERICAL INTEGRATION OF THE INVERSE OF • THE EXCHANGE COEFFICIENT WITH HEIGHT

MACRO INT,A,B,C,D,E=NUMINT(COEF1,COEF2,POWER,ZS,MONOBL)

```
• SEE EQN 4.22 AND 4.23
F1=COEF1*(1.-COEF2*ZS(1)/MONOBL)**POWER
F2=COEF1*(1.-COEF2*ZS(2)/MONOBL)**POWER
F3=COEF1*(1.-COEF2*ZS(3)/MONOBL)**POWER
F4=COEF1*(1.-COEF2*ZS(4)/MONOBL)**POWER
F5=COEF1*(1.-COEF2*ZS(5)/MONOBL)**POWER
A=F5
E=(F1-4.*F2+6.*F3-4.*F4+F5)/(24.*DZS4)
D=(F2-3.*F3+3.*F4-F5)/(6.*DZS3)-6.*E*DZS
C=(F3-2.*F4+F5)/(2.*DZS2)-3.*D*DZS-7.*E*DZS2
B=(F4-F5)/DZS-C*DZS-D*DZS2-E*DZS3
• SEE EQN 4.42
INT=A*INTN+B*ZIS+C*Z2S+D*Z3S+E*Z4S
ENDMAC
```

• MACRO DESCRIBING THE CO2 ASSIMILATION, TRANSPIRATION • AND LEAF TEMPERATURE OF THE INDIVIDUAL LEAVES

```
MACRO EHL,SHL,TL,NCO2A,LRES= ...
TRPH(VIS,NIR,LWR)
ABSRAD=VIS+NIR*LWR
AMAX =AMAX1(AFCEN(AMTB,TADT),0.001)
• SEE EQN 3.8
NCO2A =(AMAX+DPL)*(1.-EXP(-VIS*EFF/AMAX))-DPL
CO2F =68.4*(ECO2C-RCO2I)
• SEE EQN 3.9
SRESL =CO2F/(AMAX1(.001,NCO2A)*1.66)-RA*0.783
IF (SRESL.GT.SRW) GO TO 700
SPESL =SRW
NCO2A =AMIN1(CO2F/(1.66*SRW+1.3*RA),NCO2A)
700 LPES =RESCW*SRESL/(SRESL+RESCW)
IF (DEW(I).GT.0.,OR. LHLL(I).LT.0.) LRES=0.
ENP =0.3*NCO2A
• SEE EQN 3.11
EHL =(SLOPE*(ABSRAD-ENP)+DRYP)/(PSCH*(RA*0.93+LRES)/RA+SLOPE)
SHL =ABSRAD-EHL-ENP
TL =TADT+SHL*RR
ENDMAC
```

* FUNCTIONS, PARAMETERS AND TABLES

FUNCTION SRADTB=0.,-1.E6, 1.E6,-1.E6
 FUNCTION NRADTB=0.,-1.E6, 1.E6,-1.E6

***** USER MUST DEFINE THE FOLLOWING FUNCTIONS, PARAMETERS AND TABLES *****

* OBSERVED WEATHER DATA AS A FUNCTION OF HOUR OF THE DAY IN STANDARD SOLAR TIME

FUNCTION TATB = 0.,13.5, 6.,12.9, 10.,16.5, 14.,20., 16.,20.6, ...
 18.,14.1, 24.,13.5
 FUNCTION VPATB = 0.,13., 6.,12., 8.5,13., 13.,11.2, 18.,15., 24.,13,
 FUNCTION WINDRB=0.,.7, 7.,.7, 8.,.7, 9.,.2, 11.,.3, 16.,.1, 17.,.7, ...
 24.,.7
 FUNCTION NRADTB=0.,-40., 6.,-30., 6.5,0., 8.5,105., 9.8,400., ...
 11.2,660., 12.1,690., 13.2,630., 14.1,530., 15.1,380., ...
 16.1,200., 17.1,14., 18.1,-84., 24.,-40.

PARAM ECO2C=330.
 PARAM CROPHT=2.5,REFHT=3.
 PARAM DFACT=0.8,ZNOTF=0.07
 * ZNOTF RATIO OF ROUGHNESS LENGTH AND CROP HEIGHT
 PARAM LAI=3.73
 PARAM LAT=45.,DLONG=0,
 PARAM DAY=270,
 PARAM START=0.

*** PHYSICAL DATA

PARAM GR=9.81
 CONST SIGMA=5.6696E-8
 CONST PI=3.1415927
 PARAM KARMAN=0.35
 PARAM RHOCp=1240.,PSCH=0.67
 PARAM LHVAP=2.5E9
 PARAM SCOF=4.7

FUNCTION FRDIFT=0.,1., 5.,1., 15.,0.323, 25.,.219, 35.,.176, ...
 45.,.16, 55.,.145, 65.,.136, 90.,.133
 TABLE BU(1-9)=.03,.087,.133,.163,.174,.163,.133,.087,.03

*** PLANT DATA

PARAM SCN=0.85,SCV=0.2
 PARAM WIDTH=0.05
 FUNCTION AMTB=10.,.001, 15.,25., 20.,50., 25.,60., 35.,60., 40.,20.
 PARAM RCO2I=90.
 PARAM EFF=0.62,RESCW=2000.
 FUNCTION SRWTB=.5,1.E4, 0.6,3.E3, 0.7,800., 0.8,600., 0.9,130., 1.5,130.
 FUNCTION WSTTB=.5,-50., .7,-17., .8,-14., .84,-12.5, .88,-10., ...
 .90,-8.1, 1.,0., 1.5,40.5

TABLE F(1-9)=9*0.
 ** UNLESS SPECIFIED BY USER, A SPHERICAL LEAF ANGLE DISTRIBUTION IS ASSUMED

FUNCTION HTB=0.,0., 100.,0.
 ** IF HTR IS NOT SPECIFIED BY USER, A PARABOLIC DISTRIBUTION OF LEAF
 * AREA DENSITY WITH HEIGHT IS ASSUMED BY THE FOLLOWING FUNCTION
 FUNCTION RHTB=0.,0., 0.028,0.1, 0.104,0.2, 0.216,0.3, 0.352,0.4, ...
 0.5,0.5, 0.648,0.6, 0.784,0.7, 0.896,0.8, 0.972,0.9, 1.,1.

PARAM WRESPL=10.E6
 PARAM SCRS=3.5E-2
 FUNCTION TREDTB=0.,.08, 10.,.08, 20.,.29, 33.,.94, 37.,1., 48.,0.87
 PARAM WSTSL=0.1
 PARAM DRAGC=0.3

*** SOIL DATA, SOIL IS ALWAYS ASSUMED AT FIELD CAPACITY

PARAM TCOM1=0.02
 PARAM MULT=1.2
 PARAM LAMBDA=1.3
 PARAM HRES=0.05
 PARAM RESS=0.

** WHEN SOIL SURFACE IS WET, THIS RESISTANCE IS ZERO,
 * WHEN IT IS DRY, THIS RESISTANCE IS VERY LARGE, E.G., 1.E6
 PARAM VHCAP=2.E6
 PARAM SRESP=10.

TABLE TI(1-10)=12.2,12.9,13.6,14.3,15.0,15.5,15.7,15.7,15.4,15.2
 * TI INITIAL TEMPERATURE OF THE DIFFERENT SOIL LAYERS

*** CONTROL VARIABLES

PARAM NUMLL=3
 * NUMLL NUMBER OF LAYERS IN WHICH CANOPY IS DIVIDED
 ** CAUTION: THIS NUMBER APPEARS IN WRITE STATEMENTS SEVERAL TIMES,
 * AND IN END NUMBER OF INTEGRAL STATEMENTS OF DT,DV,DEW,DEWT.
 * ADVICE: NUMLL=3 IS SUFFICIENTLY ACCURATE FOR TOTAL FLUXES.

* SPECIFY TIMER CARD IN SECONDS (ONE DAY=86400 SECONDS)
 TIMER FINTIM=0.,PRDEL=1800.,OUTDEL=10800.,DELT=1.
 METHOD PECT

INITIAL

***** SECTION 4 *****

* STRATIFICATION IN AIR AND SOIL

* ASSIGNING INITIAL VALUES TO SOME CONTROL VARIABLES

```

PROCED WCCPI,SRADF=CONTR(LAI)
  WCCPI=2.5E-3*LAI*0.975
  DO 72 I=1,NUMLL
    IDT(I)=-4.
    IDV(I)=-2.
    IDEW(I)=0.
  72 IDEWT(I)=0.
  SRADF =1.
  LASTTL=0.
  LASTDV=0.
  LASTDT=0.
  ZHCR =0.
  ZHNR =0.
  TELFO =0.
  TELLER=0.
  TELN =0.
ENDPRO
  
```

* AERODYNAMICS AND STRATIFICATION ABOVE THE CANOPY

PROCED D,ZNOT,ZS1,ZA1,DZS,INTN,INTAN=ABL(SRADF)
 * BETTER FORMULATIONS FOR D AND ZNOT GIVEN IN SECTION 4.4(LATER DEVELOPMENT

```

D =DFACT*CROPHT
ZNOT =0.1*INSW(CPOPHT-1.,CPOPHT,SQRT(CROPHT) )
ZA1 =REFHT-D
ZA(1)=ZA1
ZA(5)=CROPHT-D
Z1A =ZA1-ZA(5)
Z2A =(ZA1*ZA1-ZA(5)*ZA(5) )*0.50
Z3A =(ZA1**3-ZA(5)**3)/3.
Z4A =(ZA1**4-ZA(5)**4)*0.25

ZS1 =ZA1
ZS(1)=ZS1
ZS(5)=ZNOT
Z1S =ZS1-ZS(5)
Z2S =(ZS1*ZS1-ZS(5)*ZS(5) )*0.50
Z3S =(ZS1**3-ZS(5)**3)/3.
Z4S =(ZS1**4-ZS(5)**4)*0.25
DZS =Z1S*0.25
DZS2 =DZS*DZS
DZS3 =DZS*DZS2
DZS4 =DZS*DZS3
DO 40 J=2,4
  ZA(J)=ZA1-(J-1)*Z1A*0.25
  ZS(J)=ZS1-(J-1)*DZS
  
```

```

INTN=ALOG(ZS1/ZS(5) )
INTAN=ALOG(ZA1/ZA(5) )
ENDPRO

```

```

* AERODYNAMICS AND STRATIFICATION IN THE CANOPY
PROCED NUML1,DL,LMIX,ALPHA=LAYER(D,NUMLL)
NUML1=NUMLL+1
DL=LAI/NUMLL
* ACCORDING TO EQN 4.44 A FACTOR 4/PI MUST BE ADDED (LATER DEVELOPMENT)
LMIX=SQRT(WIDTH*CROPHT/LAI)
* SEE EQN 4.49 , ADDITION OF IW IS LATER DEVELOPMENT
ALPHA=SQRT(DRAGC*LAI*CROPHT/(2.*LMIX))
* IF NO MEASURED LEAF AREA DISTRIBUTION IS AVAILABLE (HTB), A ...
* PARABOLIC ONE (RHTB) IS ASSUMED
IF (AFGEN(HTB,100.).EQ.0.) GO TO 22
DO 20 I=1,NUMLL
20 H(I)=AFGEN(HTB,LAI-(I-1)*DL)
GO TO 21
22 DO 23 I=1,NUMLL
23 H(I)=CROPHT*AFGEN(RHTB,1.-(I-1.)/NUMLL)
21 H(NUML1)=0.
DO 24 I=1,NUMLL
DIK(I)=H(I)-H(I+1)
ITCAP(I)=1./(DIK(I)*RHOCP)
24 IVCAP(I)=ITCAP(I)*PSCH
ENDPRO

```

```

* INITIALIZATION AND STRATIFICATION IN THE SOIL
PROCED DIST1=SOILI(XL)
DIST1 =0.5*TCOM1
DIST(1)=DIST1
TCOM(1)=TCOM1
HCI(1) =TCOM1*VHCAP*TI(1)
DO 70 I=2,10
TCOM(I)=TCOM(I-1)*MULT
DIST(I)=0.5*(TCOM(I)+TCOM(I-1) )
70 HCI(I) =TI(I)*TCOM(I)*VHCAP
ENDPRO

```

***** SECTION 5 *****

```

* RADIATION CHARACTERISTICS
* AVERAGE PROJECTION OF LEAVES (OAV)
* AND LIGHT DISTRIBUTION FUNCTIONS Z AND S , ACCORDING TO APPENDIX B
PROCED SUMF,ZISSN,RAD,DEC,SSIN,CCOS=GEOM(DL)
RAD =PI/180.
DEC =-23.45*COB(PI*(DAY+10.173)/182.621)
COSDEC=COB(RAD*DEC)
SINDEC=SIN(RAD*DEC)
SNLT=SIN(RAD*LAT)
CSLT=COB(RAD*LAT)
SSIN=SNLT*SINDEC
CCOS=CSLT*COSDEC
SUMF=F(1)+F(2)+F(3)+F(4)+F(5)+F(6)+F(7)+F(8)+F(9)
IF (SUMF,EQ.0.) GO TO 90
DO 64 IS=1,9
FLIS=(10*IS-5)*RAD
SI=SIN(FLIS)
CO=COB(FLIS)
DD=0.
DO 60 IL=1,9
FLIL=(10*IL-5)*RAD
AA=SI*COB(FLIL)
BB=CO*SIN(FLIL)
CC=AA
IF (IS,GE,IL) GO TO 36
SQ=SQRT(BB*BB-AA*AA)
CC=2.*(AA*ATAN(AA/SQ)+SQ)/PI

```

```

* CC IS 0 (SEE EQN 2.3), AND DD IS OAV (SEE EQN 2.4)
36 DD=DD+CC*F(IL)
   DO 56 SN=1,9
   FLSN=SN/10.
   FA=FLSN-AA
   CC=1.
   IF (IS,LT,IL) GO TO 57
   IF (FLSN-BB,GE,AA) GO TO 56
   IF (FLSN+BB,GT,AA) GO TO 61
   CC=0.
   GO TO 56
61 SQ=SQRT(BB*BB-FA*FA)
   CC=ATAN(FA/SQ)/PI+0.5
   GO TO 56
57 IF (FLSN-AA,GE,BB) GO TO 56
   IF (FLSN+AA,GE,BB) GO TO 61
   SQ=SQRT(BB*BB-FA*FA)
   CC=ATAN(FA/SQ)
   FA=FLSN-AA
   SQ=SQRT(BB*BB-FA*FA)
   CC=(ATAN(FA/SQ)+CC)/PI
56 S(IL,SN)=CC
60 S(IL,10)=1.
   EE=0.
   DO 63 SN=1,10
   CC=0.
   DO 62 IL=1,9
62 CC=CC+F(IL)*S(IL,SN)
   Z(IS,SN)=CC-EE
63 EE=CC
64 OAV(IS)=DD
   GO TO 91

* A SPHERICAL LEAF ANGLE DISTRIBUTION IS ASSUMED
90 ZISSN=0.1
   DO 92 IS=1,9
92 OAV(IS)=0.5
91 CONTINUE
ENDPRO

```

```

* SIMPLIFIED EQUATIONS FOR REFLECTION AND EXTINCTION
* COEFFICIENTS UNDER DIRECT RADIATION
PROCED REFY,REFN=EXTI(RAD)
SONI=SQRT(1.-SCN)
SQV =SQRT(1.-SCV)
REFV=(1.-SQV)/(1.+SQV)
REFN=(1.-SONI)/(1.+SONI)
* SEE EQN 2.21
DO 65 IS=1,9
* KB(IS+1)=OAV(IS)/SIN( (10*IS-5)*RAD)
* SEE EQN 2.34
KDN(IS+1) =KB(IS+1)*SONI*0.94623+0.03533
65 KDV(IS+1) =KB(IS+1)*SQV *0.94623+0.03533
* SEE EQN 2.42
KB(1)=KB(2)
KB(11)=KB(10)
KDV(1) =KDV(2)
KDV(11) =KDV(10)
KDN(1) =KDN(2)
KDN(11) =KDN(10)
DO 66 IS=1,11
RFN(IS)=REFN*2.*KB(IS)/(KB(IS)+1.)
RFV(IS)=REFV*2.*KB(IS)/(KB(IS)+1.)
* SEE EQN 2.45
66 RFV(IS)=AMAX1(0.,1.117*(1.-EXP(-RFV(IS) ) )-0.0111)
RFN(IS)=AMAX1(0.,1.117*(1.-EXP(-RFN(IS) ) )-0.0111)
* SEE EQN 2.46
ENDPRO

```

```

* REFLECTION AND EXTINCTION OF DIFFUSE RADIATION(SEE EQN 2.37)
PROCED XL,XVDF,XNDF,RFOVV,RFOVN=EXDIF(REFY)
RFOVV=0.
RFOVN=0.
SUMBL=0.

```

```

SUMVI=0.
SUMNI=0.
DO 67 J=1,9
RFOVY=RFOVY+BU(J)*RFV(J+1)
RFOYN=RFOYN+BU(J)*RFN(J+1)
SUMBL=SUMBL+BU(J)*EXP(-KB(J+1)*LAI)
SUMVI=SUMVI+BU(J)*EXP(-KDV(J+1)*LAI)
67 SUMNI=SUMNI+BU(J)*EXP(-KDN(J+1)*LAI)
KBDF =-ALOG(SUMBL)/LAI
KDFV=-ALOG(SUMVI)/LAI
KDFN=-ALOG(SUMNI)/LAI
XNDF=EXP(-DL*KDFN)
XVDF=EXP(-DL*KDFV)
XL =EXP(-DL*KBDF)
XLN =XL*NUMLL
* SEE EQN 2.41
ENDPRO

```

DYNAMIC

***** SECTION 6 *****

```

* CONTROL OF EXECUTION

* TIMING AND PROGRAM CONTROL
PROCD HOUR,SRADM,NRADM,DIFTL,DIFDT=CONTR1(TIME)
EXPROG=IMPULS(0.,180.)
HOUR =AMOD(TIME/3600,+START,24.)
SRADM=AFGEN(SRADTB,HOUR)
NRADM=AFGEN(NRADTB,HOUR)
IF (TIME.EQ.0. .OR. EXPROG.GT.0.5) GO TO 175
IF (ABS(LASTSR-SRADM).GT.AMAX1(5.,0.01*SRADM) ) GO TO 176
IF (ABS(LASTNR-NRADM).GT.AMAX1(3.,0.01*ABS(NRADM) ) ) GO TO 176
DIFTL=ABS(TL(1)-LASTTL)
IF (DIFTL.GT.1.) GO TO 176
DIFDT=ABS(DT(1)-LASTDT)
IF (DIFDT.GT.0.001*CT) GO TO 176
DO 191 I=1,NUMLL
IF (DEW(I)*DEWL(I).LT.0.) GO TO 177
191 CONTINUE
GO TO 170
175 CONTINUE
ENDPRO

```

```

PROCD TELLER,PRT,DT0,DV0,ENLOSS=CONTR2(DT1,DV1,TELF0)
TELLER=TELLER+1.
PRT=IMPULS(0.,PRDEL)
IF (PRT.LT.0.5) GO TO 851
DT0=DT1*ABTURR/RINC(1)
DV0=DV1*ABTURR/RINC(1)
ENLOSS=SHFL1+LHFL1+C+0.3*TNCO2A
ENDPRO

```

***** SECTION 7 *****

```

* WEATHER CONDITIONS ABOVE THE CANOPY

* OBSERVED WEATHER CONDITIONS
PROCD SVPA,TA,TABS,VPD,SLOPE,WINDR,WINDR2,CT=WEER(HOUR,DZ8)
VPA =AFGEN(VPATB,HOUR)
TA =AFGEN(TATB,HOUR)
TA239=TA+239.
TABS =TA+273.

```

```

SVPA =6.11*EXP(17.4*TA/TA239)
SLOPE=4158.6*SVPA/(TA239*TA239)
VPD =SVPA-VPA
WINDR=AFGEN(WINDRB, HOUR)
WINDR2=WINDR*WINDR
CT=INTN*WINDR2*TABS/(GR*4.*DZS)
ENDPRO

* CALCULATION OF SUN HEIGHT
PROCD HSUN,SNHS,SNHSS=GLOBE(HOUR,RAD,DEC,SSIN,CCOS,SRW)
* SEE EQN 2.107
SNHSS=SSIN*CCOS*COS(RAD*(HOUR+12,-DLONG)*15.)
SNHS =AMAX1(0.,SNHSS)
HSUN =ATAN(SNHS/SQRT(1.-SNHS*SNHS) )/RAD
ENDPRO

* INTERPOLATION OF REFLECTION AND EXTINCTION COEFFICIENTS
PROCD RDRV,RDRN,KDRV,KDRN,KDR=INTERP(HSUN)
FISUN=(HSUN+15.)*0.1
ISUN =FISUN
IS=FISUN*0.5
FI =FISUN-ISUN
RDRV =RFV(ISUN) *(1.-FI)+RFV(ISUN+1) *FI
RDRN =RFN(ISUN) *(1.-FI)+RFN(ISUN+1) *FI
KDR =KB(ISUN) *(1.-FI)+KB(ISUN+1) *FI
KDRN =KDN(ISUN) *(1.-FI)+KDN(ISUN+1) *FI
KDRV =KDV(ISUN) *(1.-FI)+KDV(ISUN+1) *FI
ENDPRO

* CALCULATION OF FRACTION OVERCAST AND APPARENT SKY TEMPERATURE
PROCD DIFOV,DIFCL,SUNDCL,FOV,FCL,LFOV,LFCL,NRAD,SRAD,SKT,LWRI,TELN=...
CURRAD(KDR)
176 LASTDT=DT(1)
LASTDV=DV(1)
LASTTL=TL(1)
LASTNR=NRADM
LASTSR=SRADM
TELN=TELN+1.
* SEE TABLE 2.1
FRDIF =AFGEN(FRDIFT,HSUN)
DIFCL =580.*SNHS*FRDIF
DIFOV =116.*SNHS
SUNDCL=580.*SNHS*(1.-FRDIF)
NSRO =(1.-RFOVV+0.7*(1.-RFOVN) )*DIFOV
NSRC =(2.-RDRV-RDRN)*SUNDCL+(2.-RFOVV-RFOVN)*DIFCL
SRC =2.*(SUNDCL+DIFCL)
SRO =1.7*DIFOV
SKTCL =1.2*TA-21.
* SEE EQN 2.67
SKTOV =TA-2.
SKTCL4=(SKTCL+273.)*.4
SKTOV4=(SKTOV+273.)*.4
LWRCI =SIGMA*(SKTCL4-ETS4)
LWROI =SIGMA*(SKTOV4-ETS4)
IF (SRADM,LT.-1000.) GO TO 300
LFOV =1.
LFCL =0.
SUNDCL=0.
DIFCL=0.
DIFOV=SRADM/1.7
IF (SNHS,EQ.0. ,OR. SRADM,EQ.0.) GO TO 302
FOV=(SRC-SRADM)/(NOT(SRC-SRO)+SRC-SRO)
FCL=1.-FOV
LFOV=LIMIT(0.,1.,FOV)
LFCL=1.-LFOV
IF (LFOV,EQ.0.) GO TO 302
SPADF =SRADM/INSW(LFOV-FOV,SRO,SRC)
SUNDCL=SPADF*SUNDCL
DIFCL =SPADF*DIFCL
DIFOV =SPADF*DIFOV
302 IF(NRADM,LT.-1000.) GO TO 304

```

```

310 LWRI =NRADM-LFCL*((2,-RDRV-RDRN)*SUNDCL+(2,-RFOVV-RFOVN)* ...
DIFCL)-LFOV*(1,7-RFOVV-0,7*RFOVN)*DIFOV
311 SKT =(LWRI/SIGMA+ETS4)**0,25-273.
GO TO 306
304 SKT =FOV*SKTOV *(1,-FOV)*SKTCL
SKT4 =(SKT+273,)**4
LWRI =SIGMA*(SKT4-ETS4)
GO TO 306
300 FOV =(NSRC+LWRCI-NRADM)/(NSRC-NSRO+LWRCI-LWROI)
FCL =1,-FOV
LFOV =LIMIT(0,,1,,FOV)
LFCL =1,-LFOV
LWRI =LFOV*LWROI+LFCL*LWRCI
NRADOV=NSRO+LWRI
NRADCL=NSRC+LWRI
IF (LFOV,EQ,FOV) GO TO 311
IF (SNHS,GT,0,) GO TO 309
LWRI =NRADM
GO TO 311
309 SRADF=(NRADM-LWRI)/INSW(LFOV-FOV,NSRO,NSRC)
IF(SRADF,GT,0,) GO TO 307
WRITE(6,807) SRADF
807 FORMAT(1H ,20H WARNING SRADF IS E15.5,10H ,BUT SET AT ZERO /)
SPADF=0.
307 IF(SRADF,LT,2,) GO TO 308
WRITE(6,808) SRADF
808 FORMAT(1H ,20H WARNING SRADF IS E15.5,10H ,BUT SET AT TWO /)
SPADF=2.
308 SUNDCL=SUNDCL+SRADF
DIFCL =DIFCL +SRADF
DIFOV =DIFOV +SRADF
GO TO 310
306 NPADCL=(2,-RDRV-RDRN)*SUNDCL+(2,-RFOVV-RFOVN)*DIFCL+LWRI
NRADOV=(1,-RFOVV+0,7*(1,-RFOVN) )*DIFOV+LWRI
NRAD =LFOV*NRADOV + LFCL*NRADCL
SRAD =LFOV*DIFOV*1,7+2,*LFCL*(SUNDCL+DIFCL)
SKT4 =(SKT+273,)**4
ENDPRO

```

***** SECTION 8 *****

* WATER STATUS OF THE CANOPY (SECTION 3.4.4)

```

PROCED SRW,RWCP,WSTCP=STRESS(CT)
RWCP =WCCP/(LAI*2,5E-3)
WSTCP=AFGEN(WSTTB,RWCP)
SRW =AFGEN(SRWTR,RWCP)
ENDPRO

```

* WATER BALANCE OF THE CANOPY

```

PROCED WLOSS,WUPTCP,WCCPRT,TRZ,ACRS=WABAL(WSTCP,TS)
WLOSS =LHFL1/LHVAP
TRZ =(TEMP(3)+TEMP(4)+TEMP(5) )/3.
ACRS =SCRS*1,E-6*AFGEN(TREDTB,TRZ)
WUPTCP=(WSTSL-WSTCP)/(WRESPL*1./ACRS)
WCCPRT=WUPTCP-WLOSS
WCCP =INTGRL(WCCPI,WCCPRT)
ENDPRO

```

***** SECTION 9 *****

* TURBULENCE AND WIND

* ABOVE VEGETATION AERODYNAMICS (SECTION 4.2)

```

PROCED RICHN,MONOBL,INTM,WINDC,USTAR,ABTURP,DZETA= ...
ABOVE(WINDP,TABS,INTM,INTAN,ZA1,DIFOV,SRW)
RICHN=(REFHT-D-ZNOT)*GR*(LASTDT+0,1*LASTDV)/(WINDR2+TABS)
* SEE EQN 4,40
IF (RICHN,GT,+0,001) GO TO 41
IF (RICHN,LT,-0,001) GO TO 43

```

```

* NEUTRAL CONDITIONS, (SECTION 4.2.1)
42 USTAR =WINDR*KARMA/INTN
   ABTURR=0.74*INTAN/(KARMA*USTAR)
   WINDC =WINDR -USTAR*INTAN/KARMA

* STABLE CONDITIONS WHEN RICHN IS POSITIVE.
41 AA =SCOF*(1.-SCOF*RICHN)
   IF (AA,LT,0.) GO TO 45
   BB =INTN*(0.74-2.*SCOF*RICHN)
   CC =-INTN*INTN*RICHN
* SEE EQNS 4.37,4.38,4.39
   DZETA=(SQRT(BB*BB-4.*AA*CC)-BB)/(AA+AA)
* SEE EQN 4.36
   GO TO 46

* EXTREME STABILITY, LAMINAR FLOW
45 DZETA =1.E10
46 INTM =INTN*SCOF*DZETA
* SEE EQN 4.33
   USTAR =KARMA*WINDR/INTM
   MONOBL=(ZAI-ZNOT)/DZETA
   ABTURR=(0.74*INTAN+ZIA*SCOF/MONOBL)/(KARMA*USTAR)
* SEE EQN 4.29
   WINDC =WINDR -USTAR*(INTAN+ZIA*SCOF/MONOBL)/KARMA
   GO TO 50

* UNSTABLE CONDITIONS WHEN RICHN IS NEGATIVE.
43 CONTINUE
   DZETA=IMPL(-0.001,1.E-3,DZETA1)
   MONOBL=ZIS/DZETA
   INTM,AM,BM,CM,DM,EM=NUMINT(1.,15.0,-0.25,ZS,MONOBL)
   INTN,AH,BH,CH,DH,EH=NUMINT(0.74, 9.0,-0.50,ZS,MONOBL)
   DZETA1=RICHN*INTM*INTM/INTN
* SEE EQN 4.43
   USTAR =KARMA*WINDR/INTM
   MONOBL=(ZAI-ZNOT)/DZETA
   KU =KARMA*USTAR
   ABTURR=(AH*INTAN+BH*ZIA+CH*Z2A+DH*Z3A+EH*Z4A)/KU
* SEE EQN 4.29
   INTAM=AM*INTAN+BM*ZIA+CM*Z2A+DM*Z3A+EM*Z4A
   WINDC =WINDR -USTAR*INTAM/KARMA
50 CONTINUE
ENDPRO

* INSIDE VEGETATIVE CANOPY AERODYNAMICS, EDDY DIFFUSIVITY AND WINDSPEED
PROCD PHI=INSIDE(ALPHAK,LMIX,TARS,WINDC)
   WIND(1) =WINDC
   GRLMIX =GR*LMIX*LMIX
* RICH(1)=-GRLMIX*DT(1)/(TABS*(0.5*DIK(1)+ZIA)*WIND(1)*WIND(1) )
* SEE EQN 4.50
   I =1
   GO TO 121
* DO 123 I=2,NUMLL
120 WIND(I) =ANAXI(WINDC*EXP(-ALPHAK*(1.-H(I)/CROPHY) ),0.0001)
* SEE EQN 4.48
   RICH(I)=GRLMIX*(DT(I-1)-DT(I) )/ ...
   (TABS*(0.5*DIK(I-1)+DIK(I) )*WIND(I)**2)
* SEE EQN 4.50
121 IF (RICH(I).GT.0.) GO TO 122
   PHI =0.74/SQRT(1.-9.*RICH(I) )
   GO TO 123
122 PHI =0.74+(0.74-9.4*RICH(I)-0.74*SQRT(8.9262*RICH(I)+1.) ) ...
   /(9.4*RICH(I)-2.)
* SEE EQN 4.51
123 IF (RICH(I).GT.0.21) PHI=1.E10
   K(I)=LMIX*WIND(I)/PHI
* SEE EQN 4.52 (ADDITION OF IW IS LATER DEVELOPMENT)
   I =I+1
   IF (I.LE.NUMLL) GO TO 120
ENDPRO

* CALCULATION OF RESISTANCES BETWEEN LAYERS, REFHT AND SOIL SURFACE
* FROM TURBULENCE AND WINDSPEED

```

```

PROCED RSSH,RSSE=TURBR(NUML1,ALPHAK,LMIX,ABTURR,PHI)
  RINC(1)=0.5*DIK(1)/K(1)+ABTURR
  TCOND(1)=RHOC/PCON(1)
  VCOND(1)=TCOND(1)/PSCH
  DO 149 I=2,NUMLL
    RINC(I)=(DIK(I-1)+DIK(I))*0.5/K(I)
    TCOND(I)=RHOC/PCON(I)
  149 VCOND(I)=TCOND(I)/PSCH
  WIND(NUML1)=WIND(1)*EXP(-ALPHAK)
  * SEE EQN 4.48
  K(NUML1)=WIND(NUML1)*LMIX/0.74
  RINC(NUML1)=0.5*DIK(NUMLL)/K(NUML1)
  RSS=185.*SQRT(HRES/WIND(NUML1))
  * SEE EQN 3.5
  RSSH=RSS+RINC(NUML1)
  RSSE=0.93*RSS+RINC(NUML1)
ENDPRO

```

***** SECTION 10 *****

```

* RADIATION AND ENERGY BALANCE OF THE LEAVES
* RADIATION CONDITIONS INSIDE CANOPY AND ON SOIL SURFACE.
* ENERGY BALANCE OF INDIVIDUAL LEAVES, ACCUMULATION OF HEAT LOSS
* AND TRANSPIRATION
PROCED TLHL,TSHL,TNCO2A,TNCO2R,NRADS,ETS=...
  SOURCE(KDR,SPW,SUNDCL,SNHSS,TA,PSSH)
  177 CONTINUE
  XD=EXP(-DL*KDR)
  XNDR=EXP(-DL*KDRN)
  XVDR=EXP(-DL*KDRV)
  VISDF=(1.-RFOVV)*DIFCL*(1.-XVDF)/DL
  NIRDFF=(1.-RFOVN)*DIFCL*(1.-XNDF)/DL
  * SEE EQN 3.35
  FVDR=(1.-RDRV)*SUNDCL*(1.-XVDR)/DL
  FNDR=(1.-RDRN)*SUNDCL*(1.-XNDR)/DL
  * SEE EQN 3.36
  NDIR=(1.-SCN)*SUNDCL*(1.-XD)/DL
  VDIR=(1.-SCV)*SUNDCL*(1.-XD)/DL
  * SEE EQN 3.39
  VISDFC=VISDF+FVDR-VDIR
  NIRDFC=NIRDFF+FNDR-NDIR
  * SEE EQN 3.40
  VSPER=(1.-SCV)*SUNDCL/SNHSS
  NSPER=(1.-SCN)*SUNDCL/SNHSS
  FSR=(1.-XD)/(DL*KDR)
  * SEE EQN 3.38
  VISDFO=(1.-RFOVV)*DIFOV*(1.-XVDF)/DL
  NIRDFO=(1.-RFOVN)*0.7*DIFOV*(1.-XNDF)/DL
  * SEE EQN 3.35
  TSHL=0.
  TLHL=0.
  * DARK RESPIRATION OF LEAVES
  DPL=6.*EXP(0.07*(TA-30.))
  TNCO2A=0.
  XLFD=1.-XL
  XLFU=XLFD/XL
  ETS4=0.
  NLWRS=0.
  DO 154 I=1,NUMLL
  * EXCHANGE OF THERMAL RADIATION BETWEEN SKY, LEAVES AND SOIL SURFACE
  * SEE EQNS 2.68 AND 2.69
  NLWR(I)=0.
  DO 162 J=1,NUMLL
    IF (I-J) 167,162,164
  167 NLWRM(I,J)=(0.0281*(TL(I)+TL(J))+4.61)*(TL(I)-TL(J))*...
    (1.-XL)*(1.-XL)*XL*(J-I-1)
    GO TO 165
  164 NLWRM(I,J)=-NLWRM(J,I)
  165 NLWR(I)=NLWR(I)-NLWRM(I,J)
  162 CONTINUE
  LWSOIL=(0.0281*(TL(I)+TS)+4.61)*(TS-TL(I))*XLN*XLFU
  NLWR(I)=NLWR(I)+LWSOIL
  NLWRS=NLWRS-LWSOIL

```



```

TL4  =(TL(I)+273.)*.4
LWR  =(NLWR(I)+SIGMA*(SKT4-TL4)*XLFD)/DL
DEWL(I)=DEW(I)
RA=185.*SQRT(WIDTH/WIND(I) )*.5
*
SEE EQN 3,5
RR=RA/RHOCP
TADT=TA+DT(I)
DRYP=(VPD+SLOPE*DT(I)-DV(I) )/RR
*
SEE EQN 3,13
LHLL0,SHLL0,TLO,NCO2A0,LRES0= ...
TRPH(VISDFO,NIRDF0,LWR)
IF (HOUR,EQ.12.) WRITE (6,600) LRES0
600  FORMAT (11H LRES0 IS E10,5/)
IF (SNHS,EQ.0.) GO TO 230
NCO2AC=0.
SHLLCL=0.
LHLLCL=0.
TLCL =0.
IF (LFCL,EQ.0.) GO TO 261
DO 260 SN=1,10
SNINC=-0.05+0.1*SN
VIS  =VISDFC+VSPER*SNINC
NIR  =NIRDFC+NSPER*SNINC
LHLLC,SHLLC,TL SUN,NPHTSU,LRESSU= ...
TRPH(VIS,NIR,LWR)
IF (HOUR,EQ.12.) WRITE (6,601) LRESSU
601  FORMAT (13H LRESSU IS E10,5/)
IF (SUMF,NE.0.) ZISSN=Z(IS,SN)
SHLLCL=SHLLCL+ZISSN*SHLLC
LHLLCL=LHLLCL+ZISSN*LHLLC
NCO2AC=NCO2AC+ZISSN*NPHTSU
*
SEE EQN 3,42
260  TLCL =TLCL +ZISSN*TL SUN
*1010 FORMAT (31H STOMATAL RESISTANCE AND LIGHT,2E15,5//)
SHLLCL=SHLLCL*FSR
LHLLCL=LHLLCL*FSR
TLCL =TLCL *FSR
NCO2AC=NCO2AC*FSR
LHLLS,SHLLS,TL SHAD,NPHTSH,LRESSH= ...
TRPH(VISDFC,NIRDFC,LWR)
IF (HOUR,EQ.12.) WRITE (6,602) LRESSH
602  FORMAT (13H LRESSH IS E10,5/)
SHLLCL=SHLLCL+SHLLS *(1.-FSR)
LHLLCL=LHLLCL+LHLLS *(1.-FSR)
TLCL =TLCL +TL SHAD*(1.-FSR)
NCO2AC=NCO2AC+NPHTSH*(1.-FSR)
261  SHLL(I) =(LFOV*SHLL0 +LFCL*SHLLCL)*DL
LHLL(I) =(LFOV*LHLL0 +LFCL*LHLLCL)*DL
NCO2A(I)=(LFOV*NCO2A0+LFCL*NCO2AC)*DL
*
SEE EQN 3,43
TL(I)  = LFOV*TLO  +LFCL*TLCL
FSR  =FSR  *XD
VISDFO=VISDFO*XVDF
NIRDF0=NIRDF0*XNDF
VISDF  =VISDF  *XVDF
NIRDF  =NIRDF  *XNDF
FVDR  =FVDR  *XVDR
FNDR  =FNDR  *XNDR
VDIR  =VDIR  *XD
NDIR  =NDIR  *XD
VISDFC=VISDF+FVDR-VDIR
NIRDFC=NIRDF+FNDR-NDIR
*
SEE EQN 3,40
GO TO 231
230  SHLL(I) =SHLL0 *DL
LHLL(I) =LHLL0 *DL
NCO2A(I)=NCO2A0*DL
TL(I)  =TLO
231  TLHL  =TLHL  +LHLL(I)
TSHL  =TSHL  +SHLL(I)
ETS4  =ETS4+XLFD*(TL(I)+273)*.4
XLFD  =XLFD*XL
XLFU  =XLFU/XL
154  TNCO2A=TNCO2A+NCO2A(I)
ETS4  =ETS4+XLN*(TS+273)*.4
ETS  =ETS4*.25 - 273.

```

```

TNCO2R=TNCO2A/3600.
FVDP =FVDP *DL/(1.-XVDR)
FNDR =FNDR *DL/(1.-XNDR)
VISDFO=VISDFO*DL/(1.-XVDF)
NIRDFO=NIRDFO*DL/(1.-XNDF)
TS4 =(TS+273.)**4
NLWRS =NLWRS+SIGMA*XLN*(SKT4-TS4)
VISDF =VISDF *DL/(1.-XVDF)
NIRDF =NIRDF *DL/(1.-XNDF)
NRADS =LFOV *(VISDFO+NIRDFO) +NLWRS + ...
      LFCL *(VISDF +NIRDF +FVDR+FNDR)
ABSNP =NPAD -NPADS
ENDPRO

```

***** SECTION 11 *****

```

* ENERGY BALANCE OF THE SOIL
* SOIL TEMPERATURES
PROCED TEMP1=STEMP(TLHL)
178 CONTINUE
      DO 146 I=1,10
146  TEMP(I)=HC(I)/(TCOM(I)*VHCAP)
      TEMP1=TEMP(1)
ENDPRO

```

```

* ENERGY BALANCE OF SOIL SURFACE (SECTION 3.3 )
PROCED VPDB,LHFLB,SHFLB,TS,G= ...
SOILS(NUML1,TA,SVPA,SLOPE,VPD,NRADS,RSSH,RSSE,DIST1,TEMP1)
Y=RHOCP*DIST1/(DIST1*RHOCP+LAMBDA*RSSH)
* SEE EQN 3.25
PSCHAP=(RSSE+RESS)*PSCH/RSSH
* SEE EQN 3.26
VPDR=VPD-DV(NUMLL)+SLOPE*DT(NUMLL)
DRYPB=VPDR*RHOCP/RSSH
LHFLB=(SLOPE*Y*(NRADS+(TEMP(1)-TA-DT(NUMLL))*LAMBDA/DIST1) ...
+DRYPB)/(SLOPE*Y+PSCHAP)
* SEE EQN 3.24
SHFLB=(LHFLB*PSCHAP-DRYPB)/SLOPE
* SEE EQN 3.29
SHFL(NUML1)=SHFLB
LHFL(NUML1)=LHFLB
G =NRADS-SHFLB-LHFLB
* SEE EQN 3.23
TS =TEMP(1)+G*DIST1/LAMBDA
ESS=SVPA+SLOPE*(TS-TA)
* ESS IS THE SATURATED VAPOUR PRESSURE AT THE SOIL SURFACE
HFL(1)=-G
      DO 147 I=2,10
147  HFL(I)=(TEMP(I)-TEMP(I-1))*LAMBDA/DIST(I)
      DO 148 I=1,10
148  NHFL(I)=HFL(I+1)-HFL(I)
ENDPRO

```

***** SECTION 12 *****

```

* ENERGY AND MASS BALANCE OF THE AIR LAYERS IN THE CANOPY
* FLUXES BETWEEN LAYERS
PROCED SHFL1,LHFL1=FLUX(G)
170 CONTINUE
IF (ABS( (SHFL1-SHFLB-TSHL)/TSHL).LT.0.005 .AND. ...
      ABS( (LHFL1-LHFLB-TLHL)/TLHL).LT.0.005) GO TO 172
SHFL(1)=DT(1)*TCOND(1)
LHFL(1)=DV(1)*VCOND(1)
SHFL1=SHFL(1)
LHFL1=LHFL(1)
      DO 153 I=2,NUMLL
      SHFL(I)=(DT(I)-DT(I-1))*TCOND(I)
      LHFL(I)=(DV(I)-DV(I-1))*VCOND(I)
153
ENDPRO

```

```

* NET FLUXES OF LAYERS
PROCED NSF1=NFLUX(SHFL1,LHFL1)
      DO 155 I=1,NUMLL
        NSF(I)=SHFL(I+1)-SHFL(I)
        NLF(I)=LHFL(I+1)-LHFL(I)
      NSF1=NSF(1)
ENDPRO

```

```

* RATES OF THE INTEGRALS THAT DESCRIBE THE STATE OF THE LAYERS
PROCED TELFO=RATE(NSF1)
      DO 158 I=1,NUMLL
        DDTDT(I)=(NSF(I)+SHLL(I))*ITCAP(I)
        DDVDT(I)=(NLF(I)+LHLL(I))*IVCAP(I)
        IF (DEW(I).GT.0.) GO TO 157
        DDEWT(I)=0.
        DDEW(I) =AMAX1(0.,-LHLL(I) )
        GO TO 158
      157 DDEWT(I)=1.
        DDEW(I) =-LHLL(I)
      158 CONTINUE
      GO TO 173
    172 CONTINUE
      TELFO=TELF0+1.
      DO 156 I=1,NUMLL
        DDTDT(I)=0.
        DDVDT(I)=0.
      156 CONTINUE
    173 CONTINUE
ENDPRO

```

```

PROCED INVL=PROCO2(NUML1,PRT)
      CO2FL(NUML1)=SRESP
      DO 210 I=1,NUMLL
        INVL=NUML1-I
        CO2FL(INVL)=CO2FL(INVL+1)-NCO2A(INVL)
      210 CO2(I)=ECO2C+(SRESP-TNCO2A)*RINC(I)/68.4
        IF (NUMLL.EQ.1) GO TO 212
        DO 211 I=2,NUMLL
          CO2(I)=CO2(I-1)+CO2FL(I)*RINC(I)/68.4
        211 CONTINUE
      212 CONTINUE
ENDPRO

```

NOSORT

***** SECTION 13 *****

```

* INTEGRALS AND OUTPUT
** LAST ARGUMENT OF THESE STATEMENTS MUST EQUAL THE NUMBER OF LAYERS
DT1 =INTGRL( IDT1,DDTDT1,3)
DV1 =INTGRL( IDV1,DDVDT1,3)
DEW1 =INTGRL( IDEW1 ,DDEW1 ,3)
DEWT1=INTGRL( IDENT1,DDEWT1,3)
**
HC1 =INTGRL(HC11 ,NHFL1 ,10)
DNCO2A=INTGRL(0.,TNCO2R)
DLHFL =INTGRL(0.,LHFL1)
DSHFL =INTGRL(0.,SHFL1)
DNRAD =INTGRL(0.,NRAD)
DLHFLB=INTGRL(0.,LHFLB)
DSHFLB=INTGRL(0.,SHFLB)
DSOILF=INTGRL(0.,C)
WRITE (6,900) TIME, HOUR
WRITE (6,901) DT0, (DT(I),I=1,NUMLL)
WRITE (6,903) DVO, (DV(I),I=1,NUMLL)
WRITE (6,902) (NCO2A(I),I=1,NUMLL)
WRITE (6,904) (SHLL(I),I=1,NUMLL)
WRITE (6,905) (LHLL(I),I=1,NUMLL)
WRITE (6,907) (DEW(I),I=1,NUMLL)
WRITE (6,908) (DEWT(I),I=1,NUMLL)

```

```

WRITE (6,909) (TL(I),I=1,NUMLL)
WRITE (6,1001) (DDTDT(I),I=1,NUMLL)
WRITE (6,1002) (DDVDT(I),I=1,NUMLL)
WRITE (6,1003) (SHFL(I),I=1,NUML1)
WRITE (6,1004) (LHFL(I),I=1,NUML1)
WRITE (6,1007) ECO2C,(CO2(I),I=1,NUMLL)
WRITE (6,1008) ( (WIND(I),K(I) ),I=1,NUMLL)
SIX=IMPULS(0.,21600.)
IF (SIX.LT.0.5) GO TO 851
WRITE (6,1005) (TEMP(I),I=1,10)
TRCOEF=0.006*DLHFL/(NOT(DNCO2A)+DNCO2A)
DBOWR =DSHFL/(NOT(DLHFL)+DLHFL)
WRITE (6,1006) DNCO2A,DLHFL,DSHFL,DNRAD,DLHFLB,DSHFLB,DSOILF, ...
TRCOEF,DBOWR
1006 FORMAT (61H DNCO2A,DLHFL,DSHFL,DNRAD,DLHFLB,DSHFLB,DSOILF,TRCOEF,
$DBOWR /9E12.3//)
1005 FORMAT (12H TEMP(1-10) 10F11.3/)
900 FORMAT (21H TIME AND HOUR 2F15.2/)
901 FORMAT (11H DT 20F15.3/)
902 FORMAT (11H NCO2A 20E15.5/)
903 FORMAT (11H DV 20F15.3/)
904 FORMAT (11H SHLL 20E15.5/)
905 FORMAT (11H LHLL 20E15.5/)
907 FORMAT (11H DEW 20E15.5/)

908 FORMAT (11H DEWT 20E15.5/)
909 FORMAT (11H TL 20F15.3/)
1001 FORMAT (11H DDTDT 20E15.5/)
1002 FORMAT (11H DDVDT 20E15.5/)
1003 FORMAT (11H SHFL 21E15.5/)
1004 FORMAT (11H LHFL 21E15.5/)
1007 FORMAT (11H CO2 21F15.1/)
1008 FORMAT (25H WIND K (INSIDE)/20(2E12.3/ )

851 CONTINUE
CALL DEBUG(10,0.)
CALL DEBUG(10,3600.)
CALL DEBUG(1,86400.)
PRINT TS,G,INTM,INTN,SHFL1,LHFL1,NRAD,NRADS,ENLOSS,TELLER, ...
TELFO,TELN,ABTURR,RWCP,SRW,USTAR,MONOBL,DZETA,TA, ...
RSSE,VPD,VPDB,SHFLB,LHFLB,TNCO2A,SRAD,FOV,RICHN, ...
SKT,LWRI,ETS

END
TIMER FINTIM=86400.,PRDEL=3600.
END
STOP
ENDJOB

```

Input weather data for the runs of Section 6.4

```

END
* 31 AUGUSTUS 1972, FLEVOPOLDER, MAIS
TIMER FINTIM=86400.,PRDEL=1800.
PARAM KAPMAN=0.4,DFACT=0.74,ZNOTF=0.077
FUNCTION TATB= 0.,14., 6.,12., 10.,16.25, 10.5,17.05, 11.,17.85, ...
              11.8,18.0, 12.5,18.7, 13.3,18.45, 13.8,19.7, 14.5,19.6, ...
              15.,19.9, 15.7,19.7, 16.3,18.6, 16.8,19.05, 24.,14.
FUNCTION VPATB= 0.,14., 10.,14.5, 10.5,14.25, 11.,14., 11.8,13.8, ...
              12.5,13.35, 13.3,13.55, 13.8,13.35, 14.5,12.9, 15.,12.9, ...
              15.7,12.35, 16.3,13., 16.8,13.1, 24.,12.
FUNCTION WINDRB= 0.,3., 10.,3.15, 10.5,3.49, 11.,3.95, 11.8,3.83, ...
              12.5,4.19, 13.3,3.55, 13.8,3.71, 14.5,3.6, 15.,3.62, ...
              15.7,3.68, 16.3,3.6, 16.8,3.8, 24.,2.
FUNCTION NRADTB=0.,-20., 6.,0., 7.,10., 8.,100., 10.,304., ...
              10.5,360., 11.,407., 11.8,334.5, 12.5,518., 13.3,309., ...
              13.8,425., 14.5,343., 15.,335., 15.7,240., 16.3,140., ...
              16.8,206., 18.,0., 19.,-30., 24.,-20.
PARAM CROPHT=2.2, REFHT=3., LAI=3.5
PARAM DAY=243.
PARAM LAT=52., DLONG=-0.6
TABLE TI(1-10)=10=15.
PARAM RCO2I=120.
FUNCTION AMTB=0.,.001, 15.,50., 25.,60., 35.,60., 40.,20., 45.,0.
PARAM LAMBDA=1.15
END
* 1 SEPTEMBER 1972, FLEVOPOLDER, MAIS
PARAM DAY=244.
FUNCTION TATB= 0.,14., 6.,12., 10.5,17.6, 12.7,17.8, 13.3,19.4,...
              13.9, 18.3, 14.5,19.2, 15.1,18.6, 15.7,18.9, ...
              16.4,18.7, 17.0,18.3, 24.,14.
FUNCTION VPATB= 0.,12., 10.5,12.3, 12.7,13.0, 13.3,13.1, ...
              13.9,12.4, 14.5,12.3, 15.1,12.4, 15.7,12.3, ...
              16.4,12.1, 17.0,12.0, 24.,12.
FUNCTION WINDRB= 0.,2.0, 10.5,2.0, 12.7,2.0, 13.3,2.5, 13.9,2.3,...
              14.5,2.3,15.1,3.3, 15.7,3.4, 16.4,3.3, 17.0,3.6,24.,3.
FUNCTION NRADTB=0.,-20., 6.,0., 7.,10., 8.,100., 10.5,360., ...
              12.7,183., 13.3,370., 13.9,145., 14.5,307., 15.1,176.,...
              15.7,246., 16.4,208., 17.0,125., 18.0,0., 19.,-30., ...
              24.,-20.
END
* 14 AUGUSTUS 1973, FLEVOPOLDER, MAIS
PARAM DFACT=0.74,ZNOTF=0.077
TIMER FINTIM=61200.
PARAM DAY=226.
FUNCTION TATB= 0.,18., 6.,16., 10.2,22.8, 11.,23.5, 11.8,23.9, ...
              12.5,24.5, 13.3,25.2, 14.3,26.1, 15.,26.4, ...
              15.5,26.4, 16.3,26.5, 16.8,26.5
FUNCTION VPATB= 0.,14., 10.2,14.9, 11.,14.3, 11.8,14.0, 12.5,15.0,...
              13.3,14.8, 14.3,13.6, 15.,14., 15.5,14., 16.3,14.2, ...
              16.8,15.
FUNCTION WINDRB= 0.,3., 10.2,3.9, 11.,4.1, 11.8,4.0, 12.5,3.8, ...
              13.3,4.2, 14.3,3.7, 15.,3.5, 15.5,3.3, 16.3,3.2, 16.8,2.8
FUNCTION NRADTB= 0.,-20.,6.,0., 7.,10., 8.,100., 10.2,407., 11.,457.,...
              11.8,496., 12.5,511., 13.3,514., 14.3,471., ...
              15.0,424., 15.5,369., 16.3,301., 16.8,231.
PARAM REFHT=3., CROPHT=2.2, LAI=5.4, RESS=0.
END
* 23 AUGUSTUS 1973, FLEVOPOLDER, MAIS
PARAM DAY=235.
FUNCTION TATB=0.,15., 6.,13., 10.,16.2, 10.8,17.4, 11.3,18.4, ...
              12.,19.2, 12.5,20.1, 13.3,20.6, 14.,21.2, 14.8,21.2, ...
              15.3,21.4, 15.8,21.5, 16.5,21.6
FUNCTION VPATB=0.,11., 10.,11.8, 11.3,11.8, 12.,11.7, 12.5,11.5, ...
              13.3,11.5, 14.,11.6, 14.8,11.7, 15.3,11.4, 15.8,11.2,...
              16.5,11.1
FUNCTION WINDRB=0.,2., 10.,2.6, 10.8,2.8, 11.3,3.1, 12.,3.1, ...
              12.5,2.7, 13.3,2.3, 14.,2.3, 14.8,2.5, 15.3,2.5, ...
              15.8,2.3, 16.5,2.3

```

FUNCTION NRADTB=0.,-20., 6.,0., 7.,10., 8.,100., 10.,320., ...
10.8,378., 11.3,426., 12.,456., 12.5,477., 13.3,470., ...
14.,413., 14.8,376., 15.3,334., 15.8,285., 16.5,234.

PARAM RESS=1,E4

END
STOP
ENDJOB

List of abbreviations for MICROWEATHER

Com-puter-name	description	symbol in text	chapter	unit
A	COEFFICIENT IN TAYLOR SERIES	α		
AA	IN PROC. GEOM, INTERMEDIATE VARIABLE	α		
AA	IN PROC. ABOVE, COEFFICIENT OF SECOND ORDER EQN	α	4	
ABL	NAME OF PROCEDURE	α		
ABOVE	PROCEDURE FOR TURBULENT EXCHANGE ABOVE CROP	α		
ABS	TAKES ABSOLUTE VALUE OF THE ARGUMENT	α		
ABSNR	NET RADIATION ABSORBED BY THE CANOPY	R		$J M^{-2} S^{-1}$
ABSRAD	TOTAL ABSORBED RADIANT ENERGY PER LEAF AREA	R	3	$J M^{-2} S^{-1}$
ABTURR	RESISTANCE TO HEAT BETWEEN CROPHT AND REFHT	r	4	$S M^{-1}$
ACRS	ACTUAL CONDUCTANCE OF THE ROOT SYSTEM	r		$KG H_2O M^{-2} BAR^{-1} S^{-1}$
AFGEN	ARBITRARY FUNCTION GENERATOR OF CSMP	r		
AH	A FOR HEAT	r		
ALOG	NATURAL LOGARITHM	r		
ALPHAK	EXTINCTION FACTOR FOR WINDSPEED	r	4	
AM	A FOR MOMENTUM	r		
AMAX	RATE OF CO2 ASSIMILATION OF A LEAF AT LIGHT SATURATION	r	3	$KG CO_2 HA^{-1} H^{-1}$
AMIN1	CSMP FUNCTION THAT TAKES THE SMALLEST OF ITS ARGUMENTS	r		
AMOD	CSMP FUNCTION FOR SAW TOOTH DEPENDENCE	r		
AMTB	LIGHT SATURATED NET CO2 ASSIMILATION AS DEPENDENT ON TEMPERATURE	r		$KG CO_2 HA^{-1} H^{-1}$
B	COEFFICIENT IN TAYLOR SERIES	β		
BB	IN PROC. GEOM, INTERMEDIATE VARIABLE	β		
BB	IN PROC. ABOVE, COEFFICIENT OF SECOND ORDER EQN	β	4	
BH	B FOR HEAT	β		
BM	B FOR MOMENTUM	β		
BU	RELATIVE CONTRIBUTION OF NINE ZONES OF A UNIFORM OVERCAST SKY	B_n	2	
C	COEFFICIENT IN TAYLOR SERIES	γ		
CC	IN PROC. GEOM, INTERMEDIATE VARIABLE	γ		
CC	IN PROC. ABOVE, COEFFICIENT OF SECOND ORDER EQN	γ	4	
CCOS	INTERMEDIATE VARIABLE	γ		
CH	C FOR HEAT	γ		
CM	C FOR MOMENTUM	γ		
CO	INTERMEDIATE VARIABLE	γ		
COEF1	COEFFICIENT IN EQN 4.22 AND 4.23	γ	4	
COEF2	COEFFICIENT IN EQN 4.22 AND 4.23	γ	4	
CONTR	NAME OF CONTROL PROCEDURE	γ		
CONTR1	NAME OF CONTROL PROCEDURE	γ		
CONTR2	NAME OF CONTROL PROCEDURE	γ		
COSDEC	COSINE OF SUN DECLINATION	γ		
CO2	CO2 CONCENTRATION INSIDE THE CANOPY	γ		VPM
CO2F	INTERMEDIATE VARIABLE	γ		$KG CO_2 HA^{-1} H^{-1} S M^{-1}$
CO2FL	CO2 FLUX BETWEEN ADJACENT AIR LAYERS	γ		$KG CO_2 HA^{-1} H^{-1} S M^{-1}$
CROPHT	HEIGHT OF THE CROP	Z_c	4	M
CSLT	COSINE OF LATITUDE OF EXPERIMENTAL PLOT	γ		
CT	CHARACTERISTIC GROUP OF VARIABLES, WHICH DETERMINES THE ALLOWED RANGE OF DIFDT	γ		K
CURRAD	PROCEDURE FOR CURRENT RADIATION CONDITIONS	γ		
D	IN MACRO, COEFFICIENT IN TAYLOR SERIES	δ		
D	IN MAIN PROGRAM, ZERO PLANE DISPLACEMENT	d	4	M
DAY	NUMBER OF THE DAY IN THE YEAR, reckoned from 1 JANUARY	t_d	2	D
DBOWR	AVERAGE DAILY BOWEN RATIO	γ		
DD	INTERMEDIATE VARIABLE	γ		
DDEW	RATE OF CHANGE OF DEW	γ		$J M^{-2} S^{-1}$
DDEWT	RATE OF CHANGE OF DEWT	γ		
DDTDT	RATE OF CHANGE OF THE AIR TEMPERATURE IN A LAYER	γ		$K S^{-1}$

DDVDT	RATE OF CHANGE OF THE WATER VAPOUR PRESSURE IN A LAYER	-		MBAR S ⁻¹
DEC	DECLINATION OF SUN WITH RESPECT TO THE EQUATOR	6	2	-
DEW	AMOUNT OF DEW IN A LAYER OF THE CANOPY	-		J M ⁻²
DEWL	VALUE OF DEW AT THE LAST CALCULATION	-		J M ⁻²
DEWT	DURATION OF LEAF WETNESS	-		S
DFACT	RATIO OF ZERO PLANE DISPLACEMENT AND CROP HEIGHT	-		-
DH	D FOR HEAT	-		-
DIFCL	DIFFUSE VISIBLE RADIATION OF A STANDARD CLEAR SKY	S _{0,c}	2,3	J M ⁻² S ⁻¹
DIFDT	DIFFERENCE BETWEEN CURRENT DT AND DT DURING THE LAST CALCULATION	-		K
DIFOV	DIFFUSE VISIBLE RADIATION OF A STANDARD OVERCAST SKY	S _{0,o}	2,3	J M ⁻² S ⁻¹
DIFTL	SAME AS DIFDT, BUT FOR TL	-		K
DIK	THICKNESS OF A LAYER INSIDE THE CANOPY	-		M
DIST	DISTANCE BETWEEN THE CENTRES OF THE SOIL LAYERS	-		M
DISTI	DISTANCE BETWEEN SOIL SURFACE AND CENTRE OF THE TOP SOIL LAYER	d ₁	3	M
DL	LAI OF A LAYER	L _s	2,3	M ² LEAF M ⁻² GROUND
DLHFL	DAILY TOTAL OF LHFLI	-		J M ⁻² D ⁻¹
DLHFLB	DAILY TOTAL OF LHFLB	-		J M ⁻² D ⁻¹
DLONG	DIFFERENCE IN HOURS WITH STANDARD SOLAR TIME	-		H
DM	D FOR MOMENTUM	-		-
DNRAD	DAILY TOTAL OF NRAD	-		J M ⁻² D ⁻¹
DPL	DARK RESPIRATION RATE OF LEAVES	F ₀	3	KG CO ₂ HA ⁻¹ H ⁻¹
DRAGC	DRAG COEFFICIENT OF THE LEAVES	c	4	-
DRYP	DRYPING POWER OF THE AIR AT REFERENCE HEIGHT	6	3	MBAR J M ⁻² S ⁻¹ K ⁻¹
DRYPB	DRYP IN THE LOWEST AIR LAYER	6	3	MBAR J M ⁻² S ⁻¹ K ⁻¹
DSHFL	DAILY TOTAL OF SHFLI	-		J M ⁻² D ⁻¹
DSHFLB	DAILY TOTAL OF SHFLB	-		J M ⁻² D ⁻¹
DSOILF	DAILY TOTAL OF THE SOIL HEAT FLUX G	-		J M ⁻² D ⁻¹
DT	DIFFERENCE BETWEEN AIR TEMPERATURE INSIDE THE CANOPY AND THAT AT REFERENCE LEVEL	-		K
DT0	DT AT CROP HEIGHT	-		C
DV	DIFFERENCE BETWEEN WATER VAPOUR PRESSURE INSIDE THE CANOPY AND THAT AT REFERENCE LEVEL	-		MBAR
DV0	DV AT CROP HEIGHT	-		MBAR
DYNAMIC	NAME OF DYNAMIC SEGMENT	-		-
DZETA	DIMENSIONLESS HEIGHT DIFFERENCE BETWEEN REFHT AND D PLUS ZNOT	Δζ	4	-
DZS	DISTANCE BETWEEN CONSECUTIVE LEVELS OF ZS	-		M
DZS2	DZS SQUARED	-		M ²
DZS3	DZS, RAISED TO THE THIRD POWER	-		M ³
E	COEFFICIENT IN TAYLOR SERIES	-		-
ECO2C	EXTERNAL CO ₂ CONCENTRATION	-		VPM
EE	INTERMEDIATE VARIABLE	-		-
EH	E FOR HEAT	-		-
EFF	DERIVATIVE OF CO ₂ ASSIMILATION VERSUS ABSORBED VISIBLE RADIATION AT LOW LIGHT INTENSITY	ε	3	KG CO ₂ M ² S HA ⁻¹ H ⁻¹ J ⁻¹
EHL	EVAPORATIVE HEAT LOSS OF LEAVES PER LEAF AREA	λE	3	J M ⁻² S ⁻¹
EM	E FOR MOMENTUM	-		-
ENLOSS	ENERGY FLUX, LOST FROM THE CANOPY SPACE	-		J M ⁻² S ⁻¹
ENP	ENERGY USED FOR CO ₂ ASSIMILATION, PER LEAF AREA	H	3	J M ⁻² S ⁻¹
ESS	SATURATED VAPOUR PRESSURE AT THE SOIL SURFACE TEMPERATURE	-		MBAR
ETS	EFFECTIVE RADIANT TEMPERATURE OF THE CANOPY, SEEN FROM ABOVE	-		C
EQ	STANDS FOR EQUAL IN IF-STATEMENT	-		-
ETS4	ETS IN KELVIN, RAISED TO THE POWER 4	-		K
EXDIF	NAME OF PROCEDURE	-		-
EXTI	NAME OF PROCEDURE	-		-
EXPROG	SWITCH FOR EXECUTION OF PART OF THE PROGRAM	-		-
F	LEAF ANGLE DISTRIBUTION	F	2,3	-
FA	INTERMEDIATE VARIABLE	-		-
FCL	FRACTION OF TIME THAT SKY IS CLEAR	-		-
FI	INTERMEDIATE VARIABLE IN INTERPOLATION	-		-
FINTIM	TOTAL DURATION OF SIMULATION RUN	-		S
FISUN	INTERMEDIATE VARIABLE USED FOR INTERPOLATION	-		-
FLIL	INTERMEDIATE FLOATING VARIABLE	-		-
FLIS	INTERMEDIATE FLOATING VARIABLE	-		-
FLUX	PROCEDURE FOR FLUXES IN THE AIR	-		-
FLSN	INTERMEDIATE FLOATING VARIABLE	-		-

FNDR	ABSORBED NEAR-INFRARED RADIATION UNDER A CLEAR SKY, ONLY ORIGINATING FROM DIRECT SOLAR RADIATION, BUT INCLUDING THAT DIFFUSED BY OTHER LEAVES	R_{nb}	3	$J M^{-2} LEAF S^{-1}$
FOV	FRACTION OF TIME THAT SKY IS OVERCAST	f	3	-
FRDIF	FRACTION DIFFUSE UNDER CLEAR SKY	-	-	-
FRDIFT	TABLE OF FRACTION DIFFUSE AS FUNCTION OF THE SINE OF SUN HEIGHT	-	-	-
FSR	FRACTION OF SUNLIT LEAVES IN A LAYER	-	-	-
FVDR	SEE FNDR, BUT FOR VISIBLE RADIATION	-	-	-
F1-F5	CORRECTION FACTOR FOR BUOYANCY EFFECTS	ϕ	4	-
G	SOIL HEAT FLUX	G	3	$J M^{-2} S^{-1}$
GEOM	PROCEDURE FOR LIGHT DISTRIBUTION OVER THE LEAVES	-	-	-
GLOBE	PROCEDURE FOR SOLAR POSITION	-	-	-
GR	ACCELERATION OF GRAVITY	g	4	$M S^{-2}$
GRLMIX	INTERMEDIATE VARIABLE	-	-	$M^2 S^{-2}$
GT	STANDS FOR GREATER THAN IN IF-STATEMENT	-	-	-
H	HEIGHT AT THE TOP OF A LAYER	-	-	M
HC	HEAT CONTENT OF A SOIL LAYER	-	-	$J M^{-2}$
HCI	INITIAL HEAT CONTENT OF A SOIL LAYER	-	-	$J M^{-2}$
HFL	HEAT FLUX BETWEEN SOIL LAYERS	-	-	$J M^{-2} S^{-1}$
HOUR	TIME OF THE DAY IN HOURS	t_h	2	H
HRES	AVERAGE HEIGHT OF THE CLOUDS	-	-	M
HSUN	HEIGHT OF THE SUN IN DEGREES	-	-	-
HTB	HEIGHT AS FUNCTION OF THE CUMULATIVE LEAF AREA INDEX	-	-	M
I	RUNNER IN DO LOOP	-	-	-
IDEW	INITIAL DEW	-	-	$J M^{-2}$
IDWT	INITIAL DEWT	-	-	S
IDT	INITIAL VALUE OF DT	-	-	K
IDV	INITIAL VALUE OF DV	-	-	MBAR
IF	STARTS A CONDITIONAL STATEMENT	-	-	-
IL	NUMBER OF INCLINATION CLASS OF LEAVES	λ	2,3	-
IMPL	IMPLICIT LOOP, PROVIDED BY CSMP	-	-	-
IMPULS	CSMP FUNCTION OF TIME	-	-	-
INITIAL	NAME OF INITIAL SEGMENT	-	-	-
INSIDE	PROCEDURE FOR TURBULENT EXCHANGE INSIDE CROP	-	-	-
INT	RESULT OF NUMERICAL INTEGRATION OF $\phi/(z-d)$	-	-	-
INTAM	INT FOR MOMENTUM BETWEEN Z_c AND Z_r	-	-	-
INTAN	INT UNDER NEUTRAL CONDITIONS BETWEEN Z_c AND Z_r	-	-	-
INTERP	PROCEDURE FOR INTERPOLATION	-	-	-
INTH	INT FOR HEAT BETWEEN $D+Z_0$ AND Z_r	-	-	-
INTM	INT FOR MOMENTUM BETWEEN $D+Z_0$ AND Z_r	-	-	-
INTN	INT UNDER NEUTRAL CONDITIONS BETWEEN $D+Z_0$ AND Z_r	-	-	-
INVL	NUMBER OF THE LAYER, RECKONED FROM BELOW	-	-	-
IS	NUMBER OF INCLINATION CLASS OF SUN	-	-	-
ISUN	NUMBER OF THE INCLINATION CLASS OF THE SUN, SHIFTED OVER 5 DEGREES	-	-	-
ITCAP	INVERSE CAPACITY FOR SENSIBLE HEAT OF AN AIR LAYER	-	-	$K M^2 J^{-1}$
IVCAP	INVERSE CAPACITY FOR LATENT HEAT OF AN AIR LAYER	-	-	MBAR $M^2 J^{-1}$
J	RUNNER IN DO LOOP	-	-	-
K	TURBULENT EXCHANGE COEFFICIENT INSIDE THE CANOPY	K	4	$M^2 S^{-1}$
KARMAN	VON KARMAN'S CONSTANT	k	4	-
KB	EXTINCTION COEFFICIENT FOR DIRECT RADIATION AND BLACK LEAVES	K_b	2	$M^2 GROUND M^{-2} LEAF$
KBDF	EXTINCTION COEFFICIENT FOR DIFFUSE RADIATION AND BLACK LEAVES	-	-	$M^2 GROUND M^{-2} LEAF$
KDFN	EXTINCTION COEFFICIENT FOR DIFFUSE NEAR-INFRARED RADIATION	-	-	$M^2 GROUND M^{-2} LEAF$
KDFV	IDEM FOR DIFFUSE VISIBLE RADIATION	-	-	$M^2 GROUND M^{-2} LEAF$
KDN	IDEM UNDER DIRECT NEAR-INFRARED RADIATION	-	-	$M^2 GROUND M^{-2} LEAF$
KDP	SEE KB	-	-	-
KDRN	SEE KDN	-	-	-
KDRV	SEE KDV	-	-	-
KDV	IDEM UNDER DIRECT VISIBLE RADIATION	-	-	$M^2 GROUND M^{-2} LEAF$
KEEP	CONTROL VARIABLE GENERATED BY CSMP,	-	-	-
KN	SEE KDN	-	-	-
KU	INTERMEDIATE VARIABLE	-	-	$M S^{-1}$
KV	SEE KDV	-	-	-
LAI	LEAF AREA INDEX	LAI	-	$M^2 LEAF M^{-2} GROUND$
LAMBDA	THERMAL CONDUCTIVITY OF THE SOIL	λ'	3	$J M^{-1} S^{-1} K^{-1}$
LASTDT	VALUE OF DT DURING LAST CALCULATION	-	-	C

LASTDV	VALUE OF DV DURING LAST CALCULATION	-		MBAR
LASTNR	VALUE OF NRAD DURING LAST CALCULATION	-		$J M^{-2} S^{-1}$
LASTSR	VALUE OF SRAD DURING LAST CALCULATION	-		$J M^{-2} S^{-1}$
LASTTL	VALUE OF TL DURING LAST CALCULATION	-		C
LAT	LATITUDE OF EXPERIMENTAL PLOT	λ	2	-
LAYER	PROCEDURE FOR STRATIFICATION IN THE CANOPY	-		-
LFCL	COMPLEMENT OF LFOV	-		-
LFOV	FOV, RESTRICTED BETWEEN 0 AND 1	-		-
LHFL	LATENT HEAT FLUX PER GROUND AREA AT THE BOUNDARY BETWEEN TWO LAYERS OF AIR	-		$J M^{-2} S^{-1}$
LHFLB	LATENT HEAT FLUX AT THE BOTTOM	λE	3	$J M^{-2} S^{-1}$
LHFL1	LATENT HEAT FLUX AT THE TOP OF THE CANOPY	-		$J M^{-2} S^{-1}$
LHLL	LATENT HEAT LOSS PER GROUND AREA OF A CANOPY LAYER	-		$J M^{-2} S^{-1}$
LHLLC	LATENT HEAT LOSS OF SUNLIT LEAVES UNDER A CLEAR SKY	-		$J M^{-2} LEAF S^{-1}$
LHLLCL	LATENT HEAT LOSS OF A LAYER UNDER A CLEAR SKY, EXPRESSED PER LEAF AREA	-		$J M^{-2} LEAF S^{-1}$
LHLL0	SEE LHLLCL, BUT FOR AN OVERCAST SKY	-		-
LHLLS	LATENT HEAT LOSS OF SHADED LEAVES UNDER A CLEAR SKY	-		$J M^{-2} LEAF S^{-1}$
LHVAP	LATENT HEAT FOR VAPORIZATION OF WATER	λ	3	$J KG^{-1} H_2O$
LMIX	MIXING LENGTH INSIDE THE CANOPY	l_m	4	M
LPES	LEAF RESISTANCE TO WATER VAPOUR	r_{lv}	3	$S M^{-1}$
LPES0	LPES UNDER AN OVERCAST SKY	-		$S M^{-1}$
LRESSH	LRES OF SHADED LEAVES UNDER A CLEAR SKY	-		$S M^{-1}$
LRESSU	LRES OF SUNLIT LEAVES UNDER A CLEAR SKY	-		$S M^{-1}$
LT	STANDS FOR LESS THAN IN IF-STATEMENT	-		-
LWR	NET ABSORBED LONG WAVE RADIATION PER LEAF AREA	R_l	2	$J M^{-2} S^{-1}$
LWRCI	LWRI UNDER A CLEAR SKY	-		$J M^{-2} S^{-1}$
LWRI	NET LONG WAVE RADIATION ABOVE THE CANOPY	-		$J M^{-2} S^{-1}$
LWROI	LWRI UNDER AN OVERCAST SKY	-		$J M^{-2} S^{-1}$
LWSOIL	NET THERMAL RADIANT FLUX PER GROUND AREA BETWEEN SOIL SURFACE AND A LAYER OF LEAVES	-		$J M^{-2} S^{-1}$
MONOBL	MONIN-OBUKHOV LENGTH	L	4	M
MULT	MULTIPLICATION FACTOR FOR THICKNESSES OF SUBSEQUENT SOIL LAYERS	-		-
NCO2A	IN MACRO, NET CO2 ASSIMILATION PER LEAF AREA	F_n	3	$KG CO_2 HA^{-1} H^{-1}$
NCO2A	IN PROCEDURE, NET CO2 ASSIMILATION OF A LAYER PER GROUND AREA	-		$KG CO_2 HA^{-1} H^{-1}$
NCO2AC	NET CO2 ASSIMILATION OF A LAYER UNDER A CLEAR SKY	F_{cl}	3	$KG CO_2 HA^{-1} LEAF H^{-1}$
NCO2AO	NET CO2 ASSIMILATION UNDER AN OVERCAST SKY	F_{ov}	3	$KG CO_2 HA^{-1} LEAF H^{-1}$
NDIR	ABSORBED DIRECT NEAR-INFRARED RADIATION UNDER A CLEAR SKY	$R_{n,d}$	3	$J M^{-2} LEAF S^{-1}$
NE	STANDS FOR NOT EQUAL IN IF-STATEMENT	-		-
NFLUX	PROCEDURE FOR NET FLUXES IN THE AIR	-		-
NIR	ABSORBED NEAR-INFRARED RADIATION PER LEAF AREA	R_n	3	$J M^{-2} S^{-1}$
NIRDF	ABSORBED NEAR-INFRARED RADIATION UNDER A CLEAR SKY, BUT ONLY FROM THE DIFFUSE SKYLIGHT	$R_{n,d}$	3	$J M^{-2} LEAF S^{-1}$
NIRDFC	ABSORBED DIFFUSE AND DIFFUSED NEAR-INFRARED RADIATION UNDER A CLEAR SKY	-		$J M^{-2} LEAF S^{-1}$
NIRDPO	ABSORBED NEAR-INFRARED RADIATION UNDER AN OVERCAST SKY	$R_{n,o}$	3	$J M^{-2} LEAF S^{-1}$
NHFL	NET HEAT FLUX OF A SOIL LAYER	-		$J M^{-2} S^{-1}$
NLF	NET LATENT HEAT FLUX PER GROUND AREA GAINED BY A LAYER OF AIR INSIDE THE CANOPY	-		$J M^{-2} S^{-1}$
NLWR	NET THERMAL RADIANT FLUX PER GROUND AREA BETWEEN A LAYER OF LEAVES AND OTHER LAYERS AND THE SOIL SURFACE	-		$J M^{-2} S^{-1}$
NLWRM	NET THERMAL RADIANT FLUX PER GROUND AREA BETWEEN TWO LAYERS OF LEAVES	-		$J M^{-2} S^{-1}$
NLWRS	NET THERMAL RADIANT FLUX ON THE SOIL SURFACE, BOTH FROM LEAVES AND SKY	-		$J M^{-2} S^{-1}$
NHFL	NET HEAT FLUX BETWEEN ADJACENT SOIL LAYERS	-		$J M^{-2} S^{-1}$
NOT	CMP FUNCTION, USED TO PREVENT ZERO DIVISION	-		-
NPHTSH	NET CO2 ASSIMILATION OF SHADED LEAVES UNDER A CLEAR SKY	F_{sh}	3	$KG CO_2 HA^{-1} LEAF H^{-1}$
NPHTSU	NET CO2 ASSIMILATION OF SUNLIT LEAVES UNDER A CLEAR SKY	F_{su}	3	$KG CO_2 HA^{-1} LEAF H^{-1}$
NRAD	CALCULATED NET RADIATION	-		$J M^{-2} S^{-1}$
NRADCL	NET RADIATION UNDER A CLEAR SKY	-		$J M^{-2} S^{-1}$
NRADM	MEASURED NET RADIATION	-		$J M^{-2} S^{-1}$
NRADOV	NET RADIATION UNDER AN OVERCAST SKY	-		$J M^{-2} S^{-1}$
NRADTB	TABLE OF MEASURED NRAD AS FUNCTION OF HOUR	-		$J M^{-2} S^{-1}$
NRADS	NET RADIATION ABSORBED BY THE SOIL SURFACE	R	3	$J M^{-2} S^{-1}$

NSF	NET SENSIBLE HEAT FLUX PER GROUND AREA GAINED BY A LAYER OF AIR INSIDE THE CANOPY	-		$J M^{-2} S^{-1}$
NSPER	ABSORBED NEAR-INFRARED RADIATION OF A LEAF , PERPENDICULAR TO THE SOLAR BEAM	-		$J M^{-2} LEAF S^{-1}$
NSRC	NET SOLAR RADIATION CLEAR	-		$J M^{-2} S^{-1}$
NSRO	NET SOLAR RADIATION OVERCAST	-		$J M^{-2} S^{-1}$
NUMINT	NAME OF THE MACRO FOR NUMERICAL INTEGRATION	-		-
NUMLL	NUMBER OF LAYERS INSIDE THE CANOPY	M	2	-
NUML1	NUMLL PLUS ONE	-		-
OAV	AVERAGE PROJECTION OF LEAVES IN NINE DIRECTIONS	\bar{O}	2	-
PHI	CORRECTION FACTOR FOR BUOYANCY	ϕ	4	-
PI	CIRCUMFERENCE OF A CIRCLE , DIVIDED BY ITS DIAMETER	π		-
POWER	EXPONENT IN BUSINGER'S EQNS ,4.22 AND 4.23	-		-
PROEL	TIME INTERVAL FOR OUTPUTTING PRINT RESULTS	-		S
PROCO2	NAME OF PROCEDURE FOR THE CO2 PROFILE	-		-
PRT	SWITCH FOR OUTPUT	-		-
PSCH	PSYCHROMETRIC CONSTANT	γ	3	MBAR K^{-1}
PSCHAP	APPARENT PSYCHROMETRIC CONSTANT	γ_a	3	MBAR K^{-1}
RA	RESISTANCE TO HEAT OF BOUNDARY LAYER ROUND LEAF	$r_{s,h}$	3	$S M^{-1}$
RAD	ONE DEGREE IN RADIANS, OR 180 DIVIDED BY PI	-		-
RATE	PROCEDURE FOR RATES OF THE FAST PROCESSES	-		-
RCO2I	INTERNAL CONCENTRATION, MAINTAINED BY STOMATAL REGULATION	C_i	3	VPM
RDRM	SEE RFN	-		-
RDRV	SEE RFY	-		-
REFHT	HEIGHT OF REFERENCE LEVEL ABOVE THE GROUND	z_r	4	M
REFN	REFLECTION COEFFICIENT OF A CANOPY WITH HORIZONTAL LEAVES, IN THE NEAR-INFRARED REGION	ρ_h	2	-
REFV	REFLECTION COEFFICIENT OF A CANOPY WITH HORIZONTAL LEAVES, IN THE VISIBLE REGION	ρ_h	2	-
RESCW	CUTICULAR RESISTANCE TO TRANSPIRATION	-		$S M^{-1}$
RESS	SOIL SURFACE RESISTANCE TO EVAPORATION	-		$S M^{-1}$
RFN	REFLECTION COEFFICIENT OF A CANOPY FOR NEAR-INFRARED RADIATION, UNDER DIRECT IRRADIATION	-		-
RFOVM	REFLECTION COEFFICIENT OF A CANOPY FOR NEAR-INFRARED RADIATION, UNDER DIFFUSE IRRADIATION	-		-
RFOVV	REFLECTION COEFFICIENT OF A CANOPY FOR VISIBLE RADIATION, UNDER DIFFUSE IRRADIATION	-		-
RFV	REFLECTION COEFFICIENT OF A CANOPY FOR VISIRLE RADIATION, UNDER DIRECT IRRADIATION	-		-
RHOCP	VOLUMETRIC HEAT CAPACITY OF AIR	ρc_p	3	$J M^{-3} K^{-1}$
RHTB	RELATIVE HEIGHT AS FUNCTION OF THE RELATIVE LAI FOR A PARABOLIC LEAF AREA DENSITY DISTRIBUTION	-		-
RICHI	RICHARDSON NUMBER INSIDE THE CANOPY	Ri	4	-
RICHN	RICHARDSON NUMBER ABOVE THE CANOPY	Ri	4	-
RINC	RESISTANCE TO AERIAL EXCHANGE BETWEEN ADJACENT AIR LAYERS	-		$S M^{-1}$
RN	SEE RFN	-		-
RR	HEAT EXCHANGE RESISTANCE	-		$K M^2 S J^{-1}$
RSS	BOUNDARY LAYER RESISTANCE ON SOIL SURFACE	r_s	3	$S M^{-1}$
RSSE	RSS TO WATER VAPOUR PLUS TURBULENT RESISTANCE TO THE CENTRE OF THE BOTTOM LAYER OF AIR	$r_{s,v}$	3	$S M^{-1}$
RSSH	SAME AS RSSE, BUT TO HEAT	$r_{s,h}$	3	$S M^{-1}$
RV	SEE RFY	-		-
RWCP	RELATIVE WATER CONTENT OF THE PLANTS	θ	3	-
S	CUMULATIVE DISTRIBUTION OF LEAVES OVER 10 CLASSES OF SINES OF INCIDENCE	S	3	-
SCN	SCATTERING COEFFICIENT OF LEAVES FOR NEAR-INFRARED RADIATION	σ_n	2	-
SCOP	STABILITY COEFFICIENT	-		-
SCRS	MINIMUM CONDUCTANCE OF THE ROOT SYSTEM	-		$KG H2O BAR^{-1} M^{-2} S^{-1}$
SCV	SCATTERING COEFFICIENT OF LEAVES FOR VISIBLE RADIATION	σ_v	2,3	-
SHFL	SENSIBLE HEAT FLUX PER GROUND AREA AT THE BOUNDARY BETWEEN TWO LAYERS	-		$J M^{-2} S^{-1}$
SHFLB	SENSIBLE HEAT FLUX AT THE BOTTOM	-		$J M^{-2} S^{-1}$
SHFL1	SENSIBLE HEAT FLUX AT THE TOP OF THE CANOPY	-		$J M^{-2} S^{-1}$
SHL	SENSIBLE HEAT LOSS OF LEAVES PER LEAF AREA CANOPY LAYER	C	3	$J M^{-2} S^{-1}$
SHLL	SENSIBLE HEAT LOSS PER GROUND AREA OF A CANOPY LAYER	-		$J M^{-2} S^{-1}$

SHLLC	SENSIBLE HEAT LOSS OF SUNLIT LEAVES UNDER A CLEAR SKY	-	J M ⁻² LEAF S ⁻¹
SHLLCL	SENSIBLE HEAT LOSS OF A LAYER UNDER A CLEAR SKY ,EXPRESSED PER LEAF AREA	-	J M ⁻² LEAF S ⁻¹
SHLLO	SEE SHLLCL,BUT FOR AN OVERCAST SKY	-	J M ⁻² LEAF S ⁻¹
SHLLS	SENSIBLE HEAT LOSS OF SHADED LEAVES UNDER A CLEAR SKY	-	J M ⁻² LEAF S ⁻¹
SI	INTERMEDIATE VARIABLE	-	-
SIGMA	STEFAN-BOLTZMANN CONSTANT	σ 2	J M ⁻² S ⁻¹ K ⁻⁴
SINDEC	SINE OF SUN DECLINATION	-	-
SIX	SWITCH FOR OUTPUT,ONCE PER SIX HOURS	-	-
SKT	APPARENT RADIANT TEMPERATURE OF THE SKY	T _{sky} 2	C
SKTCL	SKT FOR A STANDARD CLEAR SKY	-	C
SKTCL4	SKTCL IN KELVIN, RAISED TO THE POWER 4	-	K ⁴
SKTOV	SKT FOR A STANDARD OVERCAST SKY	-	C
SKTOV4	SKTOV IN KELVIN, RAISED TO THE POWER 4	-	K ⁴
SKT4	SKT IN KELVIN ,RAISE TO THE POWER 4	-	K ⁴
SLOPE	SLOPE OF SATURATED VAPOUR PRESSURE CURVE AT AIR TEMPERATURE	S 3	MBAR K ⁻¹
SN	NUMBER OF CLASS OF SINE OF INCIDENCE	4 3	-
SNHS	SAME AS SNHSS,BUT 0 WHEN SNHSS IS NEGATIVE	-	-
SNHSS	SINE OF THE HEIGHT OF THE SUN	-	-
SNINC	SINE OF INCIDENCE OF SUNLIGHT ON A LEAF	-	-
SNLT	SINE OF LATITUDE OF EXPERIMENTAL PLOT	-	-
SOILI	PROCEDURE FOR STRATIFICATION IN THE SOIL	-	-
SOILS	PROCEDURE FOR FLUXES IN THE SOIL AND ON ITS SURFACE	-	-
SOURCE	PROCEDURE FOR ENERGY BALANCE OF LAYERS	-	-
SO	INTERMEDIATE VARIABLES TO OBTAIN APCSINE	-	-
SORT	SQUARE ROOT FUNCTION	-	-
SQNI	FACTOR FOR THE REDUCTION OF THE EXTINCTION COEFFICIENT FOR NEAR-INFRARED RADIATION	-	-
SQV	FACTOR FOR THE REDUCTION OF THE EXTINCTION COEFFICIENT FOR VISIBLE RADIATION	-	-
SRAD	INCOMING SOLAR RADIATION	S 2,3	J M ⁻² S ⁻¹
SRADF	CALCULATED MULTIPLICATION FACTOR FOR THE SOLAR RADIATION UNDER EITHER A CLEAR OR AN OVERCAST SKY	-	-
SRADM	MEASURED SOLAR RADIATION	-	J M ⁻² S ⁻¹
SRADTB	MEASURED SOLAR RADIATION AS FUNCTION OF TIME	-	J M ⁻² S ⁻¹
SRC	SOLAR RADIATION UNDER A CLEAR SKY	-	J M ⁻² S ⁻¹
SRESL	STOMATAL RESISTANCE,CHECKED BY LIGHT	-	S M ⁻¹
SRESP	RATE OF SOIL RESPIRATION	-	KG CO ₂ HA ⁻¹ H ⁻¹
SRO	SOLAR RADIATION UNDER AN OVERCAST SKY	-	J M ⁻² S ⁻¹
SRW	STOMATAL RESISTANCE,CHECKED BY WATER STRESS	-	S M ⁻¹
SRWTB	MINIMAL STOMATAL RESISTANCE AS FUNCTION OF THE RELATIVE WATER CONTENT	-	S M ⁻¹
SSIN	INTERMEDIATE VARIABLE	-	-
START	HOUR OF THE DAY,WHEN SIMULATION IS STARTED	-	H
STEMP	PROCEDURE FOR SOIL TEMPERATURES	-	-
STRESS	PROCEDURE FOR THE WATER STRESS OF THE CANOPY	-	-
SUMBL	CANOPY TRANSMISSIVITY FOR LONG WAVE RADIATION	-	-
SUMF	SUM OF TEN CLASSES OF P,SHOULD EQUAL 1	-	-
SUMNI	CANOPY TRANSMISSIVITY FOR DIFFUSE NEAR-INFRARED RADIATION	-	-
SUMVI	CANOPY TRANSMISSIVITY FOR DIFFUSE VISIBLE RAD.	-	-
SUNDCL	DIRECT VISIBLE RADIATION STANDARD SKY CLEAR	S _b 2,3	J M ⁻² S ⁻¹
SUNPER	DIRECT IRADIATION OF THE SUN, PERPENDICULAR ON THE BEAM,EITHER IN VISIBLE OR NEAR-INFRARED	S _p 3	J M ⁻² S ⁻¹
SVPA	SATURATED VAPOUR PRESSURE	e _s 3	MBAR
TA	AIR TEMPERATURE AT THE REFERENCE LEVEL	-	C
TABS	TA PLUS 273,ABSOLUTE TEMPERATURE	-	K
TADT	TA PLUS DT	-	C
TATB	MEASURED TA AS FUNCTION OF HOUR OF THE DAY	-	C
TA239	TA + 239 ,USED IN EQN 3.21	-	C
TCOM	THICKNESS OF THE LAYERS IN THE SOIL	-	M
TCOM1	THICKNESS OF THE TOPMOST SOIL LAYER	-	M
TCOND	CONDUCTANCE FOR SENSIBLE HEAT BETWEEN TWO LAYERS	-	J M ⁻² S ⁻¹ K ⁻¹
TEHL	EVAPORATIVE HEAT LOSS OF LEAVES PER GROUND AREA	-	J M ⁻² S ⁻¹
TELFO	NUMBER OF TIMES ,THAT THE PATES OF THE FAST PROCESSES ARE SET AT ZERO	-	-
TELLER	TELLER COUNTS HOW MANY TIMES PROGRAM IS EXECUTED	-	-
TELM	NUMBER OF TIMES THAT THE RADIATION PART HAS BEEN EXECUTED	-	-

TEMP	TEMPERATURE OF THE LAYERS IN THE SOIL	-		C
TI	INITIAL VALUES OF TEMP	-		C
TIME	SIMULATED TIME ELAPSED SINCE START OF SIMULATION	-		S
TL	LEAF TEMPERATURE, AVERAGED FOR A LAYER	T_l	3	C
TLCL	TL UNDER A CLEAR SKY	-		C
TLHL	LATENT HEAT LOSS, TOTALIZED OVER ALL CANOPY LAYERS	-		$J M^{-2} GROUND S^{-1}$
TLO	TL UNDER AN OVERCAST SKY	-		C
TLSHAD	TL OF SHADED LEAVES UNDER A CLEAR SKY	-		C
TL SUN	TL OF SUNLIT LEAVES UNDER A CLEAR SKY	-		C
TNCO2A	TOTAL NET CO2 ASSIMILATION OF THE CANOPY	-		$KG CO2 HA^{-1} H^{-1}$
TNCO2R	SAME AS TNCO2A, BUT PER SECOND	-		$KG CO2 HA^{-1} S^{-1}$
TRCOEF	TRANSPIRATION COEFFICIENT	-		$KG H2O KG^{-1} CH2O$
TREDTB	REDUCTION FACTOR FOR ROOT CONDUCTANCE AS FUNCTION OF SOIL TEMPERATURE	-		-
TRPH	MACRO THAT DESCRIBES THE ENERGY BALANCE OF THE INDIVIDUAL LEAVES	-		-
TRZ	TEMPERATURE OF THE ROOTING ZONE	-		C
TS	TEMPERATURE OF THE SOIL SURFACE	T_s	3	C
TSHL	SENSIBLE HEAT LOSS TOTALIZED OVER ALL CANOPY LAYERS	-		$J M GROUND S$
TS4	TS IN KELVIN, RAISED TO THE POWER 4	-		K
TURBR	PROCEDURE FOR TURBULENT RESISTANCES	-		-
USTAR	FRICTION VELOCITY	u^*	4	$M S^{-1}$
VAPHT	HEAT OF VAPORIZATION OF WATER	λ	3	$J KC^{-1}$
VCOND	CONDUCTANCE FOR LATENT HEAT BETWEEN TWO LAYERS	-		$J M^{-2} S^{-1} MBAR^{-1}$
VDIR	SEE NDIR, BUT FOR VISIBLE RADIATION	-		-
VIS	ABSORBED VISIBLE RADIATION PER LEAF AREA	R_v	3	$J M^{-2} S^{-1}$
VISDF	SEE NIRD, BUT FOR VISIBLE RADIATION	-		-
VISDFC	SEE NIRD, BUT FOR VISIBLE RADIATION	-		-
VISDFO	SEE NIRD, BUT FOR VISIBLE RADIATION	-		-
VHCAP	VOLUMETRIC HEAT CAPACITY OF THE SOIL	-		$J M^{-3} K^{-1}$
VPA	VAPOUR PRESSURE OF AIR AT REFERENCE LEVEL	-		MBAR
VPATB	TABLE OF MEASURED VPA AS FUNCTION OF HOUR	-		MBAR
VPD	VAPOUR PRESSURE DEFICIT AT REFERENCE HEIGHT	-		MBAR
VPDB	VPD IN THE LOWEST AIR LAYER	-		MBAR
VSPER	SEE NSPER, BUT FOR VISIBLE RADIATION	-		MBAR
WABAL	PROCEDURE FOR THE WATER BALANCE OF THE CANOPY	-		-
WCCP	WATER CONTENT OF THE CANOPY	-		$KG H2O M^{-2}$
WCCPI	INITIAL WCCP	-		$KG H2O M^{-2}$
WCCPRT	RATE OF CHANGE OF WCCP	-		$KG H2O M^{-2} S^{-1}$
WEER	PROCEDURE FOR INPUT WEATHER CONDITIONS	-		-
WIDTH	AVERAGE WIDTH OF THE LEAVES	w	4	M
WIND	HORIZONTAL WIND VELOCITY INSIDE THE CANOPY	u	4	$M S^{-1}$
WINDC	WIND VELOCITY AT CROP HEIGHT	u_c	4	$M S^{-1}$
WINDR	WIND VELOCITY AT REFERENCE HEIGHT	u_r	4	$M S^{-1}$
WINDRB	TABLE OF MEASURED WINDR AS FUNCTION OF HOUR	-		$M S^{-1}$
WINDR2	WINDR SQUARED	-		$M^2 S^{-1}$
WLOSS	WATER LOSS OF THE CANOPY	-		$KG H2O M^{-2} S^{-1}$
WRESPL	XYLEM RESISTANCE TO THE TRANSPIRATION STREAM OF WATER	-		$BAR M^2 S KG$
WSTCP	WATER STRESS OF THE CANOPY	ψ	3	BAR
WSTSL	WATER STRESS IN THE SOIL	-		BAR
WSTTB	PLANT WATER STRESS AS FUNCTION OF ITS RELATIVE WATER CONTENT	-		BAR
WUPTCP	WATER UPTAKE OF THE CANOPY	-		$KG H2O M^{-2} S^{-1}$
XD	TRANSMISSIVITY OF A LAYER, SEE XB	-		-
XL	TRANSMISSIVITY OF A LAYER, SEE XBDP	-		-
XLFD	INTERMEDIATE VARIABLE USED FOR INTERCEPTION OF THERMAL RADIATION	-		-
XLFU	SEE XLFD	-		-
XLN	TRANSMISSIVITY OF THE WHOLE CANOPY, SEE XBDP	-		-
XNDF	TRANSMISSIVITY OF A LAYER, SEE XDFN	-		-
XNDR	TRANSMISSIVITY OF A LAYER, SEE XDN	-		-
XVDF	TRANSMISSIVITY OF A LAYER, SEE XDFV	-		-
XVDR	TRANSMISSIVITY OF A LAYER, SEE XDFV	-		-
Y	INTERMEDIATE VARIABLE	Y	3	-
Z	DISTRIBUTION FUNCTION OF SINE OF INCIDENCE, AVERAGED OVER THE ACTUAL LEAF ANGLE DISTRIBUTION	-		-
Z1A-25A	INTERMEDIATE VARIABLES IN TAYLOR SERIES	-		-
Z1B-25B	INTERMEDIATE VARIABLES IN TAYLOR SERIES	-		-
ZA	FIVE EQUIDISTANT LEVELS BETWEEN CROP HEIGHT AND REFERENCE HEIGHT, RECKONED FROM THE ZERO PLANE D	-		M
ZAI	ZA AT REFERENCE LEVEL	-		M

ZAS	ZA AT CROP HEIGHT	-	M
ZISSN	Z FOR A SPHERICAL LEAF ANGLE DISTRIBUTION	-	-
ZNOT	ROUGHNESS LENGTH	z ₀	M
ZNOTF	RATIO OF ZNOT AND CROPHT	-	-
ZS	FIVE EQUIDISTANT LEVELS BETWEEN ROUGHNESS LENGTH AND REFERENCE HEIGHT, RECKONED FROM THE ZERO PLANE D	-	M
ZS1	ZS AT REFERENCE LEVEL	-	M
ZS5	ZS AT THE LEVEL D+ZNOT	-	M

6 Results

6.1 Introduction

The behaviour of the submodels used was discussed in Chapters 2, 3 and 4, and separately evaluated. In this chapter the composite model is evaluated qualitatively by a case study (Section 6.2). It is investigated whether the daily courses of typical output variables make sense, and whether they are explainable from the behaviour of the submodels. Then the sensitivity of the model for the parameters or for its structure is tested (Section 6.3). This may lead to important conclusions for the choice of priorities in research. However, in complicated models the relation between output and input variables is almost as unpredictable as in nature. It is therefore dangerous to extrapolate the conclusions of a sensitivity analysis to the whole region of likely circumstances. The relations between input and output variables may be smooth in some situation but exhibit a discontinuity in another. It may be considered a modeller's task to explore the terrain of input-output relations and to describe its most conspicuous features. Discontinuities and sudden changes must be explained from the behaviour of the submodels used. A rigorous selection in the number of input and output variables considered is unavoidable.

In Section 6.4 the model is evaluated quantitatively by comparison with actual measurements.

6.2 A case study

6.2.1 Description

First a situation is studied, which can be considered as typical. It concerns a mature maize crop on a fine day at the end of the summer. The weather conditions are given in Fig. 30 where it can be seen that temperature ranges from 13.5 to 20.6°C, humidity from 11.2 to 15 mbar, wind speed from 0.2 to 3 m s⁻¹ and net radiation from -84 to 690 J m⁻² s⁻¹. The height of the crop is 2.5 m, the height of the

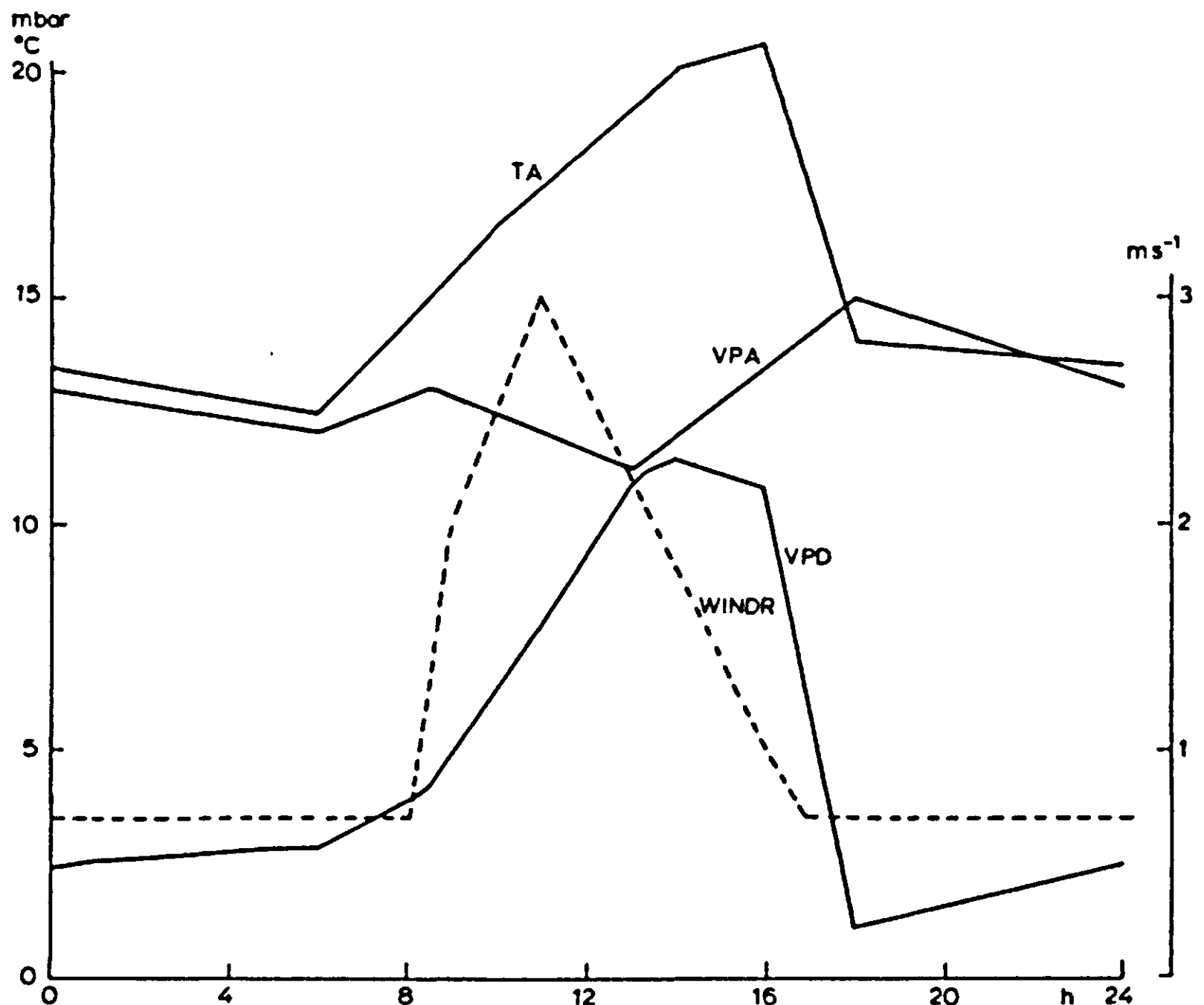


Fig. 30 | Daily courses of weather conditions used for a case study. The scales for air temperature (TA), water vapour pressure in the air (VPA) and vapour pressure deficit (VPD) are given on the left ordinate and that for wind speed (WINDR) on the right ordinate. These conditions hold for the reference level at some height above the crop.

measurements is 3 m and the leaf area index is 3.7. It is assumed that the soil water status is at field capacity and that the soil surface is wet. These conditions are taken from Brown (1964). I used these measured data and not entirely fictive ones to ensure at least some degree of reality in the range of the input data and their mutual relations. For the night, however, no data were available so I had to cook these up. Brown's data refer to the top of the canopy. I shifted the level of reference from this 2.5 m height to 3 m height so that the model effects of stabilization in this layer of air would show up in the simulated results. This manipulation is permitted because I never use Browns other measurements for evaluation purposes. The net radiation is an

input variable in this case, from which the solar radiation is computed according to the method described in Section 5.2.3.

6.2.2 *Daily courses of energy fluxes*

Fig. 31a gives the daily course of net radiation together with the simulated courses of sensible and latent heat fluxes above the canopy. Fig. 31b gives the simulated fluxes of net radiation at the soil surface, the sensible and latent heat fluxes at the soil surface and the heat flux into the soil.

To begin with the daytime conditions, we notice that the peak of total latent heat loss occurs later in the day than that of the total sensible heat loss. This shift in time is mainly due to the increase of the vapour pressure deficit (VPD) during the afternoon (Fig. 30). This effect is so strong that the effect of a water stress (see Section 3.4.4) during the afternoon is masked, even though it results in an increase in stomatal resistance from 150 to 360 s m^{-1} (both sides of the leaf together). The water stress does, however, show up in the CO_2 -assimilation as will be seen later.

The net radiation at the soil surface, averaged from 08h00 till 17h00, equals 20% of the value above the canopy, which corresponds to an effective average extinction coefficient for total net radiation of 0.43. The soil heat flux G reaches a peak of 70 W m^{-2} at noon, which amounts to 10% of the total net radiation above the canopy or 50% of the net radiation at the soil surface at that moment.

The sensible heat flux at the soil surface is negative during the day and has almost a constant value of -16 W m^{-2} . Thus the soil surface remains colder than the air just above it, mainly because of evaporation. The evaporative heat loss from the soil surface reaches a considerable value of 90 W m^{-2} just after noon, which is 28% of the total evaporative heat loss. So under the given circumstances (high radiation, wet soil and rather dry air) soil evaporation takes almost one third of the total water consumption.

In the early morning, between 07h00 and 08h00, the transport from the soil surface through the air is almost negligible because the gradients are close to zero. In this situation the soil heat flux G equals the net radiation at the soil surface.

In the nightly period until about 06h00 the air above the canopy is in an inverse situation. Then the soil heat flux G is necessarily equal

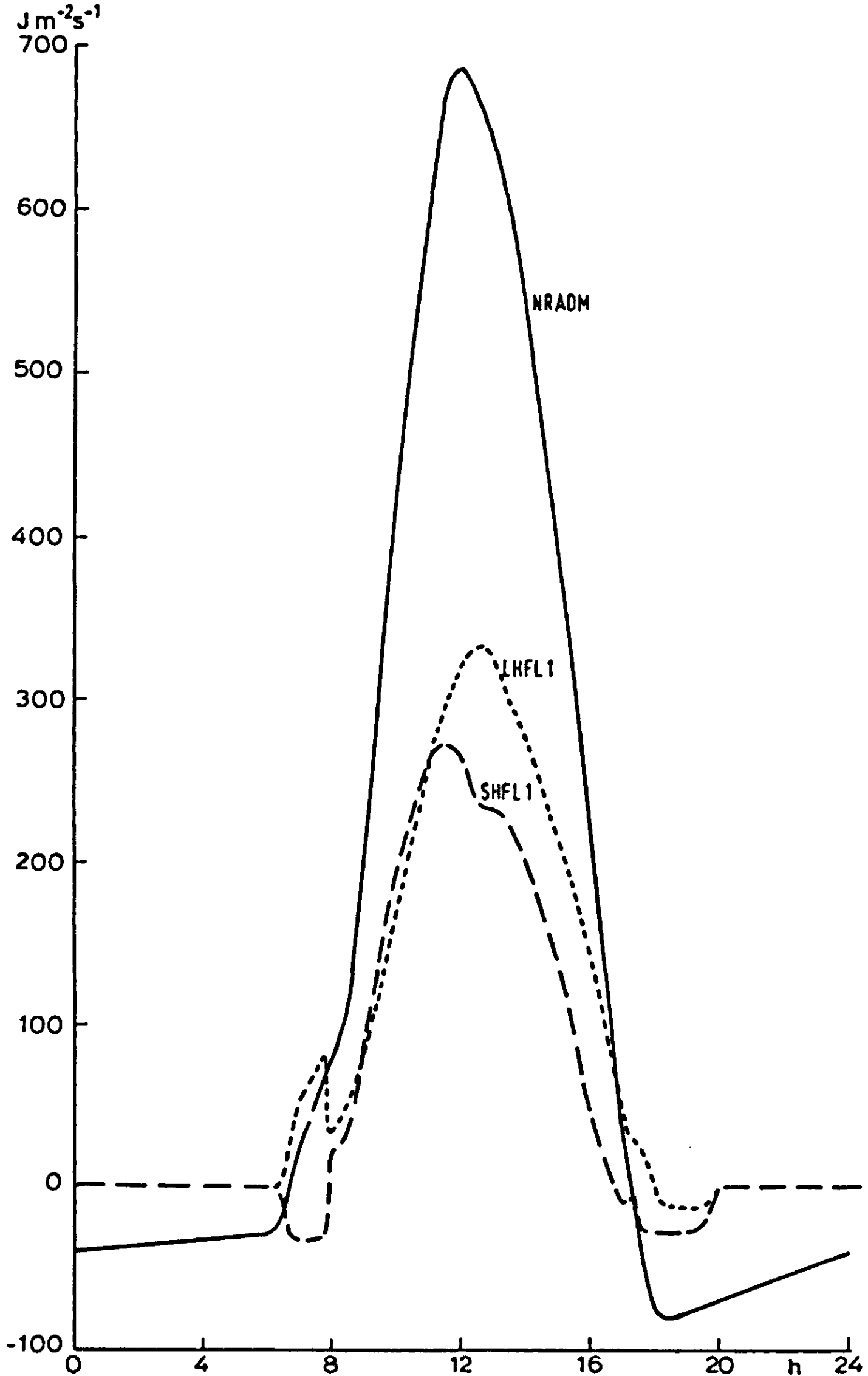


Fig. 31a | The solid line gives the daily course of the net radiation that is used as a forcing function for the case study. The broken lines LHFL1 and SHFL1 give the simulated latent heat flux and sensible heat flux into the air above the canopy.

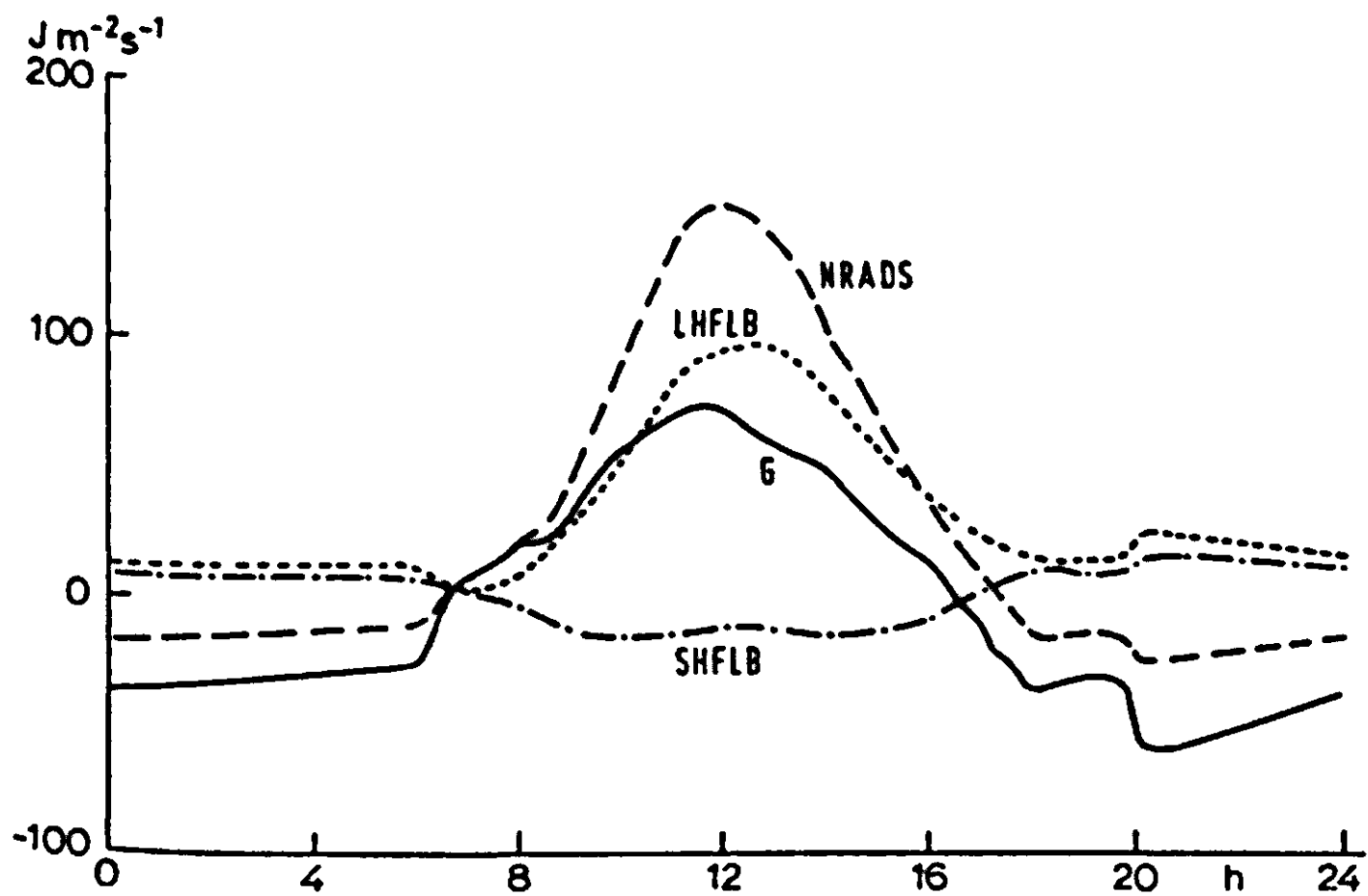


Fig. 31b | Simulated energy fluxes in the case study. NRADS is the net radiation just above the soil surface, LHFLB the latent heat loss from the soil surface to the air, SHFLB the sensible heat loss from the soil surface to the air and G the heat flux from the soil surface into the soil underneath.

to the net radiation above the canopy. Although there is no exchange above the canopy, lapse conditions inside ensure transport of heat and moisture from the soil surface to the leaves (Section 4.3.2). The upward thermal radiant flux almost entirely originates from the leaves, which in turn receive energy from condensation of water vapour to dew, from sensible heat transfer by the air and from thermal radiation exchange with the soil surface. As can be seen in Fig. 31b the radiative exchange between soil surface and leaves (NRADS) equals about 50% of the total soil heat flux, the latent heat flux about 30% and the sensible heat flux about 20%.

The water vapour, released by the soil surface, condenses again as dew on the leaves, but almost exclusively on the topmost layer. Since this layer is the one most exposed to the sky, it is cooled most by loss of radiation. Below this layer with an LAI of 1.3 the quantities of dew are negligible. During the whole night the top layer collects about 0.27 mm of water expressed per ground area. This corresponds to an average heat flux of $15 W m^{-2}$ due to condensation. The nightly net radiation was $-50 W m^{-2}$ on the average, so that 30%

of this was released by condensation of dew, previously evaporated from the soil surface.

Inversion starts at 20h00 (Fig. 31) as can be seen from a resulting drop in soil heat flux and net radiation at the soil surface, and from the blocking of exchange in the air above the canopy. Leaf temperatures change also dramatically (Fig. 32).

6.2.3 Daily courses of temperatures and humidities

The simulated average leaf temperature of the top layer is given in Fig. 32 together with the measured air temperature and the simulated soil surface temperature. The leaf temperature stays 4–6°C below air temperature during the inversion period. Upon the increase of net

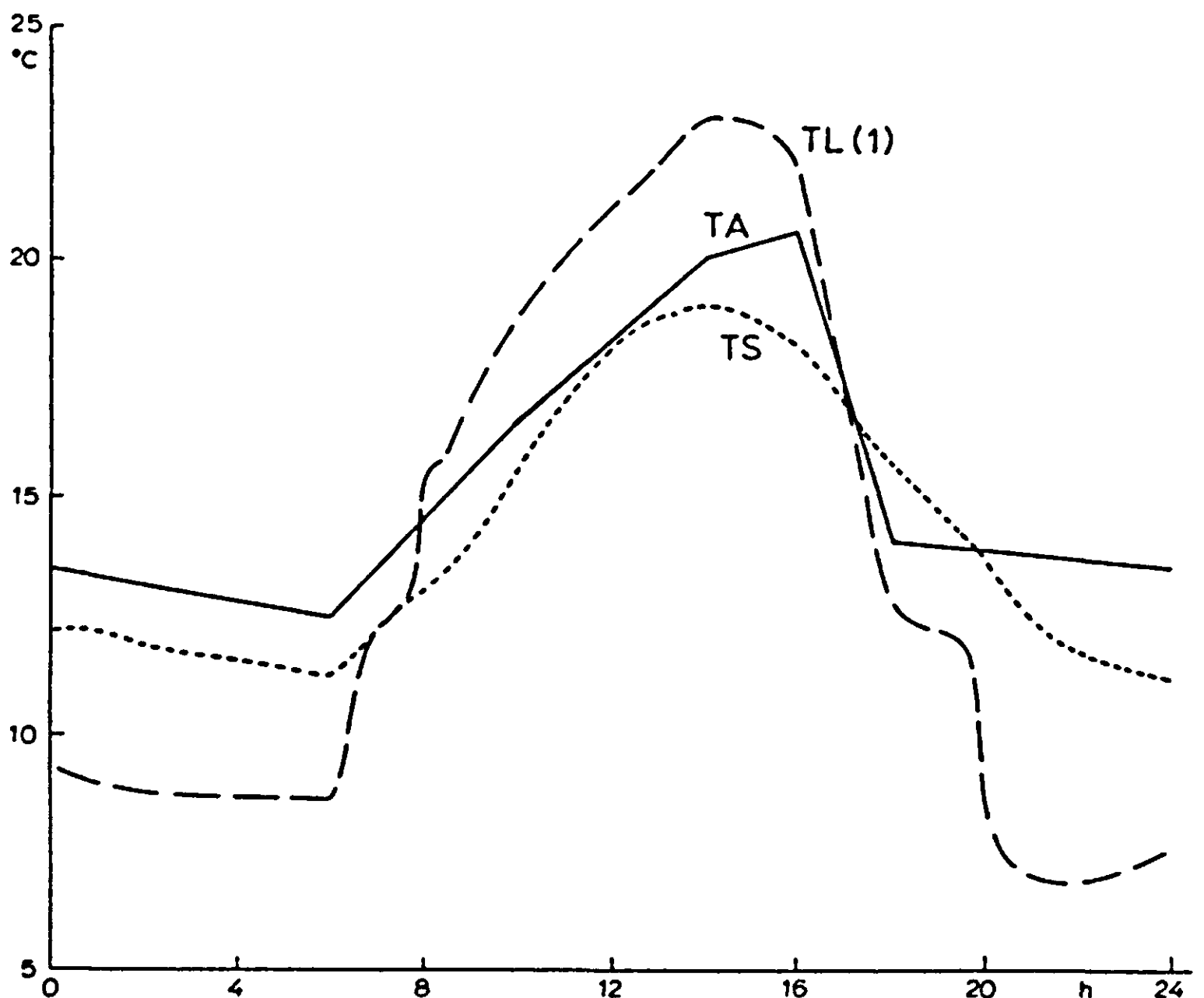


Fig. 32 | Daily courses of some temperatures in the case study. The solid line is the air temperature TA(forcing function), the broken line is the simulated average leaf temperature of the top layer of the canopy TL(1), and the dotted line is the simulated soil surface temperature TS.

radiation in the early morning, the inversion vanishes and the leaf temperature rises to about one degree below air temperature. At 08h00 a second steep increase occurs which can be traced back to the disappearance of the dew from the leaves. From 08h00 till 10h00 the leaf temperature rises gradually with respect to air temperature till a steady difference of 2.5–3°C is reached, in spite of a twofold variation in the net radiation. After 16h00 the leaf temperature drops again. It should be noticed that at 17h00 air, leaf and soil surface temperature are almost equal, so that the heat fluxes are zero and the buoyant forces disappear. At 20h00 the inversion situation starts again. The soil surface temperature has clearly a more gradual course than leaf temperatures with a maximum round 14h00.

In Fig. 33 some profiles are given of air temperature and humidity. Humidity always increases with depth, but temperature sometimes exhibits a maximum (9h00 and 15h00) or a minimum (18h00). At noon the maximum lies near the soil surface. This result conflicts with the measurements, that showed a maximum at about 1.5 m height. During an inversion both temperature and humidity have a

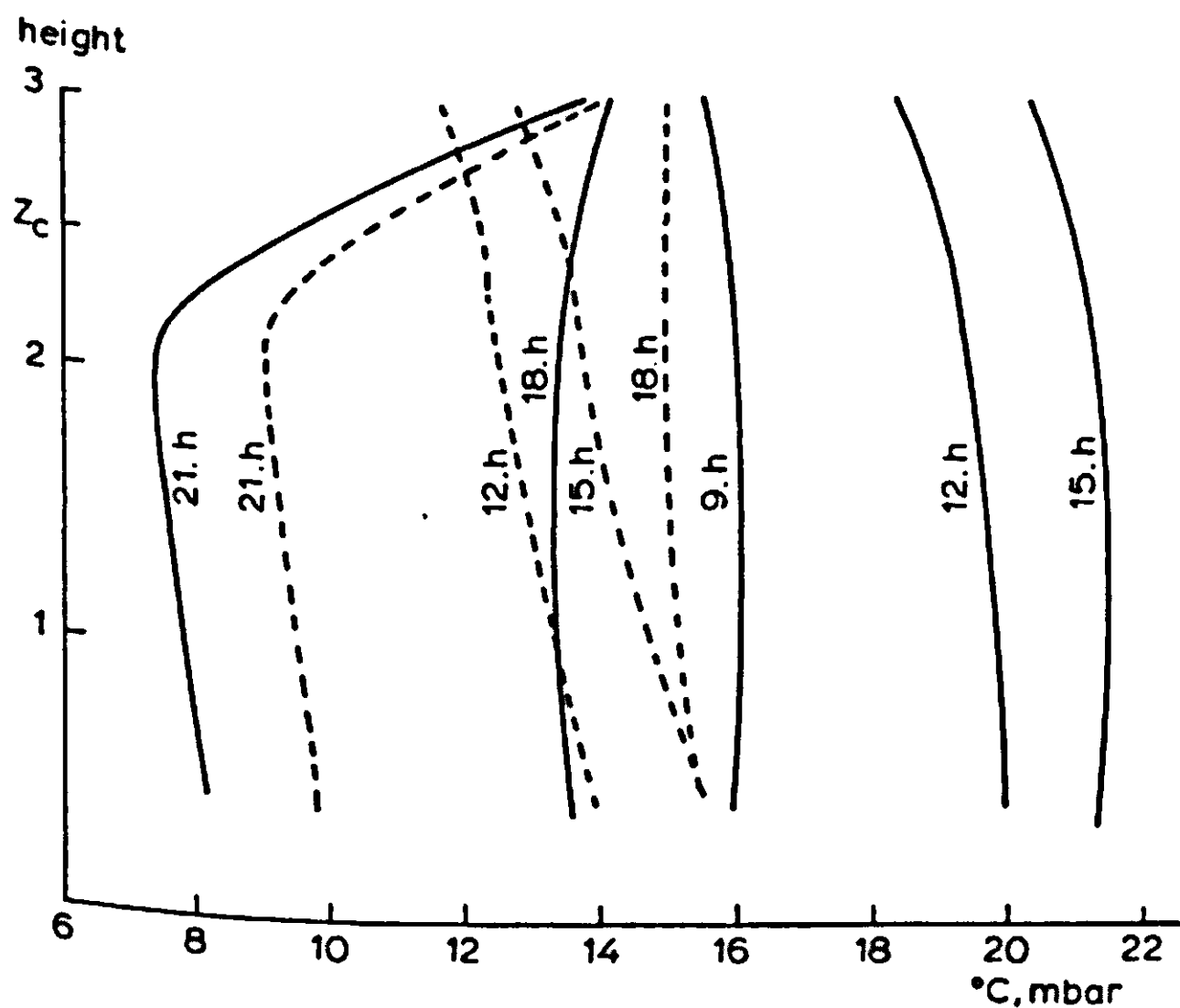


Fig. 33 | Some profiles of simulated air temperatures (solid lines) and humidity (broken lines) in the case study.

minimum at the top of the canopy (21h00). Heat and moisture are both withdrawn from the air by the cold leaves, which have a temperature below the dew point of the air.

6.2.4 *Net CO₂-assimilation*

The relation between net CO₂-assimilation of the canopy and computed solar radiation is given by Line A in Fig. 34. In the dark, the net CO₂-assimilation ranges between -5 and -8 kg CO₂ ha⁻¹ h⁻¹, expressed per ground area, because the respiration depends on leaf temperature. At low light intensities net assimilation increases fast, but the rate of increase levels off at higher light intensities. The maximum slope of this curve can be calculated by multiplying the light use efficiency of individual leaves (0.62 kg CO₂ ha⁻¹ h⁻¹ J⁻¹ m² s) by the fraction of visible radiation in the solar radiation (0.5) times a reduction factor due to reflection of visible radiation (1 minus 0.08 = 0.92). A response as indicated by Line B is obtained.

This slope is maintained below a solar radiation of 70 W m⁻², but it soon falls off because of light saturation of the individual leaves. Most of the sunlit leaves are light saturated, when the sun is higher than about 25 degrees in the sky, which is the case between about 8h00 and 16h00. In this situation the total assimilation can, nevertheless, increase with solar radiation for three reasons: first total sunlit leaf area increases as sun rises, second there is a concurrent increase in temperature so that the maximum rate of photosynthesis increases, and third the diffuse and scattered radiation available for shaded leaves increases with total solar radiation.

The first effect is evaluated by another simulation run from 9h00 till 12h00, in which everything is kept constant except solar height. The incoming solar radiation SRAD is fixed at 600 W m⁻² and only consists of direct radiation. Air temperature is 18°C and humidity 12 mbar. Under these circumstances net CO₂-assimilation increases from 44 kg ha⁻¹ h⁻¹ at 9h00 till 54 at 12h00. In Fig. 34 the values occurring simultaneously with the standard case (Line A) are indicated by Line C. The slope of Line C is only about 25% of the slope of the simulated standard curve A, so that the first effect is not very important. However, for a high LAI the increase is faster as the ground loss of visible or photosynthetically active radiation (PhAR) increases from 2.6% of the incoming visible flux at 9h00 till 18% at

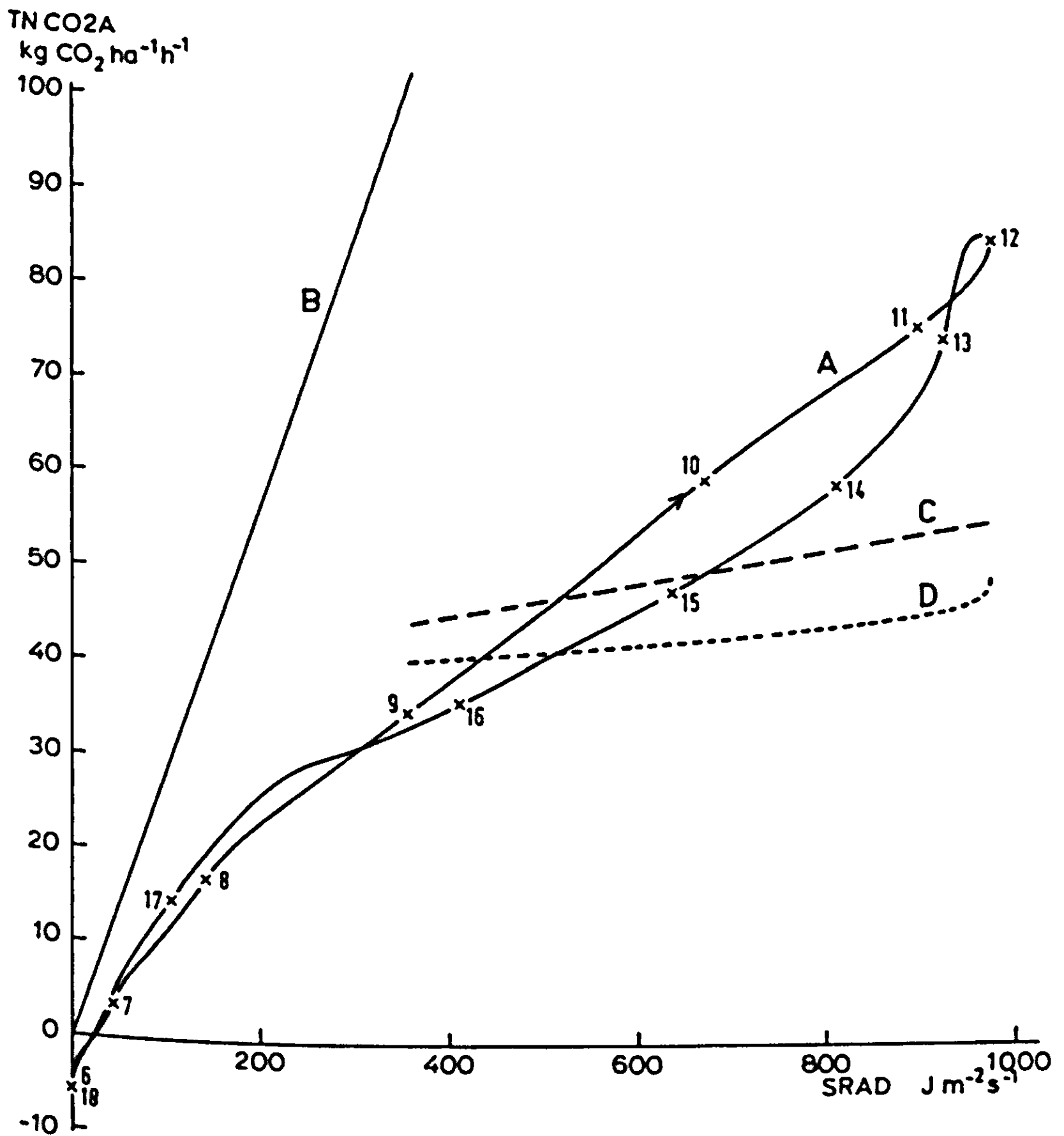


Fig. 34 | Simulated net CO₂ assimilation TNCO₂A in the case study, plotted versus the simulated incoming solar radiation SRAD (line A). The hours of the day are indicated along the curve. Line B gives the gross CO₂ assimilation, if all absorbed visible radiation is used with the maximal efficiency. Line C gives the isolated effect of solar height only and line D the isolated air temperature effect only (incoming radiation constant).

12h00 in the present situation with LAI at 3.7. The temperature effect mentioned secondly, can be evaluated in a similar way and is indicated by Line D.

From this we see that the increase of net assimilation around noon is entirely due to an increase in temperature (Fig. 30), as the photosynthetic rate of the light-saturated leaves is higher. On the average, however, the temperature effect contributes only about 15% to the total increase in assimilation during the period from 09h00 till 12h00. The remaining 60% must be attributed to the effect of the increase of the solar radiation itself, some of which is available as diffuse and scattered radiation for shaded leaves.

After 12h30 the net CO₂-assimilation drops sharply, and stays then much lower than the morning values. The reason is that a water stress has developed, which causes some closure of the stomata. Because of the limitation to CO₂ diffusion, the maximum rate of net CO₂-assimilation is reduced from about 40 to about 28 kg CO₂ ha⁻¹ h⁻¹. After 16h30 the mesophyll resistance again takes over the controlling function from the stomatal resistance, and soon radiation becomes the only limiting factor.

6.2.5 Dew

Dew formation is simulated in the same way as transpiration (Eqn (3.12)) except that the leaf resistance is made zero, either when the leaf surface is wet, or when the leaf transpiration rate is negative. An integral for each leaf layer keeps track of the amount of dew. Dew only occurs when the leaves are cooled by the loss of thermal radiation to the sky to such an extent that the leaf temperature drops below dew point.

Since the top leaves are most exposed, they are subject to the strongest cooling and the heaviest dew fall. In the case studied the top layer collects 4/5 of the total amount of dew, the middle layer 1/5 and the bottom layer no dew at all. When the air is saturated with water, the rate of condensation corresponds to a factor $s/(s + \gamma)$ of the net radiant heat loss of the leaves. At 10°C this fraction is about 0.5. Under non-inversion conditions and a LAI of about 3.5, 20% of the net radiation above the canopy is provided by the soil, but under an inversion this percentage rises to 45. The temperature difference between leaves and soil surface may then be as large as 5 degrees,

causing a thermal radiant flux of about 30 W m^{-2} . Hence, the fraction of the net radiation above the canopy that can be used for condensation of water vapour is about $0.5 \times 0.8 = 0.4$ under non-inversion conditions and about $0.5 \times 0.55 = 0.275$ under inversion conditions. Moreover, this smaller fraction during inversion refers to an absolutely smaller net radiant flux above the canopy! The leaf temperatures may be 5 degrees lower when there is an inversion, so that the difference between leaf temperature and apparent sky temperature may be reduced by about 25%. Thus the maximum rate of dewfall under an inversion is about half $\left(\frac{0.275}{0.4} \times 0.7\right)$ of the value under non-inversion conditions. Indeed Monteith (1957) observed that the heaviest dew fall does not occur on still nights (presumably with an inversion), but at moderate wind speeds of $1\text{--}3 \text{ m s}^{-1}$. With the above figures, an upper limit of the amount of dew can be easily calculated. A net radiation of -100 W m^{-2} , which only occurs under an entirely clear sky, means that -40 W m^{-2} can be used for condensation if no inversion occurs and the air is saturated with water vapour. This corresponds to a dewfall rate of 0.058 mm h^{-1} . If this rate continues for 10 hours, the total amount of dew is about 0.6 mm.

In practice, these optimal conditions will not be fulfilled all the time so that the maximum amount of dew recorded is about 0.5 mm (Slatyer & McIlroy, 1961; Burrage, 1972).

Simulation of dew is not easy because much depends on the occurrence of an inversion. When no inversion develops, temperature and humidity of the air above the canopy are very important and also wind speed. Under an inversion, the current air conditions lose their effect because the exchange above the canopy is blocked. Then dew can only come from the soil so that past weather conditions become important. When statistical techniques are used for dew prediction, these considerations should be reflected in the structure of the regression equations used.

6.3 Sensitivity analysis

6.3.1 Introduction

A sensitivity analysis is made to see how important the input variables and system properties are for the behaviour of the model. This is mainly done by applying changes that are so small that the response

of the model is still in the linear region. For discrete characteristics, such as the number of layers, this cannot be done. The same holds for structural changes in the model, although these can sometimes be considered as extremes of parametric changes. For instance, omitting stability effects from the model is a structural change, but this can be gradually achieved by decreasing the buoyancy parameters in the equations for stability corrections (Eqns (4.22) and (4.23)). Therefore a clear distinction between structural changes and parametric changes can hardly be made.

Two types of output variables can be distinguished, current values on the one hand and their values integrated over time or space on the other. The first group contains profiles of leaf and air temperatures, and fluxes. The second group contains, for instance, daily totals of net CO₂-assimilation, transpiration and duration of leaf wetness.

6.3.2 *Input weather data*

An important question for practical measurement is how frequently should the weather data be sampled (Stigter et al., 1976). This is sometimes equivalent to the question: what is the required speed of the response of the sensors? Therefore I investigated the effect of periodic variations in the input weather data on mean values of output variables, by applying a sine wave with various periods and an amplitude of 1 °C or 1 mbar for temperature and humidity, respectively, and 10% of the measured mean for wind speed and net radiation. The effect was always less than 1% for the daily total net CO₂-assimilation and less than 2% for the daily total evapotranspiration for a period of the sine wave up to 1000 seconds.

This result is essentially due to virtually all processes being linear in the region of variation of 1 °C, 1 mbar or 10% of radiation and wind speed. However, wind speed usually varies by more than 10%, and since resistances are proportional to roughly the inverse of wind speed, errors may occur when the average wind speed is used. The effect of sizeable temporal variation in wind speed is further discussed in Section 6.3.7. Apart from wind speed, hourly averages of the weather data are sufficiently accurate, so that slow sensors may also be used. The influence of a systematic change in the input weather data was investigated by shifting temperature and humidity by 1 °C or 1 mbar, respectively, in either direction, and multiplying wind speed and net

Table 24 Simulated values of some variables and daily totals at 24h00 for a series of variations in weather conditions.

variable	unit	standard	TA+1	TA-1	VPA+1	VPA-1	WIND	WIND	NRAD	NRAD
DNCO2A	kg CO ₂ ha ⁻¹	417	405	427	436	402	417	420	434	400
DLHFL	10 ⁶ J m ⁻²	6.95	7.49	6.53	6.57	7.40	7.48	6.95	7.36	6.95
DSHFL	10 ⁶ J m ⁻²	4.72	4.32	4.69	4.28	4.64	3.62	4.91	5.73	3.03
DNRAD	10 ⁶ J m ⁻²	11.7	11.7	11.7	11.7	11.7	11.7	11.7	12.9	10.6
DLHFLB	10 ⁶ J m ⁻²	2.56	2.73	2.40	2.25	2.82	2.63	2.53	2.79	2.40
DSHFLB	10 ⁶ J m ⁻²	-0.087	-0.144	-0.111	-0.206	-0.074	-0.302	-0.005	0.005	-0.279
DSOILF	10 ⁶ J m ⁻²	-0.510	-0.612	-0.103	0.255	-0.851	0.025	-0.691	-0.755	0.012
DEW(1)	10 ⁶ J m ⁻²	0.352	0.393	0.264	0.283	0.380	0.052	0.384	0.420	0.110
DEW(2)	10 ⁶ J m ⁻²	0.094	0.089	0.095	0.105	0.085	0.026	0.082	0.099	0.042
DEW(3)	10 ⁶ J m ⁻²	-	-	-	0.002	-	-	-	-	-
DEWT(1)	h	13.8	14.1	6.4	7.0	13.8	6.1	14.2	14.0	6.1
DEWT(2)	h	13.4	13.7	6.3	7.6	13.3	6.1	13.8	13.7	6.1
DEWT(3)	h	1.7	0.2	5.0	6.5	-	0.2	0.3	0.8	0.1
TL(1)	°C	7.52	7.24	11.22	12.24	6.71	11.65	6.82	6.23	11.61
TL(2)	°C	7.82	7.52	11.35	12.36	7.01	11.77	7.14	6.56	11.76
TL(3)	°C	8.42	8.11	11.77	12.59	7.66	12.20	7.82	7.22	12.16
TRZ	°C	13.54	13.25	14.42	14.98	12.88	14.61	13.13	12.98	14.61
INVERSION		YES	YES	NO	NO	YES	NO	YES	YES	NO

radiation by 1.1 or 0.9. The results for the 8 variations together with the standard situation are listed in Table 24, which gives daily totals of net CO₂-assimilation DNCO₂A, total latent heat flux DLHFL, total sensible heat flux DSHFL, daily net radiation DNRAD, daily latent heat flux from the soil surface DLHFLB, daily sensible heat flux from the soil surface DSHFLB and the daily total soil heat flux DSOILF. The total amount of dew for each of the leaf layers used is given at midnight, expressed in the heat of condensation per ground area (J m⁻²), and duration of leaf wetness in the preceding 24 hours expressed in hours (DEWT). It must be realized that the leaves may be recorded as wet in this model, even when the amount of dew is very small. The average leaf temperature TL in each of the layers and the average temperature in the rooting zone of the soil between 4.5 and 15 cm depth (TRZ) are given in °C. At midnight 24 hours earlier TRZ was initialized at 14.3°C.

The daily total net CO₂-assimilation DNCO₂A decreases with air temperature in spite of an increase in saturation level. This decrease is partly due to increased respiration, but is mainly an effect of an enhanced afternoon depression through a larger transpiration. This effect is even clearer with humidity. Wind speed has a negligible effect, and a 10% increase in net radiation produces almost 5% increase in net CO₂-assimilation.

The daily total of latent heat flux increases considerably with temperature and decreases with humidity. It increases with wind speed, but when it is corrected for dew formation hardly any effect remains. Net radiation has a strong effect on the total latent heat loss as well as on the sensible heat loss.

The rooting zone temperature TRZ shows an unexpected reaction to air temperature. When air temperature decreases by 1 degree, TRZ is almost 1 degree higher than in the standard situation! This can be explained by a qualitative difference between both situations. In the standard case an inversion developed during the night, but not for the case with lower air temperature, as is obvious from the leaf temperatures at midnight. When there is an inversion the leaf temperatures range between 6–9°C, and between 11–13°C otherwise.

In the inversion situation more heat is released by the soil than otherwise (see Fig. 31b around 20h00) so that the soil becomes colder, and TRZ and DSOILF are decreased. The exchange with the air

above is blocked so that the daily total sensible heat loss DSHFL is increased, as during the night the leaves are colder than the air above them.

As pointed out before, inversion plays a major role in dew formation. As soon as inversion does form, the effect of the humidity and temperature of the air above is negligible. Then the most important factor is net radiation. When the inversion is not formed all weather data are equally important.

The duration of leaf wetness is almost 14 hours for the top layer when there is an inversion. When no inversion develops it is less, but how long leaf wetness lasts entirely depends on the weather data.

Amount of dew and duration of leaf wetness cannot be calculated by an easy rule. The great number of complex relations must be integrated in a simulation program to evaluate their combined effect.

Table 25 gives the midday values of net CO₂-assimilation TNCO₂A, soil heat flux G, sensible heat flux SHFL1, latent heat flux LHFL1 and the differences of the temperatures and humidities in the three air layers with those at the height of reference. Unlike the daily totals, the midday values are hardly affected by nightly inversion.

The net assimilation at noon is increased by air temperature, because of the rise in saturation level. The effect is of the order of 3–4 kg CO₂ ha⁻¹ h⁻¹ °C⁻¹. This is less than to be expected from the sunlit leaf area and the saturation level alone, but there is a compensatory effect of the increased respiration. In this case the net assimilation is practically insensitive to humidity and wind speed, but net radiation is very important.

The effects of air temperature on sensible and latent heat fluxes are opposite, and of the order of 10% per degree K and 5% per mbar. Fortunately the effect of wind speed is very small. A 10% error in wind speed produces about the same error in the calculated sensible or latent heat fluxes as an error of 0.1 K in air temperature or 0.2 mbar in air humidity. Under field circumstances more accuracy is hard to achieve, but not necessary anyway because net radiation is the real problem. If again an accuracy of 1% is aimed at, it means that net radiation should be measured with an accuracy of 1%, as the latent and sensible heat fluxes are about proportional to net radiation. Thus the measurement of net radiation is usually the main source of error. Therefore there is a need for a separate measurement of solar radiation as this can be done more accurately. Moreover, this avoids the

Table 25 Simulated values of some variables at 12h00 for the same series of variations in weather conditions as in Table 24.

variable	unit	standard	TA+1	TA-1	VPA+1	VPA-1	WIND	WIND	NRAD	NRAD
TNCO2A	kg CO ₂ ha ⁻¹									
G	h ⁻¹	83.75	86.59	79.66	84.22	83.31	83.24	84.36	87.97	79.35
SHFL1	J m ⁻² s ⁻¹	70.4	72.8	65.6	69.0	67.8	64.1	73.7	77.3	60.8
LHFL1	J m ⁻² s ⁻¹	263.2	230.7	297.8	279.4	248.7	267.0	260.3	300.4	227.1
DT(1)	J m ⁻² s ⁻¹	320.2	349.2	291.8	305.4	337.5	322.9	319.8	342.7	299.6
DT(2)	K	1.094	0.962	1.233	1.159	1.035	1.017	1.189	1.244	0.948
DT(3)	K	1.518	1.317	1.735	1.625	1.423	1.410	1.654	1.732	1.310
DV(1)	K	1.701	1.435	1.992	1.854	1.571	1.580	1.862	1.961	1.455
DV(2)	mbar	0.892	0.976	0.810	0.849	0.941	0.824	0.979	0.950	0.838
DV(3)	mbar	1.514	1.639	1.393	1.445	1.597	1.404	1.659	1.616	1.423
DT(3)/DT(2)	mbar	2.263	2.423	2.110	2.164	2.389	2.115	2.462	2.408	2.135
DV(3)/DV(2)	-	1.121	1.090	1.148	1.141	1.104	1.121	1.126	1.132	1.111
DT(3)/DV(3)	-	1.495	1.478	1.515	1.498	1.496	1.506	1.484	1.490	1.500
Inversion during the night	K mbar ⁻¹	0.752	0.592	0.944	0.857	0.658	0.747	0.756	0.814	0.681
		YES	YES	NO	NO	YES	NO	YES	YES	NO

use of an empirical and unreliable equation for sky temperature.

With an increasing air temperature above the canopy, the inside air temperatures rise more slowly. A similar compensatory effect occurs for humidity. The shape of these aerial profiles is hardly changed, when wind speed or net radiation are varied.

The fraction of diffuse radiation under clear conditions is a function of sun height (Table 1). Deviations from this standard table have a marked effect on the rate of net CO₂-assimilation. In Table 26 the

Table 26 Influence of the proportion of the diffuse component in the total solar radiation.

<i>at 24h00</i>	standard	only direct	only diffuse
DNCO2A	417	298	618
DLHFL	6.95	6.62	7.59
DSHEL	4.72	5.27	3.68
DNRAD	11.7	11.7	11.7
DLHFLB	2.56	2.57	2.57
DSHFLB	-0.087	-0.115	-0.016
DSOILF	-0.510	-0.645	-0.201
DEW(1)	0.352	0.365	0.312
DEW(2)	0.094	0.093	0.048
DEW(3)	0.00	0.00	0.00
DEWT(1)	13.8	13.6	13.8
DEWT(2)	13.4	13.4	13.3
DEWT(3)	1.7	1.5	0.00
<i>at 12h00</i>			
TNCO2A	83.75	69.59	117.46
G	70.4	71.6	65.7
SHFL1	263.2	280.2	230.0
LHFL1	320.2	305.6	351.9
DT(1)	1.094	1.163	0.959
DT(2)	1.518	1.624	1.287
DT(3)	1.701	1.824	1.415
DV(1)	0.892	0.850	0.983
DV(2)	1.514	1.448	1.672
DV(3)	2.263	2.187	2.461

simulated results of two situations are compared, either all radiation is direct or all radiation is diffuse. The profiles of air temperature and humidity, and also of dew, are hardly affected. The effect on the net CO₂-assimilation is very large, so much so that about 1.5% transfer of the total global radiation from direct to diffuse brings about a one percent change in net CO₂-assimilation. Because of the coupling between photosynthesis and transpiration the latent heat flux is also affected, but to a lesser extent. These results indicate that separate measurements of diffuse and direct radiation are almost as important as measuring the total solar radiation.

6.3.3 Compartmentalization in canopy and soil

The soil is divided into 10 layers, increasing in thickness downwards by a factor 1.2. The top layer is 2 cm thick. A previous simulation study (Goudriaan & Waggoner, 1972) showed that the soil heat flux is hardly affected when the thickness of the compartments is reduced by a factor 10. It may therefore well be that the thickness of the compartments can be further increased without an appreciable effect. Here no such attempt is made, as the soil part consumes only a tiny fraction of the simulation program and does not limit the time interval of integration.

The main body of the simulation program concerns the processes in the air and foliage and consumes most of the computing time. Therefore the number of layers in the canopy must be as few as possible, dependent on the purpose of the simulation. In the equations for extinction of radiation, an integrated form with depth in the canopy is used so that the number of layers has no effect on factors like sunlit leaf area and radiation distribution. Compartmentalization of the foliage is only necessary to account for profiles of temperature, humidity and wind speed, and for profiles of dew. It also affects exchange at the soil surface.

The effect of neglecting the profiles can be studied by using unnaturally large exchange coefficients, but maintaining the normal boundary layer resistances on the leaves. The result of such a simulation is given in Table 27. The net CO₂-assimilation is lower than that in the standard case because the temperature in the canopy does not increase with depth. The increase of DLHFL, the decrease of DSHFL and the increase of DSOILF are partly attributed to the absence of inversion.

Table 27 Influence of the number of layers in the air inside the canopy.

variable	Number of layers				
	0	1	3 (standard)	9	
<i>at 24h00</i>					
DNCO2A	kg CO ₂ ha ⁻¹	393	468	417	411
DLHFL	10 ⁶ J m ⁻²	7.91	7.08	6.95	6.86
DSHFL	10 ⁶ J m ⁻²	3.32	4.73	4.72	4.66
DLHFLB	10 ⁶ J m ⁻²	2.98	2.41	2.56	2.40
DSHFLB	10 ⁶ J m ⁻²	-0.385	0.002	-0.087	-0.036
DSOILF	10 ⁶ J m ⁻²	-0.083	-0.694	-0.510	-0.358
DEW					
(all layers)	10 ⁶ J m ⁻²	-	0.396	0.446	0.449
TRZ	°C	14.54	13.14	13.54	13.85
<i>12h00</i>					
TNCO2A	kg CO ₂ ha ⁻¹ h ⁻¹	76.52	91.01	83.75	83.17
G	J m ⁻² s ⁻¹	50.2	70.2	70.4	70.6
SHFL1	J m ⁻² s ⁻¹	294.9	258.5	263.2	258.1
LHFL1	J m ⁻² s ⁻¹	309.5	322.5	320.2	325.4
SHFLB	J m ⁻² s ⁻¹	-9.0	-10.6	-14.6	-14.6
LHFLB	J m ⁻² s ⁻¹	104.0	86.9	92.4	92.8

This also accounts for the vapour pressure deficit not becoming small enough to form dew.

The fluxes at 12h00 are also considerably changed by a lower air temperature inside the canopy: CO₂-assimilation, soil heat flux and transpiration decrease and the sensible heat loss increases.

The resistance between the centre of the foliage and the height of reference can be introduced by using just one layer, and allowing for the profile in the air above the canopy. Now inversion can develop and the amount of dew is indeed almost the same as that for three layers (standard). Gradients inside the canopy are, however, omitted. Still the agreement between the one-layer and three-layer programs is remarkable. Only CO₂-assimilation is overestimated because the

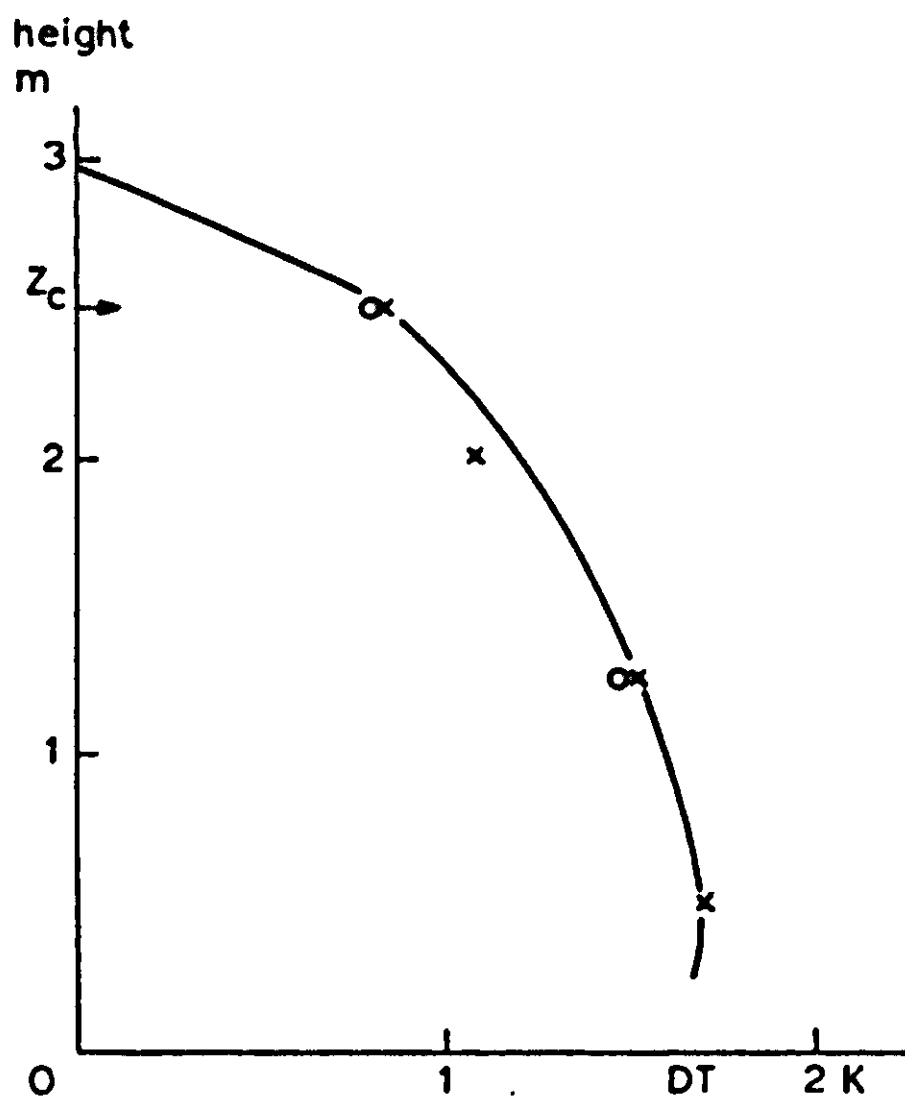


Fig. 35 | Simulated air temperature profiles at 12h00 in the standard case for a one layer (open circle), three layer (crosses) and nine layer (solid line) program.

temperature of the important top layer of leaves is too high.

One may expect that the three-layer program is accurate enough. This expectation is confirmed by comparison with the results of the nine-layer program. In Fig. 35 the simulated temperature profiles are given for all three programs: one, three and nine layers. These comparisons show that it is not worthwhile to use more than three layers inside the vegetation.

6.3.4 Height of reference

If the simulation program is correct, changing the height of measurement will have no effect because the measured data change accordingly.

However, for the purpose of the case study the weather data measured at a height of 2.5 m are transferred to a height of 3 m without changing them. The results of this manipulation are given in Table 28 for some other heights as well.

The results at 12h00 show that both temperature and humidity in the

Table 28 Influence of the height of reference z_r .

variable	z_r				
	2.5	2.75	3.	3.25	5.
<i>at 24h00</i>					
DNCO2A	394	410	417	424	447
DLHFL	7.88	7.65	6.95	6.96	6.90
DSHFL	3.44	3.50	4.72	4.88	4.61
DLHFLB	3.19	2.77	2.56	2.49	1.99
DSHFLB	-0.531	-0.350	-0.088	-0.027	-0.088
DSOILF	-0.145	-0.006	-0.508	-0.669	-0.349
DEW(1)	-	-	0.353	0.387	0.353
DEW(2)	-	-	0.094	0.075	0.027
DEW(3)	-	-	-	-	-
DEWT(1)	-	3.2	13.7	14.5	14.9
DEWT(2)	-	3.5	13.4	13.9	13.8
DEWT(3)	-	-	1.9	0.2	0.1
TL(1)	12.98	12.70	7.52	6.61	5.65
TL(2)	12.93	12.67	7.82	6.96	6.16
TL(3)	12.98	12.80	8.44	7.70	7.23
TRZ	14.43	14.60	13.54	13.15	13.65
<i>at 12h00</i>					
TNCO2A	78.17	81.26	83.75	85.55	89.37
G	49.9	59.9	70.4	75.8	92.7
SHFL1	288.5	275.6	263.2	254.9	233.2
LHFL1	316.6	318.8	320.2	322.9	328.2
DT(1)	0.18	0.67	1.09	1.44	2.75
DT(2)	0.47	1.05	1.52	1.90	3.30
DT(3)	0.59	1.22	1.70	2.10	3.54
DV(1)	0.13	0.52	0.89	1.22	2.59
DV(2)	0.55	1.06	1.51	1.91	3.48
DV(3)	1.09	1.74	2.26	2.71	4.45

canopy increase when the height of measurement z_r is increased. This increase is partly due to the distance between the canopy and the height of measurement being larger so that the resistance is larger, and partly to an overall decrease in wind speed, as the same wind speed is

supposed to be measured at a higher level. Both effects are of the same magnitude. The increase in temperature causes an appreciable increase in CO_2 assimilation and soil heat flux. The evapotranspiration hardly increases, but the sensible heat loss is reduced and the soil heat flux is increased at the same time.

From the values of the leaf temperatures T_L at midnight, it is clear that for the heights 2.5 m and 2.75 m no inversion is formed, as is also reflected in the absence of dew. Earlier in the evening some dew was formed, as can be noticed from DEWT, but it evaporated later. For the other heights, where inversion does occur, the total amount of dew is practically constant. The transition to inversion situations means a decrease in rooting zone temperature TRZ and in daily total soil heat flux DSOILF, because more heat is released from the soil during the night. The total soil evaporation decreases considerably with height of reference because of a lower wind speed and lower vapour pressure deficit underneath the canopy. Crop transpiration increases slightly, but total evapotranspiration is still a decreasing function of z_r .

6.3.5 *Plant properties*

In Table 29 the results are given for a variation of the scattering coefficients for visible (SCV) and near-infrared radiation (SCN). The increase of SCV from 0.20 to 0.25 improves the distribution of radiation so that more is available for the shaded leaves. This effect explains the increase of the net CO_2 -assimilation. Also the transpiration increases a little because of the relation between stomatal opening and net CO_2 -assimilation.

Since the formation of the inversion is hardly affected, the amount of dew and of duration of leaf wetness are not influenced either and are consequently omitted from the table.

A decrease in scattering coefficient for near-infrared radiation SCN from 0.85 to 0.80 slightly decreases the net CO_2 -assimilation. This is an indirect effect, mediated by a lower reflection. Therefore a lower solar radiation is computed to arrive at the measured net radiation. This example shows how important it is to choose adequate input variables.

The decrease in total latent heat flux LHFL1 comprises a decrease in soil evaporation (because less radiation is transmitted) and a small

Table 29 Influence of some plant properties. The change with respect to the standard run is indicated by the arrow.

variable	standard	SCV 0.20 → 0.25	SCN 0.85 → 0.80	RESCW 2000 → ∞	RCO2I 90 → 120	F spherical → planophile	F spherical → erectophile
DNCO2A	417	435	410	437	396	420	410
DLHFL	6.95	7.02	6.88	6.39	7.15	6.94	7.17
DLHFLB	2.56	2.57	2.48	2.60	2.54	2.49	2.46
<i>12h00</i>							
TNCO2A	83.75	86.64	82.97	84.40	83.27	80.96	84.60
G	70.4	71.5	66.5	70.6	70.0	52.6	72.0
SHFL1	263.2	267.9	270.2	286.3	246.1	308.6	247.9
LHFL1	320.2	323.6	317.2	297.0	337.7	314.2	320.0
DT(3)/DT(2)	1.121	1.126	1.104	1.144	1.121	1.039	1.137
DT(3)/DV(3)	0.752	0.731	0.770	0.752	0.679	0.844	0.710

increase in crop transpiration. The effect on evapotranspiration is equal for both scattering coefficients, but, of course, CO₂-assimilation is more sensitive in the visible region.

Next the effects of the cuticular conductance for water vapour and internal regulatory CO₂-concentration are investigated. Increasing them has qualitatively the same effect, transpiration increases and net CO₂-assimilation decreases because of a prolonged period of water stress. However, whereas cuticular transpiration only affects water status, the regulatory CO₂-concentration also influences the sensitivity for a given water stress. Therefore the regulatory CO₂-concentration has a larger effect on net CO₂-assimilation, as can be seen from the size of the changes that result in a one percent change in daily net CO₂-assimilation and evapotranspiration. In the standard situation the internal regulatory CO₂-concentration is set at 90 vpm. This value is rather low as has been shown in another report (Goudriaan & van Laar, in press). The cuticular conductance is estimated at $0.5 \cdot 10^{-3} \text{ m s}^{-1}$ (resistance 2000 s m^{-1}). A one percent variation in evapotranspiration is brought about by a 10 vpm change in RCO₂I and $0.06 \cdot 10^{-3} \text{ m s}^{-1}$ in cuticular conductance. The corresponding range of the cuticular resistance RESCW is from 1780 till 2270 s m^{-1} . Hence it is difficult to determine accurately enough cuticular resistance and regulatory CO₂-concentration.

A widely discussed crop property is the leaf angle distribution. However, the sensitivity to this property does not justify the attention it has received. In accordance with results of de Wit (1965), I found that the daily totals are hardly affected, even for the extreme planophile and erectophile situations. A closer inspection of the relation between the net CO₂-assimilation and solar radiation (Fig. 36) for some leaf angle distributions shows that at low and high radiation levels (solar angles) the effect of the leaf angle distribution is opposite. At a low radiation level the planophile leaf angle distribution is advantageous because the light distribution over the leaves is more uniform. With increasing solar angle the light distribution of a vertical (and spherical) leaf angle distribution becomes more uniform. The total effect is never larger than 10% except during the late afternoon. Because of the water stress that is still present then, the maximum CO₂-assimilation of the leaves is still reduced so that the light distribution over the leaves is more important.

In the situation at midnight it is remarkable that no inversion is form-

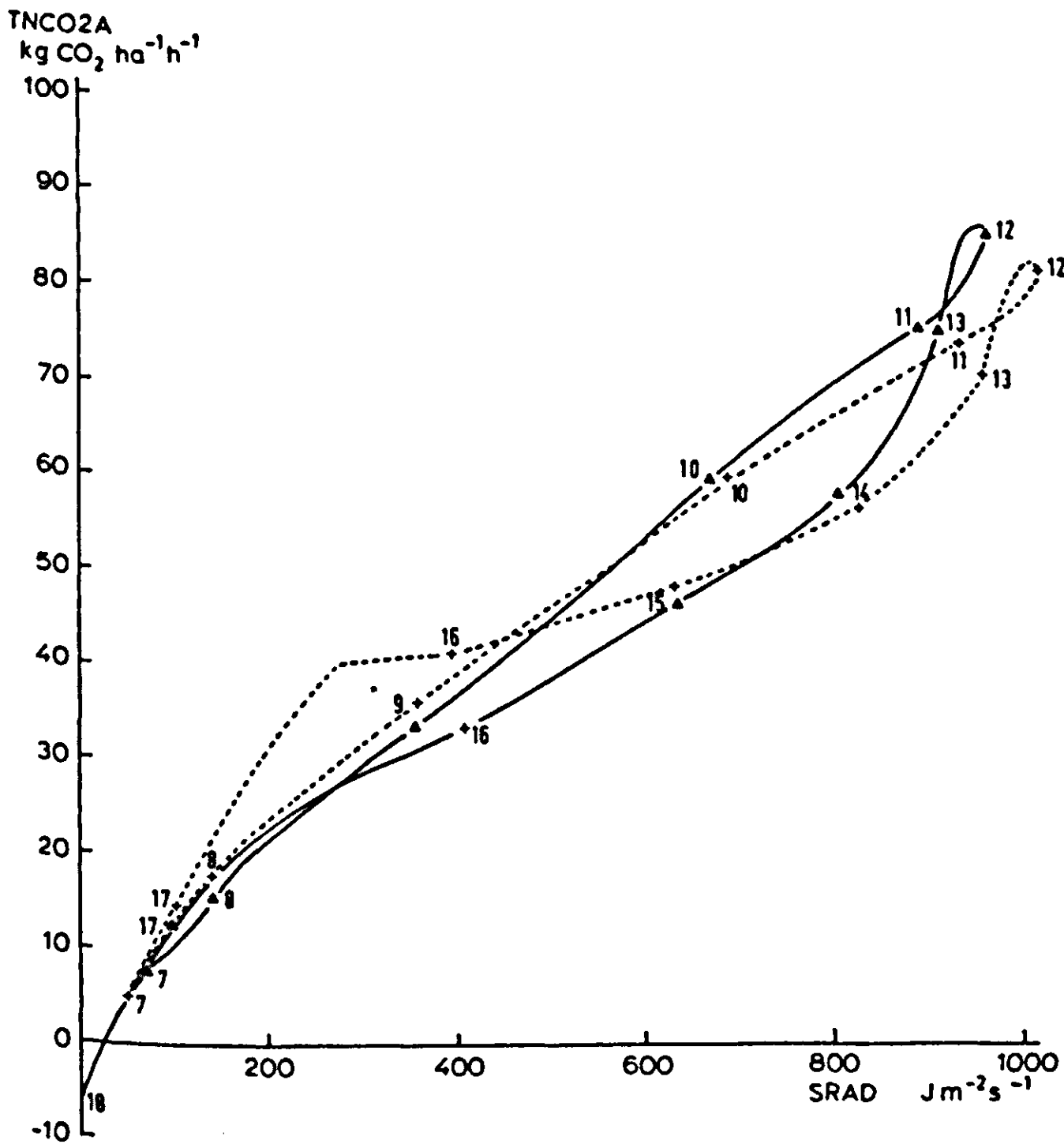


Fig. 36 | Simulated net CO₂-assimilation TNCO₂A in the case study, plotted versus the simulated incoming solar radiation SRAD. For the solid line the leaf angle distribution is vertical, and for the broken line horizontal (see also Fig. 34, spherical leaf angle distribution).

ed above the canopy with vertical leaf angle distribution. The slightly better transmission (lower extinction coefficient) of thermal radiation from the soil surface to the higher leaves is capable of preventing the inversion. This also explains the much lower dew formation in this case, and hence the increased daily total evapotranspiration.

The photosynthesis curve is determined by three parameters, the maximum rate of net CO₂-assimilation AMAX, the slope at low light intensity or efficiency EFF and the dark respiration DPL. The influences of each of these three are given in Table 30. A change in AMAX is reflected for about 30% and of EFF for about 60% in the

Table 30 Influence of some plant properties.

variable	AMAX	EFF	DPL	SRW	RWCP	no water-stress
	*1.1	*1.1	*1.1	*1.1	*1.1	
DNCO2A	431	443	403	410	428	468
DLHFL	7.01	7.03	6.94	6.89	7.03	7.29
DLHFLB	2.56	2.55	2.56	2.57	2.56	2.53
<i>at 12h00</i>						
TNCO2A	88.43	87.25	83.28	83.75	83.75	83.75
LHFL1	328.0	324.4	319.7	320.3	320.3	320.3
$\frac{DT(3)}{DT(2)}$	1.123	1.117	1.122	1.121	1.121	1.121

daily total of net CO₂-assimilation. According the one percent criterion, AMAX should be known within 3% and EFF within 1.6% accuracy, so that again some problems are encountered. Although the dark respiration has a much lower absolute value than AMAX, it exerts the same influence on daily total net CO₂-assimilation. When it is changed by 3%, DNCO2A alters by 1%. Whereas both AMAX and EFF increase the daily total evapotranspiration by 1% when they are 10% higher, DPL has hardly any influence on it.

The reason is that the influence of DPL gradually decreases as the saturation level is approached, so that during the periods of highest transpiration its effect is the smallest.

The influence of the leaf area index is small in the situation studied: the LAI is practically optimal for daily net CO₂-assimilation. As much as 10% increase in LAI is needed to increase the daily net CO₂-assimilation DNCO2A by only 1%. With a LAI of more than 5 the daily total is adversely affected by higher LAI because of increased respiration. This effect is probably less pronounced when the respiration is modelled according to the approach developed by Penning de Vries (1973).

Increasing the leaf area index decreases soil evaporation faster than it

increases plant transpiration, so that a 10% increase in LAI reduces evapotranspiration by 1%. Of course, when the soil surface is dry, an increase in LAI will increase crop evapotranspiration, again with a relative sensitivity of about 0.1 (1% per 10%). If only crop transpiration is considered, there is a remarkable constancy in the ratio of daily net CO₂-assimilation and daily crop transpiration when the LAI is changed and when the scattering coefficients are changed. The ratio remains at a value corresponding to 43 kg transpired water per kg assimilated CO₂. When the more realistic value of 120 vpm for the regulatory CO₂-concentration is used, this ratio rises to 47. Nevertheless, this is extremely low compared with measured transpiration coefficients. However, soil evaporation should still be taken into account as well as a growth respiration of about 25%. Moreover, about one third of the assimilation products goes below ground for production and maintenance of roots. When the remaining part is expressed as carbohydrates (CH₂O) instead of as CO₂, the transpiration coefficient becomes 200 kg water per 1 kg dry matter (CH₂O) above ground. This is a reasonable value (de Wit, 1958).

The sensitivity to the aerodynamic crop properties such as drag coefficient, zero plane displacement and roughness length of the vegetation is small. The drag coefficient may vary by 50% before the daily fluxes are influenced by 1% and zero plane displacement and roughness length by 20%. This 20% variation is a rather narrow range compared with the large experimental errors that occur in their determination.

6.3.6 *Soil properties*

The volumetric heat capacity of the soil VHCAP and the soil conductivity for heat LAMBDA influence the soil heat flux G and the total amount of heat stored in the soil. Hence the temperature and vapour pressure profiles in the air are also affected. In Table 31 the results are given for a run where both VHCAP and LAMBDA are increased by about 10 percent. The soil heat flux G at 12h00 is increased by 7 percent. In Fig. 31b G reaches a maximum at 12h00. The phase of the daily cycle of the soil heat flux is hardly influenced by the thermal properties of the soil, so that the moment of the maximum value of G is rather conservative. The influence of the soil properties on the profiles in the air is quite small. At 12h00 the air temperature in the

Table 31 Influence of some soil properties.

variable	standard	LAMBDA	WSTSL	TI (all layers)
<i>24h00</i>		1.3 → 1.5 $2.0 \times 10^6 \rightarrow 2.2 \times 10^6$	-0.1 → -5	4 K lower
DNCO2A	417	418	347	406
DLHFL	6.95	6.90	6.44	6.46
DSHFL	4.72	4.56	5.30	4.65
DSHFLB	-0.088	-0.134	-0.108	-0.231
DLHFLB	2.56	2.48	2.60	2.21
DSOILF	-0.508	-0.313	-0.499	0.124
DEW(1)	0.353	0.325	0.352	0.384
DEW(2)	0.094	0.094	0.094	0.090
DEW(3)	-	-	-	-
DEWT(1)	13.7	13.7	13.7	14.3
DEWT(2)	13.4	13.3	13.4	14.1
DEWT(3)	1.9	-	1.9	1.4
TL(1)	7.52	8.45	7.54	5.52
TL(2)	7.82	8.75	7.83	5.81
TL(3)	8.44	9.34	8.48	6.48
TRZ	13.54	14.04	13.57	11.59
TS	11.15	12.05	11.18	9.19
<i>12h00</i>				
TNCO2A	83.75	83.69	64.79	83.44
G	70.4	75.0	71.5	92.6
SHFL1	263.2	261.5	302.9	254.8
LHFL1	320.2	317.3	284.4	306.3
SHFLB	-14.57	-15.80	-16.3	-20.3
LHFLB	92.38	89.72	94.9	79.8
DT(1)	1.094	1.087	1.254	1.060
DT(2)	1.518	1.503	1.736	1.448
DT(3)	1.701	1.673	1.935	1.569
DV(1)	0.892	0.884	0.789	0.854
DV(2)	1.514	1.498	1.373	1.436
DV(3)	2.263	2.231	2.110	2.112

lowest air layer is decreased by 0.03°C and the vapour pressure by 0.03 mbar. Therefore the influence of the thermal properties of the soil is small during daytime, presumably because the exchange in the air is relatively large. This conclusion is confirmed by the fact that the influence is much larger during the night. Although the amounts of dew are almost the same, the leaf temperatures are increased by 0.9 degrees. This increase is entirely determined by a simultaneous increase in soil surface temperature TS of 0.9 degrees, so that the difference in temperature between leaves and soil surface is not changed. Thus even for a closed crop surface the thermal properties of the soil may be decisive for the occurrence of night frost.

In the next run the influence is investigated of the water stress of the soil $WSTSL$, which is changed from -0.1 to -5 bar. This change results in a serious stomatal closure and consequently a depression of the net CO_2 -assimilation and plant transpiration. For nighttime conditions the effect is negligible.

The size of the daytime effect, however, very much depends on the plant's reaction to water stress.

Since the initial soil temperatures are an uncertain factor and depend on past weather conditions, I examined the effect on the results of an overall decrease in initial soil temperature of 4 K.

After 24 hours the temperatures of the leaves and the upper soil layers are still about 2 K lower than in the standard case, so that the initial perturbation is halved. The daily totals of CO_2 assimilation and latent and sensible heat fluxes are slightly decreased. At noon, the soil heat flux G is increased by 22.2 W m^{-2} at the expense of the soil evaporation $LHFLB$ (12.6 W m^{-2} less), of the sensible heat loss $SHFLB$ (5.6 W m^{-2} less) and by an increase in net radiation at the soil surface from 148.2 to 152.1 (3.9 W m^{-2} more). The latter increase is accomplished by a change in thermal radiation, because the soil surface temperature at noon decreased from 18.17°C standard to 17.33°C . It must be noted that this decrease is much less than the one during the night, because of a much larger exchange with the air during the day. For the same reason the simulated profiles of temperature and humidity in the air are also little affected, and their shapes remain essentially the same. The influence of the initial soil temperature on factors other than soil heat flux is small.

6.3.7 *Turbulent exchange*

As shown in Table 27 all fluxes, except the soil heat flux G , are only slightly influenced by assuming a very high turbulent exchange in the canopy. Probably in general turbulent exchange is not important for fluxes, but is important for the profiles of temperature and humidity. Table 32 gives the results for when the values of the exchange coefficients are changed. In the first column the exchange coefficients are halved over the whole depth ($KF = 0.5$). This about doubles the gradients inside, and increases the soil heat flux G because of the higher air temperature. The quantities of dew, and the duration of leaf wetness are hardly affected.

So far the exchange coefficient decreased exponentially with depth. However this decrease was derived under the assumption of a homogeneous distribution for leaf area density (Section 4.3.1). Therefore it is worthwhile to investigate the effect of variations in the profile of turbulent exchange. First the exchange coefficient in the lowest air layer is increased by a factor two ($KF(1-3) = 1., 1., 2.$). This corresponds qualitatively to a sparser leaf area density in the lowest part of the canopy. Except for the air temperature and humidity in this layer (Table 32) there is hardly any effect.

In a following run the exchange in the middle layer was halved ($KF(1-3) = 1., 0.5, 2.$), so that the lower half of the canopy and the soil become more isolated from the air above. This leads to increased temperatures and humidities in the bottom layer during the daytime, and consequently a higher soil temperature. This in turn delays the formation of inversion in the evening, so that at midnight both soil and leaves are about 1 K warmer. Also the duration of wetness has been shorter and the total amount of dew less.

For standard simulation the turbulent exchange coefficient inside the canopy is also influenced by a modified Richardson's number (Section 4.3.2), containing wind speed and temperature gradients. Since this is a theoretically rather weak spot, I looked at how sensitive the results are when this correction is omitted. The change is negligible, only affecting the last decimal of some of the variables given. Therefore incorporation of corrections for stability and buoyancy inside the canopy seems only relevant at low wind speeds, when large temperature gradients may be expected. In agreement with the discussion in Section 4.5 a spatial variation of the exchange coefficient up

Table 32 Influence of the turbulent exchange in the air inside the canopy.

variable	standard	KF(1-3) = 0.5,0.5,0.5	KF(1-3) = 1.,1.,2.	KF(1-3) = 1.,0.5,2.
<i>24h00</i>				
DNCO2A	417	429	415	423
DLHFL	6.95	6.83	7.01	7.09
DSHFL	4.72	4.78	4.69	4.14
DLHFLB	2.56	2.40	2.64	2.54
DSOILF	-0.510	-0.459	-0.547	-0.088
DEW(1)	0.352	0.360	0.355	0.283
DEW(2)	0.094	0.095	0.096	0.114
DEW(3)	-	-	-	-
DEWT(1)	13.8	13.9	13.8	8.0
DEWT(2)	13.4	13.7	13.4	8.8
DEWT(3)	1.7	2.3	2.1	0.7
TL(1)	7.52	7.17	7.56	8.61
TL(2)	7.82	7.61	7.86	9.04
TL(3)	8.42	8.44	8.35	9.45
TRZ	13.54	13.55	13.48	14.33
<i>12h00</i>				
TNCO2A	83.75	85.31	83.68	84.24
G	70.4	79.8	68.4	69.2
SHFL1	263.2	258.0	262.5	262.0
LHFL1	320.2	316.0	322.8	322.5
DT(1)	1.09	1.32	1.09	1.09
DT(2)	1.52	2.13	1.51	1.91
DT(3)	1.70	2.46	1.60	2.00
DV(1)	0.89	1.08	0.90	0.90
DV(2)	1.51	2.28	1.53	2.15
DV(3)	2.26	3.67	1.91	2.53

to 50% has a negligible effect. Temporal variations (gustiness) are much more important as is shown in Table 33. Here the situation at noon is compared for fluctuating wind and steady wind (in brackets), both averaged over the period mentioned above each column. For all frequencies evapotranspiration and soil heat flux increase so that the

Table 33 A sine wave with an amplitude of 0.8 of the mean was superimposed on the mean wind speed. In top of each column is the period over which the average value is given. In brackets are the values for a steady wind (standard).

<i>at 12h00</i>	cycle period 10 s 0–300 seconds after noon	cycle period 100 s 1700–1800 s after noon	cycle period 1000 s 600–3600 s after noon
G	81.9 (70.4)	66.8 (63.1)	63.9 (63.0)
SHFL1	253.9 (263.2)	233.1 (238.6)	232.8 (243.3)
LHFL1	326.4 (320.2)	338.9 (333.7)	336.1 (325.3)
DT(2)	1.46 (1.52)	1.58 (1.48)	1.73 (1.50)
DT(3)	1.61 (1.70)	1.64 (1.65)	1.90 (1.67)
DV(2)	1.54 (1.51)	1.82 (1.69)	2.05 (1.66)
DV(3)	2.26 (2.26)	2.63 (2.50)	2.99 (2.47)

sensible heat loss decreases. For the long cycle the average gradient increases. For the 100 s period the difference DT(3)–DT(2) is decreased from 0.17 to 0.07°C, whereas the sensible heat flux only changed slightly. Therefore the apparent exchange coefficient for heat increases by a factor 2.5. This effect may be one of the reasons for a maximum of the exchange coefficient often being observed in the middle of the canopy.

In Table 34 the effect of fluctuating wind is given for the nightly situation. From 0h00 to 0h30 the program was run with a cycle period

Table 34 A sine wave, with amplitudes ranging from 0 to 0.5 of the mean, and a cycle period of 100 s, was superimposed on the mean wind speed. The situation is given half an hour after midnight when the simulation was started.

time = 1800 s	Amplitude/mean			
	0	0.1	0.2	0.5
DT(1)	-2.17	-2.11	-1.59	-1.41
DV(1)	0.06	0.15	0.25	0.22
ABTURR	163.	147.	69.	55.
DEW(1) J m ⁻²	2677.	1645.	–	–

of 100 seconds and a range of amplitudes of the sine wave, superimposed on the wind speed. For the steady wind speed the inversion is well under way after half an hour. When the fluctuation is only 20%, inversion is practically prevented. Also dew formation is absent. These examples show that fluctuation of wind speed is one of the important micrometeorological phenomena. Wind speed is not sufficiently characterized by its average value, but the frequency structure of the fluctuations must be known. This is an unfortunate conclusion, both from a measurement and a simulation point of view. For simulation the problem of the stiff equations becomes more complicated (Section 5.5). Hence wind speed has to be recorded in much more detail than is usually done, although it may be that the frequency distributions are rather conservative. Anyway they should be included in an improved version of this simulation program.

6.4 Experimental evaluation¹

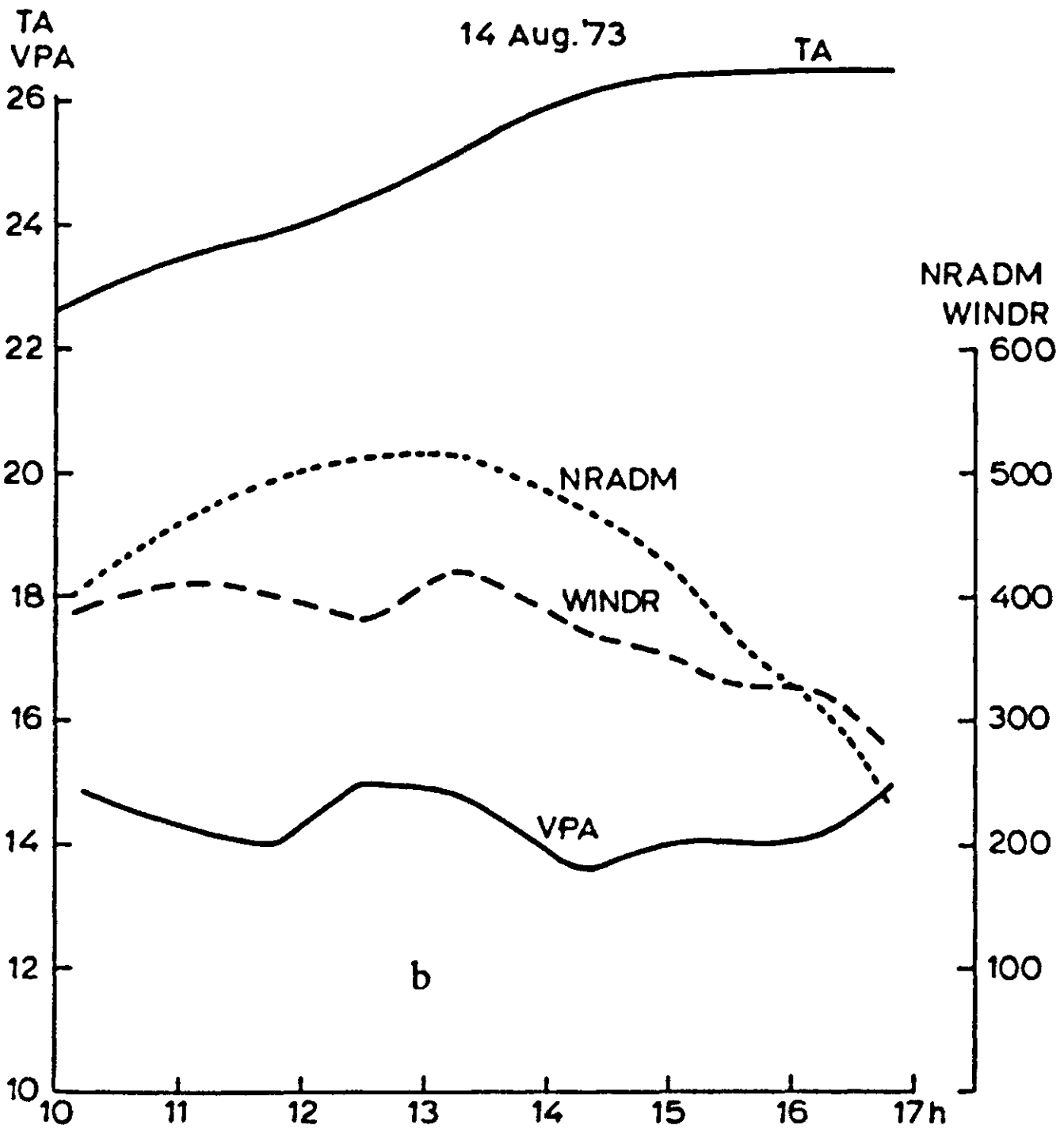
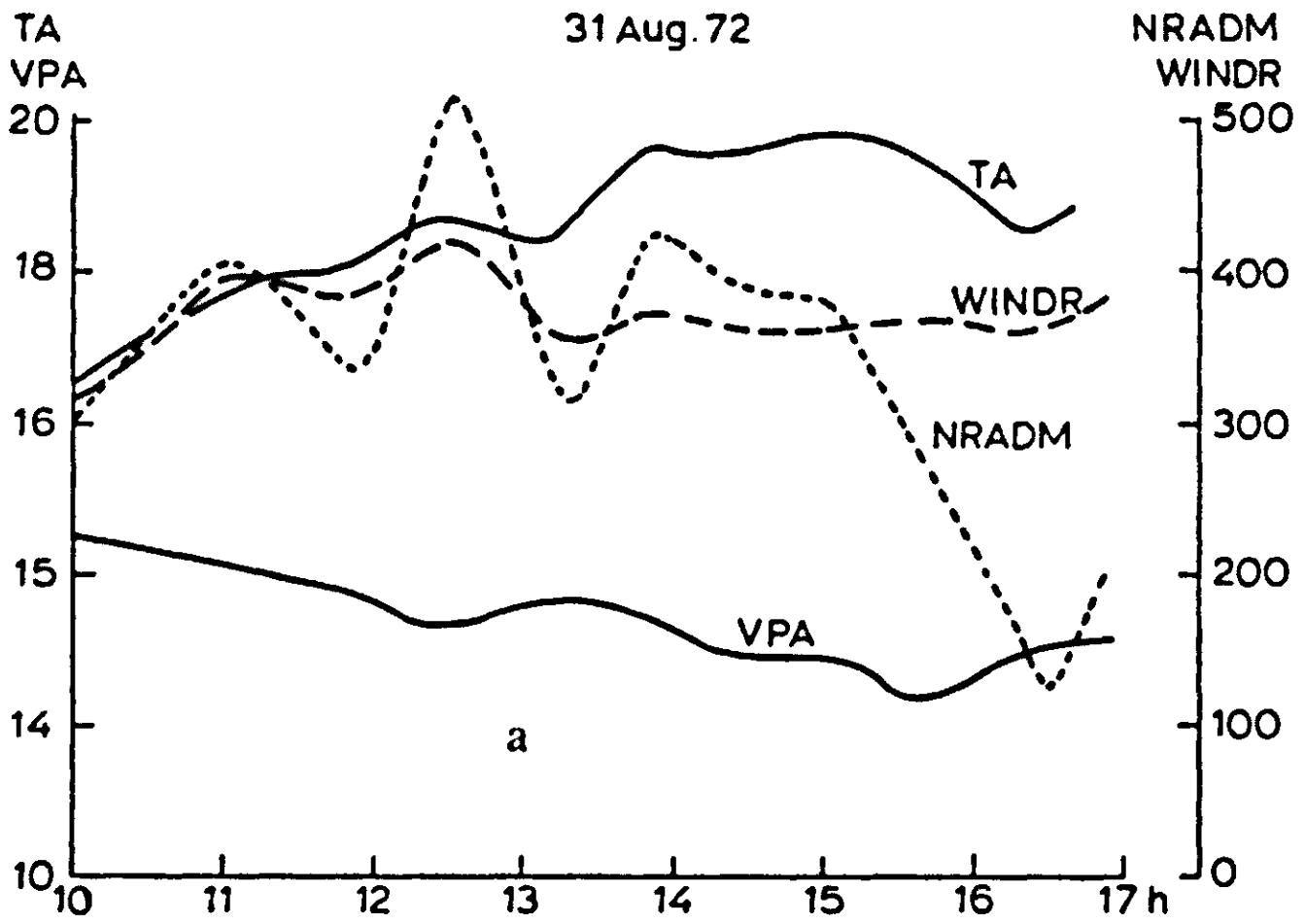
6.4.1 Introduction

In an evaluation not only the end results (final outputs) of the model should be compared with measured data, but also intermediate results of submodels. This comparison facilitates error spotting in the model because it enables one to see at least in which submodels the errors are located.

The model as described in Chapters 2, 3, 4 and 5 was developed independently of the results given in this section. The sensitivity analysis was deliberately done for another case to avoid subjective adaptation of the model to the experimental results. Only after completion of the model building and the sensitivity analysis were the simulation runs made for the experimental data sets, referred to in this section.

In this way attuning of the parameters to the specific experimental conditions and a consequent loss of generality of the model, is avoided.

¹ The experimental work was done by the following members of the Department for Physics and Meteorology of the Agricultural University of Wageningen: Dr C. J. Stigter, Dr F. A. Bottemanne, Ir J. Birnie, Ir J. G. Lengkeek, Ir T. Reitsma and by L. Sibma of the Institute for Biological and Chemical Research on Field Crops and Herbage in Wageningen.



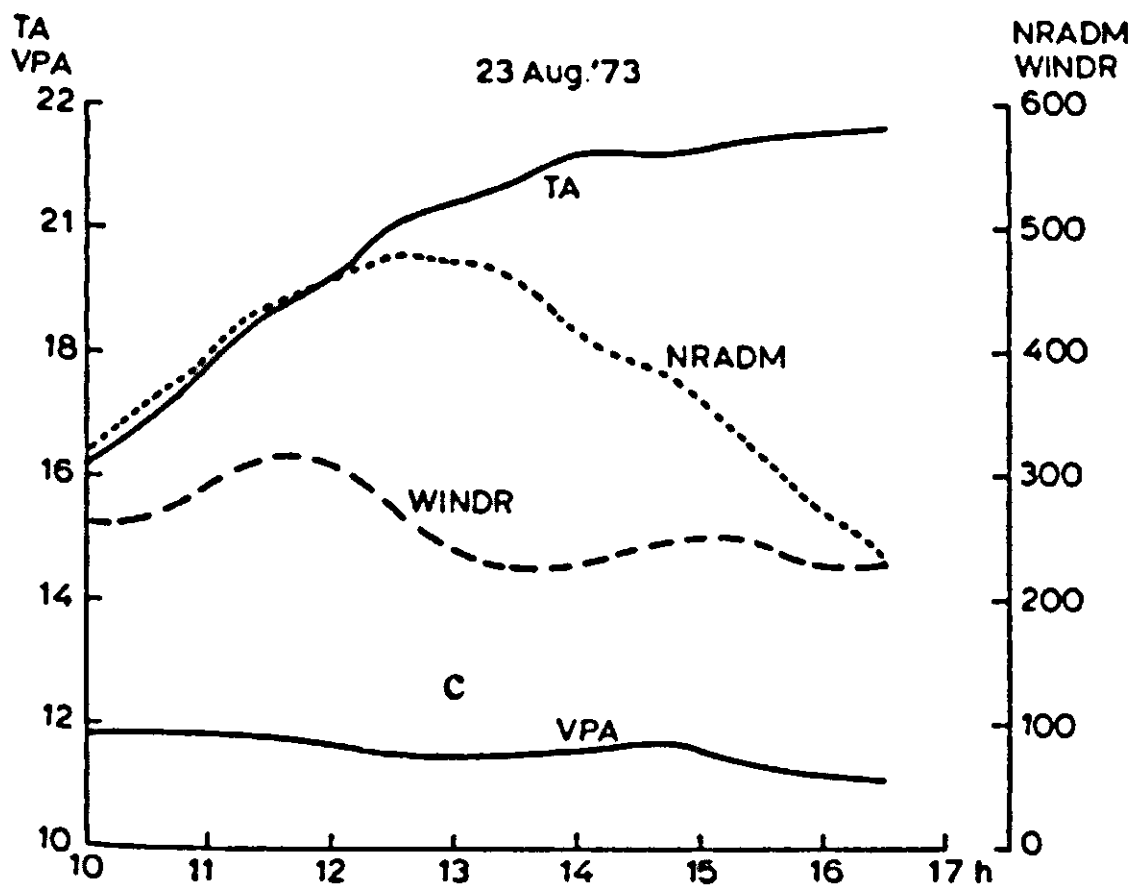


Fig. 37 | Measured course of the meteorological input data at 3 m height above the soil on 31 August 1972 (a), 14 August 1973 (b) and 23 August 1973 (c).

- TA (——) air temperature left ordinate in °C
- VPA (——) air humidity left ordinate in mbar
- WINDR (-----) wind speed right ordinate in $cm s^{-1}$
- NRADM (-----) net radiation right ordinate in $J m^{-2} s^{-1}$

The only changes that were made in the model used in the case study and sensitivity analysis of Sections 6.2 and 6.3, are correction of some programming errors, as discussed in Section 5.6. It was felt that this should be done and that it would follow up too rigid an approach to evaluate a model with errors that had been detected and not changed. The experimental set up has been described by Stigter et al. (1977), but is briefly repeated here.

6.4.2 Experimental conditions

The measurements were done on several days in 1972 and 1973. Three days were chosen for the evaluation because of their relatively undisturbed radiation, 31 August 1972, 14 August 1973 and 23 August 1973. The measured meteorological characteristics of these days are given in Figs 37a, b and c. All days were rather windy. The net radia-

tion fluctuated a little on 31 August 1972, but the two days in 1973 were perfectly clear. Especially on 14 August 1973 the air was hot and dry, with a vapour pressure deficit rising to 20 mbar towards the end of the afternoon.

A detailed description of the experimental sites and the data logging and scanning equipment has been given by Stigter et al. (1977) and by Stigter et al. (in prep.). The planting pattern was almost uniform with a row distance of 40 cm and 3 maize plants per metre in a row. Within the canopy the air temperatures and humidities were measured at 30 cm height intervals and with three to seven repetitions at each level. The scanning rate was chosen such that only minor errors were expected in the determination of the means. The sensors for temperature were small platinum resistance thermometers of a type comparable with those described by Long (1968) and with a radiation shield for those above the soil. The soil heat flux was sampled with heat flux plates. The air humidity was measured with thermocouple psychrometers, and the omnidirectional air movement inside and just above the canopy with heated-sphere thermocouple anemometers. Both types of instruments were protected against asymmetrical irradiation on the junctions. The wind profiles above the canopy were measured with cup anemometers up to a height of nearly 6 m, so that the values of the friction velocity, the roughness length and the zero plane displacement could also be determined (Bottemanne & Reitsma, 1973). Temperature was also measured so that Richardson's number could be determined as well. The measuring sites were far enough from the edges to ensure sufficient fetch for the profiles of wind, temperature and humidity, at least for the wind direction on the days of measurement. The masts could only be approached from the side opposite to this wind direction, for a minimum disturbance of the aerial conditions. One of the intermediate variables and a result of one of the submodels (Section 3.2) is the leaf resistance. This was sampled with a leaf diffusion resistance meter (porometer), constructed by Stigter et al. (1973, 1974, 1975). Results are given by Stigter & Lammers (1974), and used here for comparison with simulated values.

The net radiation above the canopy was measured with a Funk net radiometer. The net radiation inside the canopy, at a height of about 1 m, was recorded with four movable net-radiometers. The radiometers and the equipment to move each of them over a path of 1 m were specially constructed for this purpose.

The leaf area index and its distribution with height were measured by periodical stratified sampling of 25-cm layers. The leaf areas were determined by a automatic area meter (model AAM-5) of the Daiichi Boeki Shokai Company, Tokyo.

6.4.3 Comparison of measured and simulated output values

a. Extinction of net radiation

The net radiation, measured and simulated at a height of 1 m is given as a fraction of that above the canopy in Figs. 38a and b for two days, 31 August 1972 and 14 August 1973. Both, measured and simulated fractions are given as a function of time. The simulated fraction exhibits a slight maximum around noon and declines as the sun gets lower. The measured fraction shows peaks and dips which can be ascribed to some crop inhomogeneities, but on the whole the simulated fraction gives a satisfactory representation of the measured fractions. In 1973 the transmitted fraction is slightly underestimated. Here the measured leaf area index was as high as 5, compared with 3.5 in 1972.

b. Wind profiles

Simulated and measured wind profiles are given in Figs. 39a, b and c for 31 August 1972, 14 August 1973 and 23 August 1973. The agreement is satisfactory in view of the crude assumptions.

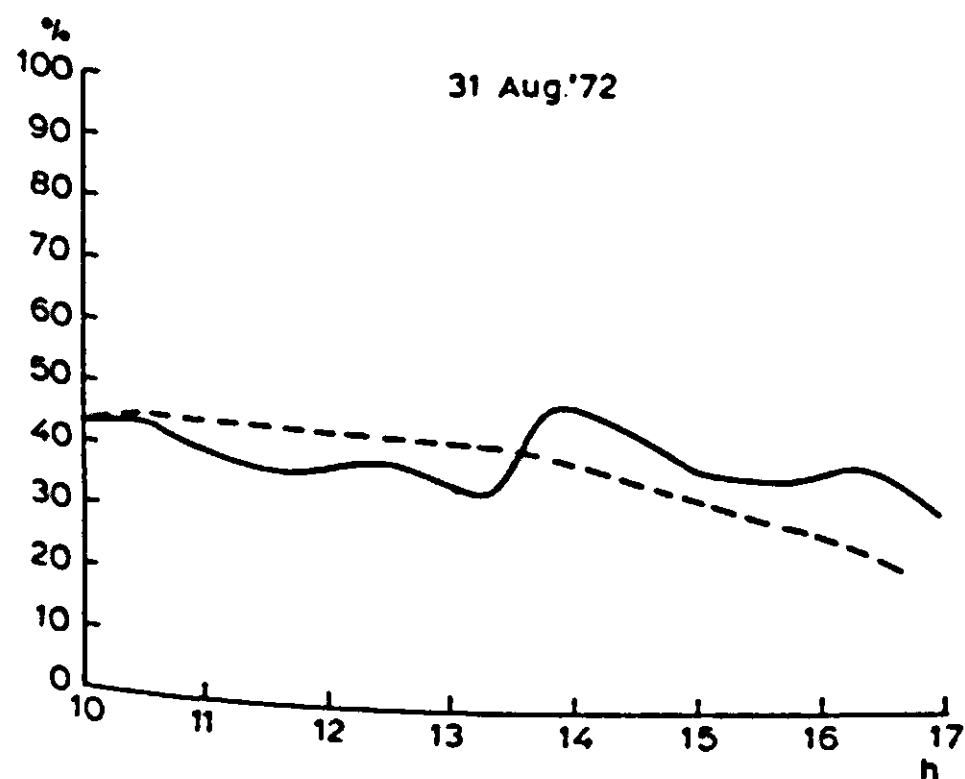


Fig. 38a

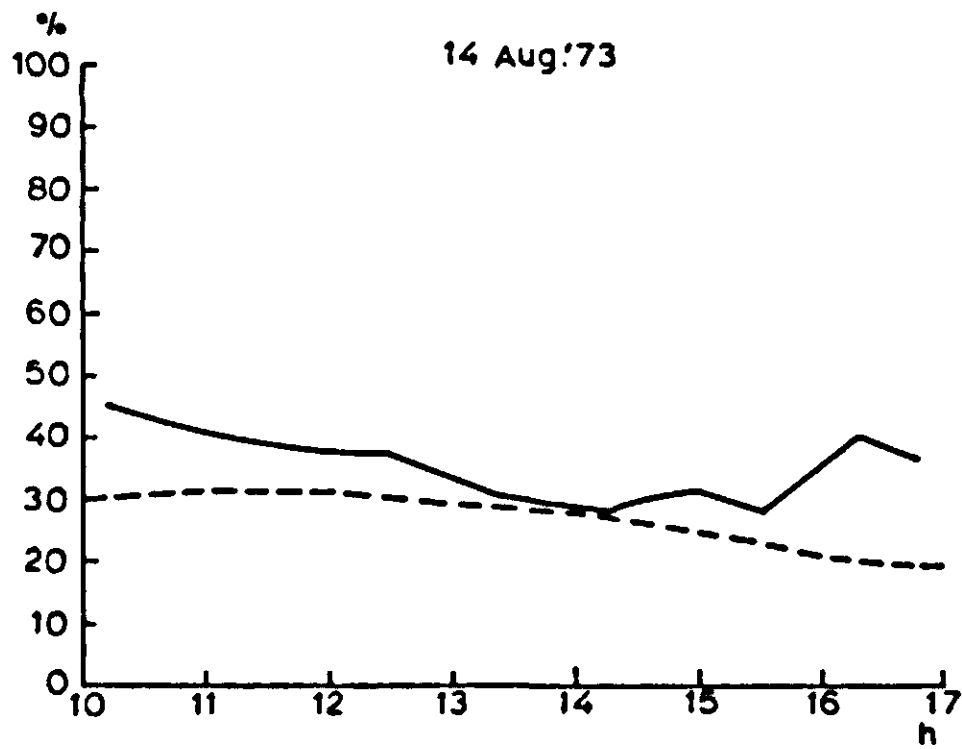


Fig. 38b

Fig. 38 | Measured and simulated percentage transmission of net radiation at a height of 0.95 m on 31 Aug. 1972 (a) and 14 August 1973(b).

—— measured, - - - - - simulated

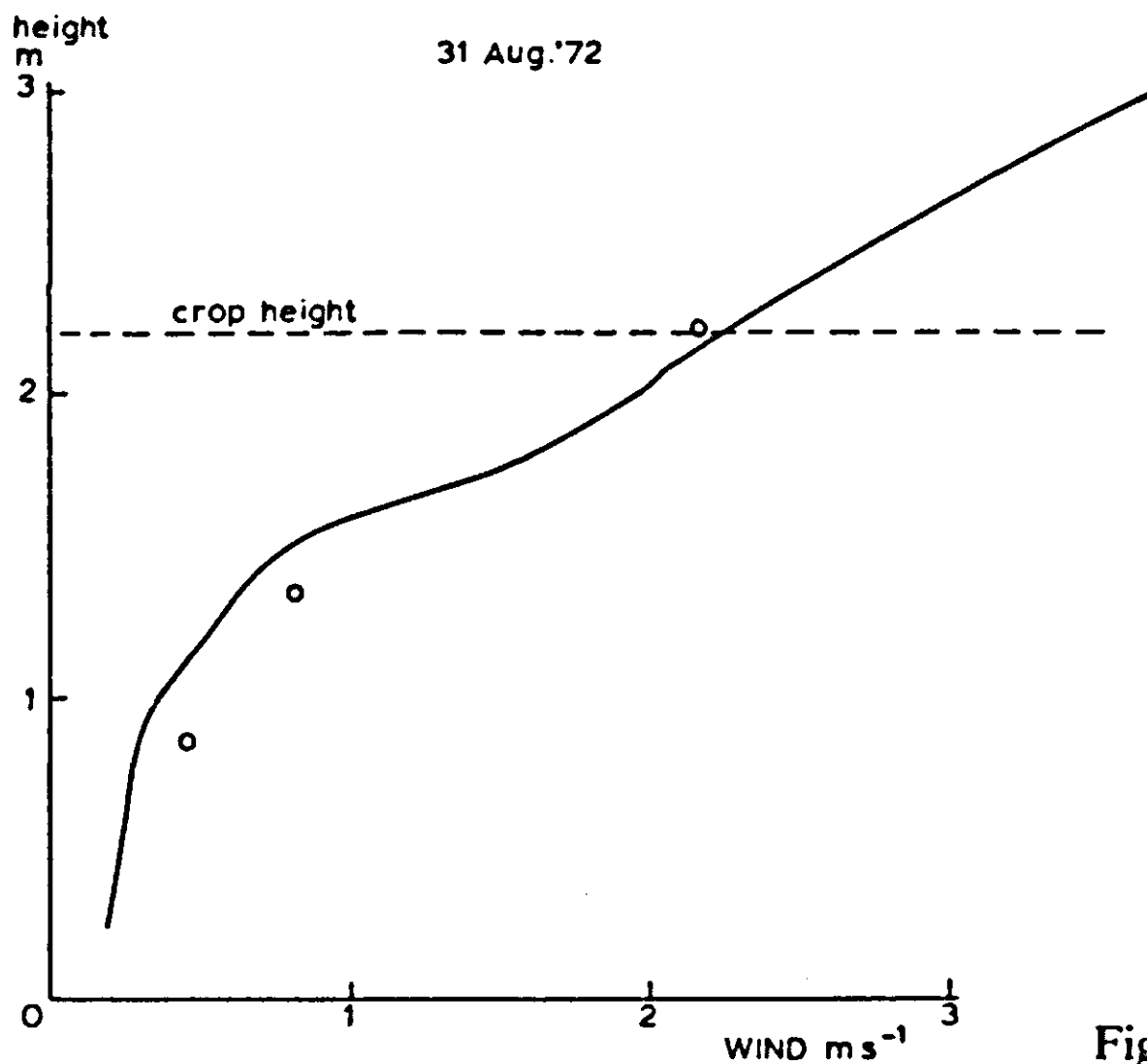


Fig. 39a

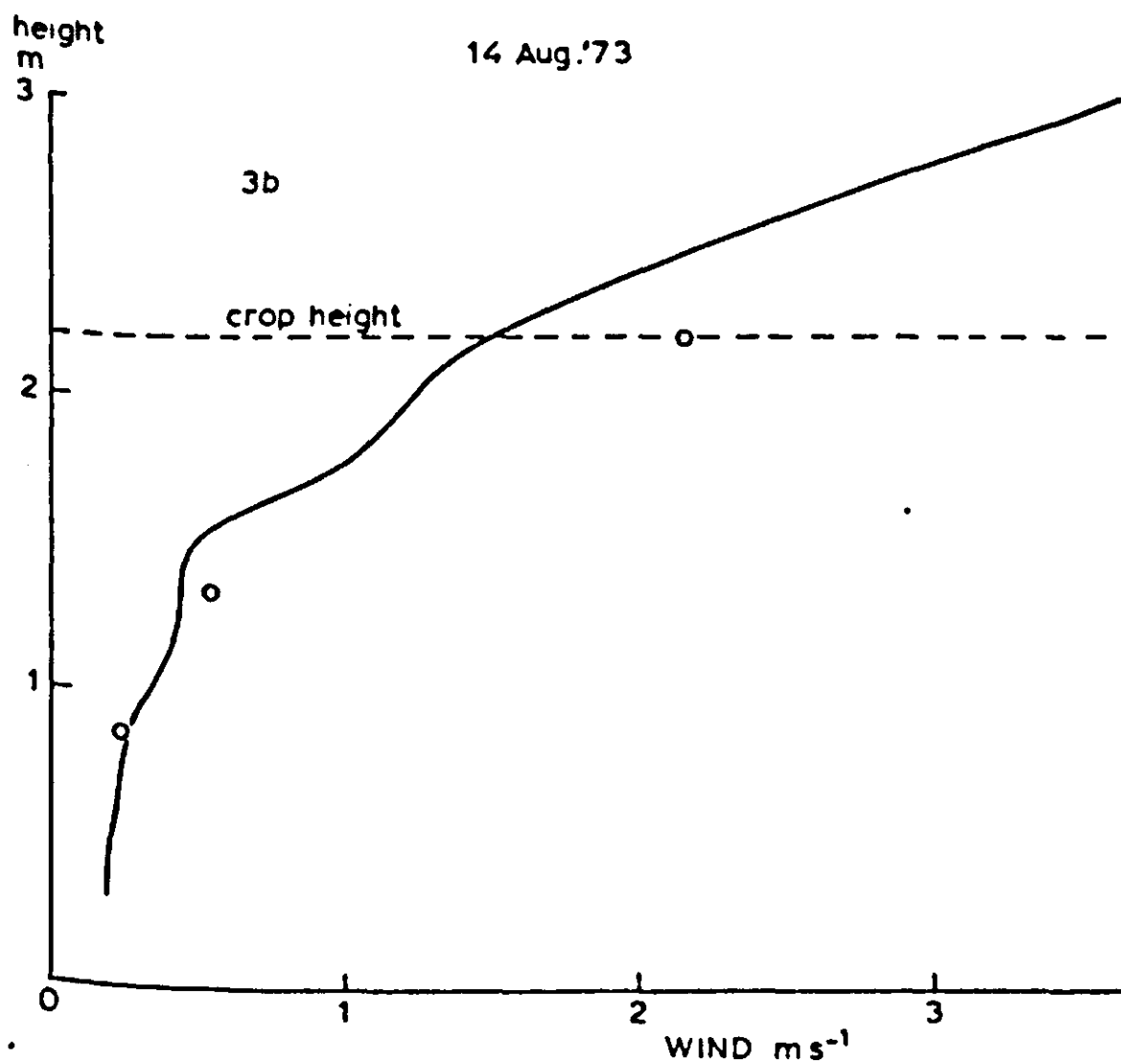


Fig. 39b

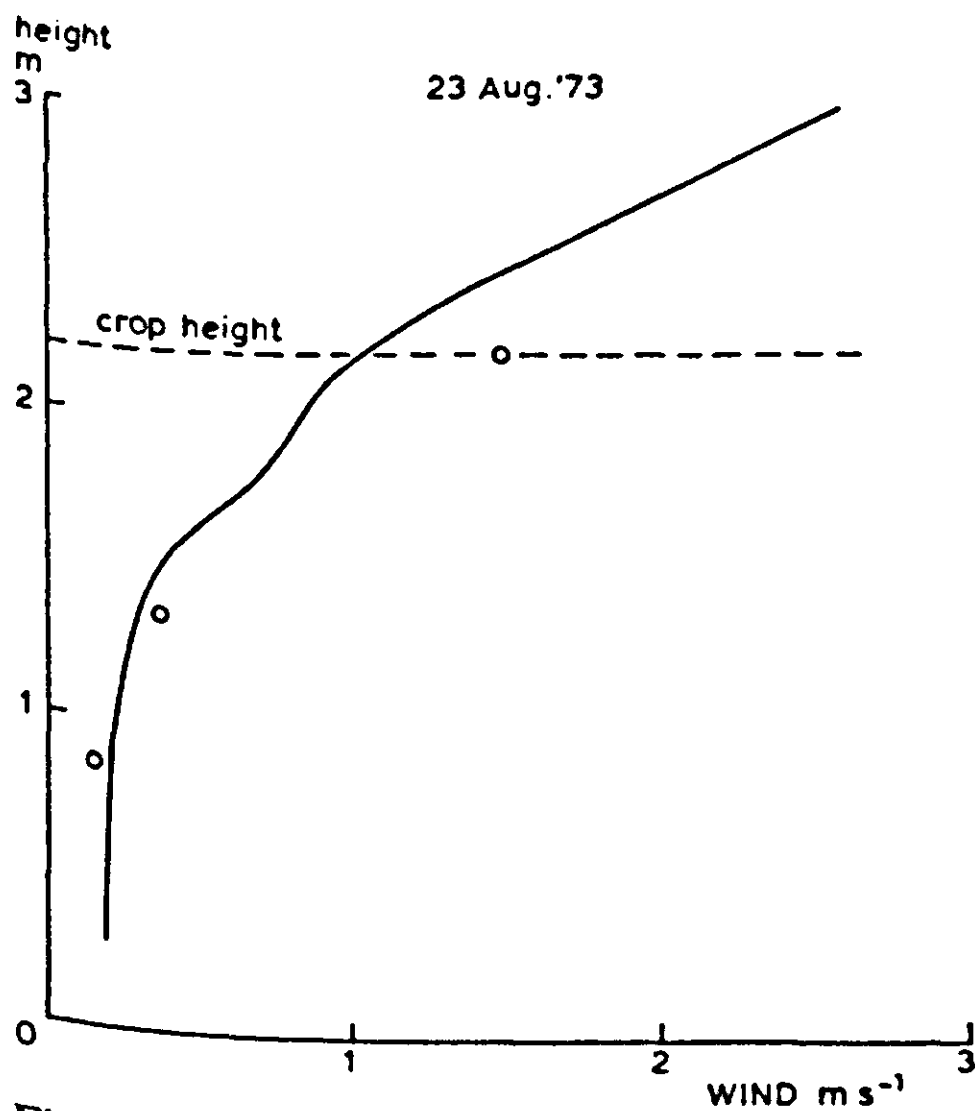


Fig. 39c

Fig. 39 | Measured and simulated wind speeds, averaged over the period 10h00–17h00, on 31 August 1972 (a), 14 August 1973 (b) and 23 August 1973 (c).

— measured, ○ simulated, - - - - - crop height

c. Leaf resistances

The measured leaf resistances were reported by Stigter & Lammers (1974). One of their main conclusions is that sunlit leaves show little variation in leaf resistance. This is also indicated by the simulation, and is a consequence of the leaf photosynthesis being saturated by light. In the range of sines of incidence of direct radiation from 0.4 to 1, the simulated leaf resistance decreases only 20%. The simulated differences with height in the canopy are negligible. In Fig.40a and b the simulated values for leaf conductance (inverse resistance) for sunlit leaves are given for a sine of incidence of 0.35, as a reasonable average of the sunlit leaves. The conductances are given as a sum of those for either side of the leaf. The shaded leaves exhibit a marked decrease in leaf conductance with depth. Leaf conductance is a better characteristic than leaf resistance, because the rate of transpiration is

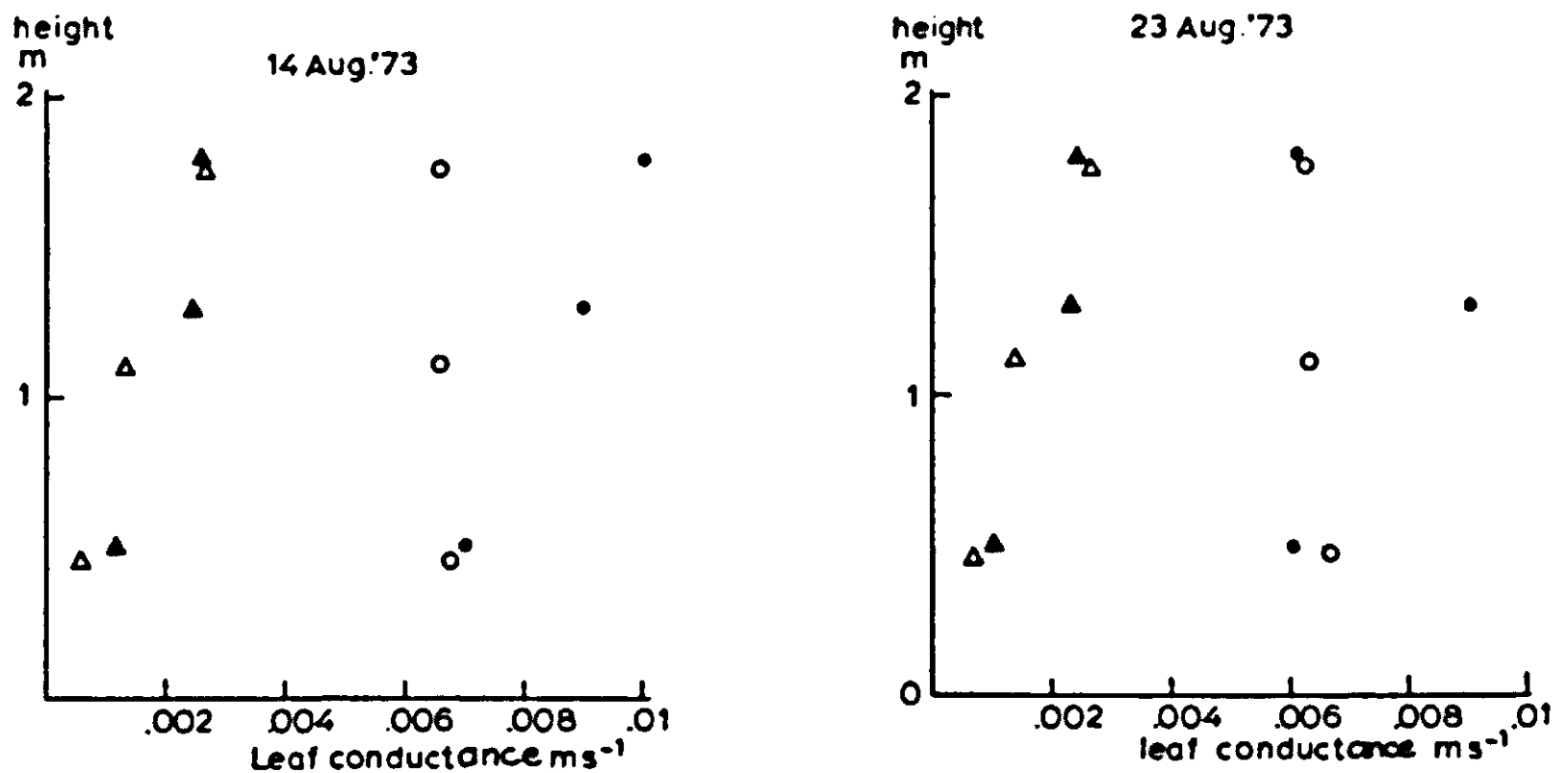


Fig. 40 | Measured and simulated leaf conductances for water vapour, on 14 August 1973 (a) and 23 August 1973 (b).

shaded sunlit
 ▲ ● measured.
 △ ○ simulated

approximately proportional to conductance. For the deepest layer the leaf conductance is underestimated, so that the transpiration rate is also slightly underestimated there. On the whole the simulated values agree quite well with the measured data.

d. Soil heat flux and soil surface temperature

On 31 August 1972 and 14 August 1973 the soil surface was wet, whereas on 23 August 1973 it was dry. Therefore the simulation was done with a zero resistance for evaporation on the first two dates, and with a very high resistance on the third date. On the first two days

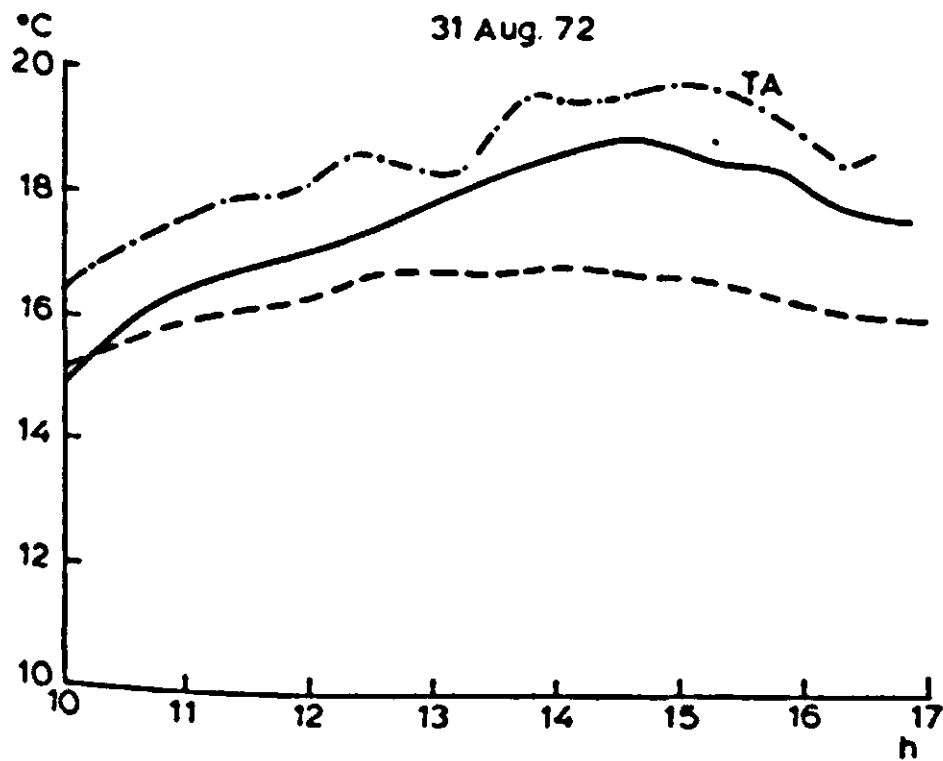


Fig. 41a

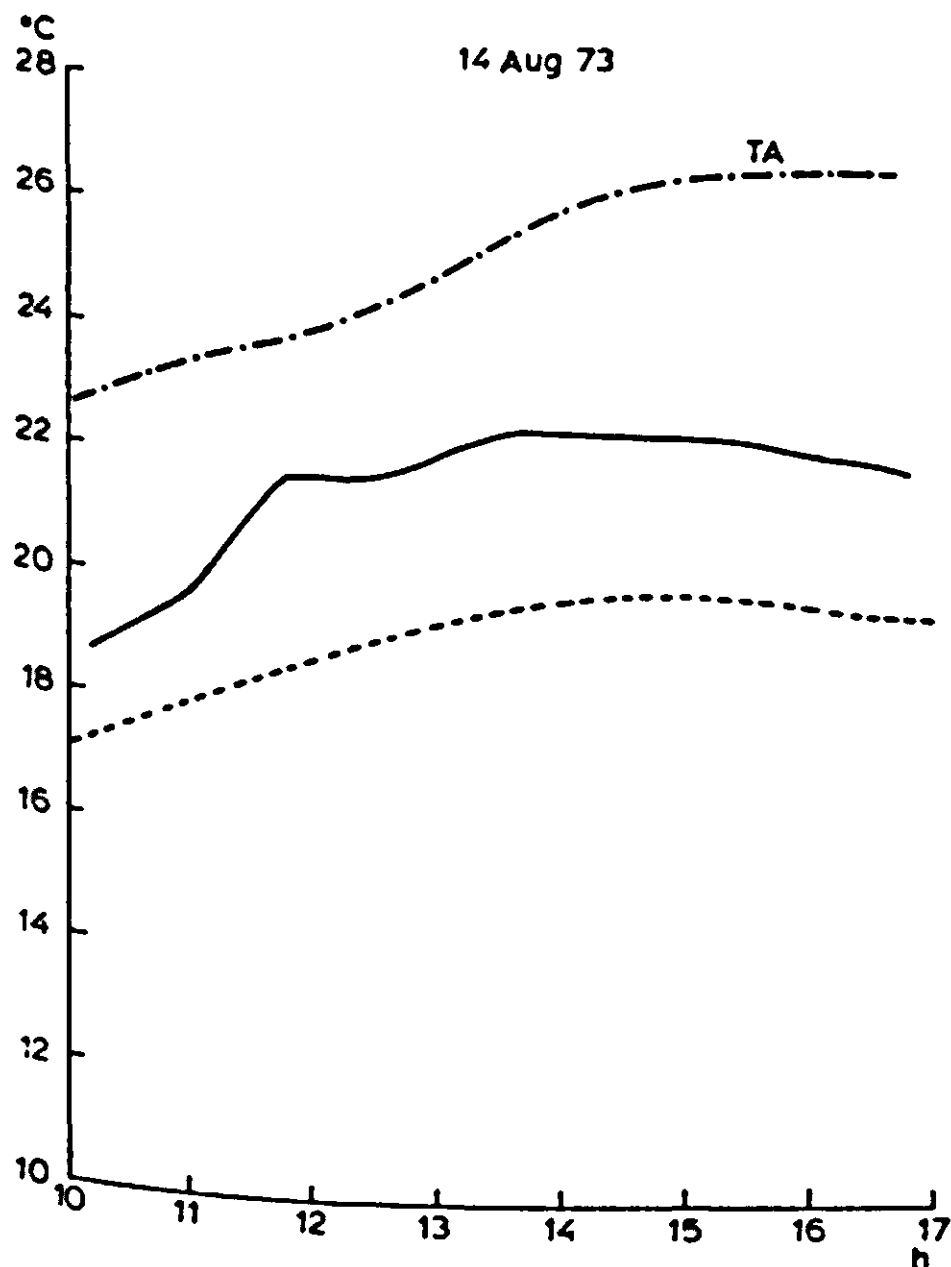


Fig. 41b

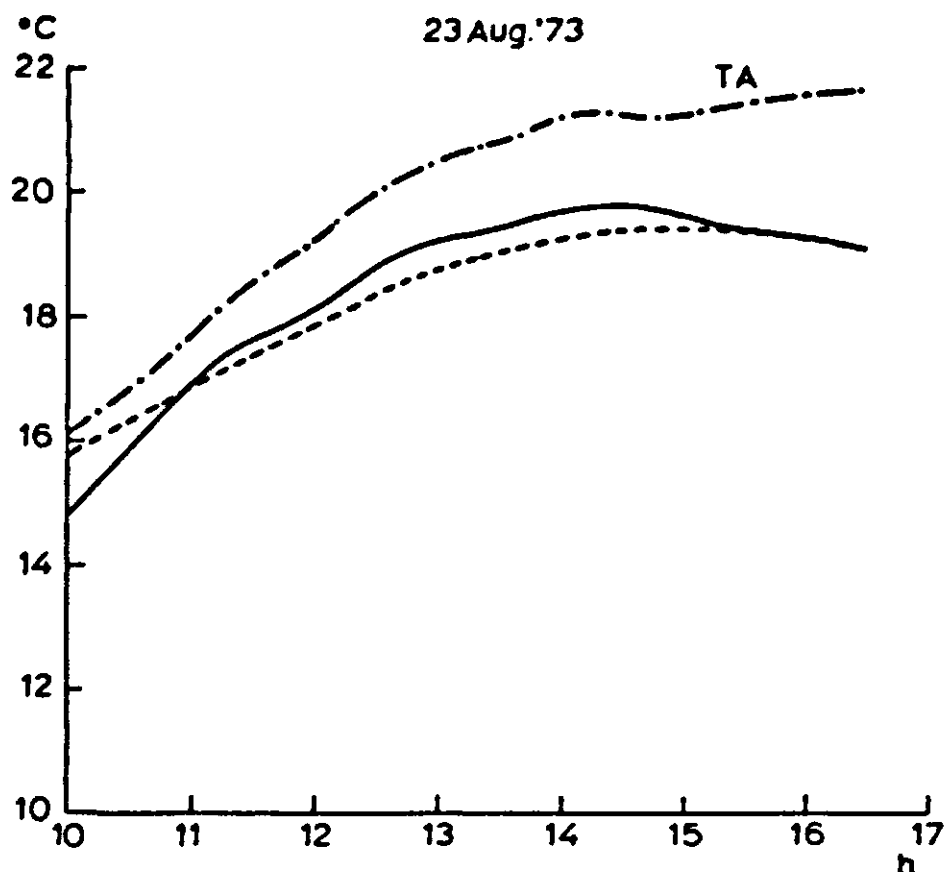


Fig. 41c

Fig. 41 | Measured and simulated temperature in the soil at 2 cm depth. on 31 August 1972 (a), 14 August 1973 (b) and 23 August 1973 (c).

————— measured, - - - - - simulated
 TA - ······ measured air temperature at 3 m height

the simulated soil temperature at 2 cm depth is too low with a maximum difference of 3 K (Figs. 41a, b and c). probably due to a too high evaporation rate. Later during the day the soil surface may have dried to some extent. This effect was not taken into account in the simulation and can also explain the phase shift between the simulated and measured soil heat fluxes (Figs. 42a, b and c). Invariably the maximum in the measured soil heat flux occurs much later than in the simulated value.

However, the soil heat flux has also been calculated from measured temperature differences between 2 and 5 cm depth, and a constant conductivity for heat of $1.15 \text{ J m}^{-1} \text{ }^\circ\text{C}^{-1} \text{ s}^{-1}$. These results are indicated by the open circles. It is remarkable that for these data the phase shift coincides better with the simulated values. It is possible that the heat flux plates inhibited an upward water movement, thereby forming their own local dry soil layer above them.

Fig. 42 | Measured and simulated soil heat fluxes at 2 cm depth.

- flux measured by heat plates
- flux, calculated from measured temperatures at 2 and 5 cm depth
- - - simulated heat flux at 2 cm depth

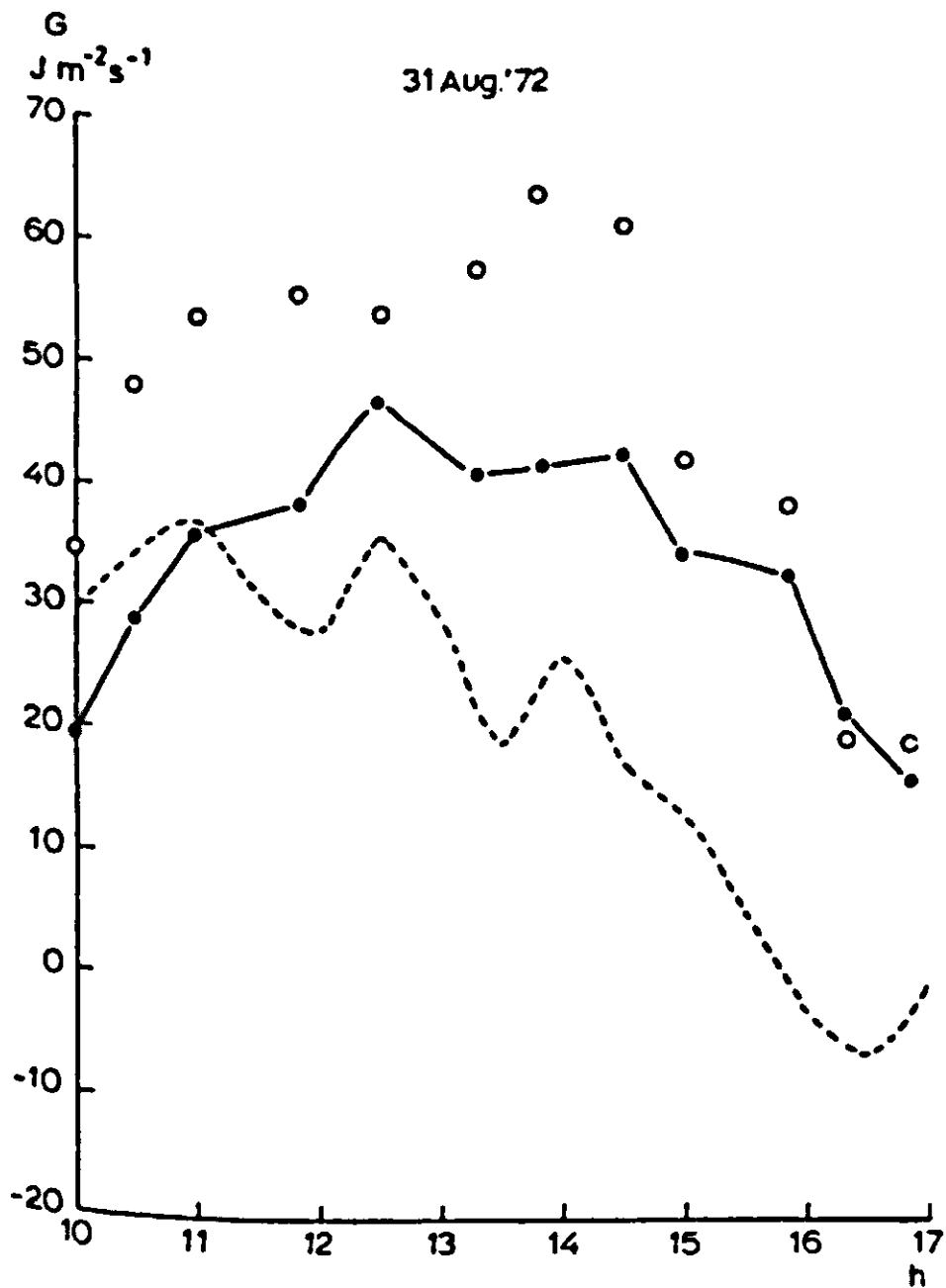


Fig. 42a

Fig. 42 is continued on page 218.

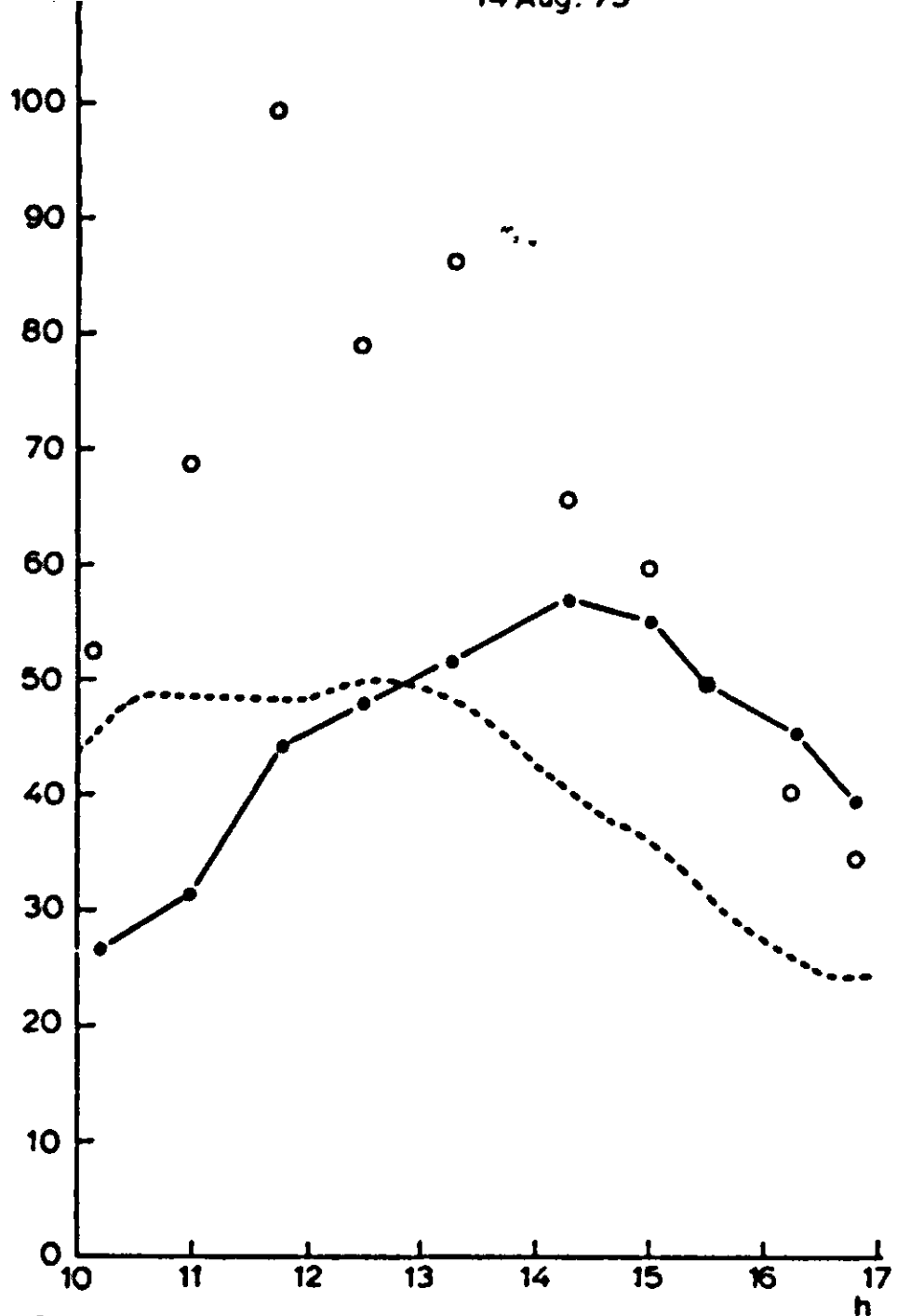


Fig. 42b

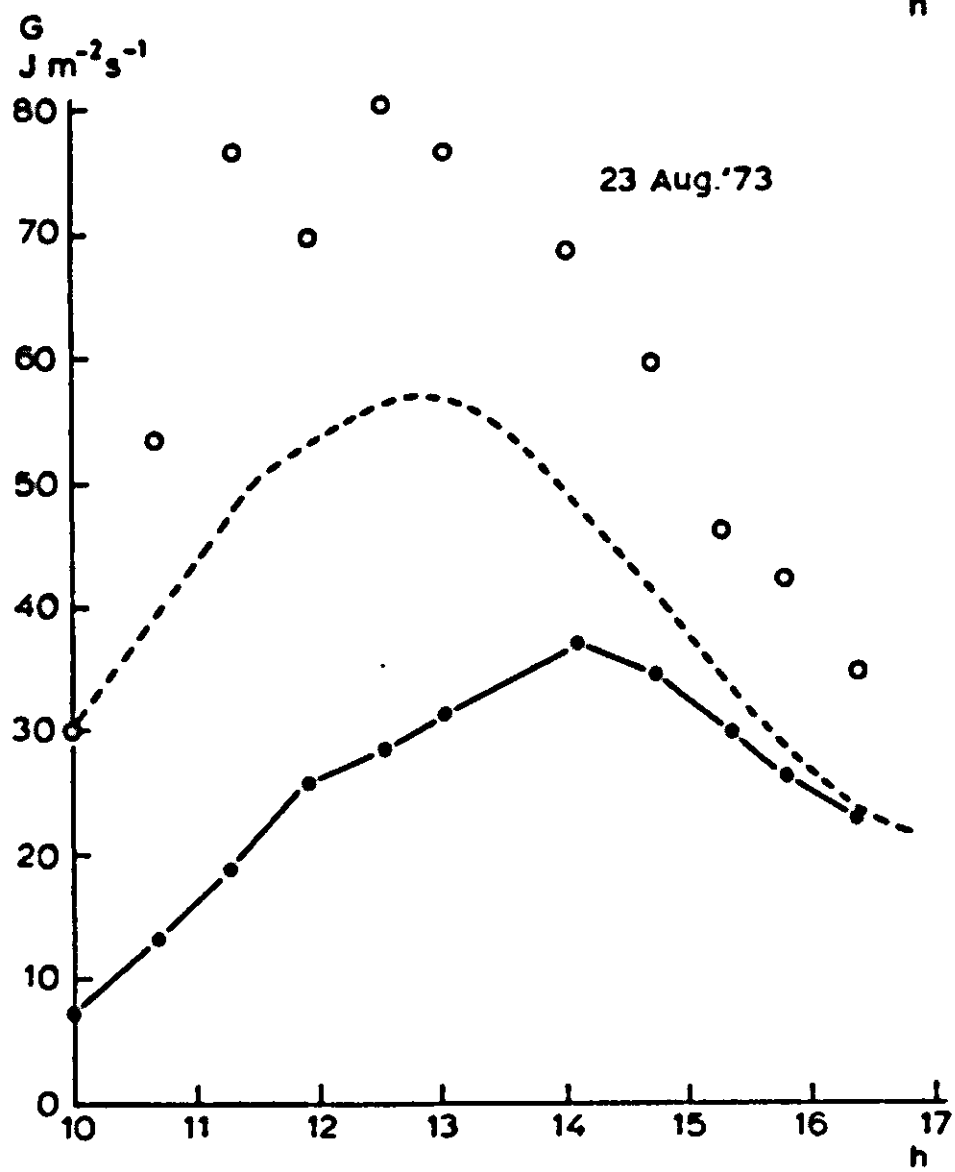


Fig. 42c

e Profiles of air temperature and humidity

In Figs. 43, 44 and 45 measured and simulated profiles of air temperature and humidity are given for 3 moments of the days 31 August 1972, 14 August 1973 and 23 August 1973. The deviations between measured and simulated data are obvious, and have two characteristics in common:

- 1 The simulated gradients are not steep enough, especially at about 2 m height, just under the top of the vegetation.
- 2 The simulated temperature profiles do not show a maximum, which frequently occurs in the measured data between 0.5 and 2 m height.

The simulated and measured air temperatures and humidities can also be compared more directly by plotting them against each other. The results should be close to a 1:1 line. Fig. 46 shows that such a comparison looks more satisfying than the previous one, although it concerns the same data. Most of the variation of the measured temperature and humidity difference between inside and above the canopy can be explained by the model. There is still a systematic underestimation which has essentially the same cause as those mentioned under 1 and 2.

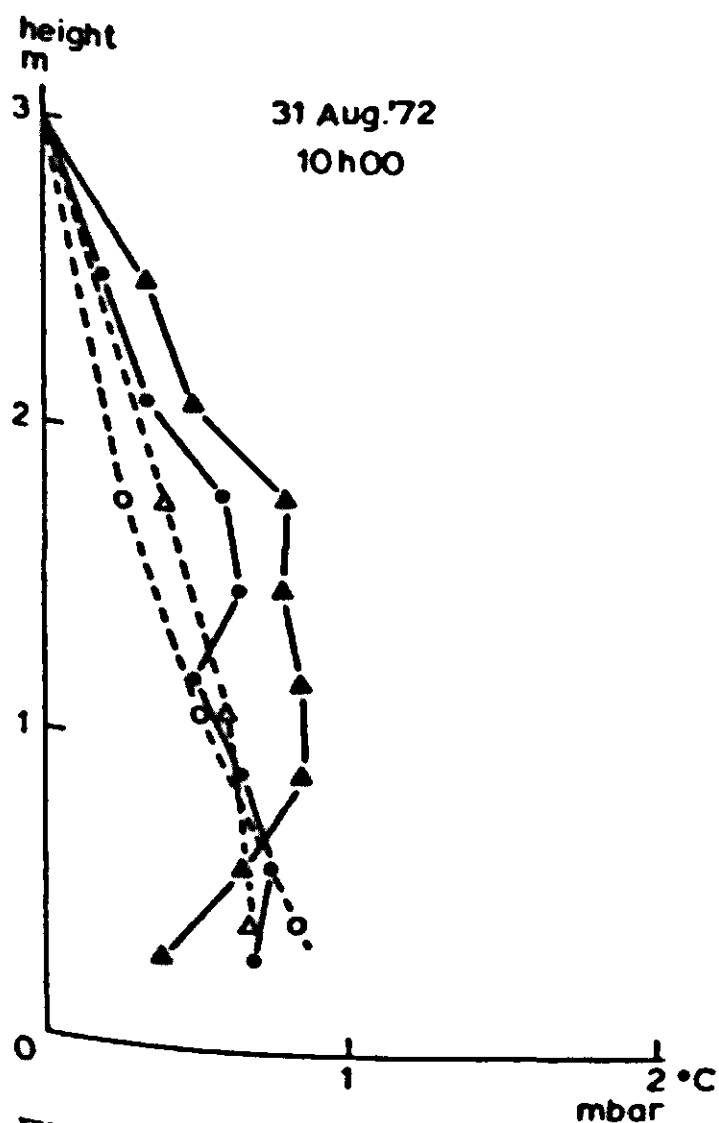


Fig. 43a

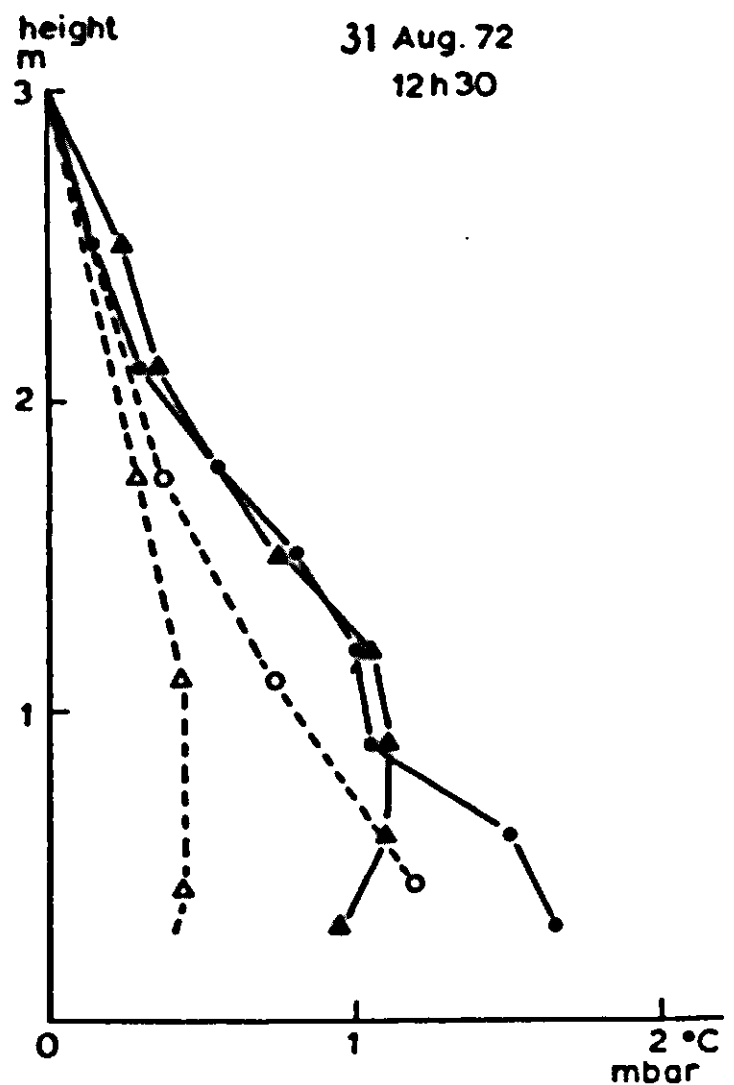


Fig. 43b

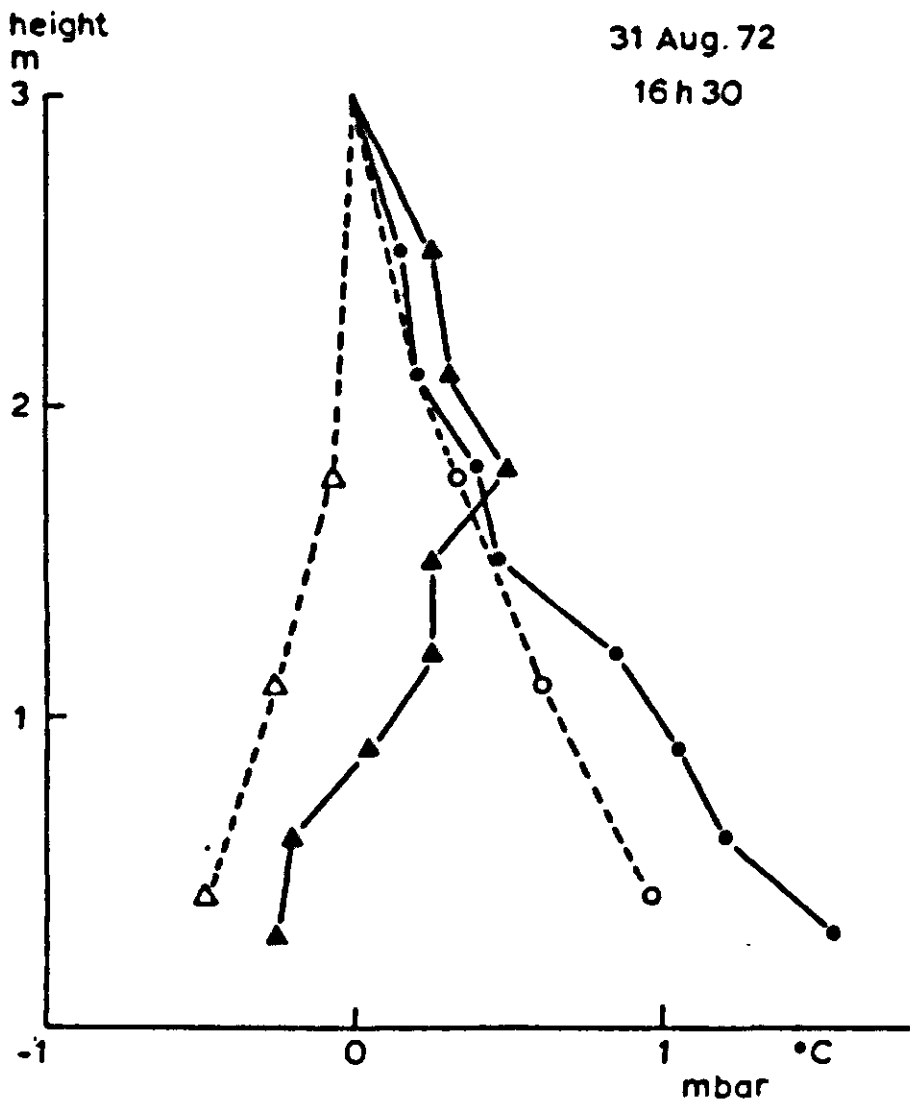


Fig. 43c

Fig. 43 | Measured and simulated profiles of air temperature and humidity on 31 August 1972 for the moments 10h00(a), 12h30(b) and 16h30(c).

measured	simulated		
▲ —▲	△ - - - △	air temperature	°C
● —●	○ - - - ○	air humidity	mbar

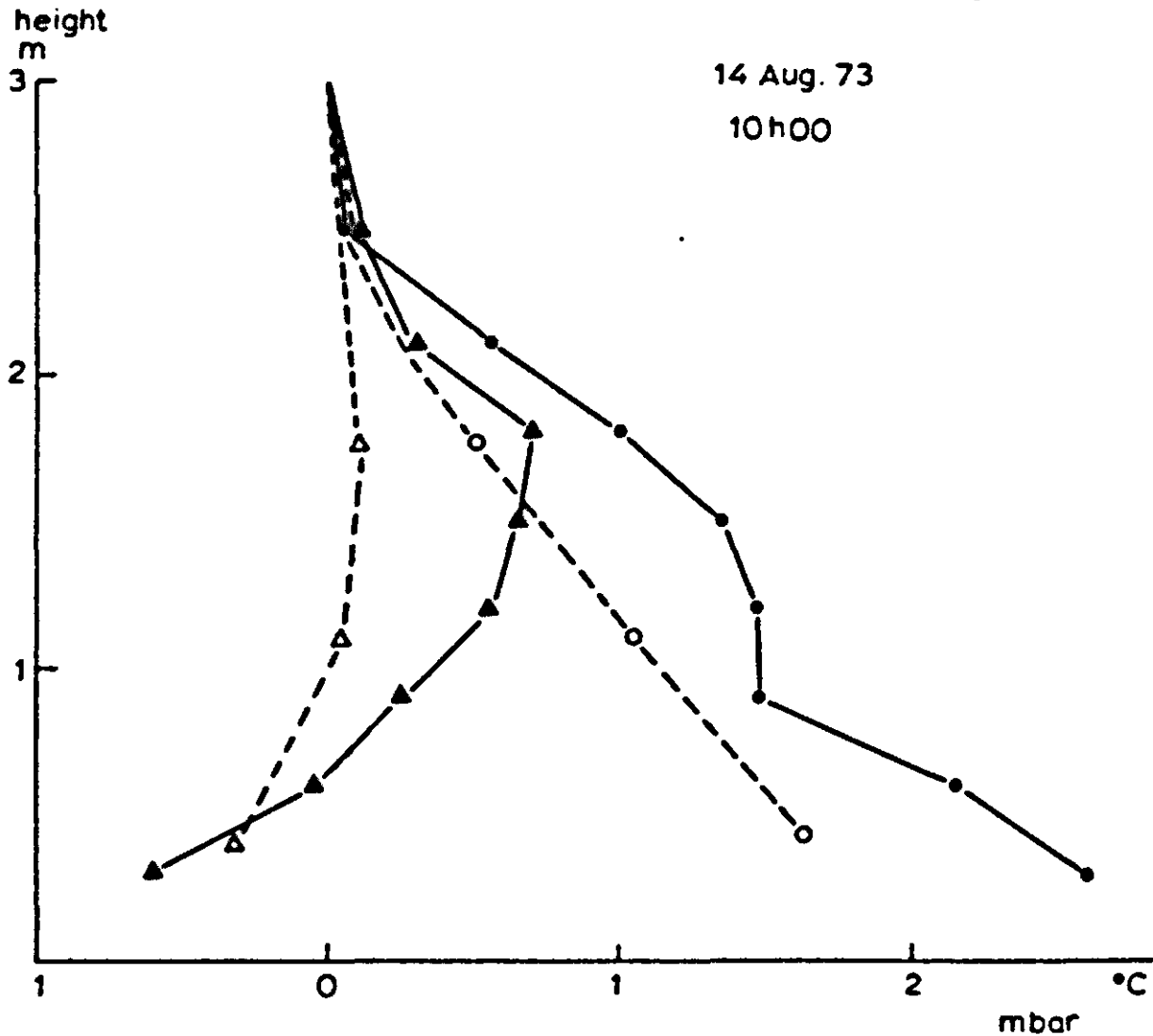


Fig. 44a

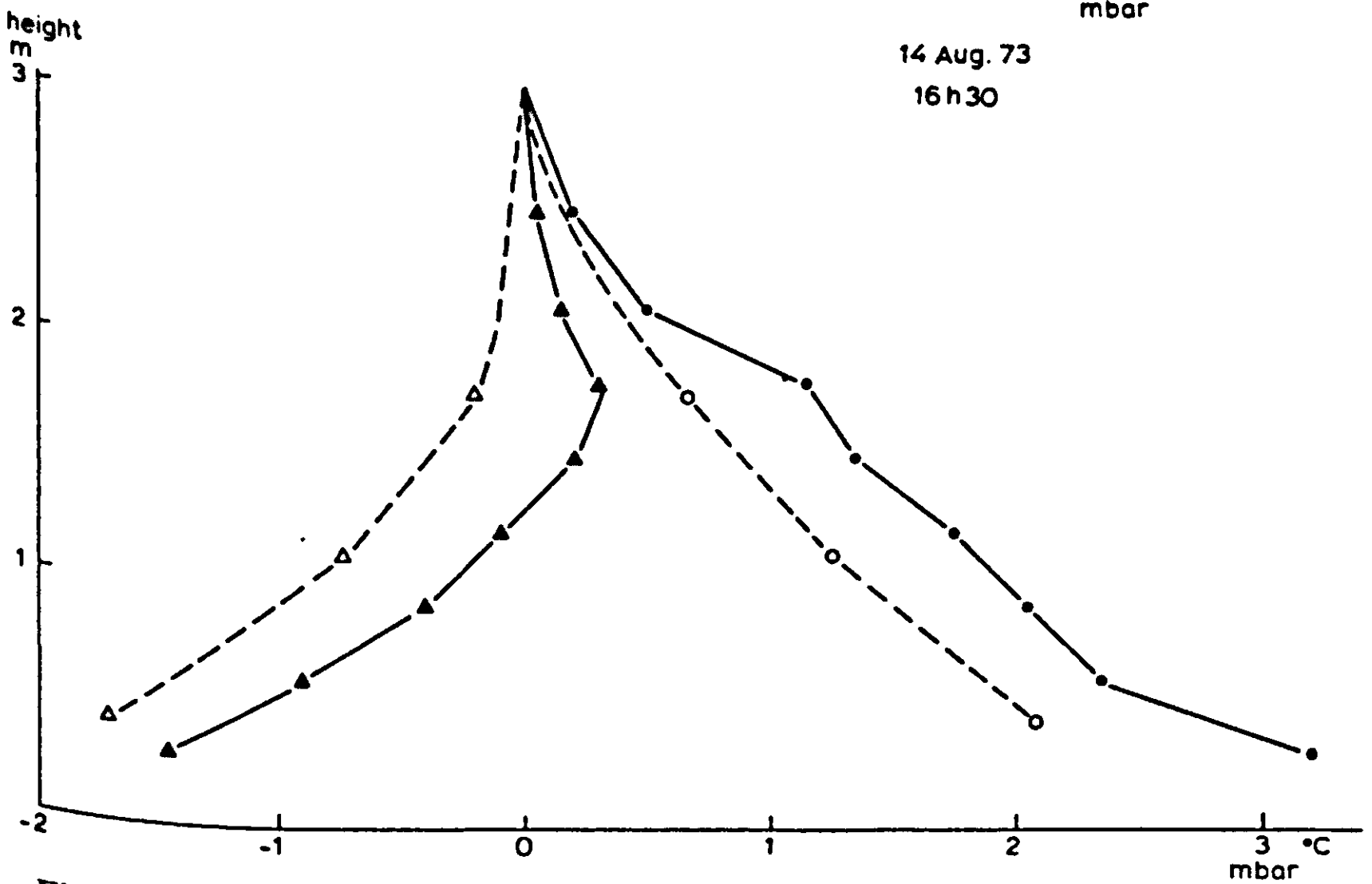
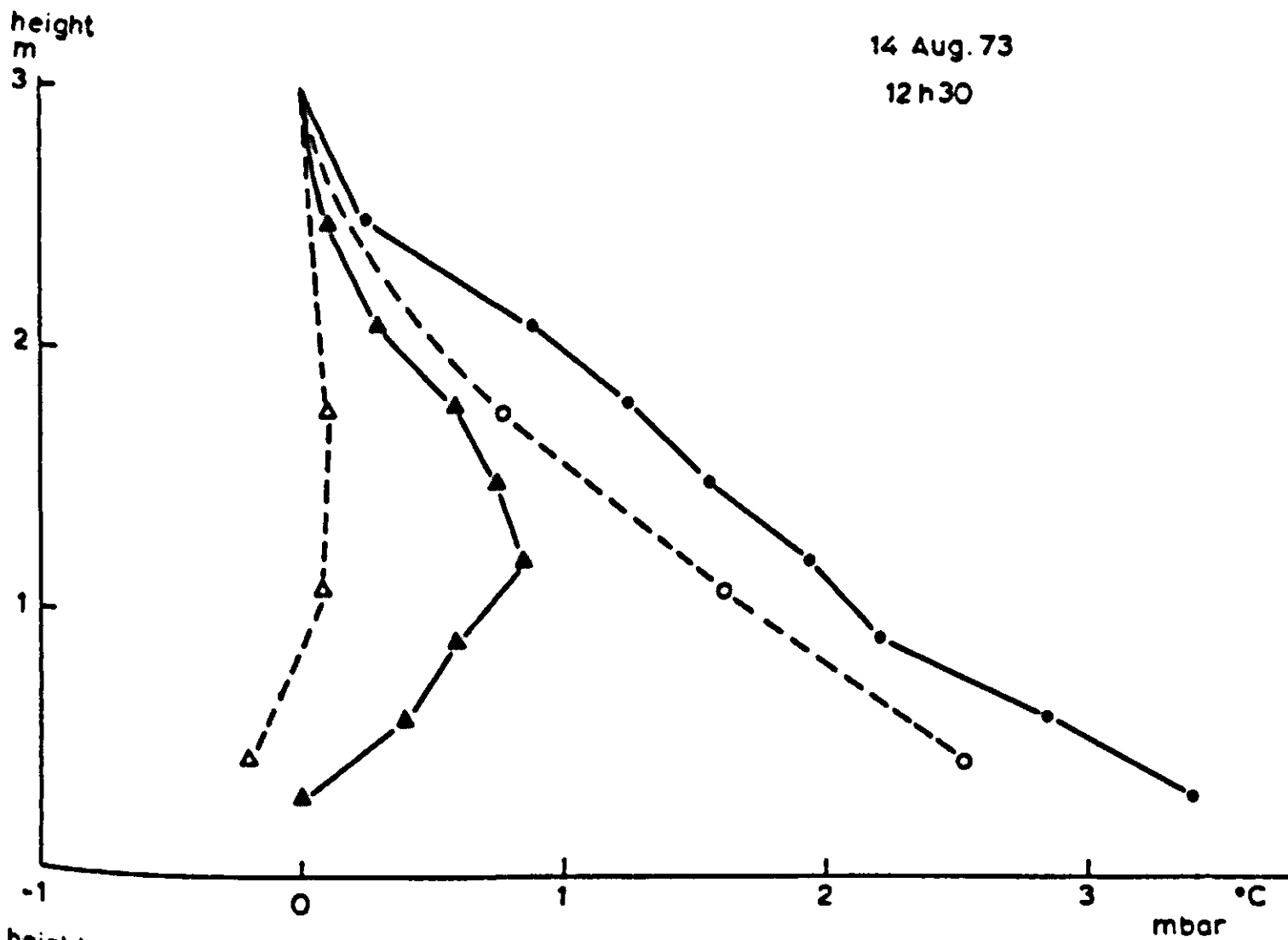


Fig. 44 | Measured and simulated profiles of air temperature and humidity on 14 August 1973 for the moments 10h00(a), 12h30(b) and 16h30(c).

measured	simulated	air temperature	°C
▲——▲	△-----△	air humidity	mbar
●——●	○-----○		

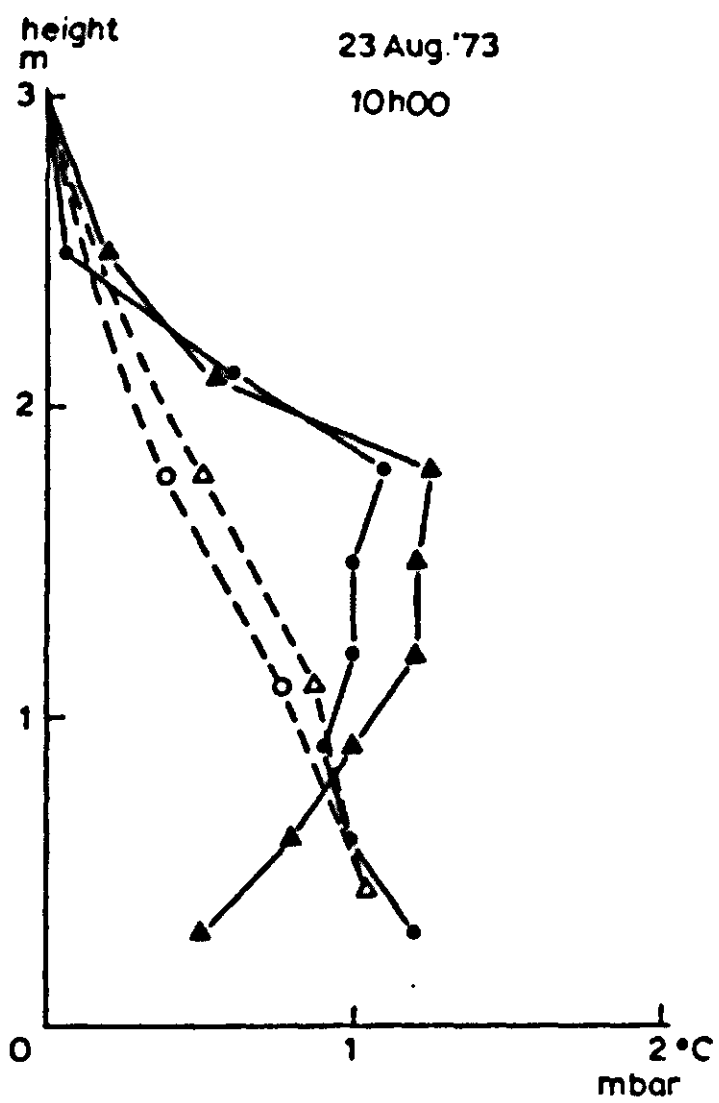


Fig. 45a

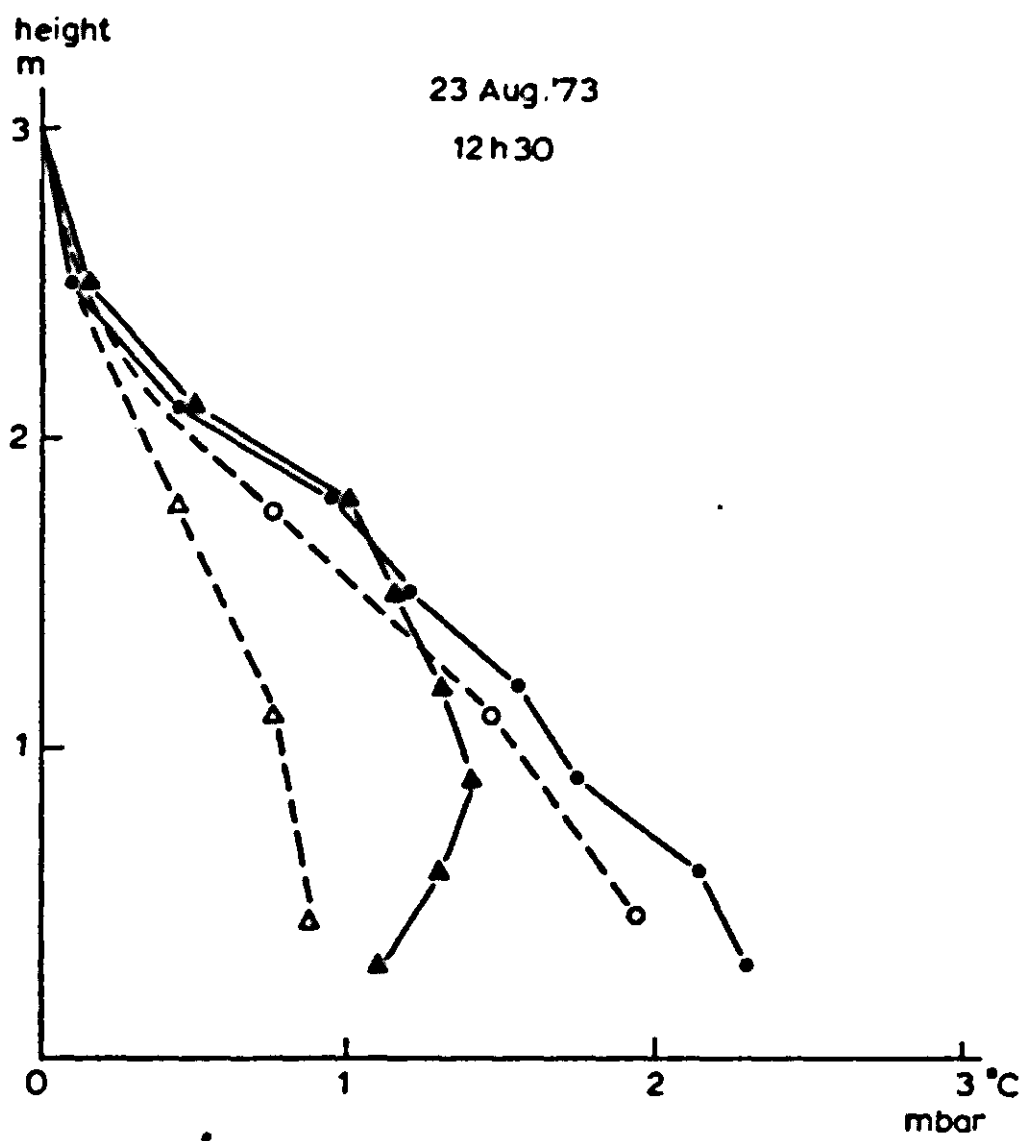


Fig. 45b

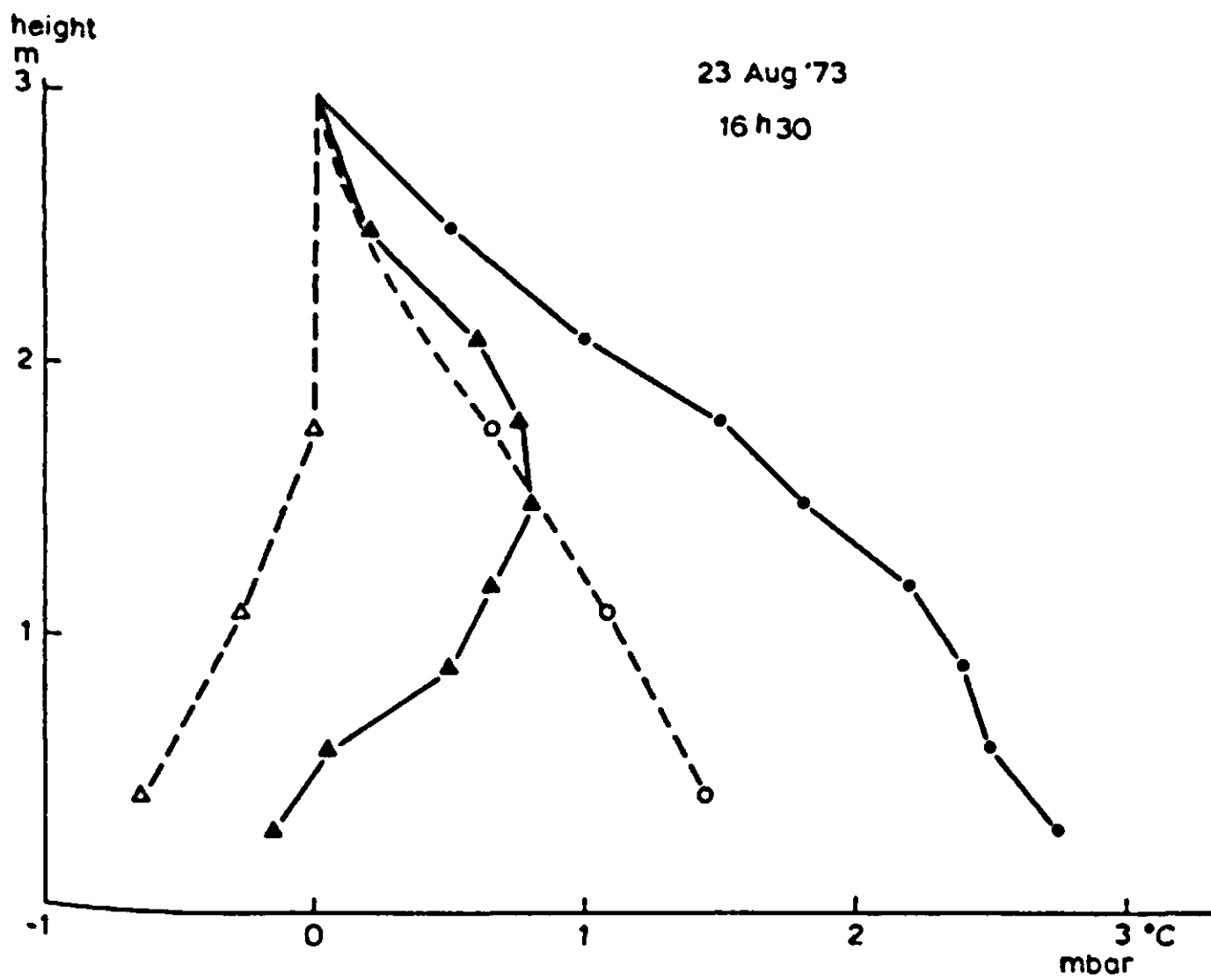


Fig. 45c

Fig. 45 | Measured and simulated profiles of air temperature and humidity on 23 August 1973 for the moments 10h00(a), 12h30(b) and 16h30(c).

measured	simulated		
▲—▲	△-----△	air temperature	°C
●—●	○-----○	air humidity	mbar

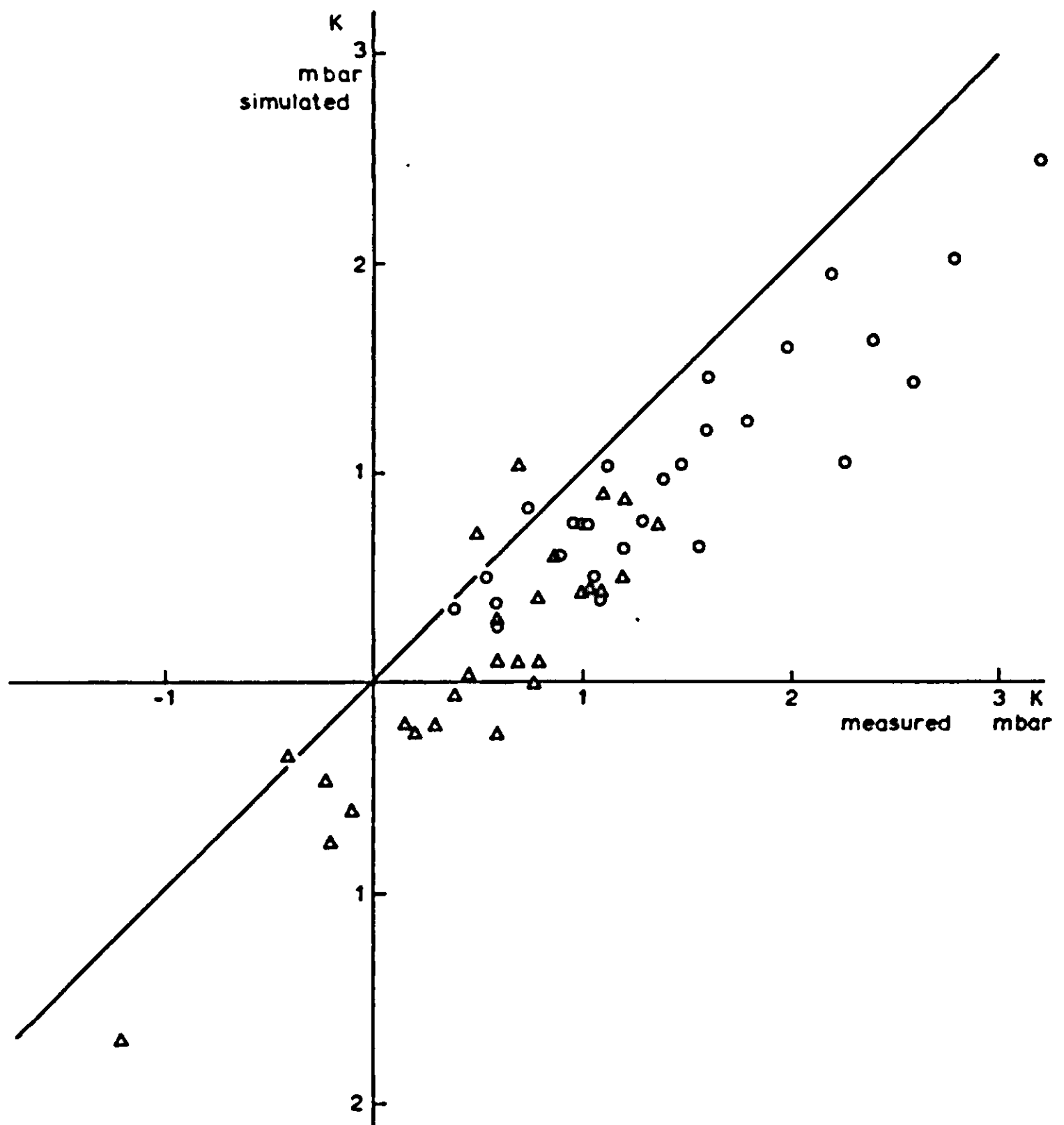


Fig. 46 | Simulated and measured differences between the temperatures (Δ) and humidities (\circ) inside the canopy and those above for different days, times and depths.

6.4.4 Discussion

One of the purposes of the simulation effort is to indicate important gaps in our knowledge by tracing back the sources of deviation between simulation and measurement. The comparisons a, b and c justify the conclusion that the radiation and leaf resistance submodels are sufficiently correct and do not cause the deviations. The simulation of the energy balance of the soil surface has probably some shortcomings, but since the energy fluxes at the soil surface do not

References

- Anderson, M. C., 1966. Stand structure and light penetration. II. A theoretical analysis. *J. appl. Ecol.* 3: 41–54.
- Bottemanne, F. A. & Tj. Reitsma, 1973. Windprofielmetingen boven grasland; Windprofielmetingen boven mais. Reports 73–1a and 73–1. Laboratory of Physics and Meteorology, Wageningen. (In Dutch).
- Brandt, A. B. & S. V. Tageeva, 1967. Optičeskije parametry rastitel'nych organizmov. Nauka, Moscow (In Russian).
- Brown, K. W., 1964. Vertical fluxes within the vegetative canopy of a corn-field. Interim Report 64–1, U.S.D.A. and Cornell University, Ithaca, N.Y.
- Budde, W., 1960. Standards of reflectance. *J. optical Soc. Am.* 50: 217–220.
- Burikov, J., 1968. The peculiarities of the radiation regime of the plant cover depending on its structure, In: *Actinometry and atmospheric optics*, Tallin.
- Burrage, S. W., 1972. Dew on wheat *Agric. Met.* 10: 3–12.
- Businger, J. A., J. C. Wijngaard, Y. I. Izumi & E. F. Bradley, 1971. Flux-profile relationships in the atmospheric surface layer. *J. atmosph. Sci.* 181–189.
- Cionco, R. M., 1972. A wind profile index for canopy flow. *Boundary Layer Met.* 3: 255–263.
- Chamberlain, A. C., 1968. Transport of gases to and from surfaces with bluff and wave-like roughness elements. *Quart. J. of the royal meteorol. Soc.* Vol 94: 318–332.
- Cowan, I. R., 1968. The interception and absorption of radiation in plant stands. *J. appl. Ecol.* 5: 367–379.
- Gates, D. M., H. J. Keegan, J. C. Schleter & V. R. Weidner, 1965. Spectral properties of plants. *Appl. Optics* 4(1).
- Goudriaan, J. & H. H. van Laar, in press. Measurement of some relations between leaf resistance in maize, beans, lalang-grass and sunflower (Accepted by *Photosynthetica*)
- Goudriaan, J. & P. E. Waggoner, 1972. Simulating both aerial microclimate and soil temperature from observations above the foliar canopy. *Neth. J. agric. Sci.* 20: 104–124.
- Grace, J., 1971. The directional distribution of light in natural and controlled environment conditions. *J. appl. Ecol.* 8: 155–165.

- Hartog, G. den & R. H. Shaw, 1975. A field study of atmospheric processes within a vegetative canopy. In: D. A. de Vries & N. H. Afgan (Ed.), Heat and mass transfer in the biosphere, John Wiley and Sons, London.
- Hopmans, P. A. M., 1971. Rhythms in stomatal opening of bean leaves. Meded. Landb. Hogesch. Wageningen 71.3, 1-86.
- Inoue, E., 1963. On turbulent structure of airflow within crop canopies. J. Met. Soc. Japan, II, 41(6): 317-326.
- Jarvis, P. G., G. B. James & J. J. Landsberg, 1976. Coniferous forest. In: J. L. Monteith (Ed.), Vegetation and the atmosphere, Vol. 2: 171-236.
- Kalma, J. D. & R. Badham, 1972. The radiation balance of a tropical pasture, I. The reflection of short-wave radiation. Agric. Meteorol., 10: 251-259.
- Kanemasu, E. T., 1974. Seasonal canopy reflectance patterns of wheat, sorghum and soybean. Remote Sensing Envir. 3: 43-47.
- Kaufmann, S. 1976. Het verdampingsbeeld van enkele bodemtypen. Thesis, Agricultural University, Wageningen.
- Keulen, H. van & D. Hillel, 1974. A simulation study of the drying front phenomenon. Soil Sci. 118(4): 270-273.
- Keulen, H. van, 1975. Simulation of water use and herbage growth in arid regions. Pudoc, Wageningen 184 pp.
- Kyle, W. J., 1971. Daytime radiation regimes within a corn canopy. Publications in climatology No 2, McMaster University, Hamilton, Ontario, USA.
- Laar, H. H. van, D. Kremer & C. T. de Wit, 1977. Maize. In: Th. Alberda et al., Crop photosynthesis. Methods and compilation of data obtained with a mobile field equipment. Agric. Res. Rep. 865. Pudoc. Wageningen. p. 12-21.
- Laar, H. H. van & F. W. T. Penning de Vries, 1972. CO₂ assimilation light response curves of leaves, some experimental data. Versl. Inst. biol. scheik. Onderz. LandbGewassen, 62, Wageningen.
- Legg, B. & J. L. Monteith, 1975. Heat and mass transfer within plant canopies, In D. A. de Vries and N. H. Afgan (Ed), 'Heat and mass transfer in the biosphere'. pp. 167-186. John Wiley & Sons, London.
- Lemeur, R., 1971. Mathematical model for the study of parallel, isotropic and scattered radiation in theoretical and real canopies. Ph. D. Thesis, University of Ghent, Ghent, 102 pp (In Dutch).
- Lemeur, R. & B. L. Blad, 1974. A critical review of light models for estimating the short-wave radiation regime of plant canopies. Agric. Met. 14: 255-286.
- List, R. J., 1949. Smithsonian meteorological tables, Smithsonian Institution Press, Washington.

- Long, I. F., 1968. Instruments and techniques for measuring the microclimate of crops. In: R. M. Wadsworth (Ed.), 'The measurement of environmental factors in terrestrial ecology', Blackwell Sc. Publ., 1-32. Oxford.
- May, R. M., 1973. Stability and complexity in model ecosystems. Princeton University Press, Princeton.
- Monin, A. S. & A. M. Obukhov, 1954. Basic regularity in turbulent mixing in the surface layer in the atmosphere. Publ. USSR Acad. Sci., geophys. Inst. No 24.
- Monsi, M. & T. Saeki, 1953. Über den Lichtfaktor in den Pflanzengesellschaften und seine Bedeutung für die Stoffproduktion. Jap. J. Bot. 14: 22-52.
- Monteith, J. L., 1957. Dew. Q. J. Met. Soc. 83: 322-341.
- Monteith, J. L., 1973. Principles of environmental physics. Edward Arnold, London, 241 pp.
- Monteith, J. L., 1976. Vegetation and the atmosphere, Vol. 2. Academic Press. London.
- Moon, P. & D. E. Spenser, 1942. Illumination from a non-uniform sky. Trans. Illum. Engng Soc., N.Y. 37: 707-712.
- Mullamaa, U. A. R. & V. K. Pyldmaa, 1975. Variability of direct solar radiation. In: J. Ross (Ed.), *Oblačnost'i radiacija*. Tartu, 1975.
- Norman, J. M. & P. G. Jarvis, 1974. Photosynthesis in Sitka spruce (*Picea sitchensis* (Bong.) Carr). III. Measurements of canopy structure and interception of radiation. J. of appl. Ecol. Vol. 11 No. 1: 375-398.
- Pearman, G. I., H. L. Weaver & C. B. Tanner, 1972. Boundary layer heat transfer coefficients. Agric. Met. 10: 83-92.
- Penman, H. L., 1948. Natural evaporation from open water, bare soil and grass. Proc. Roy. Soc. A., 193; 120-146.
- Penning de Vries, F. W. T., 1973. Substrate utilization and respiration in relation to growth and maintenance in higher plants. Ph. D. Thesis, Agricultural University, Wageningen.
- Prandtl, L., 1932. Meteorologische Anwendung der Strömungslehre. Beitr. Phys. Atmosphäre, 19: 188-202.
- Priestly, C. H. B., 1959. Turbulent transfer in the lower atmosphere. The University of Chicago Press. Chicago.
- Rabbinge, R., 1976. Biological control of fruit-tree red spider mite. Pudoč, Wageningen 234 pp.
- Rauner, Ju. L., 1976. Deciduous forest. In: J. L. Monteith (Ed.), Vegetation and the atmosphere, Vol. 2: 241-262.
- Rodskjer, N., 1972. Measurements of solar radiation in barley and oats. Swedish J. agric. Res. 2: 71-81.

- Ross, J. & T. A. Nilson, 1966. A mathematical model of the radiation regime of vegetation. In: V. K. Pyldmaa (Ed.), Actinometry and atmospheric optics. (Translated by Israel Program of Scientific Translations, Jerusalem, 1971, pp. 253–270).
- Ross, J., 1975. Radiative transfer in plant communities. In: J. L. Monteith (Ed.), Vegetation and the atmosphere, Vol. 1: 13–52. Academic Press, London.
- Ross, J., 1975. Radiacionnyj režim i arhitektonika rastitel'nogo pokrova. Gidrometeoizdat. Leningrad, 341 pp. (In Russian).
- Rijkoort, P. J., 1968. The increase of mean wind speed with height in the surface friction layer. Meded. en Verhandelingen KNMI.
- Sinclair, T. R. & E. R. Lemon, 1974. Penetration of photosynthetically active radiation in corn canopies. Agron J. 66(2).
- Shaw, R. H., G. den Hartog, K. M. King & G. W. Thurtell, 1974. Measurements of mean wind flow and three-dimensional turbulence within a mature corn canopy. Agric. Met. 13: 419–425.
- Shaw, R. H., R. H. Silversides & G. W. Thurtell, 1974. Some observations of turbulence and turbulent transport within and above plant canopies. Boundary Layer Met. 5: 429–449.
- Slatyer, R. O. & I. C. McIlroy, 1961. Practical microclimatology. UNESCO.
- Stanhill, G., 1969. A simple instrument for the field measurement of turbulent diffusion flux. J. appl. Met. 8: 509.
- Stigter, C. J., 1972. Leaf diffusion resistance to water vapour and its direct measurement. I. Introduction and review concerning relevant factors and methods. Meded. LandbHogesch. Wageningen 72–3: 1–47.
- Stigter, C. J., J. Birnie & B. Lammers, 1973. Leaf diffusion resistance to water vapour and its direct measurement. II. Design, calibration and pertinent theory of an improved leaf diffusion resistance meter. Meded. LandbHogesch. Wageningen 73–15: 1–55.
- Stigter, C. J., 1974a, The epidermal resistance to diffusion of water vapour: an improved measuring method and field results in Indian corn (*Zea mays*). Agric. Res. Rep. 813. Pudoc, Wageningen.
- Stigter, C. J. & B. Lammers, 1974b. Leaf diffusion resistance to water vapour and its direct measurement. III. Results regarding the improved diffusion porometer in growth rooms and fields of Indian corn (*Zea mays*). Meded. LandbHogesch. Wageningen 74–21: 1–76.
- Stigter, C. J., 1975. Water diffusion porometry for leaf epidermal resistance measurements in the field. In: D. A. de Vries & N. H. Afgan (Ed.), Heat and mass transfer in the biosphere. John Wiley and Sons, London.

- Stigter, C. J., J. G. Lengkeek & J. Kooijman, 1976. A simple worst case analysis for estimation of correct scanning rate in a micrometeorological experiment. *Neth. J. of Agric. Sci* 24: 3-16.
- Stigter, C. J., J. Birnie & P. Jansen, 1977. Multi-point temperature measuring equipment for crop environment, with some results on horizontal homogeneity in a maize crop. Accepted by *Neth. J. of Agric. Sci.*
- Stigter, C. J., J. Goudriaan, F. A. Bottemanne, J. Birnie, J. G. Lengkeek, L. Sibma, Experimental evaluation of a crop climate simulation model for Indian corn (*Zea mays* L.), submitted to *Agric. Met.*
- Sul'gin, I. A., 1973. *Rastenie i solnce. Gidrometeoizdat, Leningrad, 251 pp* (In Russian).
- Szeicz, G., J. L. Monteith & J. Dos Santos, 1964. A tube solarimeter to measure radiation among plants. *J. appl. Ecol.* 1(1) 169-174.
- Tanner, C. B. & W. L. Pelton, 1960. Potential evapotranspiration estimated by the approximate energy balance method of Penman. *J. geophys. Res.* 65: 3391-3413.
- Tooming, H., 1967. Mathematical model of plant photosynthesis. *Photosynthetica* 1: 233-240.
- Uchijima, Z. & J. L. Wright, 1963. An experimental study of air flow in a corn plant-air layer. Interim Report 63-1, U.S.D.A. and Cornell University, Ithaca, N.Y.
- Udagawa, T., A. Ito & Z. Uchijima, 1974. Radiation environment in rice canopies. *Coll. Pap. agric. Met., Natn. Inst. agric. Sci., Tokyo.*
- Verhoef, W. & N. J. J. Bunnik, 1975. A model study on the relations between crop characteristics and canopy spectral reflectance. NIWARS, Delft, 89 pp.
- Waggoner, P. E., G. M. Furnival & W. E. Reifsnyder, 1969. Simulation of the microclimate in a forest. *Forest Sci.* 15: 37-45.
- Woolley, J. T., 1971. Reflectance and transmittance of light by leaves. *Pl. Physiol.* 47: 656-662.
- Wit, C. T. de, 1958. Transpiration and crop yields. *Versl. landbouwk. Onderz. (Agric. Res. Rep.)* 64.6. Pudoc, Wageningen.
- Wit, C. T. de, 1959. Potential photosynthesis of crop surfaces. *Neth. J. agric. Sci.* 7: 141-149.
- Wit, C. T. de, 1965. Photosynthesis of leaf canopies. *Agric. Res. Report. No 663.* Pudoc, Wageningen, 57 pp.
- Wit, C. T. de & H. van Keulen, 1972. Simulation of transport processes in soils. Pudoc, Wageningen, 109 pp.
- Wit, C. T. de & J. Goudriaan, 1974. Simulation of ecological processes. Pudoc, Wageningen, 167 pp.

Appendix A

The integrals of the following expressions are needed in some of the mathematical problems which occur in the radiation models. (Chapter 2).

$$a. \quad K = \int \frac{d\beta}{1 + \sin^2 \beta \operatorname{tg}^2 \lambda} \quad (\text{A1})$$

By substitution of $\alpha = 2\beta$ the solution can be found

$$K = -\frac{\cos \lambda}{2} \arcsin \left(\frac{1 - 2\sin^2 \beta - \operatorname{tg}^2 \lambda \sin^2 \beta}{1 + \sin^2 \beta \operatorname{tg}^2 \lambda} \right) + C \quad (\text{A2})$$

where C is the integration constant

$$b. \quad L = \int \cos \beta \sin \beta \arcsin \left(\frac{\operatorname{tg} \beta}{\operatorname{tg} \lambda} \right) d\beta \quad (\text{A3})$$

First the substitution $p = \arcsin \left(\frac{\operatorname{tg} \beta}{\operatorname{tg} \lambda} \right)$ is made. Then L can be written as

$$L = \int \frac{\operatorname{tg}^2 \lambda \, p \sin p \cos p \, dp}{(1 + \sin^2 p \operatorname{tg}^2 \lambda)^2} \quad (\text{A4})$$

or

$$L = \frac{1}{2} \int \frac{\operatorname{tg}^2 \lambda \, p \, d(\sin^2 p)}{(1 + \sin^2 p \operatorname{tg}^2 \lambda)^2} \quad (\text{A5})$$

or

$$L = -\frac{1}{2} \int p \, d \left\{ \frac{1}{(1 + \sin^2 p \operatorname{tg}^2 \lambda)} \right\} \quad (\text{A6})$$

Integration by parts gives

$$L = -\frac{p}{2(1 + \sin^2 p \operatorname{tg}^2 \lambda)} + \frac{1}{2} \int \frac{dp}{1 + \sin^2 p \operatorname{tg}^2 \lambda} \quad (\text{A7})$$

The right term is the previously solved integral K , divided by 2. Substitution of p and of the expression for K gives

$$L = -\frac{\cos^2\beta}{2} \arcsin\left(\frac{\operatorname{tg}\beta}{\operatorname{tg}\lambda}\right) + \frac{\cos\lambda}{2} \arcsin\left(\frac{\sin\beta}{\sin\lambda}\right) + C \quad (\text{A8})$$

where C is an integration constant.

c. It can now be shown that the following integral J equals L_s (see Eqn (2.28))

$$J = \int_0^{\pi/2} B_u(\beta) M_i(\beta) d\beta \quad (\text{A9})$$

By substitution of B_u (Eqn (2.11)) and of M_i (Eqn (2.28)), J can be written as

$$J = L_s \int_0^{\pi/2} 2\bar{O}(\beta) \cos \beta d\beta \quad (\text{A10})$$

where $\bar{O}(\beta)$ is $\sum_{\lambda=1}^9 F(\lambda) O(\beta, \lambda)$.

J is equal to L_s , if the following integral G is unity for all λ .

$$G = \int_0^{\pi/2} 2 \cos\beta O(\beta, \lambda) d\beta \quad (\text{A11})$$

Substituting the expression for $O(\beta, \lambda)$ (Eqn 2.3)) gives

$$G = \int_{\lambda}^{\pi/2} 2 \cos\beta \sin\beta \cos\lambda d\beta + \frac{4}{\pi} \int_0^{\lambda} \left\{ \sin\beta \cos\lambda \arcsin\left(\frac{\operatorname{tg}\beta}{\operatorname{tg}\lambda}\right) + (\sin^2\lambda - \sin^2\beta)^{0.5} \right\} \cos\beta d\beta \quad (\text{A12})$$

Integration of the first term between the boundaries λ and $\pi/2$ gives $\cos^3\lambda$. The integral of the second term, using the result for integral L , is $\sin^2\lambda - \cos^3\lambda + \cos^2\lambda$. The sum of these terms together is unity independently of λ . Hence G equals unity and J equals L_s .

d. To find the integral of $\bar{\psi}_{ref1}$ with respect to β' , the result for integral L must be used several times. Moreover the following relation is needed

$$(\sin^2\lambda - \sin^2\beta)^{0.5} = \sin\lambda \cos\beta \sin\alpha_c \quad (\text{A13})$$

The expression for $\int_0^{\beta'} \bar{\Psi}_{\text{refl}}$ can be simplified by using the Eqn (2.3b)

for $O(\beta, \lambda)$. The integral is now

$$\int_0^{\beta'} \bar{\Psi}_{\text{refl}} = S_p \rho \frac{4}{2\pi^2} \left[\frac{\pi^2}{4} \sin\beta \cos^2\lambda \sin^2\beta' + \frac{\pi}{2} O(\beta, \lambda) \left\{ \frac{\pi}{2} \sin\beta' O(\beta', \lambda) + \arcsin\left(\frac{\sin\beta'}{\sin\lambda}\right) - \cos\lambda \arcsin\left(\frac{\text{tg}\beta'}{\text{tg}\lambda}\right) \right\} \right] \quad (\text{A14})$$

The corresponding expression for the transmitted amount only differs by a minus sign for the first term, and of course by τ instead of ρ . The total reflected amount be the upper hemisphere is found by substituting $\pi/2$ for β' . The expression then simplifies to

$$\int_0^{\pi/2} \bar{\Psi}_{\text{refl}} = S_p \rho \frac{1}{2} \left\{ \sin\beta \cos^2\lambda + O(\beta, \lambda) \right\} \quad (\text{A15})$$

Calculation of the cumulative distribution function S (see Section 3.4)

$S(\beta, \lambda, t)$ is the fraction of leaves with inclination λ , under direct radiation with inclination β , receiving the radiation under a sine of incidence less than t . The sine of incidence is given by Eqn (2.1)

$$\sin\theta = \sin\beta \cos\lambda + \cos\beta \sin\lambda \sin\alpha \quad (2.1)$$

In Fig. 51 this relationship is plotted for β is 30 degrees and λ is 45 degrees. By changing abscissa and ordinate the sine of incidence $\sin\theta$ can be considered as the independent variable, and the azimuth α as the dependent variable. Since the cumulative fraction S is proportional to the azimuth, at least under the assumption of azimuthal isotropy,

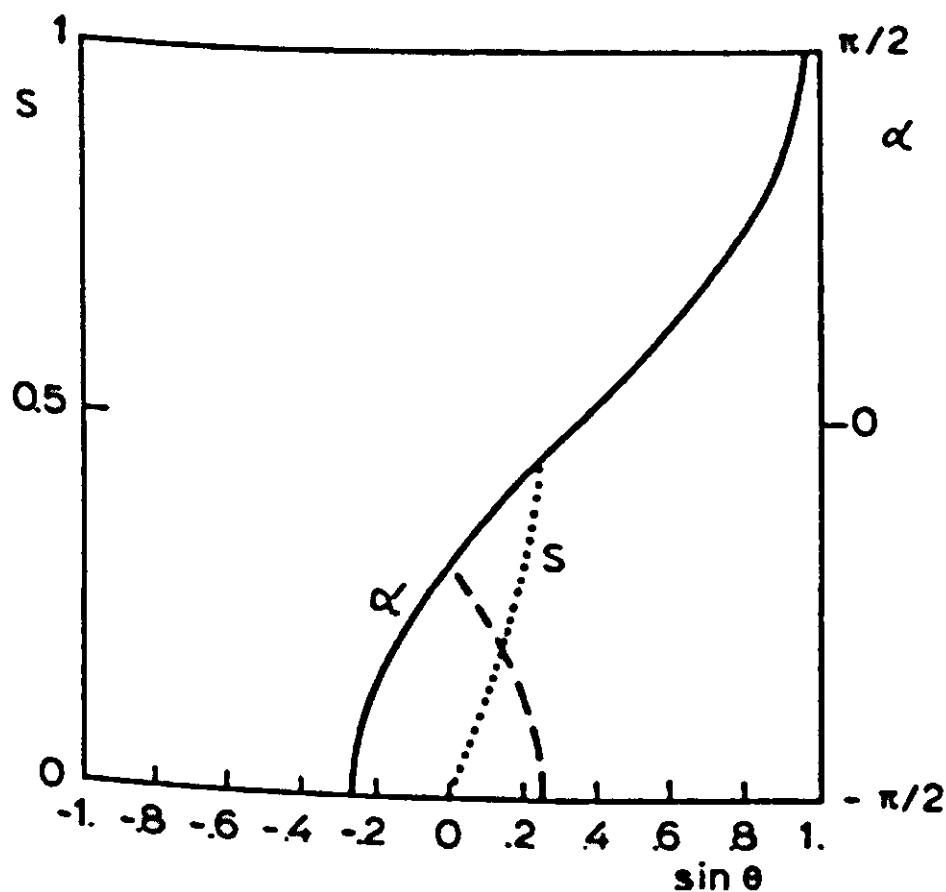


Fig. 51 | The azimuth α (solid line) and the cumulative distribution function S (dotted line) as a function of the sine of incidence of the radiation for β is 30 degrees and λ is 45 degrees. The broken line is the mirror image of α with respect to $\sin\theta$ is zero.

this is also a graph for S versus $\sin\theta$. One modification must still be made. Negative sines of incidence are equivalent to positive values, so that the negative section of the graph is projected onto the positive side (broken line) and subtracted from the positive section (resulting in the dotted line). The azimuth α ranges from $-\pi/2$ up to $\pi/2$, so that the resulting expression for S is

$$S = \frac{1}{\pi} \left\{ \arcsin \left(\frac{\sin\theta - \sin\beta \cos\lambda}{\cos\beta \sin\lambda} \right) + \arcsin \left(\frac{\sin\theta + \sin\beta \cos\lambda}{\cos\beta \sin\lambda} \right) \right\} \quad (\text{B1})$$

When the argument of an arcsine function is less than -1 , the arcsine function assumes the value $-\pi/2$, and conversely when the argument exceeds 1 , the function assumes the value $\pi/2$. This equation is programmed in Section 5 of MICROWEATHER (Section 5.6).

Index

- Absolute temperature 39, 99
Advection 234
Aerodynamic characteristics 115, 201
Afternoon depression 142
Analytical method 5, 130
Apparent
 extinction coefficient 52
 psychrometer constant 77
 radiant sky temperature 39
Assimilation of CO₂ 74 e.v., 84, 182
Azimuth 6, 54 e.v.
- Black
 body radiation see Thermal
 radiation leaves 17
Boundary layer resistance 73
Boundaries 124, 126
Buoyancy 99
Bypassing, conditional 134
- Canopy
 energy balance of 81
 radiation in 5
Clustering of leaves 6, 51 e.v.
Compartmentalization 192
Conditional bypassing 134
Conductance
 leaf 198, 214
 root 87
Convection 94 e.v.
- Daily
 courses 177
 totals 186
Damping depth 126
Declination of the sun 54
Density of air 94
Dew 184
Dew point 127
Diffuse radiation 9, 191
Dimensionless height 100
Direct radiation 9, 191
Distance
 between leaves 108
Distribution of leaves
 in angle classes 7
 in incidence classes 82
Diurnal trend 35
Drag, leaf – coefficient 110
 bulk – coefficient 116
Drying soil 80
Drying power of the air 77
- Eddy 94 e.v.
Emissivity of leaves 40
Energy balance 73 e.v.
Equivalent
 temperature 95, 99
 heat flux 95, 100
Error criterion 141
Evaporation 81, 177
Extinction coefficient 14
Extinction factor 110
- Fast processes 135

- Field capacity 86
Flow 3
Flux 3
Fraction of overcast sky 85, 89
Free convection 94
Friction velocity 97
- Gravity acceleration 99
Gustiness of wind 120, 205, 225
- Heat
 flux plates 216
 sensible – flux 73, 81, 177
 soil – flux 79, 177
 storage 73, 79
- Heterogeneous 118
Homogeneous 6, 118
Hysteresis 105
- Inclination
 of leaves 6
 of the sun 6, 54
- Initialization 124
Inversion 103, 185, 187
Irradiance 9, 61
Isotropic 7, 13, 44
Iteration 23, 108, 131
- Lapse see Unstable
Latent heat flux 73, 177 e.v.
Leaf angle distribution 7
Leaf area density 108
Leaf area index 3, 14
Leaf flutter 86
Logarithmic wind profile 95
Long-wave radiation see Thermal radiation
- Matrix 21, 130
- Microclimate 2
Microweather 1
Mixing length 96, 108
Monin-Obukhov length 99
Multiple scattering 5
- Near-infrared radiation 8, 11, 35
Net radiation 26, 128, 178
Numerical method 5, 130
Nusselt number 73
- Penman equation 78
Porometer 210
Prandtl number 74
Projection 6
Psychrometer constant 77
- Radiance 9, 36
Radiation 5 e.v.
Reciprocity 36
Reference height 98, 194
Reflection coefficient
 of the canopy 14 e.v.
 of leaves 12
 of a powder 41
 of the soil surface 13, 16
- Regular leaf arrangement 51
Regulatory internal CO₂-concentration 77, 198
Relative humidity 127
Relative plant water content 86
Relative turbulence intensity 109, 225
Relaxation method 21, 131
Resistance
 boundary layer 73
 cuticular 198
 leaf 76, 214
 root 86

scheme 118
 stomatal 76, 214
 for turbulent transfer 98
 Respiration 75, 86
 Reynolds number 74
 Richardson number 99 e.v.
 Root resistance 86
 Roughness length 96
 Rows 54
 Saturated vapour pressure ^z 77, 127
 Scattering coefficient 13, 196
 Shear stress 97
 S.I. units 3
 Slope of the saturated vapour
 pressure curve 78
 Slow processes 134
 Slow sensors 186
 Soil
 heat flux 79, 177
 temperature 79 e.v., 86
 water content 81, 86
 water stress 86
 Specular reflection 12
 Stable 102
 Standard overcast sky (SOC) 10, 41
 Stefan-Boltzmann constant 39
 Stiff systems 133
 Stomatal resistance 76, 214
 Thermal
 conductivity 79, 81
 radiation 39
 Time constant 88, 133
 Transmission
 by canopies 15
 by clouds 42
 coefficient of leaves 12
 Turbulence 94
 Turbulent exchange 94, 204
 Ultraviolet radiation 8
 Uniform overcast sky (UOC) 9
 Unstable 106
 Visible radiation 8, 11, 35
 Von Karman's constant 96
 Water
 balance 86
 Wet bulb temperature 127
 Wetness, duration of leaf 188
 Width of the leaves 73, 108
 Wind 94, 186
 Zero plane displacement 96